REACTIVITY OF NICKEL(0)–BISPHOSPHINE COMPLEXES AND NICKEL–Π COMPLEXES: EFFORTS TOWARD A WITTIG REACTION ON CARBON DIOXIDE

by

Nicholas Daniel Staudaher

A dissertation submitted to the faculty of
The University of Utah
in partial fulfillment of the requirements for the degree of

Doctor of Philosophy

Department of Chemistry

The University of Utah

December 2017

The University of Utah Graduate School

STATEMENT OF DISSERTATION APPROVAL

The dissertation of **Nicholas Daniel Staudaher**

has been approved by the following supervisory committee members:

Janis Louie	, Chair	**10/5/17** Date Approved
Matthew Kieber-Emmons	, Member	**10/5/17** Date Approved
Cynthia Burrows	, Member	**10/5/17** Date Approved
Jon Rainier	, Member	**10/5/17** Date Approved
Jules Magda	, Member	**10/5/17** Date Approved

and by **Cynthia Burrows** , Chair/Dean of

the Department/College/School of **Chemistry**

and by David B. Kieda, Dean of The Graduate School.

ABSTRACT

$Ni(COD)_2$ and Xantphos are known to form a bis-chelated $(Xantphos)_2Ni$ species, which was believed to be a thermodynamic sink and detrimental to catalysis. This species was found to react with nitriles to form a transient (Xantphos)Ni(nitrile) complex, which can be trapped by alkenes and alkynes for productive (Xantphos)Ni(alkene/alkyne) complexes. Nitrile–induced dissociation of Xantphos from $(Xantphos)_2Ni$ indicates that this species is not a thermodynamic sink and that its activation is a kinetics problem.

Aryl alkyl ketenes were synthesized in three steps: addition of an alkyl chain to the α-position of aryl acetic acids, conversion to the acyl chloride, and amine mediated dehydrohalogenation of the acyl chloride. Ketenes with primary alkyl chains form smoothly at room temperature while ketenes with secondary chains require a reaction temperature of 60 ºC. Formation of ketenes with electron rich aromatic rings requires longer reaction times than for electron poor aromatic rings.

A series of (dppf)Ni(aryl alkyl ketene) complexes were synthesized and fully characterized. The ketene is coordinated to the metal through the C=O bond in the solid state and this mode is usually the only one observed in solution. However, C=C coordination of the ketene is observed in solution for some ketenes. The mechanism of thermal decomposition of these complexes was investigated through a combination of experimental and theoretical techniques. Synergy between these techniques gave deep insight into this mechanism, which involves isomerization of the ketene from C=O

coordinated to C=C, followed by decarbonylation, giving an intermediate carbonyl carbene complex. Rearrangement of the carbene ligand is irreversible and results in a carbonyl alkene complex. While decarbonylation is usually rate limiting, carbene rearrangement is rate limiting for electron poor or sterically large ketenes.

Initial attempts toward a Ni–catalyzed Wittig reaction on CO_2 led to formation of symmetrical allenes, which raises the question: Does the trapping reagent react with free or coordinated ketene? The mechanism of ketene self–exchange was investigated. Interestingly, this ligand exchange proceeds through an autoinductive process that can be accelerated through addition of water or inhibited by a number of additives.

For my late uncle, Dick Norlin. Like me, he was a chemist, a skier, a rock climber, a cyclist, and we shared a middle name. He introduced me to cross-country skiing as a toddler, taught me to water ski, and showed me the subtle grace of the telemark turn. When I was a teenager, he took me rock climbing, something I am still passionate about. Dick was a mentor and a role model for me, and he will be sorely missed.

Nature uses only the longest threads to weave her patterns, so that each small piece of her fabric reveals the organization of the entire tapestry.

Richard Feynman

TABLE OF CONTENTS

LIST OF TABLES

Table

LIST OF ABBREVIATIONS

acac – Acetylacetanato ligand

Ac – Acetyl

Ar – Aryl

Boc – *tert*-butyloxycarbonyl

BPh_3 – Triphenylborane

cat. – Catalyst or catalytic

Cp – Cyclopentadienyl ligand

COD – 1,5-cyclooctadiene

eq. – Equation

equiv – Equivalents

DFT – Density functional theory

Dippe – 1,2-Bis(diisopropylphosphino)ethane

DMSO – Dimethylsulfoxide

DPPB – 1,4-Bis(diphenylphosphino)butane

DPPbenzene – 1,2-Bis(diphenylphosphino)benzene

DPPE – 1,2-Bis(diphenylphosphino)ethane

DPPF – 1,1'-Bis(diphenylphosphino)ferrocene

DPPP – 1,3-Bis(diphenylphosphino)propane

Dtbpe – 1,2-Bis(ditertbutylphosphino)ethane

Et – Ethyl

Et_2O – Diethyl ether

GCMS – Gas chromatography/mass spectrometry

h – Hours

HRMS – High resolution mass spectrometry

IMes – 1,3-dimesitylimidazol-2-ylidene

^{i}Bu – isobutyl

^{i}Pr – isopropyl

IR – Infrared spectroscopy

k_{obs} – Observed rateL – Ligand

M – Metal

MAO – Methylaluminoxane

Me – Methyl

MHz – Megahertz

min – Minutes

mol% – Mole percentage

NMR – Nuclear magnetic resonance spectroscopy

^{n}Bu – *Normal* butyl

ORTEP – Oak Ridge Thermal Ellipsoid Plot

Ph – Phenyl

PhCN – Benzonitrile

PMB – *para*-Methoxy benzyl

PPh_3 – Triphenylphosphine

rt – Room temperature

s – seconds

*s*Bu – secondary butyl

THF – Tetrahydrofuran

TMEDA – *N,N,N',N'*-tetramethyl ethylenediamine

TPPO – triphenylphosphine oxide

X – Halogen

Xant, Xantphos – 4,5-Bis(diphenylphosphino)-9,9-dimethylxanthene

ACKNOWLEDGEMENTS

First and foremost, I need to thank my mother, Susan Staudaher. I owe her my existence, and she slept on my couch for 3 weeks to take care of me when my collarbones were broken. I'd also like to thank my dad and brother, Steve and Shawn, as well as many aunts, uncles, cousins, and grandparents.

I also owe a great deal to my lab mates, cohorts, and other friends for emotional support, intellectual contributions, and crazy adventures. In no particular order, they include: Nabajit Lahiri, Steph Felten, Andy Clevenger, Noman Al, Ryan Stolley, Tim Lane, Ashish Thakur, Puneet Kumar, Klleber Oliveira, Joe Lovelace, Mike Johnson, Bri Esslinger, Jonas Renner, Jens Oberkofler, Adora Graham, Sarah Lefave, John Martin, Zach Niemeyer, Zak Evans, Nicolle Wiaderny, Corey Coulam, and many I've forgotten.

My committee members, Cynthia Burrows, Mark Ji, Jules Magda, and Jon Rainier, have been there every step of the way and given me excellent feedback at my qualifying exams. Matthew Kieber-Emmons has been particularly instrumental in teaching me about inorganic chemistry and DFT calculations.

I've had the opportunity to work with an amazing support staff in the U of U chemistry department. I'd like to thank Dave, Jay, Nomie, and Doug in the stockroom, our world class glassbower Kevin Teaford, and the electronics shop staff. Without Peter Flynn and Dennis Edwards, I'd still be sitting at the 500B with the FTS off wondering why the spectrometer's temperature isn't dropping. If it weren't for Dennis Romney and Tom

Gudmudson in the machine shop, I’d still be waiting for Swagelok parts to come in and the group would have no working vacuum pumps, solvent system, or glovebox.

I’m grateful for the people who have screwed my bones back together while I’ve been in graduate school: Dr. Higgins (clavicle), Dr. Curtis (medial epicondyle of the humerus), and Dr. Haller (Tibia).

Last, but certainly not least, I owe my utmost gratitude to my advisor, Janis Louie, Professor of Chemistry, Associate Dean of Academic Affairs, Ninja Warrior, and Mother of Dragons (well not really, but triplets are close). The best part about working for Janis is the freedom she gives her graduate students to pursue the research projects of their choice. A very close second is that she lets students choose their own schedules, which means I’ve spent a lot of weekdays skiing in the last five years.

CHAPTER 1

INTRODUCTION

As chemists, we are concerned with the identity of matter, its composition, and in particular, the manner in which it changes from one form to another. While the useful aspects of chemistry, such as pharmaceuticals, agrochemicals, petrochemicals, and renewable energy sources such as solar power and converting water or carbon dioxide, are obvious, the relationship between the day-to-day experiments done by a chemist and the global impact are often difficult to see. Consider the 2017 Nobel Prize in chemistry, which was awarded for the development of cryogenic electron microscopy. The development of this technique began in the late 1970s when water vitrification, or a method of freezing water without crystal growth such that biomolecules could be cooled enough for electron microscopy without destroying them, was discovered. The vitrification process was initially rejected for publication because the reviewers didn't believe water could be manipulated in such a way. However, 25 years and at least a dozen PhD students working on small improvements to the technique later, it came to fruition and was used to determine the structure of a membrane-bound protein. In 2013, a new type of electron detector was introduced, greatly improving the resolution. This technique has been used to determine the structure of many biomolecules, including the Zika virus.[1] This is a case study in the snail's pace of science, and how fundamental studies involving large groups of people over decades can have dramatic impacts on the human race, despite the lack of eureka moments in the day to day.

There are a small minority of chemists working in industrial settings where the connection between the application of their work and what they do on a daily basis is readily apparent: they do things such as fabricate devices or run reactions on a large scale and sell what they produce for a profit. In the end, all of chemistry involves manipulating matter in a way that ideally has some benefit for society, or at least can turn a profit. The chemical reaction can take many forms and have a vast range of applications. An exciting example is the reaction of iron oxide and aluminum, or the thermite reaction, which is used to weld railroad tracks. Another example is the catalytic converter, which changes some of the more toxic and polluting compounds in a car's exhaust into more innocuous chemicals. This is an example of heterogeneous catalysis, where the catalyst is in the solid state, and does not dissolve in the reaction media. The other type of catalysis is homogenous, where the catalyst dissolves in the reaction mixture. An example of homogenous catalysis is the adiponitrile process (eq 1.1),[2] where butadiene and hydrogen cyanide are converted to adiponitrile, an intermediate in the manufacture of nylon.

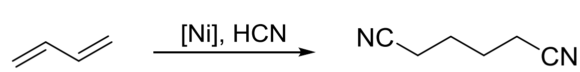

(1.1)

One way to think about a chemical reaction is to plot it on a reaction coordinate with reaction progress on the x-axis and energy on the y-axis (Figure 1.1). One key feature of this plot is that the products of the reaction are lower in energy than the reactants, otherwise the reaction would go backwards. Also, there is an energy of activation that must

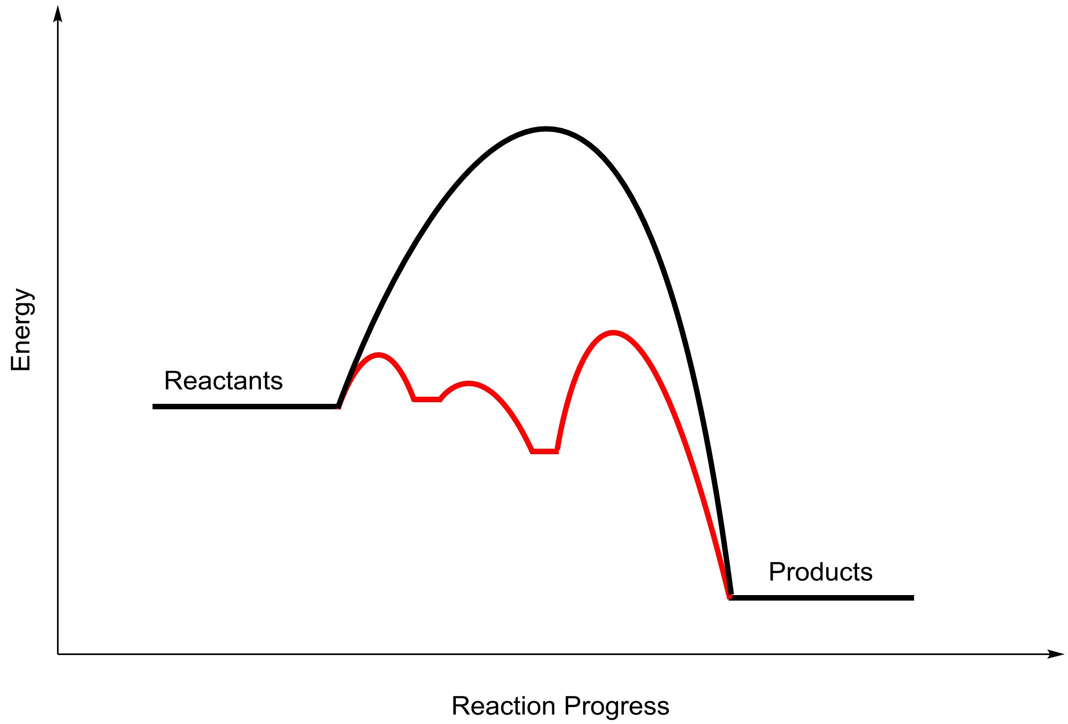

Figure 1.1. General reaction coordinate of a uncatalyzed reaction (black) and the same reaction with a catalyst (red).

be overcome for the reactants to be converted to the products. On such a plot, it is not uncommon for a desired reaction to not occur because the activation energy is insurmountable. In the absence of a catalyst, the adiponitrile process falls into this category. With a catalyst, the reaction mechanism changes in such a way that the intermediates and transition states on the reaction pathway change and the overall activation energy of the reaction is decreased. Understanding how the catalyst does this is paramount to understanding the mechanism of the reaction, as well as for improving current catalytic systems and developing new ones.

In homogenous catalysis, the catalyst can have one of a large number of structures: acids, bases, water, but transition metal complexes are by far the most ubiquitous. In this vein, the most prolific catalysts are based on the precious metals, such as Pd, Pt, Ru, Rh, and Ir.[3] Unfortunately, these metals have low natural abundance in the earth's crust and are therefore more expensive and less sustainable than the base metals. Furthermore, base metals such as nickel can do chemistries the precious metals cannot, including difficult oxidative additions to C-O[4] and C-N[5] bonds, and reductive eliminations of sp^3 hybridized carbon atoms.[6] Another lesser known example is facilitating a Wittig reaction on carbon dioxide. This reaction has received the attention of only one publication.[7] This report describes a stoichiometric reaction Aresta's complex and the most prototypical phosphorus ylide, and it produces a thermally unstable ketene complex and trimethylphosphine oxide (eq 1.2). The aim of the research described in this dissertation is to use mechanistic insight into the fundamental chemistry of Ni–ketene complexes to guide the development of a

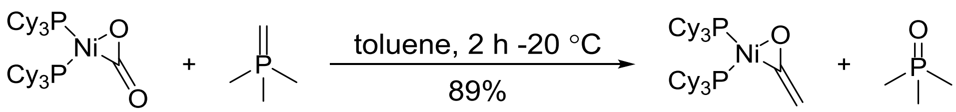

(1.2)

catalytic Wittig reaction on carbon dioxide (Figure 1.2). Not only would this reaction use carbon dioxide, a cheap, abundant C_1 synthon that is underutilized in organic synthesis, it would also add the last carbonyl functional group to the substrate scope of the Wittig reaction in a useful way.

From a mechanistic standpoint, this reaction involves a Wittig reaction on carbon dioxide coordinated to a nickel center, producing a key nickel–ketene complex intermediate. The ketene complex would then react with carbon dioxide and a trapping reagent to regenerate the catalyst and give the product. Two features of the trapping reagent are that it must render the ketene's carbonyl functionality unreactive to the Wittig reagent, and it must react with the ketene faster than the Wittig reagent, such that only one Wittig

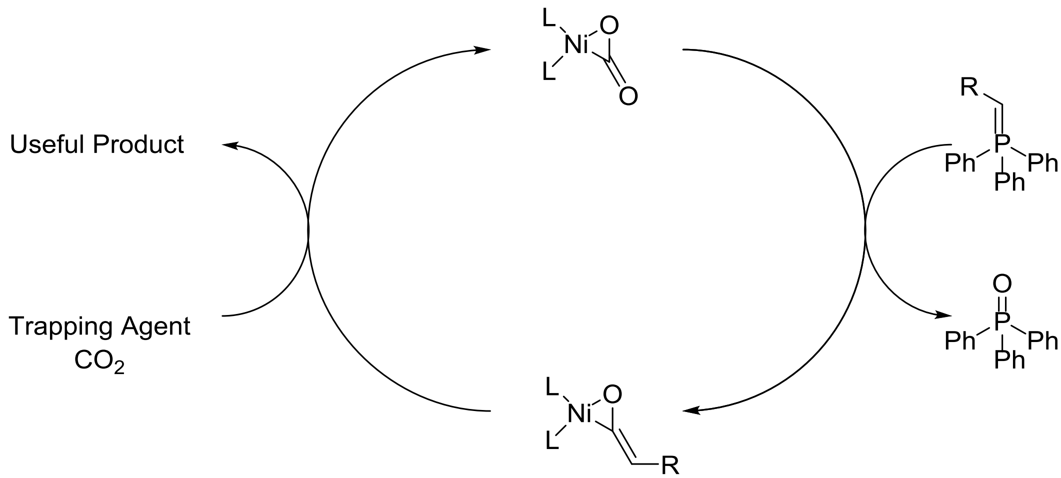

Figure 1.2. Proposed Ni catalyzed Wittig reaction on carbon dioxide.

reagent is incorporated into the product.

Few Ni–ketene complexes are known in the literature.[7-8] Of these, some are stable in solution at room temperature, but most of them decompose readily under such conditions, giving unreactive Ni–carbonyl complexes and undesired olefins. If this were to happen in our desired Wittig reaction, it would not only lead to byproduct formation (olefins), it would also result in catalyst death (Ni–carbonyl complexes). We therefore desired to have a better picture of what factors influence the stability of ketene complexes so it can be avoided in the Wittig reaction. Given that most of the known ketene complexes that are thermally stable have bidentate phosphines as the supporting ligand, we decided to start with this class of ligands. Furthermore, ligand displacement of $Ni(COD)_2$ by a phosphine and a ketene would be the most modular approach to Ni–ketene complexes. Unfortunately, most bidentate phosphines produce $(phosphine)_2Ni$ when reacted with $Ni(COD)_2$, leaving an equivalent of $Ni(COD)_2$ in solution, which rapidly decomposes ketenes. Chapter 2 therefore deals with the mechanism of formation and reactivity of the bis-chelated $(Xantphos)_2Ni$. Another challenge in the synthesis of Ni–ketene complexes is the need for stable, isolable ketenes. Unfortunately, ketenes readily dimerize and polymerize unless they have sterically large and/or electron donating groups. Due to these limitations, ketenes are almost always generated and reacted *in situ*, and preparations for them are scant and lack detail. Chapter 3 provides a detailed account of how to produce a set of 10 ketenes with yields over 5 g. Chapter 4 describes the synthesis of (dppf)Ni(ketene) complexes and their structural characteristics in the solid state and solution. The mechanism of their thermal decomposition was also elucidated in detail using a combination of experimental and theoretical methods. Key findings are that the rate determining step changes depending on the identity of the ketene, and that bidentate phosphines stabilize ketene complexes through a kinetic chelate effect. With knowledge of how to stabilize Ni–ketene complexes in hand, we turned our attention to developing the Wittig reaction by trapping a ketene with an amine, or by trapping a vinyl ketene with an alkyne, as described in Chapter 5. These efforts failed, prompting us to investigate the mechanism of ketene trapping, first by studying the mechanism of ligand exchange of ketene with itself. This ligand exchange proved to by autoinductive, where it is catalyzed by an as of yet unknown species. Due to how interesting the autoinductive nature of this elementary organometallic reaction was, it was investigated in depth, albeit few conclusions could be drawn regarding the identity of the catalyst and the mechanism of the ligand exchange.

References

1. Guarino, B. *The Washington Post* **2017**.

2. Bini, L.; Müller, C.; Vogt, D. *ChemCatChem* **2010**, *2*, 590.

3. Hartwig, J. F. *Organotransition Metal Chemistry*; University Science Books, 2010.

4. Mohadjer Beromi, M.; Nova, A.; Balcells, D.; Brasacchio, A. M.; Brudvig, G. W.; Guard, L. M.; Hazari, N.; Vinyard, D. J. *J. Am. Chem. Soc.* **2017**, *139*, 922.

5. Hie, L.; Fine Nathel, N. F.; Shah, T. K.; Baker, E. L.; Hong, X.; Yang, Y.-F.; Liu, P.; Houk, K. N.; Garg, N. K. *Nature* **2015**, *524*, 79.

6. Tellis, J. C.; Kelly, C. B.; Primer, D. N.; Jouffroy, M.; Patel, N. R.; Molander, G. A. *Acc. Chem. Res.* **2016**, *49*, 1429.

7. Wright, C. A.; Thorn, M.; McGill, J. W.; Sutterer, A.; Hinze, S. M.; Prince, R. B.; Gong, J. K. *J. Am. Chem. Soc.* **1996**, *118*, 10305.

8. (a) Sugai, R.; Miyashita, A.; Nohira, H. *Chem. Lett.* **1988**, 1403. (b) Miyashita, A.; Shitara, H.; Nohira, H. *J. Chem. Soc., Chem. Commun.* **1985**, 850. (c) Miyashita, A.; Sugai, R.; Yamamoto, J. *J. Organomet. Chem.* **1992**, *428*, 239. (d) Mindiola, D. J.; Hillhouse, G. L. *J. Am. Chem. Soc.* **2002**, *124*, 9976. (e) Curley, J. J.; Kitiachvili, K. D.; Waterman, R.; Hillhouse, G. L. *Organometallics* **2009**, *28*, 2568. (f) Hofmann, P.; Perez-Moya, L. A.; Steigelmann, O.; Riede, J. *Organometallics* **1992**, *11*, 1167. (g) Bestmann, H. J.; Denzel, T.; Salbaum, H. *Tetrahedron Lett.* **1974**, *14*, 1275.

CHAPTER 2

SYNTHESIS, MECHANISM OF FORMATION, AND CATALYTIC ACTIVITY OF XANTPHOS NICKEL Π–COMPLEXES*

Introduction

Xantphos,[1] a bidentate phosphine ligand with a rigid butterfly structure and a large bite angle, is a prolific ligand for a variety of nickel catalyzed reactions including hydrocyanation (eq 2.1),[2] alkynlcyanation (eq 2.2),[3] cross coupling (eq 2.3),[4] conversion of ethylene into 1-butene (eq 2.4),[5] and more recently, cycloaddition (eq 2.5),[6] and cross electrophile reductive couplings (eq 2.6).[7] One limitation of these reactions and Ni(0) catalyzed reactions[8] in general is that the catalyst is formed *in situ* either from addition of a ligand to $Ni(COD)_2$ or by reduction of a Ni(II) species in the presence of the ligand. Unfortunately, $Ni(COD)_2$ must be handled in a glove box and stored at low temperatures. Furthermore, COD acts as a competitive inhibitor in some of these reactions. The alternative route, namely catalyst formation from a Ni(II) species, typically requires elevated temperatures or addition of a reductant. As such, the need for air- and thermally

---

* Reproduced (adapted) with permission from Staudaher, N. D.; Stolley, R. M.; Louie, J. *Chem. Commun*. **2014**, *50*, 15577.

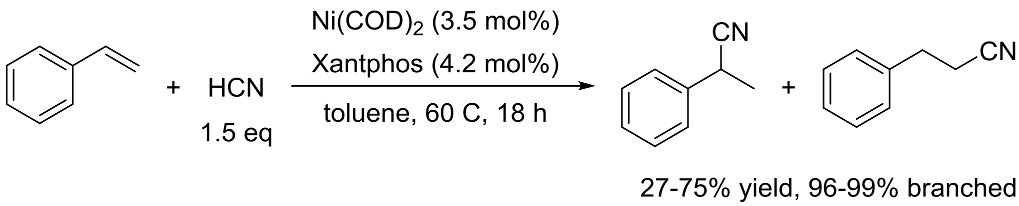

(2.1)

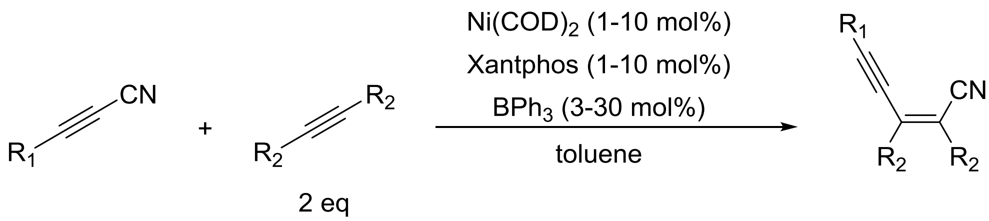

(2.2)

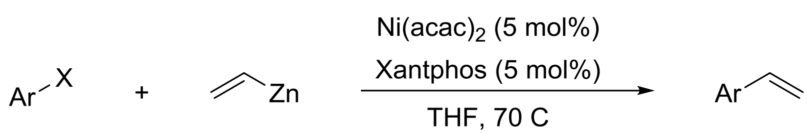

(2.3)

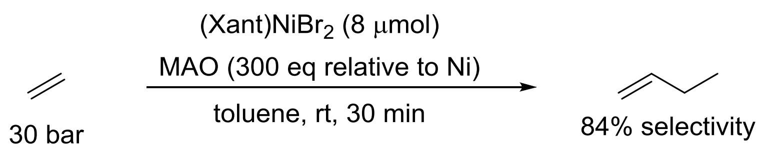

(2.4)

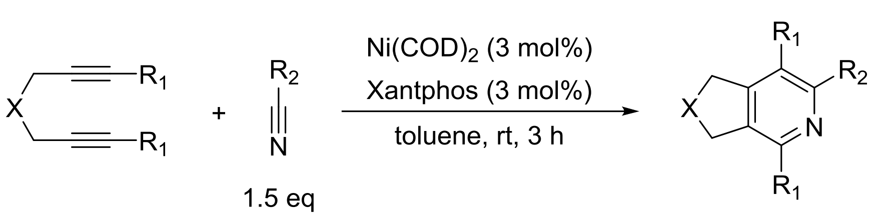

(2.5)

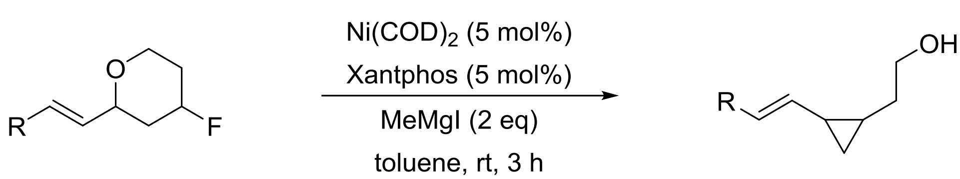

(2.6)

stable Ni pre-catalysts that are easily activated is high. The use of L_nNi (where L is the desired ligand for catalysis) as a pre-catalyst is not prevalent. In particular, $(Xant)_2Ni$ has been avoided as a pre-catalyst because it is thought to be unreactive owing to its full valence shell and coordination sphere.[2d] In fact, formation of $(Xant)_2Ni$ is generally considered detrimental to catalysis. Not surprisingly, formation of $(Xant)_2Ni$ has also thwarted efforts to prepare Xantphos-Ni π-complexes, an important intermediate in a variety of Ni/Xantphos catalyzed reactions. Herein, we report the serendipitous discovery of a synthetic route to Xantphos Ni π-complexes, an investigation into the mechanism of their formation, and an evaluation of their use as pre-catalysts. We also report the effectiveness of $(Xant)_2Ni$ to serve as a viable pre-catalyst in cross coupling and cycloaddition reactions.

Results and Discussion

We recently discovered the combination of Ni and Xantphos is one of the most effective catalysts for the cycloaddition of diynes and nitriles to afford pyridines in excellent yields.[6] Unfortunately, this catalyst system does not convert untethered alkynes to the desired pyridines. In our efforts to promote the desired 3-component coupling reaction, we reacted stoichiometric amounts of $Ni(COD)_2$ and Xantphos with an equimolar concentrations of benzonitrile and two equivalents of 3-hexyne (eq 2.7). Surprisingly, we serendipitously isolated (Xant)Ni–alkyne complex **1** in 88% yield rather than the expected pyridine product that would result from cycloaddition of 3-hexyne with benzonitrile In

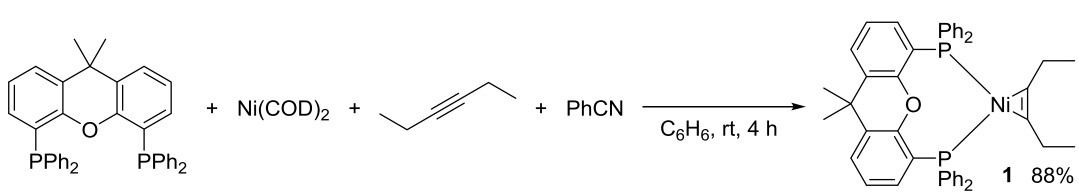

(2.7)

contrast, reduction of (Xant)$NiBr_2$[5] by Zn dust in the presence of 3-hexyne only afforded. unidentifiable paramagnetic products.

The ^{1}H NMR of (Xant)Ni(3-hexyne) **1** displayed peaks in the aromatic region and a singlet at 1.29 ppm indicative of a Xantphos ligand. In addition, the spectrum displayed a triplet at 1.12 ppm that integrated to six protons as well as a quartet at 2.15 ppm with an integration of four protons, indicating a species with a 1:1 ratio of Xantphos:3-hexyne. The ^{13}C NMR spectrum included a multiplet at 135.5 ppm, consistent with an alkyne coordinated to Ni(0).[9] IR spectroscopy revealed an alkyne peak at 1821 cm^{-1}, which is about 300 cm^{-1} shifted down from a free alkyne. These data are in accord with a (Xant)Ni(3-hexyne) structure. Crystals of this complex suitable for X-ray crystallography were grown by diffusion of pentane into a benzene solution of the complex (Figure 2.1). Notably, when 3-hexyne is added to a solution of $Ni(COD)_2$ and Xantphos, only marginal amounts of (Xant)Ni(3-hexyne) are formed in conjunction with copious $(Xant)_2Ni$ as observed by ^{31}P NMR.

Using the reaction conditions to synthesize **1**, Ni π-complexes of diphenylacetylene (**2**), dimethylfumarate (**3**), and *trans*-stilbene (**4**) were synthesized in 94%, 89%, and 76% yields, respectively (Figure 2.1). In addition, a Ni-π complex of 2-butyne-1,4-diol (**5**) was synthesized, albeit in lower yield. The formation of **5** is particularly notable in that the preferred coordination of 2-butyne-1,4-diol is by the alkyne rather than the alcohol –OH. For complex **5**, the reaction mixture is brown instead of yellow before addition of pentane for recrystallization, indicating that the alcohol groups are reacting with the nickel center, causing the lower yield.

ORTEP diagrams of **1**, **2**, and **3** are shown in Figure 2.1. Alkyne complex **1** has a

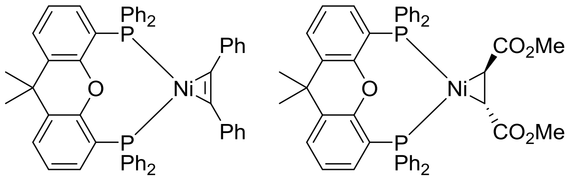

2 94% **3** 89% **4** 76% **5** 44%

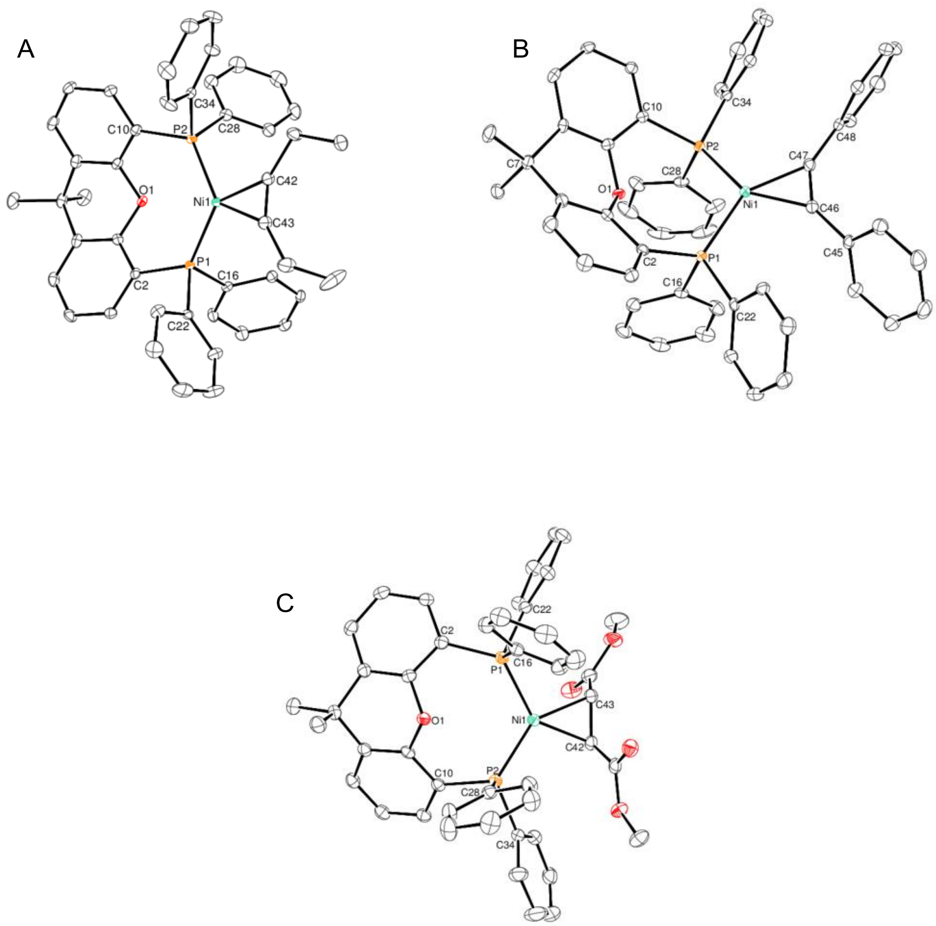

Figure 2.1. Structures and yields of complexes 2–5 and ORTEP diagrams of **1** (A) **2** (B) and **3** (C).

Ni– C(42) bond length of 1.894(2) Å and Ni–C(43) bond length of 1.905(2) Å. Complex **2** has a Ni–C(46) bond length of 1.899(3) Å and Ni–C(47) bond length of 1.895(3) Å. These bond lengths are similar to a class of (dippe)Ni(C_2R_2) (dippe = 1,2-bis(diisopropylphosphino)ethane) alkyne complexes prepared by Jones[9b] and (dtbpe)Ni(C_2R_2) (dtbpe = 1,2-bis(di-*tert*-butylphosphino)ethane) complexes prepared by Hillhouse.[9c] Alkene complex **3** has a Ni(1)–C(42) bond length of 1.972(2) and a Ni(1)–C(43) bond length of 1.997(2), which are surprisingly similar Ni–C bond lengths to (IMes)$_2$Ni(dimethylfumarate) (Ni–C bond lengths for this complex are 1.984(2) and 1.988(2)) considering the electronic and steric differences between two IMes ligands and Xantphos.[9a] Interestingly, the P–Ni–P angle is significantly different for complexes **1**, **2**, and **3** (angles are 118.92(2)º, 108.83(3)º, and 112.11(2)º, respectively). As the angle approaches Xantphos' natural bite angle of 108º,[1b] one phenyl ring on each P atom also comes closer together. In the case of complex **2**, the rings containing C(16) and C(28) have a plane-plane angle of 15.71º and a centroid–centroid distance of 3.754 Å. Each pair of carbon atoms are directly overlapping, indicating a sandwich π-stacking interaction.[10] Each diphenylacetylene phenyl ring is also π-stacking with one of the other Xantphos phenyl rings. The rings containing C(34) and C(48) have a plane-plane angle of 22.94 and a centroid–centroid distance of 3.960. The rings containing C(22) and C(45) have a plane–plane angle of 19.33 and a centroid–centroid distance of 3.821. The carbon atoms in each ring are not directly overlapping, consistent with a parallel-displaced π-stacking interaction.

We embarked on a series of NMR experiments to evaluate the ability of nitrile to disrupt the formation of the typically unreactive (Xant)$_2$Ni. Not surprisingly, when diphenylacetylene was added to a saturated solution of $(Xant)_2Ni$, no reaction occurred (eq 2.8). However, when 5 equiv. benzonitrile was also added, alkyne complex (as well as free Xantphos) was slowly generated and the reaction ultimately reached equilibrium at 24% of alkyne complex **2** (eq 2.9). Similarly, when diphenylacetylene was added to a solution of 1 equiv. $Ni(COD)_2$ and 1 equiv. Xantphos, which has been allowed to pre-coordinate for 2 min, only 5% yield of alkyne complex **2** formed while 95% of $(Xant)_2Ni$ was produced. Conversely, when diphenylacetylene and 5 equiv of benzonitrile were both added to a solution of 1 equiv. $Ni(COD)_2$ and 1 equiv. Xantphos, a significant increase in the formation of alkyne complex **2** was observed, and any $(Xant)_2Ni$ that formed was completely converted to **2** within 6 h. Taken together, these data suggest that nitrile undergoes initial ligand displacement of one Xantphos on $(Xant)_2Ni$ and subsequently is replaced with alkyne (Figure 2.2).

In some cases, the formation of $(Xant)_2Ni$ can be circumvented by changing the order of reactant addition. When diphenylacetylene and $Ni(COD)_2$ were premixed for 5 min prior to the addition of Xantphos, only alkyne complex **2** was observed, regardless of whether benzonitrile was added. Similarly, when a solution of $Ni(COD)_2$ was added to a solution of Xantphos and diphenylacetylene, only alkyne complex **2** was observed. In contrast, when *trans*-stilbene and $Ni(COD)_2$ were premixed for 5 min prior to the addition of Xantphos, $(Xant)_2Ni$ was initially the major product instead of the desired alkene complex **3** (2:1). This is consistent with a report by Tolman indicating *trans*-stilbene is less than an order of magnitude better at binding Ni(0) than COD.[11] In this case, addition of benzonitrile does facilitate the quantitative formation of Ni π-complex **4**. These reactions were repeated with 3-hexyne instead of diphenylacetylene. The same trends were observed,

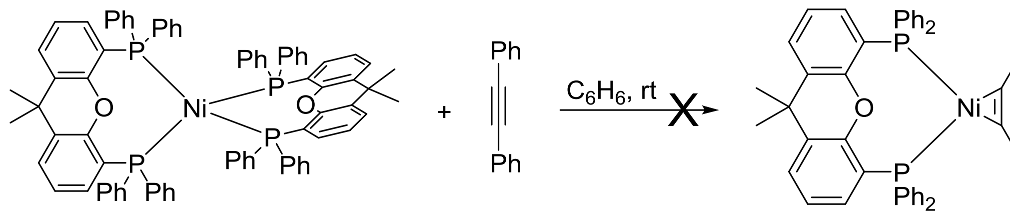

(2.8)

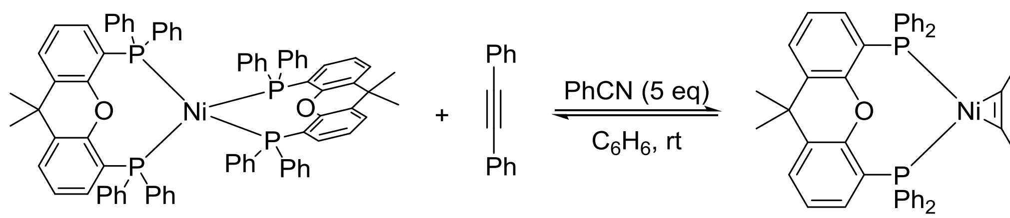

(2.9)

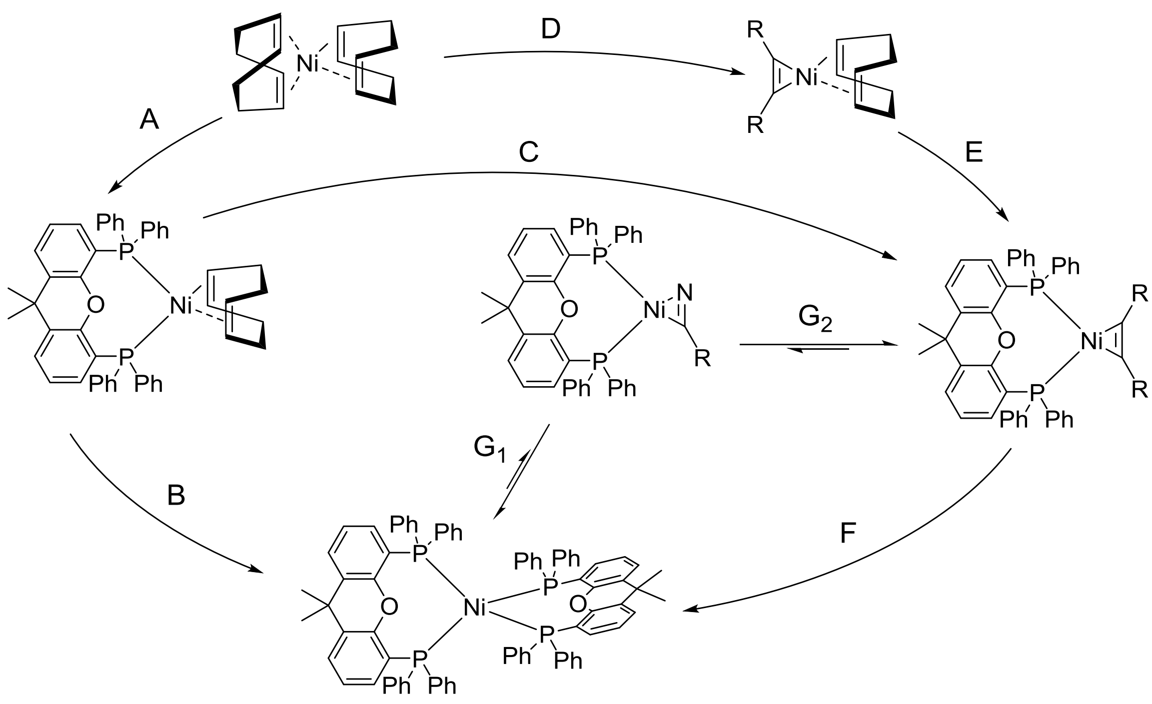

Figure 2.2. Possible ligand exchanges leading to (Xant)2Ni and (Xant)Ni(alkyne)

albeit less pronounced than those observed with diphenylacetylene.

These NMR experiments suggest the following series of reactions is possible (Figure 2.2). When Xantphos is added to $Ni(COD)_2$, Xantphos displaces on COD ligand to form a (Xant)Ni(COD) species (pathway A). The transient (Xant)Ni(COD) species can undergo a second ligand substitution by either Xantphos to form $(Xant)_2Ni$ (pathway B) or by an alkyne to form(Xant)Ni(alkyne) (pathway C). Alternatively, $Ni(COD)_2$ itself can also undergo ligand substitution by an alkyne (pathway D) followed by displacement of COD by Xantphos (pathway E). Sole formation of **2** when $Ni(COD)_2$ is added last indicates that displacement of COD from $Ni(COD)_2$ by diphenylacetylene is much faster than by Xantphos. The (Xant)Ni(alkyne) complex can react with Xantphos to form $(Xant)_2Ni$, (pathway F). If this happens in the absence of nitrile, this reaction is irreversible. However, in the presence of nitrile, $(Xant)_2Ni$ is converted to an intermediate nitrile complex which allows the formation of the desired alkyne complex (pathways G_1 and G_2).

The catalytic activity of complexes **1**–**5** as well as $(Xant)_2Ni$ with and without added benzonitrile in cross coupling were evaluated (Table 2.1). The title complexes, except 2-butyne-1,4-diol complex **5**, successfully catalyzed the cross coupling of 1-bromonaphthalene and vinyl zinc bromide in THF at 50 ºC to afford 1-vinylnapthalene in good yields (entries **1**–**4**). Surprisingly, the use of $(Xant)_2Ni$ as a catalyst also provided 1-vinylnapthalene in both the presence and absence of added nitrile (entries 6 and 7). Importantly, product yields are comparable to yields when Xantphos and $Ni(acac)_2$ are employed as catalyst.[4] Surprised by the success of $(Xant)_2Ni$ in this reaction, we assessed the ability of N-methyl-2-pyrrolidone (NMP), an additive used to keep the vinyl zinc reagent homogenous, to cause Xantphos dissociation from $(Xant)_2Ni$. When

Table 2.1. Activity of complexes in cross coupling.[a]

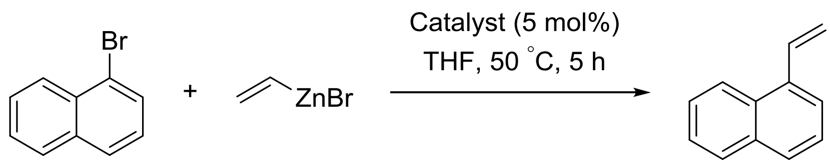

Entry	Catalyst	Conversion (%)[b]	Yield (%)[b]
1	complex **1**	89	86
2	complex **2**	97	96
3	complex **3**	97	96
4	complex **4**	99	99
5	complex **5**	15	14
6	$(Xant)_2Ni$	97	97
7	$(Xant)_2Ni$ + PhCN[c]	98	98

[a] Reaction Conditions: 1-bromonapthalene (1 eq, 0.5 M), vinyl zinc bromide (1.75 eq) [b] Determined by GC compared to naphthalene internal standard [c] 10 mol% PhCN was used

diphenylacetylene and NMP were added to a saturated solution of $(Xant)_2Ni$, formation of complex **2** was observed albeit in low yield (i.e., 8%). However, NMP is less effective than benzonitrile as ten times the equivalents of NMP, relative to benzonitrile, was required to achieve even moderate yields of complex **2**.

The activity of the complexes in cycloaddition was also assessed. Complexes **1**, **2**, and **4** (3 mol%) were added to diyne and acetonitrile at room temperature. In each case, high yields of pyridine **6** were obtained (entries 1, 2, and 4, Table 2.2). Importantly, these yields are comparable to an isolated yield of 94% when Xantphos and $Ni(COD)_2$ are employed.[6] In contrast, complex **3** was not competent in this reaction presumably due to the high affinity of dimethylfumarate for Ni(0) (entry 3). Complex **5**, which did not catalyze the cross coupling reaction, was also not an effective catalyst for this reaction

Table 2.2. Activity of complexes in cycloaddition.[a]

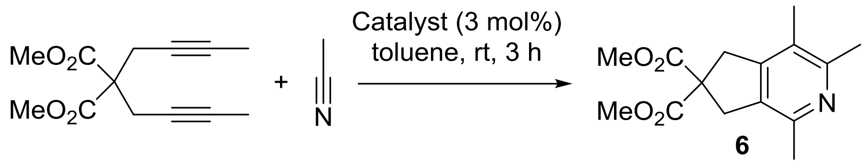

Entry	Catalyst	Conversion (%)[b]	Yield (%)[b]
1	complex **1**	97	97
2	complex **2**	>99	91
3	complex **3**	6	5
4	complex **4**	99	91
5	complex **5**	1	1
6	$(Xant)_2Ni$	65	60
7	$(Xant)_2Ni$ + PhCN[d]	81	57

[a] Reaction Conditions: Diyne (1 eq, 0.1 M), acetonitrile (1.5 eq)
[b] Determined by GC relative to naphthalene internal standard [c] 10 mol% of benzonitrile was used.

(entry 5). In addition, $(Xant)_2Ni$ did catalyze the cycloaddition with and without added benzonitrile (entries 6 and 7), A higher conversion was observed with added benzonitrile due to activation of the complex, although a slightly lower yield was observed due to incorporation of benzonitrile. It is likely that acetonitrile serves to activate the $(Xant)_2Ni$ in the same manner as benzonitrile.

To assess the possibility for using (Xant)Ni π-complexes as air stable pre-catalysts, the stability of complex **1** was evaluated. To our dismay, when a solution of **1** was exposed to air, the solution turned from yellow to brown with a marked decrease in the intensity of the singlet in ^{31}P NMR compared to internal standard. After 10 min, only 13% of the complex remained; within 20 min, complex **1** was not detected by ^{31}P NMR. The sensitivity of **1** in the solid state to air was also investigated. Within 10 min of exposing **1** in the solid state to air, only a trace amounts of **1** could be observed by ^{31}P and ^{1}H NMR spectroscopy; complete decomposition of **1** was observed after exposing a sample to air for 30 min. In contrast, $(Xant)_2Ni$ displayed surprising stability to air. This complex was slightly more stable towards air in solution. After 25 min in solution, only trace $(Xant)_2Ni$ was detected by ^{31}P NMR; no complex was detected after 35 min wherein the solution turned from orange to colorless. However, samples of $(Xant)_2Ni$ in the solid state that were exposed to atmosphere for 8 h remained intact (as examined by ^{31}P NMR spectroscopy). After 12 h, trace Xantphos and Xantphos oxides were detected, and over time, the intensity of these peaks slowly increased. Importantly, after exposure to air for 3 days, 90% of the total integration in a ^{31}P NMR of the solid sample was from $(Xant)_2Ni$. Furthermore, after 20 months, the sample was still ~60% intact. Finally, the catalytic activity of this sample was evaluated after 33 months, and a 50% yield of pyridine was observed by ^{1}H NMR, indicating that $(Xant)_2Ni$ is a relatively air-stable pre-catalyst for [2 + 2 + 2] cycloadditions of diynes and nitriles.

Conclusion

In conclusion, we have discovered a method to synthesize (Xant)Ni–alkene and –alkyne complexes, characterized them, and evaluated their catalytic activity. The mechanism of their formation was also investigated. Interestingly, we discovered nitrile is capable of facilitating the dissociation of a Xantphos ligand from $(Xant)_2Ni$ for productive alkene or alkyne coordination. However, nitrile is not necessary to form Xantphos Ni π-complexes if a strongly coordinating alkene or alkyne is allowed to pre-coordinate to Ni before Xantphos is added. These complexes showed similar catalytic activity to Xantphos and $Ni(COD)_2$ in cycloaddition of diynes and nitriles as well as to Xantphos and $Ni(acac)_2$ in Negishi coupling. Although (Xant)Ni π-complexes **1**–**5** are not bench stable, they do not need to be stored at low temperatures like $Ni(COD)_2$, and do not require activation like many Ni(II) pre-catalysts. Of particular interest, despite being Ni(0), $(Xant)_2Ni$ was shown to be reasonably air stable as a solid and was found to be a competent pre-catalyst when activated by nitrile or a coordinating solvent, even after exposure to atmosphere. This discovery should aid in the experimental simplicity of future Ni Xantphos catalyzed reactions. We believe that further work with these complexes could lend further insight into how nickel Xantphos catalyzed reactions operate and why Xantphos is an excellent ligand for a variety of transition metal catalyzed reactions.

Experimental Section

General considerations. All reactions were carried out under an atmosphere of N_2 using standard schlenk technique or in a N_2 filled glovebox. Benzene, pentane, and THF were dried over neutral alumina under N_2 using a Grubbs type solvent purification system. Xantphos was purchased from Strem and used as received. $Ni(COD)_2$ was purchased from Strem or synthesized according to the literature procedure.[12] 3-hexyne, benzonitrile, and deuterated benzene were distilled from CaH_2 and degassed by three freeze pump thaw cycles. THF-d_8 was purchased from Cambridge isotope and used as received. 2-butyne-1,4-diol was recrystallized from toluene prior to use. Diphenylacetylene, *trans*-stilbene, dimethylfumarate, and triphenylphosphine oxide were purchased from Aldrich and used as received.

^{1}H Nuclear Magnetic Resonance spectra were acquired at 300 or 400 MHz. ^{13}C

spectra were recorded at 100 MHz. ^{31}P spectra were recorded at 121 MHz. All ^{13}C and ^{31}P NMR spectra were proton decoupled. ^{1}H and ^{13}C spectra were referenced to solvent references (C_6D_6 δ 7.16 and δ 128.6; THF-d_8, δ 3.76 and δ 68.0). ^{31}P NMR shifts were reported with respect to external 85% H_3PO_4 (0 ppm). IR spectra were recorded on a Bruker Tensor 27 FT-IR spectrometer. X-ray crystallography data were collected and analyzed by Dr. Atta Arif at the University of Utah. Elemental analysis was performed by Midwest Microlabs LLC.

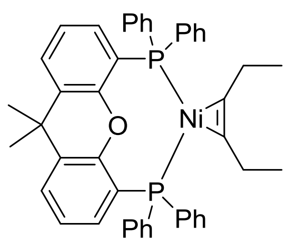

(Xantphos)Ni(3-hexyne) (1). In a drybox, $Ni(COD)_2$ (100 mg, 0.363 mmol) and Xantphos (210.4 mg, 0.363 mmol) were weighed into a 20 mL scintillation vial equipped with a Teflon coated stirbar and dissolved in 12 mL of benzene. 3-hexyne (83 μL, 0.726 mmol) followed by PhCN (50 μL, 0.486 mmol) were added to the $Ni(COD)_2$/Xantphos solution and stirred at rt for 3 h. The resultant yellow solution was then reduced in volume to about 5 mL, followed by the addition 15 mL of pentane. This solution was stored at -40 °C overnight, resulting in the formation of a yellow solid, which was removed by filtration, washed with pentane and dried to yield 198.5 mg (76% yield) of **1**. A secondary recrystallization from benzene/pentane afforded another 30 mg (88% total yield) of **1**. Crystals suitable for X-ray crystallographic analysis were prepared by slow diffusion of pentane into a benzene solution of the complex. ^{1}H NMR (300 MHz, C_6D_6): δ 7.81 (br s, 8H), 6.92-7.14 (m, 14H), 6.75-6.82 (m, 4H), 2.15 (q, J = 5.4 Hz, 4H), 1.29 (s, 6H), 1.12 (t, J = 5.4 Hz 6H). ^{13}C{^{1}H} NMR (100.6 MHz, C_6D_6): δ 159.0 (t, J_{PC} = 5.6 Hz, *Ar*), 137.9 (m, J_{PC} = 18 Hz, *Ar*), 136.5 (m, *C C*), 134.8 (t, J_{PC} = 18 Hz, *Ar*), 132.5 (s, *Ar*), 129.5 (s, *Ar*), 129.2 (s, *Ar*), 128.8 (t, J_{PC}=4.0, *Ar*) 128.8 (m, *Ar*), 125.9 (s, *Ar*), 124.2 (s, *Ar*), 37.6 (s,

$C(CH_3)_2$), 27.3 (s, CH_3), 20.7 (t, J_{PC}=7.1, CH_2), 16.9 (s, CH_3). $^{31}P\{^1H\}$ NMR (121 MHz, C_6D_6): δ 22.0 (s). IR (nujol, NaCl): 1821 (m. ν_{CC}), 1584 (w) 1434 (s) 1403 (s) 1307 (w) 1237 (w) 1219 (s) 1180 (m) 1148 (m) 1118 (m) 1088 (s) 1066 (m) 1026 (w) 998 (w) 872 (w) 793 (w) 776 (m) 757 (w) cm^{-1}. Multiple samples gave poor elemental analysis.

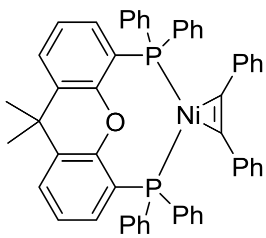

(Xantphos)Ni(diphenylacetylene) (2). In a drybox, $Ni(COD)_2$ (100 mg, 0.363 mmol) and Xantphos (210.4 mg, 0.363 mmol) were weighed into a 20 mL scintillation vial equipped with a Teflon coated stirbar and subsequently dissolved in 10 mL of benzene. A solution of diphenylacetylene (129.4 mg, 0.726 mmol) in 2 mL benzene was added followed by PhCN (50 μL, 0.486 mmol). After 5 min, the reaction turned from red to yellow and a precipitate began to form. The reaction was stirred for 4 h and 8 mL pentane was added. The reaction was stirred for an additional hour, filtered, washed with several portions of pentane, and dried under vacuum to yield 276.7 mg (94% yield) of **2** as a yellow solid. Crystals grown from diffusion of pentane into a THF solution of the complex were not suitable for X-ray crystallography. Suitable crystals were grown from a benzene solution containing 0.01 M $Ni(COD)_2$, Xantphos, benzonitrile, and 0.02 M diphenylacetylene. ^1H NMR (400 MHz, THF-d_8): δ 7.67 (d, J = 8.0 Hz, 2 H), 7.44 (m, 13H), 7.21 (t, J = 8.0 Hz, 4H), 7.25 (t, J = 8.0 Hz, 9H), 6.85 (m, 9H), 6.59 (t, J = 8.0 Hz, 2H), 1.76 (s, 6H). $^{13}C\{^1H\}$ NMR (100.8 MHz, THF-d_8): δ 158.6 (t, J_{PC} = 5 Hz, *Ar*), 138.1 (t, J_{PC} = 7 Hz, *Ar*) 136.8 (s, *Ar*), 135.8 (m, *C C*), 135.2 (t, J_{PC} = 7 Hz, *Ar*), 132.3 (s, *Ar*), 129.8 (s, *Ar*), 129.6 (s, *Ar*), 129.0 (t, J_{PC} = 5 Hz, *Ar*), 128.4 (s, *Ar*), 128.2 (s, *Ar*), 126.8 (s, *Ar*), 126.3 (m, *Ar*), 125.0 (s, *Ar*), 124.6 (s, *Ar*), 38.1 (s, $C(CH_3)_2$), 27.6 (s, CH_3).$^{31}P\{^1H\}$ NMR (121 MHz, C_6D_6): δ 22.9 (s). IR (nujol, NaCl): 1792 (s, ν_{CC}) 1589 (s) 1497 (s) 1434

(s) 1409 (s) 1309 (w) 1234 (s) 1184 (m) 1150 (w)) 1120 (w) 1096 (m) 1066 (w) 1026 (w) 1000 (w) 880 (w) 791 (w) 771 (m) cm^{-1}. Anal. Calcd. for $C_{53}H_{42}NiOP_2$: C, 78.05; H, 5.19. Found: C, 77.95; H, 5.42.

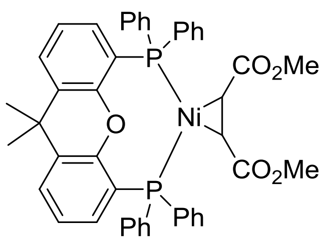

(Xantphos)Ni(dimethylfumarate) (3). In a drybox, $Ni(COD)_2$ (100 mg, 0.363 mmol) and Xantphos (210.4 mg, 0.363 mmol) were weighed into a 20 mL scintillation vial equipped with a Teflon coated stirbar and subsequently dissolved in 10 mL of benzene. Dimethylfumarate (104.9 mg, 0.727 mmol) in 2 mL benzene was added followed by PhCN (50 μL, 0.486 mmol). The reaction was stirred for 4 h, at which point it was concentrated to 5 mL. Pentane (15 mL) was added and the solution stored at -40 °C overnight, resulting in the formation of a dark solid, which was removed by filtration, washed with several portions of pentane and dried to yield 252.8 mg (89% yield) of **3** as a strikingly purple solid. Crystals suitable for X-ray crystallography were grown by diffusion of pentane into a benzene solution of the complex. ^1H NMR (400 MHz, C_6D_6): δ 7.84 (t, J = 12 Hz, 4H), 7.44 (t, J = 12 Hz, 4H), 7.15 (t, J = 8.0 Hz, 5H), 7.08 (d, J = 8.0 Hz, 2H), 7.00 (m, 7 H), 6.69 (m, 4H), 3.67 (s, 2H) 3.15 (s, 6H), 1.26 (s, 6H). $^{13}C\{^1H\}$ (100.6 MHz, C_6D_6): δ 174.4 (s, $\mathit{C}O_2CH_3$), 157.6 (t, J_{PC} = 5 Hz, *Ar*), 135.5 (t, J_{PC} = 2 Hz, *Ar*), 135.0 (d, J_{PC} = 13 Hz, *Ar*), 134.6 (dd, J_{PC} = 6 Hz, 5 Hz), 132.4 (s, *Ar*), 129.8 (d, J_{PC} = 8 Hz, *Ar*), 129.0 (t, J_{PC} = 5 Hz, *Ar*), 126.7 (s, *Ar*), 124.8 (t, J_{PC} = 3 Hz, *Ar*), 124.2 (dd, J_{PC} = 12, 3 Hz, *Ar*), 50.7 (s $CO_2\mathit{C}H_3$) 50.0 (t, J_{PC} = 8 Hz, *C*=*C*), 36.8 (s, $\mathit{C}(CH_3)_2$), 27.4 (s, $\mathit{C}H_3$). $^{31}P\{^1H\}$ NMR (121 MHz, C_6D_6): δ 16.8 (s). IR (nujol, NaCl): 1678 (s ν_{CO}), 1586 (w) 1461 (s) 1434 (m) 1410 (s) 1282 (m) 1259 (m) 1229 (s) 1205 (s) 1156 (w) 1135 (m) 1096 (w) 1036 (s) 999 (w) 881 (w) 846 (w) 793 (w) 776 (w) 754 (m) cm^{-1}. Anal. Calcd.

for $C_{45}H_{40}NiO_5P_2$: C, 69.17; H, 5.16. Found: C, 68.80; H, 4.99.

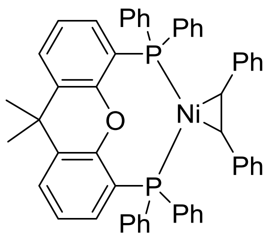

(Xantphos)Ni(*trans*-stilbene) (4). In a drybox, $Ni(COD)_2$ (100 mg, 0.363 mmol) and Xantphos (210.4 mg, 0.363 mmol) were weighed into a 20 mL scintillation vial equipped with a Teflon coated stirbar and subsequently dissolved in 10 mL of benzene. *trans*-stilbene (131.3 mg, 0.727 mmol) in 2 mL benzene was added followed by PhCN (50 μL, 0.486 mmol). The reaction was stirred for 4 h, at which point it was concentrated to 5 mL. Pentane (15 mL) was added and the solution stored at -40 °C overnight, resulting in the formation of a dark solid, which was removed by filtration, washed with several portions of pentane and dried to yield 226.6 mg (75.8% yield) of **4** as a red solid. ^{1}H NMR (400 MHz, C_6D_6): δ 7.63 (t, J = 8.0 Hz, 4H) 7.40 (m, 2H), 7.0 (m, 20H), 6.78 (m, 6H), 6.70 (t, J = 8.0 Hz, 2H), 6.40 (m, 2H) 3.97 (s, 2H), 1.23 (s, 6H). ^{13}C{^{1}H} (100.6 MHz, C_6D_6): δ 156.6 (t, J_{PC} = 6 Hz, Ar), 147.0 (s, Ar), 135.4 (t, J_{PC} = 8 Hz, Ar), 135.2 (dd, J_{PC} = 15, 2 Hz, Ar), 134.7 (t, J_{PC} = 7 Hz, Ar), 133.7 (t, J_{PC} = 6 Hz, Ar), 131.8 (s, Ar), 129.5 (s, Ar), 129.12 (s, Ar), 128.7 (t, J_{PC} = 3 Hz, Ar), 126.7 (s, Ar), 126.4 (s, Ar), 124.7 (t, J_{PC} = 2 Hz, Ar), 123.8 (s, Ar) 65.6 (t, J_{PC} = 8 Hz, *C*=*C*), 36.9 (s, *C*(CH_3)$_2$), 27.7 (s, *C*H_3). ^{31}P{^{1}H} NMR (121 MHz, C_6D_6): δ 16.3 (s). IR (nujol, NaCl): 1590 (s) 1435 (s) 1407 (s) 1378 (s) 1305 (w) 1238 (s) 1180 (w) 1149 (w) 1116 (s) 1093 (m) 1068 (w) 1028 (w) 998 (w) 881 (w) 830 (w) 790 (w) 775 (w) cm^{-1}. Anal. Calcd. for $C_{53}H_{44}NiOP_2$: C, 77.86; H, 5.42. Found: C, 77.61; H, 5.43.

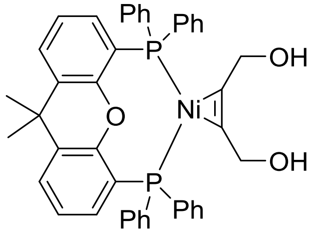

(Xantphos)Ni(2-butyne-1,4-diol) (5). In a drybox, $Ni(COD)_2$ (100 mg, 0.363 mmol) and Xantphos (210.4 mg, 0.363 mmol) were weighed into a 20 mL scintillation vial equipped with a

Teflon coated stirbar and subsequently dissolved in 10 mL of THF. A solution of 2-butyne-1,4-diol (129.4 mg, 0.726 mmol) in 2 mL THF was added followed by PhCN (50 μL, 0.486 mmol). The reaction was stirred for 4 h and concentrated to dryness. The solids were extracted with benzene and filtered, leaving a small amount of black residue. The filtrate was concentrated to ~10 mL and transferred to a 20 mL scintillation vial. 10 mL pentane was added and the solution was allowed to sit overnight to afford a yellow solid that was collected by filtration, washed with pentane, and dried under vacuum (116.6 mg, 44%). ^{1}H NMR (400 MHz, C_6D_6): δ 7.65 (s, 7H), 7.15 (d, J = 4.0 Hz, 3H), 7.03 (dd, J = 4.0 Hz, J = 8.0 Hz, 2H), 6.97 (br s, 11H), 6.71 (m, 3H), 4.09 (s, 4H), 3.05 (s, 2H), 1.27 (s, 6H). ^{13}C{^{1}H} (100.6 MHz, C_6D_6): δ 158.6 (t, J_{PC} = 5Hz, *Ar*), 137.7 (m, *Ar*), 136.3 (s, *C C*), 134.4 (t, J_{PC} = 7 Hz, *Ar*), 132.6 (s, *Ar*), 129.8 (s, *Ar*), 129.2 (s, *Ar*), 129.0 (t, J_{PC} = 5 Hz, *Ar*), 126.4 (s, *Ar*), 125.8 (m, *Ar*) 124.4 (s, *Ar*), 59.4 (t, J_{PC} = 9 Hz, *C*H_2OH), 37.4 (s, *C*$(CH_3)_2$), 27.4 (s, *C*H_3). ^{31}P{^{1}H} NMR (121 MHz, C_6D_6): δ 21.4 (s). IR (nujol, NaCl): 3280 (br, OH) 1799 (m, ν_{CC}) 1585 (w) 1478 (m) 1434 (s) 1405 (s) 1306 (w) 1225 (m) 1182 (w) 1150 (w) 1120 (w) 1093 (m) 1067 (w) 999 (m) 876 (w) 794 (w) cm^{-1}. Anal. Calcd. for $C_{43}H_{38}NiO_3P_2$: C, 71.39; H, 5.29. Found: C, 71.30; H, 5.47.

Complex 1 by reduction. In a drybox, (Xant)$NiBr_2$[5] (159.4 mg, 0.2 mmol, 1 eq) was suspended in THF (2 mL). 3-hexyne (45 μL, 0.4 mmol, 2 eq) was added, followed by a suspension of Zn (19.6 mg, 0.3 mmol, 1.5 eq) in THF (2 mL). The green suspension began turning yellow within 20 min, and was stirred overnight. Pentane (8 mL) was added and the reaction mixture stirred for an additional hour then filtered through celite. The filtrate was concentrated to dryness, taken up in benzene (4 mL), and pentane (16 mL) was added. The solution was stored at -40 ºC for 24 h. A yellow-brown solid (46.8 mg) was isolated by filtration. This material was silent by ^{31}P NMR. The ^{1}H NMR displayed peaks corresponding to THF and several weak, broad peaks.

Reaction of (Xant)$_2$Ni. (Xant)$_2$Ni (52 mg, 0.0428 mmol), triphenylphosphine oxide (6.0 mg, 0.021 mmol), and benzene (6 mL) were added to a 20 mL vial and stirred for 1 h (Figure 2.3). The residual solids were allowed to settle and the supernatant was filtered through a glass pipette fitted with a fiberglass filter. 3-hexyne, diphenylacetylene, and trans-stilbene (0.032 mmol) were added to three separate vials. Aliquots of 1.5 mL of the (Xant)$_2$Ni/TPPO solution were added to each alkene/alkyne. The resulting solutions

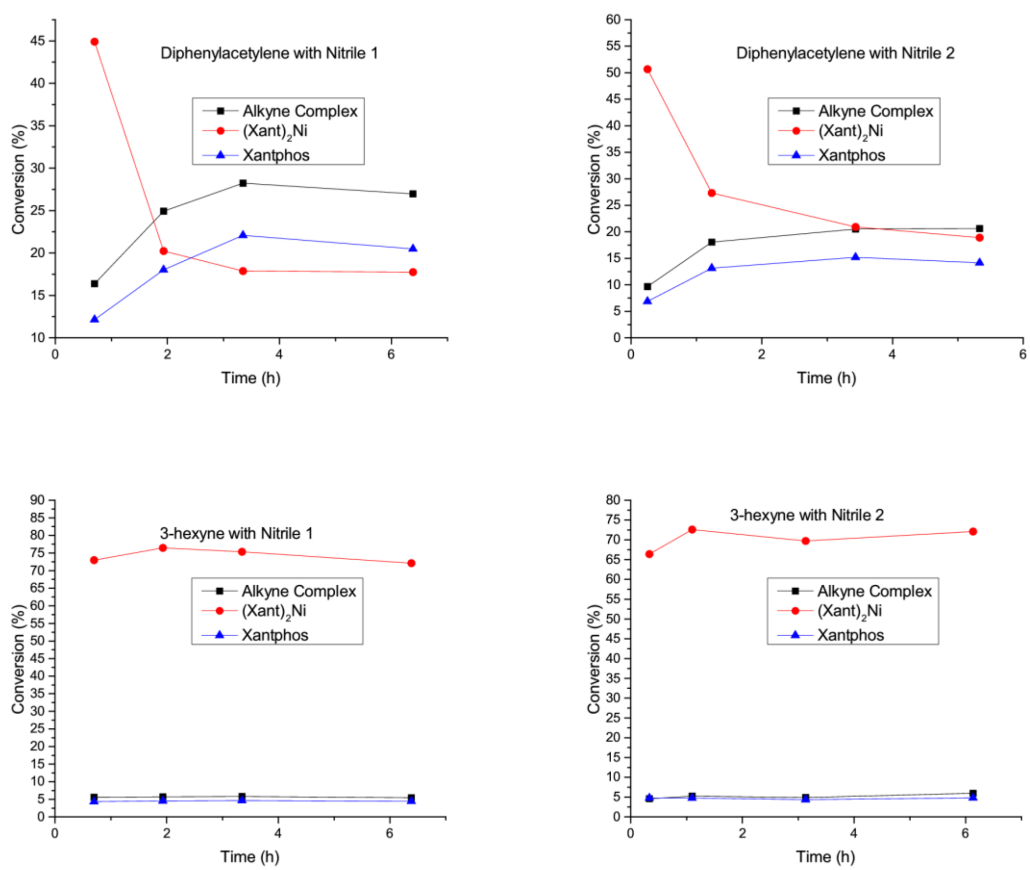

Figure 2.3. Reaction of (Xant)$_2$Ni with alkynes in the presence of benzonitrile.

were divided into two 0.75 mL portions and benzonitrile (3 μL, 0.03 mmol) was added to one of these portions. The solutions were transferred to NMR tubes, sealed with septa, and monitored by ^{31}P NMR. A spectrum of the (Xant)$_2$Ni/TPPO solution was obtained as a T_0.

(Xant)$_2$Ni (26 mg, 0.021 mmol) and TPPO (6.2 mg, 0.022 mmol) were weighed out into a vial. Benzene (3 mL) was added and the solution was stirred for 1 h, and filtered. An aliquot (1.5 mL) was added to diphenylacetylene (7.2 mg, 0.04 mmol). Half (0.75 mL) of this solution was added to N-methyl-2-Pyrrolidone (NMP) (3 μL, 0.03 mmol). The solutions were stirred for 3 h, transferred to septum-sealed NMR tubes and analyzed by ^{31}P NMR. Only trace alkyne complex and free Xantphos were observed in the tube containing NMP. The tube was brought back into the glovebox and NMP (25 μL) was added. The tube was allowed to sit overnight and the solution again analyzed by ^{31}P NMR, at which point an 8% yield of alkyne complex was observed.

Reactions of Ni(COD)$_2$, Xantphos, diphenylacetylene, and benzonitrile. The following stock solutions were prepared: Ni(COD)$_2$ (11.6 mg, 0.042 mmol) in benzene (2 mL); Xantphos (24.3 mg, 0.042 mmol), and triphenylphosphine oxide (5.8 mg, 0.021 mmol) in benzene (2 mL); and diphenylacetylene (37.4 mg, 0.210 mmol) in benzene (2 mL). A ^{31}P NMR of the Xantphos/TPPO solution was taken as a T_0.

(Xant)$_2$Ni correction. A solution of Xantphos (12.2 mg, 0.021 mmol) and triphenylphosphine oxide (2.9 mg, 0.0105 mmol) in 1.5 mL C_6H_6 was prepared. A 0.75 mL aliquot of this solution was added to Ni(COD)$_2$ (1.4 mg, 0.00525 mmol). ^{31}P NMR spectra of each solution were taken to obtain a correction factor of 2.15.

Alkyne complex correction. Experiments A, B, and C were run in parallel. The average integration of alkyne complex from experiments in which alkyne complex was produced quantitatively (B, C) was used as a T_0 for alkyne complex.

Ni(COD)$_2$, then Xantphos, then alkyne, then nitrile. (Figure 2.4) An aliquot of the Xantphos solution (0.5 mL, 1 eq) was added to an aliquot of the Ni(COD)$_2$ solution(0.5 mL, 1 eq). The resulting solution was allowed to sit for 2 min at which point an aliquot of the alkyne solution (0.5 mL, 5 eq) was added. Half (0.75 mL) of this solution was transferred to a NMR tube and sealed with a septum. Benzonitrile (3 μL, 5 eq) was added to the remainder and it was transferred to a NMR tube and sealed with a septum. The solutions were monitored by ^{31}P NMR.

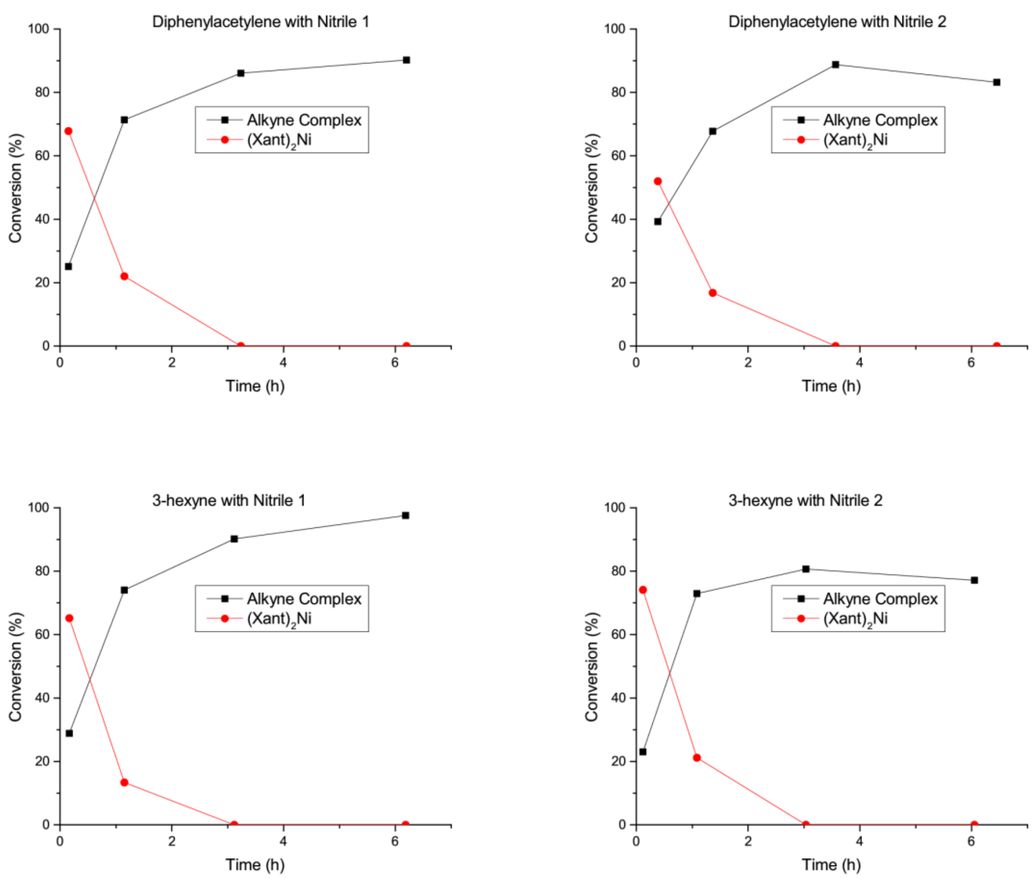

Figure 2.4. Reactions of Ni(COD)$_2$, Xantphos, and alkyne in the presence of nitrile.

Ni(COD)$_2$, then alkyne, then Xantphos, then nitrile. To an aliquot of the alkyne solution (0.5 mL, 5 eq) was added an aliquot of the Ni(COD)$_2$ solution (0.5 mL, 1 eq). The resulting solution was allowed to sit for 5 min, at which point an aliquot of the Xantphos solution (0.5 mL, 1 eq) was added. Half (0.75 mL) of this solution was transferred to a NMR tube and sealed with a septum. Benzonitrile (3 μL, 5 eq) was added to the remainder and it was transferred to a NMR tube and sealed with a septum. The solutions were monitored by ^{31}P NMR, and alkyne complex with no (Xant)$_2$Ni was observed.

Xantphos and alkyne, then Ni(COD)$_2$ and nitrile. To an aliquot of the Xantphos solution (0.5 mL, 1 eq) was added an aliquot of the alkyne solution (0.5 mL, 5 eq), followed by an aliquot of the Ni(COD)$_2$ solution (0.5 mL, 1 eq). Half (0.75 mL) of this solution was transferred to a NMR tube and sealed with a septum. Benzonitrile (3 μL, 5 eq) was added to the remainder and it was transferred to a NMR tube and sealed with a septum. The solutions were monitored by ^{31}P NMR, and alkyne complex with no (Xant)$_2$Ni was observed.

Cycloaddition. A stock solution containing dimethyl 2,2-di(but-2-yn-1-yl)malonate (diyne) (236.3 mg, 1.0 mmol, 1 eq) acetonitrile (78.3 μL, 1.5 mmol, 1.5 eq) and naphthalene (64.1 mg, 0.5 mmol, 0.5 eq) in 10 mL toluene (0.1 M in diyne) was prepared. Complexes **1-5**, (0.003 mmol, 3 mol%) were weighed into separate vials. (Xant)$_2$Ni (0.003 mmol, 3 mol%) were weighed into two separate vials. Benzonitrile (1 μL, 10 mol%) was added to one of the vials containing (Xant)$_2$Ni. Aliquots (1 mL, 0.1 mmol diyne) of the stock solution were added to each vial. The vials were stirred at room temperature for 3 h, filtered, and subjected to GC analysis. Conversions and yields were calculated based on a GC of the stock solution.

Cycloaddition with (Xant)$_2$Ni after exposure to atmosphere. Dimethyl 2,2-di(but-2-yn-1-yl)malonate (diyne) (35.4 mg, 0.15 mmol, 1 eq) acetonitrile (12 µL, 0.225 mmol, 1.5 eq) and trimethoxybenzene (1.8 mg, 0.01 mmol, 0.1 eq) in 1.5 mL toluene-d_8 (0.1 M in diyne) was prepared. An aliquot (0.75 mL) of this solution was added to (Xant)$_2$Ni (2.8 mg, 0.00225 mmol, 3 mol%) that had been exposed to atmosphere for nearly 3 years (*vide infra*) and stirred for 3 h. The remainder of the stock solution was analyzed by Q^{1}H NMR as a T$_0$. The reaction mixture could not be analyzed by ^{1}H NMR due to paramagnetic contaminants in the (Xant)$_2$Ni. This solution was exposed to atmosphere, and filtered through a small amount of silica in a pipette, eluting with EtOAc until just before the orange band from the catalyst came off. The collected liquids were concentrated on the rotovap, redissolved in toluene-d_8, and analyzed by Q^{1}H NMR, revealing 62% conversion and 50% yield.

Cross coupling. Stock solution 1, containing 1-bromonaphthalene (370.7 µL, 2.66 mmol), and naphthalene (128.0 mg, 1 mmol) in THF (2 mL, 1.33 M in aryl halide) was prepared. Stock solution 2 containing 1.0 M vinyl zinc bromide was prepared according to the literature procedure.[4] Complexes **1-5**, (0.010 mmol, 5 mol%) were weighed into separate vials. (Xant)$_2$Ni (0.003 mmol, 3 mol%) were weighed into two separate vials. Benzonitrile (1 µL, 10 mol%) was added to one of the vials containing (Xant)$_2$Ni. Stock solution 1 (150 µL, 0.2 mmol, 1 eq aryl halide) was added to each vial followed by stock solution 2 (350 µL, 0.35 mmol, 1.75 eq). The solutions were stirred at 50 ºC for 5 h. The solutions were diluted with 1 mL EtOAc, filtered, and subjected to GC analysis. Conversions and yields were calculated based on a GC of the stock solution.

Solid state air stability. Several samples ~10 mg for complex **1** and ~5 mg for

$(Xant)_2Ni$ were weighed into vials. The vials were removed from the glovebox. After ~5 min ~15 min, ~30 min, ~60 min for complex **1** and $(Xant)_2Ni$, as well as 2 h, 4 h, and 18 h for $(Xant)_2Ni$ the vials were flushed with nitrogen through a 16 G needle, capped, and brought back into the glovebox. C_6D_6 (0.5 mL) was added to the complex **1** vials and the solutions analyzed by ^{31}P and ^{1}H NMR. Benzene (0.75 mL) was added to the $(Xant)_2Ni$ vials. After 1 h, the solids were filtered off and the solutions analyzed by ^{31}P NMR. The sample of $(Xant)_2Ni$ (~100 mg) was removed from the box in a vial on 10/24/14, stored uncapped on the bench, and brought back in on 7/20/17 for evaluation as a cycloaddition catalyst (*vide supra*).

Solution air stability. A solution containing complex **1** (16.8 mg, 0.023 mmol) and TPPO (8.2 mg, 0.029 mmol) in C_6D_6 (0.75 mL, 0.03 M in **1**) was made and transferred to a septum-sealed vial. A ^{31}P spectrum was obtained as a T_0. The cap was removed, and air introduced by inserting a needle/syringe into the tube and manipulating the plunger, followed by capping the tube and shaking. Spectra were recorded after 5, 10, and 20 min. The experiment was repeated using a solution of $(Xant)_2Ni$ and TPPO prepared as described above.

Crystal data and structure refinement data for **1**, **2**, and **3** can be found in Table 2.3, Table 2.4, and Table 2.5, respectively.

.

Table 2.3. Crystal data and structure refinement for (Xant)Ni(3-Hexyne).

Identification code	jl054 CCDC# 1026030	
Empirical formula	C45 H42 Ni O P2	
Formula weight	719.44	
Temperature	150(1) K	
Wavelength	0.71073 Å	
Crystal system	Monoclinic	
Space group	$\boldsymbol{P}\ 2_1/n$	
Unit cell dimensions	a = 13.6794(3) Å	α= 90°.
	b = 15.0260(3) Å	β= 93.2001(14)°.
	c = 17.7954(4) Å	γ = 90°.
Volume	3652.08(14) $Å^3$	
Z	4	
Density (calculated)	1.308 Mg/m^3	
Absorption coefficient	0.653 mm^{-1}	
F(000)	1512	
Crystal size	0.23 x 0.23 x 0.15 mm^3	
Theta range for data collection	1.93 to 27.00°.	
Index ranges	-17<=h<=16, -19<=k<=18, -22<=l<=22	
Reflections collected	29344	
Independent reflections	7946 [R(int) = 0.0653]	
Completeness to theta = 27.00°	99.7 %	
Absorption correction	Multi-scan	
Max. and min. transmission	0.9083 and 0.8642	
Refinement method	Full-matrix least-squares on F^2	
Data / restraints / parameters	7946 / 0 / 442	
Goodness-of-fit on F^2	1.044	
Final R indices [I>2sigma(I)]	R1 = 0.0423, wR2 = 0.0713	
R indices (all data)	R1 = 0.0826, wR2 = 0.0843	
Largest diff. peak and hole	0.500 and -0.405 e.$Å^{-3}$	

Table 2.4. Crystal data and structure refinement for (Xantphos)Ni(diphenylacetylene).

Identification code	jl070 CCDC# 1026032	
Empirical formula	C59 H48 Ni O P2	
Formula weight	893.62	
Temperature	150(1) K	
Wavelength	0.71073 Å	
Crystal system	Monoclinic	
Space group	$\boldsymbol{P}\ 2_1/n$	
Unit cell dimensions	a = 12.8793(3) Å	α= 90°.
	b = 18.2497(3) Å	β= 98.8516(10)°.
	c = 19.5980(5) Å	γ = 90°.
Volume	4551.52(17) $Å^3$	
Z	4	
Density (calculated)	1.304 Mg/m^3	
Absorption coefficient	0.539 mm^{-1}	
F(000)	1872	
Crystal size	0.250 x 0.230 x 0.130 mm^3	
Theta range for data collection	2.096 to 27.001°.	
Index ranges	-16<=h<=16, -23<=k<=22, -25<=l<=25	
Reflections collected	60117	
Independent reflections	9871 [R(int) = 0.1244]	
Completeness to theta = 25.242°	99.7 %	
Absorption correction	Multi-scan	
Max. and min. transmission	0.933 and 0.877	
Refinement method	Full-matrix least-squares on F^2	
Data / restraints / parameters	9871 / 0 / 568	
Goodness-of-fit on F^2	1.084	
Final R indices [I>2sigma(I)]	R1 = 0.0516, wR2 = 0.0755	
R indices (all data)	R1 = 0.1186, wR2 = 0.0950	
Extinction coefficient	n/a	
Largest diff. peak and hole	0.366 and -0.433 e.$Å^{-3}$	

Table 2.5. Crystal data and structure refinement for (Xant)Ni(dimethylfumarate).

Identification code	jl069 CCDC# 1026031	
Empirical formula	C48 H43 Ni O5 P2	
Formula weight	820.47	
Temperature	150(1) K	
Wavelength	0.71073 Å	
Crystal system	Triclinic	
Space group	P -1	
Unit cell dimensions	a = 11.8270(2) Å	α= 73.8372(9)°.
	b = 12.1552(2) Å	β= 84.9154(12)°.
	c = 14.8937(3) Å	γ = 76.8383(11)°.
Volume	2001.73(6) $Å^3$	
Z	2	
Density (calculated)	1.361 Mg/m^3	
Absorption coefficient	0.613 mm^{-1}	
F(000)	858	
Crystal size	0.280 x 0.250 x 0.100 mm^3	
Theta range for data collection	2.231 to 27.518°.	
Index ranges	-15<=h<=15, -15<=k<=15, -19<=l<=19	
Reflections collected	17370	
Independent reflections	9192 [R(int) = 0.0291]	
Completeness to theta = 25.242°	99.9 %	
Absorption correction	Multi-scan	
Max. and min. transmission	0.941 and 0.847	
Refinement method	Full-matrix least-squares on F^2	
Data / restraints / parameters	9192 / 0 / 505	
Goodness-of-fit on F^2	1.036	
Final R indices [I>2sigma(I)]	R1 = 0.0414, wR2 = 0.0971	
R indices (all data)	R1 = 0.0665, wR2 = 0.1088	
Extinction coefficient	n/a	
Largest diff. peak and hole	0.539 and -0.650 e.$Å^{-3}$	

References

1. (a) Kamer, P. C. J.; van Leeuwen, P. W. N. M.; Reek, J. N. H. *Acc. Chem. Res.* **2001**, *34*, 895. (b) Birkholz, M.-N.; Freixa, Z.; van Leeuwen, P. W. N. M. *Chem. Soc. Rev.* **2009**, *38*, 1099. (c) Birkholz, M.-N.; van Leeuwen, P. W. N. M. In *Encyclopedia of Reagents for Organic Synthesis*; John Wiley & Sons, Ltd: 2001

2. (a) Goertz, W.; C. J. Kamer, P.; W. N. M. van Leeuwen, P.; Vogt, D. *Chem. Commun.* **1997**, 1521. (b) Goertz, W.; Kamer, P. C. J.; van Leeuwen, P. W. N. M.; Vogt, D. *Chemistry – A European Journal* **2001**, *7*, 1614. (c) Kranenburg, M.; Kamer, P. C. J.; van Leeuwen, P. W. N. M.; Vogt, D.; Keim, W. *J. Chem. Soc., Chem. Commun.* **1995**, 2177. (d) Goertz, W.; Keim, W.; Vogt, D.; Englert, U.; D. K. Boele, M.; A. van der Veen, L.; C. J. Kamer, P.; W. N. M. van Leeuwen, P. *J. Chem. Soc., Dalton Trans.* **1998**, 2981.

3. Hirata, Y.; Tanaka, M.; Yada, A.; Nakao, Y.; Hiyama, T. *Tetrahedron* **2009**, *65*, 5037.

4. Yamamoto, T.; Yamakawa, T. *J. Org. Chem.* **2009**, *74*, 3603.

5. Mora, G.; van Zutphen, S.; Klemps, C.; Ricard, L.; Jean, Y.; Le Floch, P. *Inorg. Chem.* **2007**, *46*, 10365.

6. Kumar, P.; Prescher, S.; Louie, J. *Angew. Chem. Int. Ed.* **2011**, *50*, 10694.

7. Erickson, L. W.; Lucas, E. L.; Tollefson, E. J.; Jarvo, E. R. *J. Am. Chem. Soc.* **2016**, *138*, 14006.

8. (a) Hazari, N.; Melvin, P. R.; Beromi, M. M. **2017**, *1*, 0025. (b) Kurahashi, T.; Matsubara, S. *Acc. Chem. Res.* **2015**, *48*, 1703. (c) Standley, E. A.; Tasker, S. Z.; Jensen, K. L.; Jamison, T. F. *Acc. Chem. Res.* **2015**, *48*, 1503. (d) Thakur, A.; Louie, J. *Acc. Chem. Res.* **2015**, *48*, 2354. (e) Tobisu, M.; Chatani, N. *Acc. Chem. Res.* **2015**, *48*, 1717. (f) Dander, J. E.; Garg, N. K. *ACS Catal.* **2017**, *7*, 1413. (g) Montgomery, J. *Angew. Chem. Int. Ed.* **2004**, *43*, 3890. (h) Tamaru, Y. In *Modern Organonickel Chemistry*; Wiley-VCH Verlag GmbH & Co. KGaA: 2005, p 1. (i) Tasker, S. Z.; Standley, E. A.; Jamison, T. F. *Nature* **2014**, *509*, 299.

9. (a) Clement, N. D.; Cavell, K. J.; Ooi, L.-l. *Organometallics* **2006**, *25*, 4155. (b) Edelbach, B. L.; Lachicotte, R. J.; Jones, W. D. *Organometallics* **1999**, *18*, 4040. (c) Waterman, R.; Hillhouse, G. L. *Organometallics* **2003**, *22*, 5182.

10. (a) Sinnokrot, M. O.; Sherrill, C. D. *J. Phys. Chem. A*, **2004**, *108*, 10200. (b) Hunter, C. A.; Sanders, J. K. M. *J. Am. Chem. Soc.* **1990**, *112*, 5525. (c) Sinnokrot, M. O.; Valeev, E. F.; Sherrill, C. D. *J. Am. Chem. Soc.* **2002**, *124*, 10887.

11. (a) Tolman, C. A. *J. Am. Chem. Soc.* **1974**, *96*, 2780. (b) Tolman, C. A.; Seidel, W.

C. *J. Am. Chem. Soc.* **1974**, *96*, 2774.

12. Montgomery, J. *Science of Synthesis* **2001**, *1*, 11.

CHAPTER 3

SYNTHESIS OF ARYL ALKYL KETENES[*]

Introduction

Ketenes are useful synthetic building blocks due to their propensity to undergo [2 + 2] cycloaddition reactions with several different partners including alkenes[1], aldehydes or ketones[2], and imines[3] to form a cyclobutanones, β-lactones, and β-lactams (Figure 3.1). Nucleophiles can also add to the O=***C***=C carbon.[4] These reactions have been reviewed extensively.[5] Recently, chiral nucleophilic catalysts or chiral auxiliaries have been employed to impart stereoselectivity on these cycloadditions[6] and addition[7] reactions. Furthermore, reports of transition metal catalyzed carbon-carbon bond forming reactions of ketenes are beginning to emerge, including a Ni catalyzed [2 + 2 + 2] cycloaddition reaction of diynes and ketenes, which forms cyclohexadienones,[8] and a Rh catalyzed three component reaction of silyl acetylene and two ketenes, which forms 1,3-enynes bearing carboxylic esters.[9] These reactions are of particular interest as they resist decarbonylation of transition-metal ketene complexes, which forms unreactive metal carbonyl complexes.[10]

Several methodologies exist to generate ketenes: cracking of ketene dimers,[11]

---

[*] Reproduced (adapted) with permission from: Staudaher, N. D.; Lovelace, J.; Johnson, M. P.; Louie, J. *Org. Synth.* **2017**, *94*, 1. Copyright 2017 Organic Syntheses, Inc.

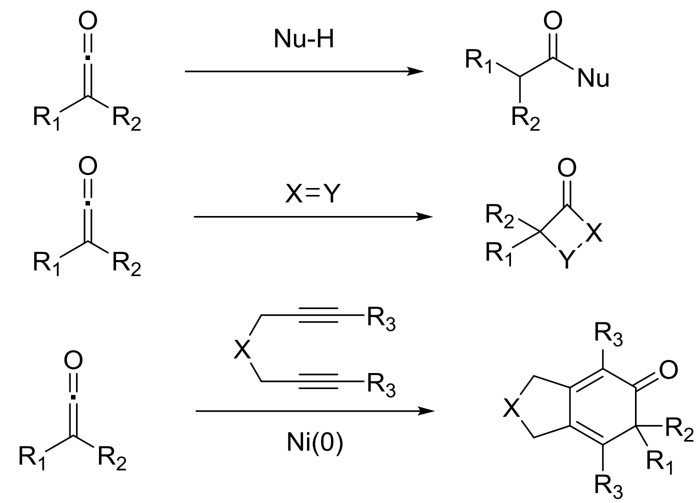

Figure 3.1. Reactions of ketenes.

pyrolysis of anhydrides,[12] Wolff rearrangement of α-diazo ketones,[13] and reduction of α-halo acid halides.[14] These methods require high temperatures, formation and handling of diazo compounds, low substrate scope, and/or extra steps. Trapping of ketenes *in situ*[15] is much more common than isolating reactive ketenes due to their tendency to dimerize, and most of these reactions produce by-products that make isolation difficult. Dehydrohalogenation[16] is therefore the most popular method of synthesizing and isolating ketenes. Some ketenes prepared in this communication have been previously reported,[7,9,17] albeit on smaller scale. These reported preparations lack the detail essential for an *Organic Syntheses* article, and are lower yielding, presumably due to the smaller scale. The synthetic strategy described herein involves three steps (Figure 3.2): alkylation of arylacetic acids, conversion of the carboxylic acid to the acid chloride, and dehydrohalogenation of the acid chloride to furnish the ketene.

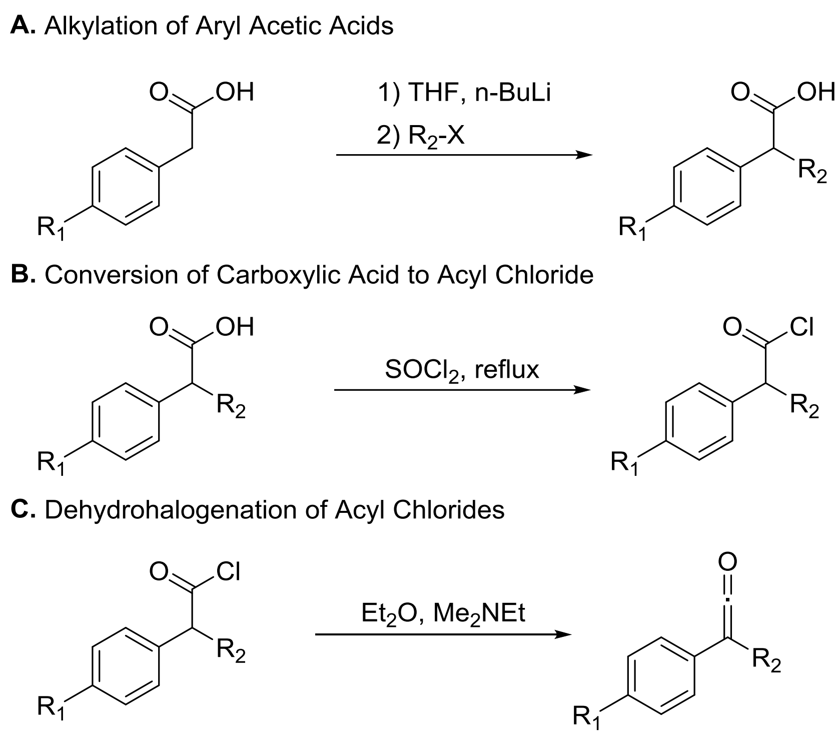

Figure 3.2. Synthetic scheme for ketene formation.

Results and Discussion

The first step, alkylation of aryl acetic acids, was found to be very general (Table 3.1). The double deprotonation proceeds well with 2.2 equivalents of butyl lithium for all substrates. The alkylation step proceeds smoothly with primary alkyl bromides. Secondary bromides reacted sluggishly and did not go to completion within 24 h, and the product was contaminated with significant amounts of aryl acetic acids. Secondary alkyl iodides were therefore employed, which reacted well.

Conversion of the resultant carboxylic acids went smoothly in refluxing excess thionyl chloride, required no optimization for different substrates, and proceeded in roughly 80% yield for all substrates (Table 3.2).

Dehydrohalogenation of the acid chlorides also went smoothly, but required

Table 3.1. Alkylation of aryl acetic acids.

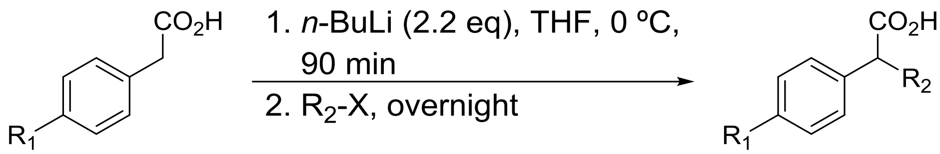

R_1	R_2-X	yield (%)
H	*n*-Bu-Br	99
F	*i*-Bu-Br	93
H	*i*-Bu-Br	97
Me	*i*-Bu-Br	98
OMe	*i*-Bu-Br	94
F	*i*-Pr-I	99
H	*i*-Pr-I	97
Me	*i*-Pr-I	95
OMe	*i*-Pr-I	98
H	*s*-Bu-I	96

Table 3.2. Conversion of carboxylic acids to acyl chlorides.

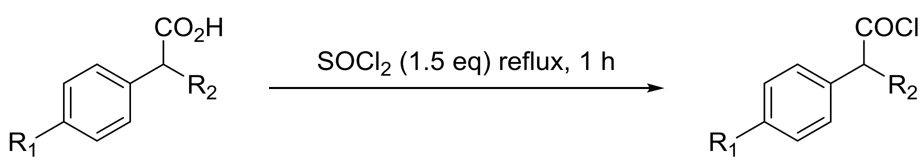

R_1	R_2	yield (%)
H	*n*-Bu	74
F	*i*-Bu	76
H	*i*-Bu	78
Me	*i*-Bu	83
OMe	*i*-Bu	86
F	*i*-Pr	83
H	*i*-Pr	82
Me	*i*-Pr	77
OMe	*i*-Pr	84
H	*s*-Bu	80

significant optimization for each compound (Table 3.3). In general, substrates with electron-rich aromatic rings required longer reaction times due to attenuated acidity of the α-proton of the acyl chloride. Acyl chlorides with secondary alkyl chains required an elevation of reaction temperature from room temperature to 60 ºC, which required a solvent/base change from ether/ethyldimethylamine to THF/triethylamine.

Conclusion

To summarize, ketenes are valuable synthetic building blocks that are most commonly generated and trapped *in situ*. Several groups have prepared them, but their descriptions of the preparations are generally lacking in detail – it took the author of this thesis four months to reliably generate any of the ketenes described in this chapter. Our method involves three straightforward steps from commercially available starting materials. Furthermore, our description of the steps is detailed enough that it can be easily

Table 3.3. Formation of ketenes.

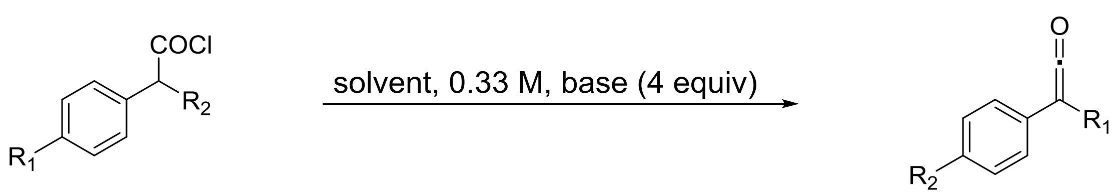

R_1	R_2	temperature	solvent	base	time (h)	yield (%)
H	*n*-Bu	rt	Et_2O	$MeNEt_2$	36	74
F	*i*-Bu	rt	Et_2O	$MeNEt_2$	36	68
H	*i*-Bu	rt	Et_2O	$MeNEt_2$	36	72
Me	*i*-Bu	rt	Et_2O	$MeNEt_2$	72	74
OMe	*i*-Bu	rt	Et_2O	$MeNEt_2$	72	61
F	*i*-Pr	60°	THF	Et_3N	24	74
H	*i*-Pr	60°	THF	Et_3N	48	77
Me	*i*-Pr	60°	THF	Et_3N	72	71
OMe	*i*-Pr	60°	THF	Et_3N	96	78
H	*s*-Bu	60°	THF	Et_3N	48	73

reproduced, as evidenced by its publication in *Organic Syntheses*, which requires reproduction of the synthesis by checkers from an outside laboratory.[18]

Experimental Section

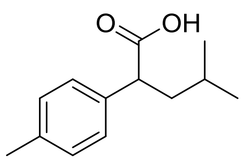

4-methyl-2-(*p*-tolyl)pentanoic acid (1a). An oven dried 1-L, one-necked round bottom flask fitted with a 4 x 2 cm egg-shaped stir bar is cooled under a stream of nitrogen. *P*-tolylacetic acid (Note 1) (17.06 g, 114 mmol, 1 equiv) is added and the flask is sealed with a rubber septum. THF (Note 2) (~700 mL) is added by cannula and the flask is placed under nitrogen through an 18 G needle. The solution is cooled to 0 °C and stirred vigorously (Note 3). *N*-Butyl Lithium (2.5 M in hexane, 100 mL, 250 mmol, 2.2 equiv) is added dropwise by cannula (Note 4) (Figure 3.3). The reaction is maintained at 0 °C for 90 min, at which point isobutyl bromide (16.0 mL, 148 mmol, 1.3 equiv) (Note 5) is added in a steady stream by syringe, causing the reaction to turn yellow. The reaction is allowed to warm to room temperature slowly (Note 6) and stirred overnight (ca. 18 h). The completion of the reaction is checked by TLC (Note 7). The reaction is quenched by the addition of water (150 mL), which causes the reaction to turn from a white to yellow suspension to clear and biphasic. The volatiles are removed by rotary evaporation (35 ºC, 4 mmHg). The solution is then acidified to pH 1 (Note 8) by addition of concentrated HCl (~15 mL). The aqueous layer is extracted with diethyl ether (4 x 150 mL). The combined organics are dried over $MgSO_4$, filtered, and concentrated by rotary evaporation (30 ºC, 4 mmHg) and then under high vacuum with stirring (2000-200 mTorr) over 12 h to yield the product as a white solid (22.97 g, 98%) (Note 9).

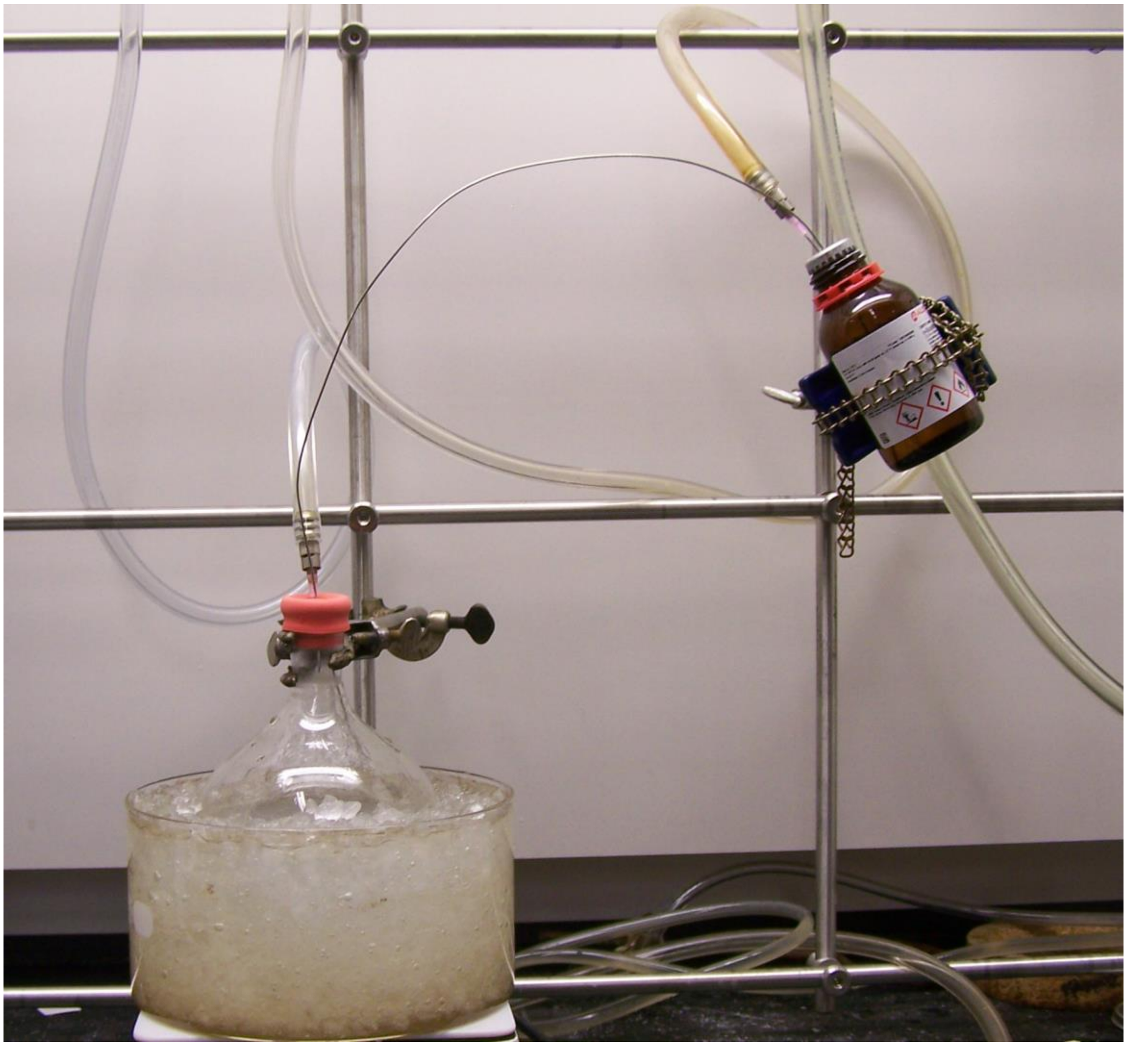

Figure 3.3. Addition of *n*BuLi to *p*-tolylacetic acid in THF.

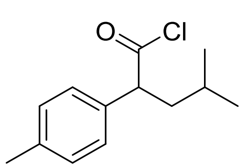

4-methyl-2-(*p*-tolyl)pentanoyl chloride (2a). An oven dried 50-mL round bottom flask with a 14/20 ground glass joint is fitted with a 1.6 x 0.7 cm egg-shaped magnetic stir bar and Liebig condenser and cooled under nitrogen. The condenser and nitrogen inlet are removed and the flask is charged with **1a** (12.00 g, 58 mmol, 1 equiv) and thionyl chloride (6.3 mL, 87 mmol, 1.5 equiv) (Note 10). The condenser and nitrogen inlet are replaced, and the flask is placed in a pre-heated thermostated oil bath set at 90 °C for 1 h. The reaction turns brown and considerable gas evolution is observed during the first 30 min of this period. The reaction is cooled to room temperature, and K_2CO_3 (~4 g) (Note 11) is added. The mixture is stirred until gas evolution ceases (~15 min), and placed on a rotary evaporator (40 ºC, 4 mmHg) for 1 h (Note 12). The flask is then fitted with a 100 mL kugelrohr bulb and the product is distilled with a kugelrohr, collecting a single fraction (200 mTorr, 130 °C, 50 rpm), at -78 °C to yield 2 (10.79 g, 82%) (Note 13).

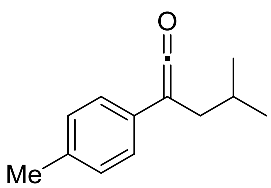

4-methyl-2-(*p*-tolyl)pent-1-en-1-one, phenyl isobutyl ketene (3a). All glassware is oven dried. A 300-mL schlenk tube with a 2.5 cm wide valve and 24/40 joint is fitted with a 3.2 x 1.6 cm egg-shaped stir bar and suba seal rubber septum (Note 14). The flask is purged (~400 mTorr) and backfilled with dry nitrogen through an 18 G needle three times as it is allowed to cool to room temperature. **2a** is then added via syringe (10.8 g, 48 mmol, 1 equiv), followed by diethyl ether (150 mL) via syringe. The solution is stirred (Note 15) and ethyl dimethyl amine (20.7 mL, 192 mmol, 4 equiv) (Note 16) is added via syringe, and the reaction begins to turn yellow and a white precipitate begins to form (Figure 3.4, left). The valve is closed and the reaction is stirred for 72 h. The reaction is then filtered as follows (Figure 3.4, right): a 1-neck (24/40) 500 mL round bottom flask with a sidearm with a ground-glass stopcock (stopcock A) is placed under a stream of argon through tube A, and fitted with a 100-mL schlenk filter with a sidearm with a ground-glass stopcock (stopcock B) and 14/20 female ground glass joint. A second tube (tube B) is connected to the schlenk line and to the filter's sidearm. The septum is removed from the reaction vessel and the vessel placed on top of the filtration apparatus. The filter apparatus is then purged (~500 mTorr) and backfilled with argon three times. The lower stopcock (tube A) is closed, and tube A placed

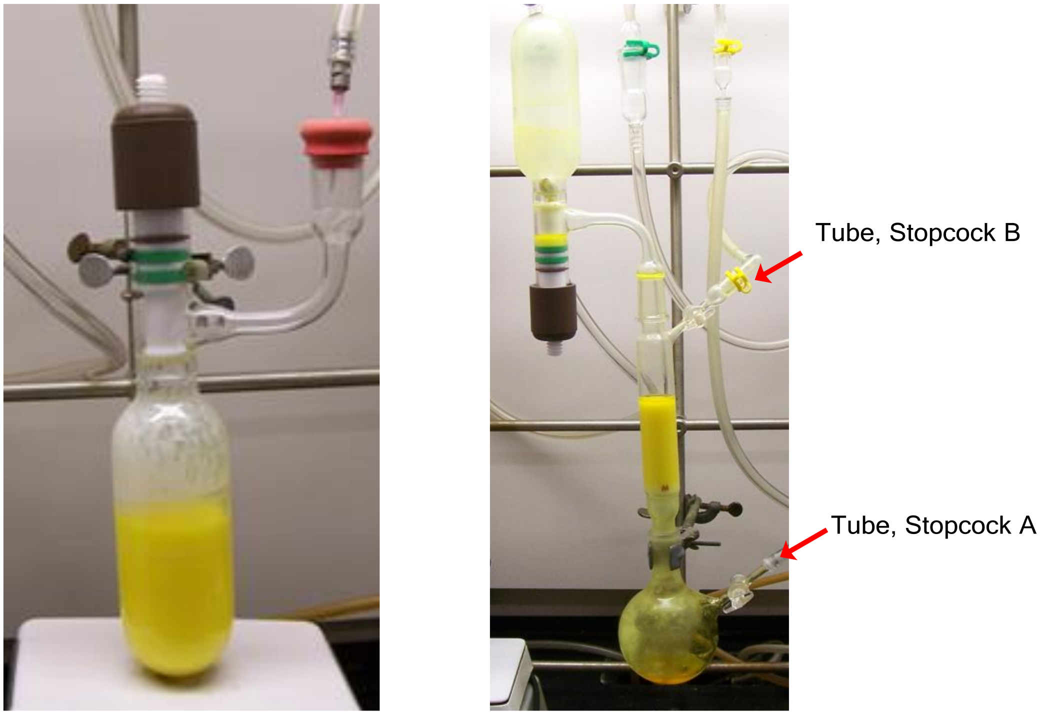

Figure 3.4. Reaction vessel and filtration assembly for step C.

under vacuum. The reaction vessel's valve is then opened slowly. When ~3 cm of reaction mixture has collected above the frit, vacuum is gently applied to the flask by quickly opening and closing stopcock A. If the level of reaction mixture approaches stopcock B, the schlenk flask's valve is closed temporarily to prevent the reaction mixture from entering tube B. When all of the liquids have entered the collection flask, stopcock B is closed, and the solvent and excess amine are removed under high vacuum. A warm water bath (~30 °C) is used to expedite the concentration, which takes ~30 min. Stopcock A is closed, and the apparatus backfilled with argon through stopcock B. Tube A is backfilled with argon and removed from the apparatus, a 14/20 suba-seal rubber septum is placed over the end of the sidearm, and tube A is fitted with a luer-lock connector and a 1.5” 18 G needle. A 50-mL round bottom flask with a 14/20 ground glass joint is fitted with a suba-seal rubber septum, which is pierced with the needle on tube A. A cannula is placed between the 50-

mL flask and the septum on sidearm A (Figure 3.5). The flask, cannula, and end of the sidearm are purged (~600 mTorr) and backfilled with argon three times. Stopcock A is then opened and the crude ketene is transferred to the round bottom flask. The flask is backfilled with argon and the cannula removed. The kugelrohr is placed under a stream of argon, and fitted with a 100-mL kugelrohr bulb, which is allowed to cool. The septum is removed from the 50-mL flask and the flask is immediately placed on the kugelrohr bulb (Figure 3.5). The distillation apparatus is then purged (~500 mTorr) and backfilled with argon three times. The ketene is then distilled in one fraction (150 mTorr, 120 °C, 50 rpm), collecting at -78 °C. Upon the distillation's completion, the apparatus is placed under argon and the ketene is allowed to warm to room temperature. Tube B is fitted with a 6" Pasteur pipette. A vial is allowed to cool under a stream of argon through the pipette on tube B. The vial is quickly capped, tared, and placed back under the argon stream. When the ketene has warmed to room temperature, any water that has condensed on the bulb is removed with a paper towel. A heavy stream of argon is then established through the manifold, and opened to tube A. In rapid succession: The kugelrohr bulb is removed and placed under argon through tube A, which has a 14/20 inlet adapter. The still pot is removed and placed on the kugelrohr (in order to ensure heavy argon flow through tubes A and B), and the ketene is poured into the vial. The argon flow to tube A is stopped, raising the flow of argon to the vial, which is capped and massed again. **3** is a yellow liquid, 6.72 g, 74% (Note 17).

1. Unless otherwise noted, all chemicals were purchased from Sigma-Aldrich (reagent grade) and used without further purification. *P*-tolylacetic acid (99%) was purchased from Acros.
2. THF (Fisher, HPLC grade, 99.9%) and ether (Fisher, ACS, 99.9%) used as reaction

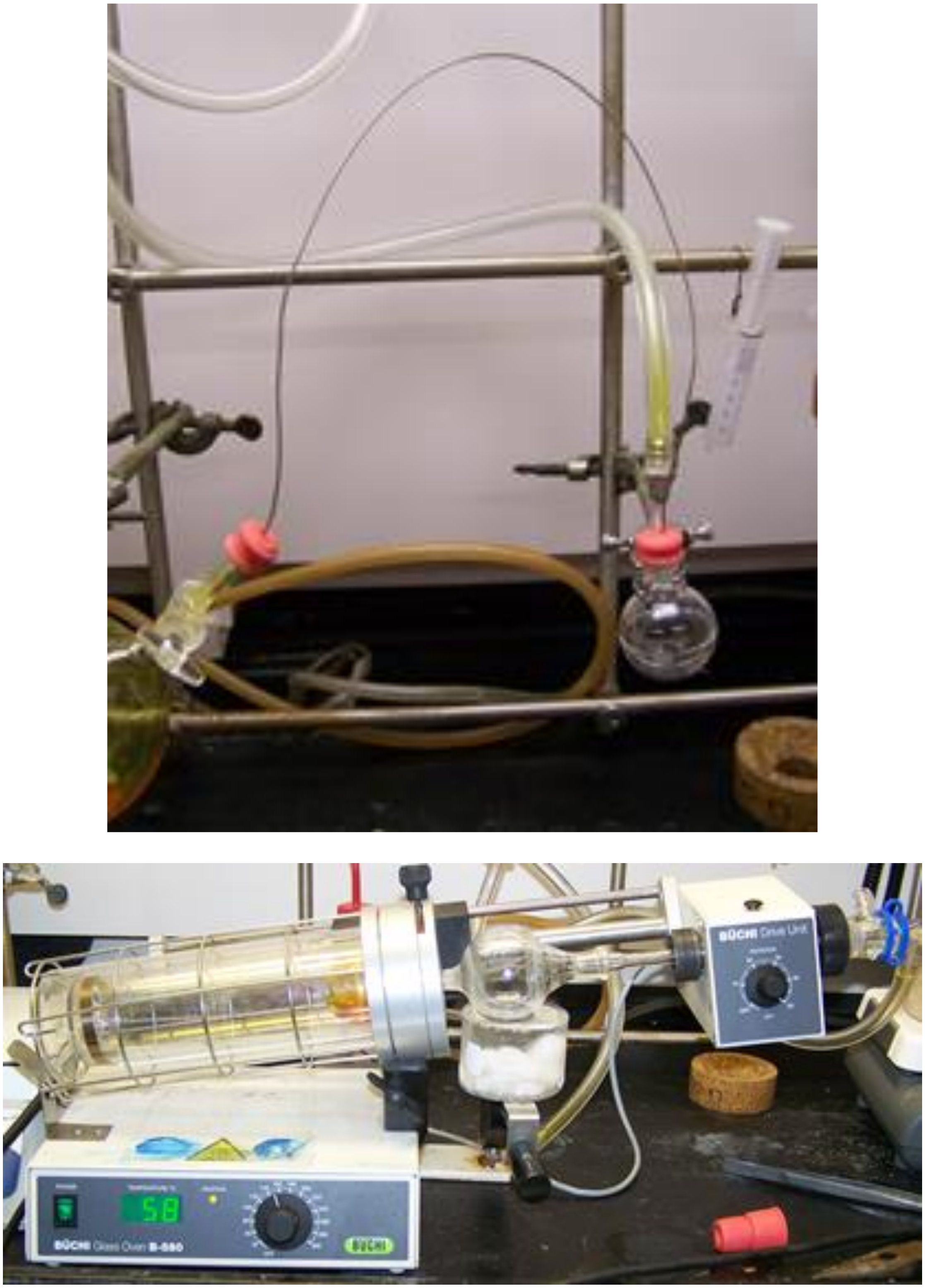

Figure 3.5. Transfer of ketene to RBF and distillation apparatus.

solvents were purchased from Fisher, sparged with dry nitrogen, and subsequently passed over columns of activated alumina and Q5 catalyst.

3. The reaction is stirred at 900-1000 RPM. The monoanion of *p*-tolylacetic acid is highly insoluble and a thick white slurry forms over the first half of the addition and dissipates over the second half.

4. An entire fresh 100 mL bottle of *n*-butyl lithium is added over a period of approximately 20 min.

5. Reagent grade isobutyl bromide (99%) was purchased from sigma-aldrich and used as received.

6. It is important to leave the reaction vessel in the ice bath. If the ice bath is removed, butane is evolved vigorously.

7. A 0.5 mL aliquot of the reaction is added to a mixture of 1 mL water, 1 mL EtOAc, and 5 drops concentrated hydrochloric acid. A TLC is taken of the organic layer, *p*-tolylacetic acid, and a co-spot of starting material and the reaction mixture. Aluminum backed Silica gel 60 F254 plates were purchased from EMD Chemicals Inc. and the plate was visualized under 254 nm UV light.

8. pH was determined by EMD Millipore colorpHast® pH Test Strips.

9. This compounds displays the following physiochemical properties: R_f = 0.43 (30% ethyl acetate / 70% hexanes), mp 61-63 ºC, ^{1}H NMR (400 MHz, $CDCl_3$) δ: 7.21 (d, *J* = 8 Hz, 2 H), 7.13 (d, *J* = 8 Hz, 2 H), 3.62 (t, *J* = 6 Hz, 1 H), 2.32 (s, 3 H), 1.92 (m, 1 H), 1.66 (m, 1 H), 1.48 (m, 1 H), 0.90 (d, *J* = 4 Hz, 6 H); ^{13}C{^{1}H} NMR (100.6 MHz, $CDCl_3$) δ: 180.8, 137.4, 135.9, 129.7, 128.3, 49.4, 42.3, 26.0, 23.0, 22.5, 21.4; IR (NaCl): 2958, 1704, 1512, 1465, 1438, 1414, 1386, 1252, 1214,

1189, 1121, 1044, 943, 835, 790, 727, 693, 671, 636; HRMS (ESI) [M + Na]+ calcd for $C_{13}H_{18}O_2$ 229.1204, found; 229.1210; Anal. Calcd. for $C_{13}H_{18}O_2$: C, 75.69; H, 8.80. Found: C, 75.54; H, 8.92.

10. Thionyl chloride (ReagentPlus, 99.5%, low iron) was purchased from Sigma Aldrich and used as received.

11. Anhydrous Potassium carbonate (Reagent grade, 100.6% assay) was purchased from JT Baker.

12. It is imperative to apply vacuum slowly to prevent bumping both on the rotovap and the kugelrohr.

13. This compound should be used immediately as it is water reactive. It displays the following spectroscopic properties: ^{1}H NMR (400 MHz, $CDCl_3$) δ: 7.18 (s, br, 4 H), 4.03 (t, *J* = 8 Hz, 1 H), 2.35 (s, 3 H), 2.02 (m, 1 H), 1.74 (m, 1 H), 0.92 (dd, *J* = 4, 8 Hz, 6 H); $^{13}C\{^{1}H\}$ NMR (100.6 MHz, $CDCl_3$) δ: 175.5, 138.4, 133.4, 130.1, 128.6, 61.6, 42.3, 25.9, 23.0, 22.3, 21.5; IR (NaCl): 2960, 2871, 1789, 1514, 1468, 1387, 1370, 1255, 1127, 1039, 983, 875, 841, 820, 752, 729, 703; HRMS (EI) [M+] calcd for $C_{13}H_{17}ClO$: 224.0968. Found: 224.0972 (HRMS was collected by the checkers of the *Organic Syntheses* article, Sheng Guo and Daiwei Ma. The compound did not ionize by ESI.); Anal. Calcd. for $C_{13}H_{17}ClO$: C, 69.48; H, 7.62. Found: C, 69.08; H, 7.54.

14. Sigma Aldrich SKU Z124656 for 24/40 joints, Z124591 for 14/20 joints.

15. The reaction is stirred between 700-900 RPM to maintain the amine hydrochloride salt in suspension.

16. Ethyl dimethyl amine and triethylamine were distilled from CaH_2 (90-95%, Alfa-

Aesar, 2mm mesh and down) and stored in bottles over KOH in a desiccator with drierite. These compounds are stable for at least 7 months stored in this fashion.

17. This compound displays the following physiochemical properties: ^{1}H NMR (400 MHz, C_6D_6) δ: 6.94 (d, *J* = 8 Hz, 2 H), 6.86 (d, *J* = 8 Hz, 2 H), 2.10 (s, 3 H), 1.96 (d, *J* = 8 Hz, 2 H), 1.61 (sept, *J* = 7 Hz, 1 H), 0.79 (d, *J* = 8 Hz, 6 H); ^{13}C{^{1}H} NMR (100.6 MHz, C_6D_6) δ: 206.8 (O=***C***=C), 134.5, 130.6, 130.2, 125.3, 38.3 (O=C=***C***), 34.0, 28.0, 22.9, 21.5; IR (NaCl): 2093 (s, CO), 2041 (m), 1885 (w), 1611 (m), 1569 (m), 1513 (s), 1466 (s), 1416 (m), 1384 (s), 1338 (m), 1314 (m), 1278 (s), 1243 (s), 1169 (m), 1125 (s), 1100 (s), 1041 (w), 1020 (m), 1006 (m), 935 (w), 872 (w), 809 (s), 717 (w), 632 (w); HRMS (GC-TOF) [M+] calcd for $C_{12}H_{14}O$ 188.1201, found 188.1205; Anal. Calcd. for $C_{12}H_{14}O$: C, 82.94; H, 8.57. Found: C, 83.33; H, 8.62. Ketenes are sensitive to water, heat, and light. However, we have found the ketenes described in this paper to be stable indefinitely in our nitrogen filled glovebox at -40 °C.

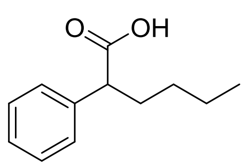

2-Phenylhexanoic acid, 1b. was synthesized according to procedure A using phenylacetic acid (15.52 g, 114 mmol, 1 eq), and *n*-butyl bromide (16 mL, 148 mmol, 1.3 eq). The yield is 21.70 g, 99% as a yellow oil. (R_f = 0.61 with 3:7 EtOAc/Hexanes; ^{1}H NMR (400 MHz, $CDCl_3$) δ: 7.34-7.26 (m, 5 H), 3.55 (t, *J* = 8 Hz, 1 H), 2.10 (m, 1 H), 1.82 (m, 2 H), 1.34-1.21 (m, 4 H), 0.88 (t, *J* = 8 Hz, 3 H); ^{13}C{^{1}H} NMR (100.6 MHz, $CDCl_3$) δ: 180.6, 139.0, 129.0, 128.4, 127.7, 51.9, 33.1, 30.0, 22.8, 14.2; IR (NaCl): 2958, 1707, 1602, 1496, 1456, 1415, 1290, 1109, 1072, 1031, 940, 757, 727, 699; HRMS (ESI-TOF) $[M + Na]^{+}$ calcd for $C_{12}H_{16}O_2$ 215.1048, found; 215.1052; Anal. Calcd. for $C_{12}H_{16}O_2$: C, 74.94; H, 8.39. Found: C, 74.83;

H, 8.48.

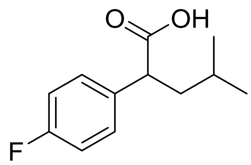

2-(4-fluorophenyl)-4-methylpentanoic acid, 1c. was synthesized according to procedure A using *p*-fluorophenylacetic acid (17.57 g, 114 mmol, 1 eq), and *i*-butyl bromide (15.5 mL, 148 mmol, 1.3 eq). The yield is 22.29 g, 93% as a white solid. R_f = 0.42 with 3:7 EtOAc/Hexanes; mp 64-72 ºC; ^{1}H NMR (400 MHz, $CDCl_3$) δ: 7.20 (m, 2 H), 6.92 (dd, *J* = 8, 8 Hz, 2 H), 3.56 (t, *J* = 8 Hz, 1 H), 1.85 (m, 1 H), 1.58 (m, 1 H), 1.38 (m, 1 H), 0.82 (dd, *J* = 4, 8 Hz, 6 H); $^{13}C\{^1H\}$ NMR (100.6 MHz, $CDCl_3$) δ: 180.6, 162.5 (d, *J* = 246.4 Hz), 134.6 (d, *J* = 4.0 Hz), 130.0 (d, *J* = 8.0 Hz), 115.8 (d, *J* = 21.1 Hz), 49.0, 42.4, 26.0, 22.9, 22.4; IR (NaCl): 2959, 1708, 1605, 1510, 1468, 1410, 1387, 1369, 1286, 1228, 1160, 1123, 1093, 1016, 931, 838, 725; HRMS (ESI-TOF) $[M - H]^-$ calcd for $C_{12}H_{15}FO_2$ 209.0978, found; 209.0988; Anal. Calcd. for $C_{12}H_{15}FO_2$: C, 68.55; H, 7.19. Found: C, 68.55; H, 7.28.

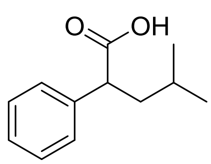

4-methyl-2-phenylpentanoic acid, 1d. was synthesized according to procedure A using phenylacetic acid (15.52 g, 114 mmol, 1 eq), and *i*-butyl bromide (15.5 mL, 148 mmol, 1.3 eq). The yield is 21.26 g, 97% as a white solid. R_f = 0.46 with 3:7 EtOAc/Hexanes; mp 60-65 ºC; ^{1}H NMR (400 MHz, $CDCl_3$) δ: 7.25-7.18 (m, 5 H), 3.59 (t, J = 8 Hz, 1 H), 1.88 (m, 1 H), 1.62 (m, 1 H), 1.42 (sept, J = 8 Hz, 1 H), 0.84 (d, J = 8 Hz, 6 H); $^{13}C\{^1H\}$ NMR (100.6 MHz, $CDCl_3$) δ: 180.7, 138.9, 129.0, 128.4, 127.7, 49.8, 42.3, 26.1, 22.9, 22.5; IR (NaCl): 2958, 1706, 1601, 1496, 1454, 1413, 1386, 1286, 1252, 1212, 1121, 1073, 1030, 936, 759, 726, 698; HRMS (ESI-TOF) $[M + Na]^+$ calcd for $C_{12}H_{16}O_2$ 215.1048, found; 215.1052; Anal. Calcd. for $C_{12}H_{16}O_2$: C, 74.97; H, 8.39. Found: C, 74.57; H, 8.57.

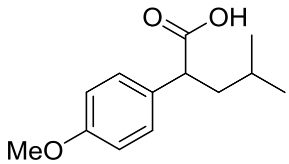

2-(4-methoxyphenyl)-4-methylpentanoic acid, 1e. was synthesized according to procedure A using *p*-methoxyphenylacetic acid (18.94 g, 114 mmol, 1 eq), and *i*-butyl bromide (15.5 mL, 148 mmol, 1.3 eq). The yield is 23.82 g, 94% as a white solid. R_f = 0.39 with 3:7 EtOAc/Hexanes; mp 66-74 ºC; ^{1}H NMR (400 MHz, $CDCl_3$) δ: 7.24 (d, *J* = 8 Hz, 2 H), 6.86 (d, *J* = 12 Hz, 2 H), 3.79 (s, 3 H), 3.60 (t, *J* = 8 Hz, 1 H), 1.91 (m, 1 H), 1.66 (m, 1 H), 1.48 (m, 1 H), 0.90 (dd, *J* = 4, 8 Hz, 6 H); ^{13}C{^{1}H} NMR (100.6 MHz, $CDCl_3$) δ: 180.9, 159.2, 131.0, 129.4, 114.4, 55.6, 48.9, 42.3, 26.0, 23.0, 22.5; IR (NaCl): 2958, 1706, 1611, 1512, 1446, 1412, 1386, 1303, 1252, 1179, 1103, 1036, 941, 835, 794, 729, 695, 631; HRMS (ESI-TOF) $[M + Na]^+$ calcd for $C_{13}H_{18}O_3$ 245.1154, found; 245.1150; Anal. Calcd. for $C_{13}H_{18}O_3$: C, 70.24; H, 8.16. Found: C, 70.05; H, 8.24.

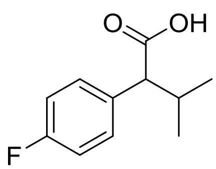

2-(4-fluorophenyl)-3-methylbutanoic acid, 1f. was synthesized according to procedure A using *p*-fluorophenylacetic acid (17.57 g, 114 mmol, 1 eq), and *i*-propyl iodide (14.7 mL, 148 mmol, 1.3 eq). The yield is 22.14 g, 99% as a white solid. R_f = 0.54 with 3:7 EtOAc/Hexanes; mp 53-58 ºC; ^{1}H NMR (400 MHz, $CDCl_3$) δ: 7.32-7.26 (m, 2 H), 7.03-6.91 (m, 2 H), 3.14 (d, *J* = 12 Hz, 1 H), 2.29 (m, 1 H), 1.07 (d, *J* = 8 Hz, 3 H), 0.71 (d, *J* = 8 Hz, 3 H); ^{13}C{^{1}H} NMR (100.6 MHz, $CDCl_3$) δ: 180.6, 162.6 (d, *J* = 246 Hz), 133.7 (d, *J* = 4 Hz), 130.4 (d, *J* = 8 Hz), 115.8 (d, *J* = 21 Hz), 59.5, 32.1, 21.7, 20.4; IR (NaCl): 2965, 1707, 1604, 1510, 1469, 1411, 1293, 1226, 1160, 1092, 1017, 934, 830, 809, 735, 695; HRMS (ESI-TOF) $[M - H]^-$ calcd for $C_{11}H_{14}FO_2$ 195.0821, found; 195.0821; Anal. Calcd. for $C_{11}H_{14}FO_2$: C, 67.33; H, 6.68. Found: C, 67.49; H, 6.57.

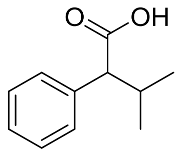

3-methyl-2-phenylbutanoic acid, 1g. was synthesized according to procedure A using phenylacetic acid (15.52 g, 114 mmol, 1 eq), and *i*-propyl iodide (14.7 mL, 148 mmol, 1.3 eq). The yield is 19.71 g, 97% as a white solid. R_f = 0.52 with 3:7 EtOAc/Hexanes; mp 50-53 ºC; ^{1}H NMR (400 MHz, $CDCl_3$) δ: 7.33-7.26 (m, 5 H), 3.14 (d, J = 12 Hz, 1 H), 2.33 (m, 1 H), 1.08 (d, J = 8 Hz, 3 H), 0.71 (d, J = 8 Hz, 3 H); $^{13}C\{^1H\}$ NMR (100.6 MHz, $CDCl_3$) δ: 180.5, 138.0, 128.9, 128.8, 127.8, 60.3, 31.9, 21.8, 20.4; IR (NaCl): 2968, 1705, 1600, 1496, 1455, 1412, 1387, 1369, 1292, 1253, 1221, 1169, 1116, 1071, 1033, 919, 837, 770, 725, 700; HRMS (ESI-TOF) $[M + Na]^+$ calcd for $C_{11}H_{14}O_2$ 201.0891, found; 201.0899; Anal. Calcd. for $C_{11}H_{14}O_2$: C, 74.13; H, 7.92. Found: C, 74.00; H, 8.26.

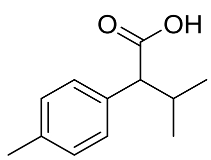

4-methyl-2-(p-tolyl)pentanoic acid, 1h. was synthesized according to procedure A using *p*-methylphenylacetic acid (17.12 g, 114 mmol, 1 eq), and *i*-propyl iodide (14.7 mL, 148 mmol, 1.3 eq). The yield is 20.82 g, 95% as a white solid. R_f = 0.43 with 3:7 EtOAc/Hexanes; mp 61-63 ºC; ^{1}H NMR (400 MHz, $CDCl_3$) δ: 7.21 (d, J = 8 Hz, 2 H), 7.13 (d, J = 8 Hz, 2 H), 3.62 (t, J = 6 Hz, 1 H), 2.32 (s, 3 H), 1.92 (m, 1 H), 1.66 (m, 1 H), 1.48 (m, 1 H), 0.90 (d, J = 4 Hz, 6 H); $^{13}C\{^1H\}$ NMR (100.6 MHz, $CDCl_3$) δ: 180.8, 137.4, 135.9, 129.7, 128.3, 49.4, 42.3, 26.0, 23.0, 22.5, 21.4; IR (NaCl): 2958, 1704, 1512, 1465, 1438, 1414, 1386, 1252, 1214, 1189, 1121, 1044, 943, 835, 790, 727, 693, 671, 636; HRMS (ESI-TOF) $[M + Na]^+$ calcd for $C_{13}H_{18}O_2$ 229.1204, found; 229.1210; Anal. Calcd. for $C_{13}H_{18}O_2$: C, 75.69; H, 8.80. Found: C, 75.54; H, 8.92.

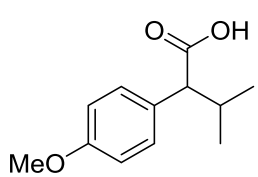

2-(4-methoxyphenyl)-3-methylbutanoic acid, 1i. was synthesized according to procedure A using *p*-methoxyphenylacetic acid (18.94

g, 114 mmol, 1 eq), and *i*-propyl iodide (14.7 mL, 148 mmol, 1.3 eq). The yield is 23.27 g, 98% as a white solid. R_f = 0.35 with 3:7 EtOAc/Hexanes; mp 137-143 ºC; ^{1}H NMR (400 MHz, $CDCl_3$) δ: 7.24 (d, J = 8 Hz, 2 H), 6.85 (d, J = 8 Hz, 2 H), 3.79 (s, 3 H), 3.08 (d, J = 12 Hz, 1 H), 2.28 (m, 1 H), 1.06 (d, J = 8 Hz, 3 H), 0.70 (d, J = 4 Hz, 3 H); ^{13}C{^{1}H} NMR (100.6 MHz, $CDCl_3$) δ: 180.5, 159.3, 130.2, 129.9, 114.3, 59.4, 55.6, 31.9, 21.8, 20.4; IR (NaCl): 2959, 1701, 1610, 1511, 1463, 1442, 1414, 1385, 1367, 1302, 1248, 1178, 1117, 1030, 941, 827, 793, 738, 696; HRMS (ESI-TOF) $[M + Na]^+$ calcd for $C_{12}H_{16}O_3$ 231.0997, found; 231.0998; Anal. Calcd. for $C_{12}H_{16}O_3$: C, 69.21; H, 7.74. Found: C, 69.43; H, 8.04.

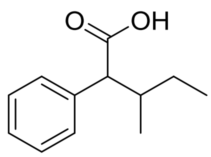

3-methyl-2-phenylpentanoic acid, 1j. was synthesized according to procedure A using phenylacetic acid (15.52 g, 114 mmol, 1 eq), and *s*-butyl iodide (17.0 mL, 148 mmol, 1.3 eq). The yield is 21.04 g, 96% as a white solid. R_f = 0.47 with 3:7 EtOAc/Hexanes; mp 54-59 ºC; ^{1}H NMR (400 MHz, $CDCl_3$). Both diastereomers are observed (1:7). δ: 7.24-7.17 (m, 5 H), 3.18 (d, J = 12 Hz, 1 H), 2.06 (m, 1 H), 1.52 (m, 1 H), 1.15 (sept, J = 6 Hz, 1 H), 0.96 (d, J = 4 Hz, 0.37 H), 0.87 (t, J = 8 Hz, 2.69 H), 0.69 (t, J = 8 Hz, 0.39 H), 0.58 (d, J = 4 Hz, 2.69 H); ^{13}C{^{1}H} NMR (100.6 MHz, $CDCl_3$) δ: 180.5, 137.9, 129.1, 128.9, 127.7, 58.7, 37.9, 28.2, 16.4, 11.5; IR (NaCl): 2966, 1705, 1601, 1496, 1456, 1415, 1382, 1289, 1214, 1184, 1072, 1032, 948, 762, 727, 700; HRMS (ESI-TOF) $[M + Na]^+$ calcd for $C_{12}H_{16}O_2$ 215.1048, found; 215.1057; Anal. Calcd. for $C_{12}H_{16}O_2$: C, 74.97; H, 8.39. Found: C, 75.25; H, 8.48.

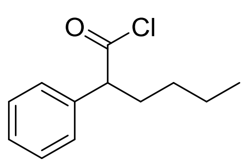

2-Phenylhexanoyl chloride, 2b. was synthesized according to procedure B using **1b** (11.15 g, 58 mmol) to yield the product as a clear oil (9.04 g, 74%) Bp 200 mTorr/150 ºC; ^{1}H NMR (400 MHz, $CDCl_3$) δ: 7.42-7.27 (m, 5 H), 3.96 (t, J = 8 Hz, 1 H), 2.18 (m, 1 H), 1.84 (m, 2 H), 1.35-

1.24 (m, 4 H), 0.88 (t, J = 8 Hz, 3 H); $^{13}C\{^1H\}$ NMR (100.6 MHz, $CDCl_3$) δ: 175.4, 136.4, 129.4, 128.7, 128.6, 63.9, 33.3, 29.6, 22.7, 14.1; IR (NaCl): 2959, 2863, 1790, 1601, 1495, 1455, 1381, 1239, 1120, 1006, 979, 913, 726, 701, 661, 619; HRMS. This compound did not ionize by ESI; Anal. Calcd. for $C_{12}H_{15}ClO$: C, 68.41; H, 7.18. Found: C, 68.45; H, 7.17.

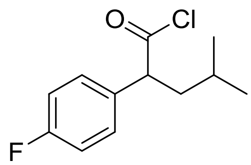

2-(4-fluorophenyl)-4-methylpentanoyl chloride, 2c. was synthesized according to procedure B using **1c** (12.19 g, 58 mmol) to yield the product as a clear oil (10.08 g, 76%) Bp 120 mTorr/120 ºC; ^1H NMR (400 MHz, $CDCl_3$) δ: 7.24 (m, 2 H), 7.04 (t, J = 8 Hz, 2 H), 4.02 (t, J = 8 Hz, 1 H), 2.01 (m, 1 H), 1.70 (m, 1 H), 1.47 (m, 1 H), 0.90 (d, J = 4 Hz, 6 H); $^{13}C\{^1H\}$ NMR (100.6 MHz, $CDCl_3$) δ: 175.4 (d, J = 2 Hz), 162.9 (d, J = 246 Hz), 132.1 (d, J = 3 Hz), 103.4 (d, J = 8 Hz), 116.4 (d, J = 22 Hz), 61.1, 42.4, 25.9, 23.0, 22.3; IR (NaCl): 2961, 2873, 1790, 1605, 1511, 1469, 1389, 1370, 1235, 1161, 1064, 984, 936, 836, 758, 735, 703; HRMS. This compound did not ionize by ESI; Anal. Calcd. for $C_{12}H_{14}ClFO$: C, 74.98; H, 6.82. Found: C, 75.34; H, 6.87.

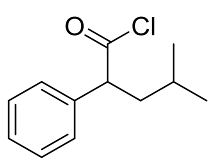

4-methyl-2-phenylpentanoyl chloride, 2d. was synthesized according to procedure B using **1d** (11.15 g, 58 mmol) to yield the product as a clear oil (9.53 g, 78%) Bp 400 mTorr/150 ºC; ^1H NMR (400 MHz, $CDCl_3$) δ: 7.36-7.22 (m, 5 H), 4.02 (t, J = 8 Hz, 1 H), 2.01 (m, 1 H), 1.71 (m, 1 H), 1.47 (sept, J = 8 Hz, 1 H), 0.89 (d, J = 8 Hz, 3 H), 0.88 (d, J = 8 Hz, 3 H); $^{13}C\{^1H\}$ NMR (100.6 MHz, $CDCl_3$) δ: 175.4, 136.4, 129.4, 128.7, 128.5, 62.0, 42.4, 25.9, 23.0, 22.3; IR (NaCl): 2959, 2932, 2863, 1791, 1707, 1601, 1495, 1455, 1382, 1290, 1240, 1120, 1031, 979, 913, 726, 699; HRMS. This compound did not ionize by ESI; several samples gave low elemental analysis. A second distillation followed by high vacuum overnight did not improve results. Anal. Calcd. for $C_{12}H_{15}ClO$: C, 68.41; H, 7.18. Found: C, 66.57; H, 7.26.

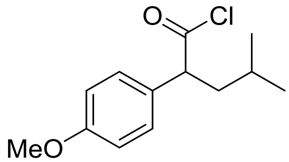

2-(4-methoxyphenyl)-4-methylpentanoyl chloride, 2e. was synthesized according to procedure B using **1e** (12.89 g, 58 mmol) to yield the product as a clear oil (12.01 g, 86%) Bp 200 mTorr/220 ºC; ^{1}H NMR (400 MHz, $CDCl_3$) δ: 7.22 (d, J = 12 Hz, 2 H), 6.90 (d, J = 12 Hz, 2 H), 4.01 (t, J = 8 Hz, 1 H), 3.81 (s, 3 H), 2.02 (m, 1 H), 1.71 (m, 2 H), 1.50 (m, 1 H), 0.92 (d, J = 8 Hz); ^{13}C{^{1}H} NMR (100.6 MHz, $CDCl_3$) δ: 175.6, 159.8, 129.8, 128.2, 114.8, 61.1, 55.6, 42.3, 25.9, 23.0, 22.3; IR (NaCl): 2959, 2872, 1789, 1611, 1513, 1466, 1387, 1369, 1305, 1255, 1180, 1127, 1035, 982, 875, 832, 757, 734, 707; HRMS. This compound did not ionize by ESI; Anal. Calcd. for $C_{13}H_{17}ClO_2$: C, 64.86; H, 7.12. Found: C, 64.91; H, 7.14.

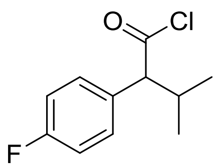

2-(4-fluorophenyl)-3-methylbutanoyl chloride, 2f. was synthesized according to procedure B using **1f** (11.38 g, 58 mmol) to yield the product as a clear oil (10.33 g, 83%) Bp 110 mTorr/100 ºC; ^{1}H NMR (400 MHz $CDCl_3$) δ: 7.35 (dd, J = 8, 12 Hz, 2 H), 7.14 (t, J = 10 Hz, 2 H), 3.72 (d, J = 12 Hz, 1 H), 2.48 (m, 1 H), 1.22 (d, J = 4 Hz, 3 H), 0.81 (d, J = 8 Hz, 3 H); ^{13}C{^{1}H} NMR (100.6 MHz, $CDCl_3$) δ: 175.0 (d, J = 2 Hz), 163.0 (d, J = 247.4 Hz), 131.1 (d, J = 3 Hz), 130.8 (d J = 10.0 Hz), 116.3 (d, J = 22 Hz), 71.1, 32.4, 21.5, 20.0; IR (NaCl): 2967, 2876, 1795, 1708, 1605, 1510, 1469, 1391, 1372, 1230, 1161, 1128, 1039, 1002, 927, 835, 796, 754, 710; HRMS. This compound did not ionize by ESI; Anal. Calcd. for $C_{11}H_{12}ClFO$: C, 61.55; H, 5.63. Found: C, 61.58; H, 5.68.

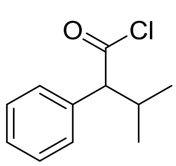

3-methyl-2-phenylbutanoyl chloride, 2g. was synthesized according to procedure B using **1g** (10.34 g, 58 mmol) to yield the product as a clear oil

(9.36 g, 82%) Bp 150 mTorr/120 ºC; ^{1}H NMR (400 MHz, $CDCl_3$) δ: 7.40-7.30 (m, 5 H), 3.68 (d, *J* = 8 Hz, 1 H), 2.45 (m, 1 H), 1.16 (d, *J* = 8 Hz), 0.75 (d, *J* = 8 Hz, 3 H).; $^{13}C\{^1H\}$ NMR (100.6 MHz, $CDCl_3$) δ: 175.0, 135.3, 129.3, 129.2, 128.6, 72.1, 32.4, 21.6, 20.1; IR (NaCl): 3032, 2966, 2875, 1800, 1706, 1495, 1455, 1390, 1371, 1273, 1168, 1128, 1034, 1000, 928, 780, 733, 700, 610; HRMS. This compound did not ionize by ESI; Anal. Calcd. for $C_{11}H_{13}ClO$: C, 67.18; H, 6.66. Found: C, 66.84; H, 6.76.

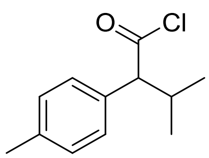

3-methyl-2-(p-tolyl)butanoyl chloride, 2h. was synthesized according to procedure B using **1h** (11.15 g, 58 mmol) to yield the product as a clear oil (9.41 g, 77%) Bp 110 mTorr/140 ºC; ^{1}H NMR (400 MHz, $CDCl_3$) δ: 7.19 (s, br, 4 H), 3.63 (d, *J* = 8 Hz, 1 H), 2.44 (m, 1 H), 2.36 (s, 3 H)1.14 (d, *J* = 4 Hz, 3 H), 0.74 (d, *J* = 4 Hz, 3 H); $^{13}C\{^1H\}$ NMR (100.6 MHz, $CDCl_3$) δ: 175.1, 138.44, 132.3, 130.0, 129.1, 71.7, 32.2, 21.6, 21.5, 20.2; IR (NaCl): 2966, 2874, 1794, 1513, 1469, 1390, 1371, 1271, 1167, 1130, 1039, 1002, 927, 818, 783, 747, 711; HRMS. This compound did not ionize by ESI; Anal. Calcd. for $C_{12}H_{15}ClO$: C, 68.41; H, 7.18. Found: C, 68.63; H, 7.23.

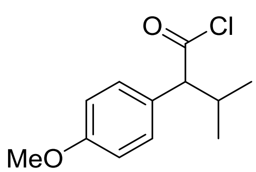

2-(4-methoxyphenyl)-3-methylbutanoyl chloride, 2i. was synthesized according to procedure B using **1i** (12.08 g, 58 mmol) to yield the product as a clear oil (11.04 g, 84%) Bp 300 mTorr/150 ºC; ^{1}H NMR (400 MHz, $CDCl_3$) δ: 7.20 (d, *J* = 8 Hz, 2 H), 6.90 (d, *J* = 8 Hz, 2 H), 3.81 (s, 3 H), 3.59 (d, *J* = 8 Hz, 1 H), 2.39 (m, 1 H), 1.13 (d, *J* = 8 Hz, 3 H), 0.74 (d, *J* = 8 Hz, 3 H); $^{13}C\{^1H\}$ NMR (100.6 MHz, $CDCl_3$) δ: 175.2, 159.9, 130.3, 127.2, 114.7, 71.2, 55.6, 32.2, 21.6, 20.1; IR (NaCl): 2965, 2875, 2838, 1795, 1611, 1584, 1512, 1466, 1390, 1371, 1304, 1256, 1181, 1130, 1036, 1001, 927, 832, 784, 751, 715; HRMS. This compound did not ionize by ESI; Anal. Calcd. for $C_{12}H_{15}ClO_2$: C, 63.58; H, 6.67. Found: C, 63.70; H, 6.66.

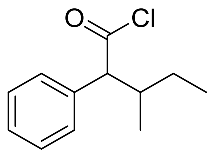

3-methyl-2-phenylpentanoyl chloride, 2j. was synthesized according to procedure B using **1j** (11.15 g, 58 mmol) to yield the product as a clear oil (9.78 g, 80%) Bp 170 mTorr/160 ºC; ^{1}H NMR (400 MHz, $CDCl_3$). Both diastereomers are observed (1:1.3) δ: 7.38-7.29 (m, 5 H), 3.78 (dd, *J* = 4, 12 Hz, 1 H), 2.26 (m, 1 H), 1.67 (m, 0.48 H), 1.32 (m, 0.68 H), 1.25 (m, 0.46 H), 1.13 (d, *J* = 8 Hz, 1.32 H), 0.99 (t, *J* = 8 Hz, 1.74 H), 0.92 (m, 0.56 H), 0.81 (t, *J* = 8 Hz, 1.30 H), 0.72 (t, *J* = 4 Hz, 1.68 H); ^{13}C{^{1}H} NMR (100.6 MHz, $CDCl_3$). Peaks from the two diastereomers are resolved, except for the carbonyl carbon. δ: 175.1, 135.2, 135.1, 129.4, 129.3, 129.3, 129.3, 128.6, 128.6, 70.8, 70.4, 38.4, 38.2, 28.1, 26.1, 17.5, 16.2, 11.4, 10.9; IR (NaCl): 3032, 2967, 2934, 2878, 1798, 1706, 1600, 1494, 1456, 1383, 1259, 1123, 982, 916, 855, 780, 729, 700, 624; HRMS. This compound did not ionize by ESI; Anal. Calcd. for $C_{12}H_{15}ClO$: C, 68.41; H, 7.18. Found: C, 68.33; H, 7.30.

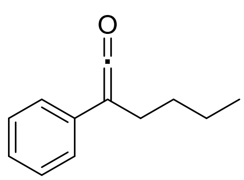

***n*-Butyl phenyl ketene, 3b.** was synthesized according to procedure C using **2b** (9.04 g, 43 mmol, 1 eq), Et_2O (130 mL) and ethyl dimethyl amine (18.5 mL, 172 mmol, 4 eq) to yield the product as a yellow oil (5.53 g, 74%) Bp 150 mTorr/110 ºC; ^{1}H NMR (400 MHz, C_6D_6) δ: 7.08 (d, *J* = 8 Hz, 2 H), 6.90 (m, 3 H), 2.00 (t, *J* = 8 Hz, 2 H), 1.25 (m, 2 H), 1.16 (m, 2 H), 0.73 (t, *J* = 8 Hz, 3 H); ^{13}C{^{1}H} NMR (100.6 MHz, C_6D_6) δ: 206.2 (O=*C*=C), 133.6, 129.9, 125.1, 40.4 (O=C=*C*), 30.9, 24.0, 23.1, 14.4. One aromatic resonance likely overlaps with the residual solvent peak. IR (NaCl): 2082 (s, CO), 2042, 1599 (s), 1497 (s), 1454 (s), 1379 (w), 1322 (w), 1248 (m), 1190 (w), 1158 (w), 1105 (w), 1076 (w), 1035 (w), 894 (w), 751 (s), 692 (s); HRMS (GC-TOF) [M^+] calcd for $C_{12}H_{14}O$ 174.1045, found 174.1045; Anal. Calcd. for

$C_{12}H_{14}O$: C, 82.72; H, 8.10. Found: C, 82.73; H, 7.99.

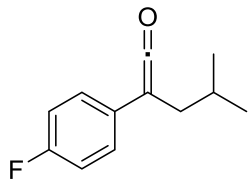

***i*-Butyl 4-fluorophenyl ketene, 3c.** was synthesized according to procedure C using **2c** (10.08 g, 44 mmol, 1 eq), Et_2O (130 mL) and ethyl dimethyl amine (19.0 mL, 176 mmol, 4 eq) to yield the product as a yellow oil (5.76 g, 68%) Bp 110 mTorr/100 ºC; ^{1}H NMR (500 MHz, C_6D_6) δ: 6.74 (m, 2 H), 6.61 (m, 2 H), 1.81 (d, J = 10 Hz, 2 H), 1.48 (sept, J = 7 Hz, 1 H), 0.75 (d, J = 5 Hz, 6 H); ^{13}C{^{1}H} NMR (100.6 MHz, C_6D_6): 205.6 (O=*C*=C), 161.1 (d, J = 244 Hz), 129.0 (d, J = 3 Hz), 126.6 (d, J = 8 Hz), 116.8 (d, J = 22 Hz), 37.8 (O=C=*C*), 34.0, 27.8, 22.8; IR (NaCl): 2097 (s, CO), 1872 (w), 1748 (w), 1634 (w), 1602 (m), 1510 (s), 1466 (s), 1419 (m), 1386 (s), 1368 (s), 1338 (m), 1305 (m), 1278 (m), 1232 (s), 1161 (s), 1100 (s), 1013 (m), 928 (w), 828 (s), 698 (w); HRMS (GC-TOF) [M$^+$] calcd for $C_{12}H_{13}FO$ calcd 192.0950, found 192.0954; Anal. Calcd. for $C_{12}H_{14}O$: C, 74.98; H, 6.82. Found: C, 75.34; H, 6.87.

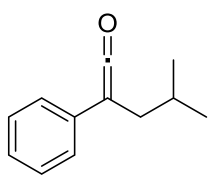

***i*-Butyl phenyl ketene, 3d.** was synthesized according to procedure C using **2b** (9.53 g, 45 mmol, 1 eq), Et_2O (135 mL) and ethyl dimethyl amine (19.6 mL, 181 mmol, 4 eq) to yield the product as a yellow oil (5.67 g, 72%) Bp 120 mTorr/100 ºC; ^{1}H NMR (400 MHz, C_6D_6) δ: 7.08 (t, J = 8 Hz, 2 H), 6.89 (m, 3 H), 1.91 (d, J = 4 Hz, 2 H), 1.55 (sept, J = 4 Hz, 1 H), 0.76 (d, J = 8 Hz, 6 H); ^{13}C{^{1}H} NMR (100.6 MHz, C_6D_6) δ: 205.6 (O=*C*=C), 133.5, 129.9, 125.2, 125.1, 38.7 (O=C=*C*), 33.7, 27.9, 22.86; IR (NaCl): 2095 (s, CO), 2042 (m), 1600 (s), 1576 (m), 1497 (s), 1466 (m), 1385 (m), 1368 (m), 1335 (w), 1278 (w), 1243 (m), 1169 (w), 1100 (w), 1075 (w), 1036 (w), 896 (w), 753 (s), 692 (s); HRMS (GC-TOF) [M$^+$] calcd for $C_{12}H_{14}O$ 174.1045, found 174.1048; Anal. Calcd. for $C_{12}H_{14}O$: C, 82.72; H, 8.10. Found: C, 82.59; H, 8.29.

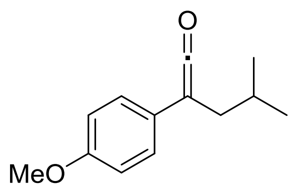

***i*-Butyl 4-methoxyphenyl ketene, 3e.** was synthesized according to procedure C using **2e** (12.01 g, 50 mmol, 1 eq), Et_2O (150 mL) and ethyl dimethyl amine (21.6 mL, 200 mmol, 4 eq) to yield the product as a yellow oil (6.21 g, 61%) Bp 140 mTorr/160 ºC; ^{1}H NMR (400 MHz, C_6D_6) δ: 6.85 (d, J = 8 Hz, 2 H), 6.74 (d, J = 8 Hz, 2 H), 3.30 (s, 3 H), 1.96 (d, J = 8 Hz, 2 H), 1.60 (sept, J = 7 Hz, 1 H), 0.80 (d, J = 8 Hz, 6 H); ^{13}C{^{1}H} NMR (100.6 MHz, C_6D_6) δ: 207.6 (O=*C*=C), 158.2, 126.7, 124.7, 115.7, 55.4, 37.5 (O=C=*C*), 34.4, 27.9, 22.9; IR (NaCl): 2100 (s, CO), 2041 (m), 1869 (w), 1786 (w), 1609 (s), 1576 (m), 1511 (s), 1465 (s), 1385 (m), 1367 (m), 1337 (w), 1287 (s), 1248 (s), 1181 (s), 1113 (w), 1040 (s), 1015 (m), 923 (w), 826 (s), 800 (m), 700 (w); HRMS (ESI) m/z $[C_{13}H_{16}O_2]^+$ calcd 204.1150, found 204.1156; Anal. Calcd. for $C_{12}H_{14}O$: C, 76.44; H, 7.90. Found: C, 76.29; H, 8.22.

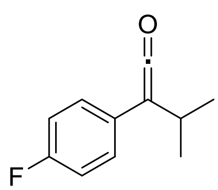

***i*-Propyl 4-fluorophenyl ketene, 3f.** was synthesized according to procedure C using **2f** (10.33 g, 48 mmol, 1 eq), THF (145 mL) and triethyl amine (26.8 mL, 192 mmol, 4 eq) to yield the product as a yellow oil (6.35 g, 74%) Bp 140 mTorr/60 ºC; ^{1}H NMR (500 MHz, C_6D_6) δ: 6.74 (m, 2 H), 6.62 (m, 2 H), 2.28 (sept, J = 7 Hz, 1 H), 0.89 (d, J = 5 Hz, 6 H); ^{13}C{^{1}H} NMR (100.6 MHz, C_6D_6) δ: 205.2 (O=*C*=C), 161.2 (d, J = 243 Hz), 128.7 (d, J = 3 Hz), 127.4 (d, J = 8 Hz), 116.8 (d, J = 21 Hz), 47.7 (O=C=*C*), 25.0, 22.4; IR (NaCl): 2082 (s, CO), 2043 (m), 1873 (w), 1749 (w), 1636 (w), 1593 (w), 1507 (s), 1462 (m), 1418 (w), 1388 (m), 1369 (m), 1305 (m), 1289 (m), 1273 (m), 1228 (s), 1161 (s), 1100 (m), 1068 (m), 1014 (w), 981 (w), 928 (w), 829 (s), 812 (s); HRMS (GC-TOF) [M^+] calcd for $C_{11}H_{11}FO$ 178.0794, found 178.0798; Anal. Calcd. for $C_{12}H_{14}O$: C, 74.14; H, 6.22. Found: C, 73.97; H, 6.06.

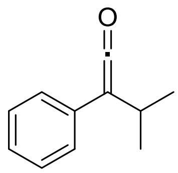

***i*-Propyl phenyl ketene, 3g.** was synthesized according to procedure C using **2g** (9.35 g, 48 mmol, 1 eq), THF (145 mL) and triethylamine (26.6 mL, 190 mmol, 4 eq) to yield the product as a yellow oil (5.87 g, 74%) Bp 150 mTorr/100 ºC; ^{1}H NMR (400 MHz, C_6D_6) δ: 7.08 (m, 2 H), 6.89 (m, 3 H), 2.43 (sept, *J* = 7 Hz, 1 H), 0.94 (d, *J* = 8 Hz, 6 H); ^{13}C{^{1}H} NMR (100.6 MHz, C_6D_6) δ: 205.5 (O=*C*=C), 133.2, 129.9, 125.8, 125.4, 48.8 (O=C=*C*), 24.6, 22.6; IR (NaCl): 2094 (s, CO), 1040 (m), 1959 (w), 1599 (s), 1574 (m), 1497 (s), 1463 (m), 1450 (s), 1388 (m), 1369 (m), 1341 (w), 1289 (m), 1276 (m), 1243 (s), 1191 (w), 1159 (m), 1112 (w), 1067 (m), 1035 (m), 977 (w), 896 (w), 867 (w), 752 (w), 692 (s); HRMS (GC-TOF) [M^+] calcd for $C_{11}H_{12}O$ 160.0888, found 160.0892; Anal. Calcd. for $C_{12}H_{14}O$: C, 82.46; H, 7.55. Found: C, 82.32; H, 7.30.

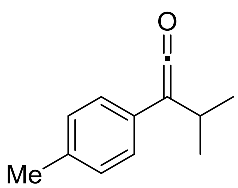

***i*-Propyl 4-methylphenyl ketene, 3h.** was synthesized according to procedure C using **2h** (9.41 g, 45 mmol, 1 eq), THF (135 mL) and triethylamine (24.9 mL, 179 mmol, 4 eq) to yield the product as a yellow oil (5.52 g, 71%) Bp 240 mTorr/100 ºC; ^{1}H NMR (400 MHz, C_6D_6) δ: 6.95 (d, *J* = 8 Hz, 2 H), 6.88 (d, *J* = 8 Hz, 2 H), 2.46 (sept, *J* = 8 Hz, 1 H), 2.09 (s, 3 H), 0.96 (d, *J* = 8 Hz, 6 H); ^{13}C{^{1}H} NMR (100.6 MHz, C_6D_6) δ: 209.2 (O=*C*=C), 134.7, 130.7, 129.9, 126.0, 48.2 (O=C=*C*), 24.8, 22.6, 21.5; IR (NaCl): 2093 (s, CO), 2040 (w), 1959 (w), 1888 (w), 1613 (w), 1568 (w), 1512 (s), 1462 (m), 1387 (m), 1368 (m), 1309 (w), 1290 (m), 1273 (w), 1242 (m), 1159 (w), 1125 (w), 1111 (w), 1067 (w), 1041 (w), 981 (w), 868 (w), 811 (s), 710 (w), 629 (w); HRMS (GC-TOF) [M^+] calcd for $C_{12}H_{14}O$ 174.1045, found 174.1043; Anal. Calcd. for $C_{12}H_{14}O$: C, 82.72; H, 8.10. Found: C, 83.05; H, 8.15.

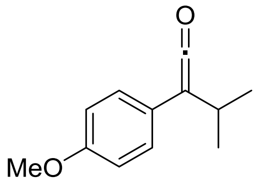

***i*-Propyl 4-methoxyphenyl ketene, 3i.** was synthesized according to procedure C using **2i** (11.04 g, 49 mmol, 1 eq), THF (150 mL) and triethylamine (27.1 mL, 195 mmol, 4 eq) to yield the product as a yellow oil (7.23 g, 78%) Bp 150 mTorr/180 ºC; ^{1}H NMR (400 MHz, C_6D_6) δ: 6.87 (d, *J* = 8 Hz, 2 H), 6.74 (d, *J* = 8 Hz, 2 H), 3.30 (s, 3 H), 2.44 (sept, *J* = 8 Hz, 1 H), 0.97 (d, *J* = 8 Hz, 6 H); ^{13}C{^{1}H} NMR (100.6 MHz, C_6D_6) δ: 207.0 (O=*C*=C), 158.4, 127.6, 124.4, 115.7, 55.41, 47.3 (O=C=*C*), 25.4, 22.6; IR (NaCl): 2094 (s, CO), 2042 (m), 1599 (s), 1577 (m), 1497 (s), 1466 (s), 1453 (s), 1386 (m), 1368 (m), 1335 (w), 1278 (m), 1243 (m), 1190 (w), 1169 (w), 1100 (w), 1075 (w), 1036 (w), 1009 (w), 993 (w), 896 (w), 811 (w), 753 (s), 730 (w), 692 (s); HRMS (ESI) m/z $[C_{12}H_{14}O_2]^+$ calcd 190.0994, found 190.0994; Anal. Calcd. for $C_{12}H_{14}O_2$: C, 75.76; H, 7.42. Found: C, 75.66; H, 7.32.

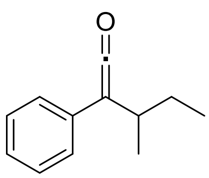

***s*-Butyl phenyl ketene, 3j.** was synthesized according to procedure C using **2j** (9.78 g, 46 mmol, 1 eq), THF (140 mL) and triethylamine (25.8 mL, 186 mmol, 4 eq) to yield the product as a yellow oil (5.90 g, 73%) Bp 160 mTorr/100 ºC; ^{1}H NMR (400 MHz, C_6D_6) δ: 7.09 (m, 2 H), 6.90 (m, 2 H), 2.29 (sext, *J* = 7.2 Hz, 1 H), 1.39 (sept, *J* = 6.7, 1 H), 1.21 (sext, *J* = 7.3 Hz, 1 H), 0.96 (d, *J* = 8.0 Hz, 3 H), 0.76 (t, *J* = 8.0 Hz, 3 H); ^{13}C{^{1}H} NMR (100.6 MHz, C_6D_6) δ: 205.3 (O=*C*=C), 133.4, 129.9, 125.9, 125.3, 47.1 (O=C=*C*), 31.42, 29.4, 19.8, 12.0; IR (NaCl): 2095 (s, CO), 2039 (w), 1959 (w), 1599 (s), 1576 (w), 1497 (s), 1453 (m), 1382 (m), 1338 (w), 1313 (w), 1274 (w), 1238 (w), 1191 (w), 1158 (w), 1104 (w), 1076 (w), 1035 (w), 1006 (w), 968 (w), 752 (s), 692 (s); HRMS (GC-TOF) [M^+] calcd for $C_{12}H_{14}O$ 174.1045, found 174.1046; Anal. Calcd. for $C_{12}H_{14}O$: C, 82.72; H, 8.10. Found: C, 82.61; H, 7.93.

References

1. (a) Frey, H. M.; Isaacs, N. S. *J. Chem. Soc. B* **1970**, 830. (b) Binsch, G.; Feiler, L. A.; Huisgen, R. *Tetrahedron Lett.* **1968**, *9*, 4497.

2. (a) Brady, W. T.; Saidi, K. *J. Org. Chem.* **1979**, *44*, 733. (b) Pons, J.-M.; Kocieński, P. *Tetrahedron Lett.* **1989**, *30*, 1833.

3. (a) Moore, H. W.; Hughes, G.; Srinivasachar, K.; Fernandez, M.; Nguyen, N. V.; Schoon, D.; Tranne, A. *J. Org. Chem.* **1985**, *50*, 4231. (b) Duran, F.; Ghosez, L. *Tetrahedron Lett.* **1970**, *11*, 245.

4. (a) Dunbar, R.; White, G. *J. Org. Chem.* **1958**, *23*, 915. (b) Andraos, J.; Kresge, A. J. *J. Am. Chem. Soc.* **1992**, *114*, 5643. (c) Kita, Y.; Matsuda, S.; Kitagaki, S.; Tsuzuki, Y.; Akai, S. *Synlett* **1991**, *1991*, 401. (d) Mićović, V. M.; Rogić, M. M.; Mihailović, M. L. *Tetrahedron* **1957**, *1*, 340. (e) Lombardo, L. *Tetrahedron Lett.* **1985**, *26*, 381.

5. (a) Tidwell, T. T. *Angew. Chem. Int. Ed.* **2005**, *44*, 6812. (b) Allen, A. D.; Tidwell, T. T. *Chem. Rev.* **2013**, *113*, 7287. (c) Tidwell, T. T. In *Ketenes*; John Wiley & Sons, Inc.: 2006. (d) Fu, N.; Tidwell, T. T. *Organic Reactions* **2015**, *87*, 257. (e) Danheiser, R. L. *Science of Synthesis (Houben-Weyl)* **2006**, *23*.

6. (a) Dymock, B. W.; Kocienski, P. J.; Pons, J.-M. *Chem. Commun.* **1996**, 1053. (b) Douglas, J.; Taylor, J. E.; Churchill, G.; Slawin, A. M. Z.; Smith, A. D. *J. Org. Chem.* **2013**, *78*, 3925. (c) Hodous, B. L.; Fu, G. C. *J. Am. Chem. Soc.* **2002**, *124*, 1578. (d) Zemribo, R.; Romo, D. *Tetrahedron Lett.* **1995**, *36*, 4159.

7. (a) Dai, X.; Nakai, T.; Romero, J. A. C.; Fu, G. C. *Angew. Chem. Int. Ed.* **2007**, *46*, 4367. (b) Hodous, B. L.; Fu, G. C. *J. Am. Chem. Soc.* **2002**, *124*, 10006.

8. Kumar, P.; Troast, D. M.; Cella, R.; Louie, J. *J. Am. Chem. Soc.* **2011**, *133*, 7719.

9. Ogata, K.; Ohashi, I.; Fukuzawa, S.-i. *Org. Lett.* **2012**, *14*, 4214.

10. (a) Ryuji, S.; Akira, M.; Hiroyuki, N. *Chem. Lett.* **1988**, *17*, 1403. (b) Grotjahn, D. B.; Bikzhanova, G. A.; Collins, L. S. B.; Concolino, T.; Lam, K.-C.; Rheingold, A. L. *J. Am. Chem. Soc.* **2000**, *122*, 5222. (c) Staudaher, N. D.; Arif, A. M.; Louie, J. *J. Am. Chem. Soc.* **2016**, *138*, 14083.

11. (a) Turro, N. J.; Leermakers, P. A.; Wilson, H. R.; Neckers, D. C.; Byers, G. W.; Vesley, G. F. *J. Am. Chem. Soc.* **1965**, *87*, 2613. (b) Andreades, S.; Carlson, H. D. *Org. Synth.* **1965**, *45*, 50.

12. (a) Danheiser, R. L.; Savariar, S.; Cha, D. D. *Org. Synth.* **1990**, *68*, 32. (b) Depres, J.; Greene, A. E. *Org. Synth.* **1990**, *68*, 41. (c) Fisher, G. J.; MacLean, A. F.;

Schnizer, A. W. *J. Org. Chem.* **1953**, *18*, 1055.

13. (a) Bachmann, W. E.; Struve, W. S. In *Organic Reactions*; John Wiley & Sons, Inc.: 2004. (b) Meier, H.; Zeller, K.-P. *Angew. Chem., Int. Ed. Engl.* **1975**, *14*, 32. (c) Smith, L. I.; Hoehn, H. H. *Org. Synth.* **1940**, *20*.

14. (a) Krepski, L. R.; Hassner, A. *J. Org. Chem.* **1978**, *43*, 2879. (b) Smith, C. W.; Norton, D. G. *Org. Synth.* **1953**, *33*, 29.

15. (a) Danheiser, R. L.; Okamoto, I.; Lawlor, M. D.; Lee, T. W. *Org. Synth.* **2003**, *80*, 160. (b) Rasik, C. M.; Salyers, E. M.; Brown, M. K. *Org. Synth.* **2016**, *93*, 401.

16. Taylor, E. C.; McKillop, A.; Hawks, G. H. *Org. Synth.* **1972**, *52*, 36.

17. (a) Rasik, C. M.; Brown, M. K. *J. Am. Chem. Soc.* **2013**, *135*, 1673. (b) Rasik, C. M.; Hong, Y. J.; Tantillo, D. J.; Brown, M. K. *Org. Lett.* **2014**, *16*, 5168.

18. Staudaher, N. D.; Lovelace, J.; Johnson, M. P.; Louie, J. *Org. Synth.* **2017**, *94*, 1.

CHAPTER 4

THE MECHANISM OF THERMAL DECOMPOSITION OF NICKEL KETENE COMPLEXES*

Introduction

Ni–Ketene complexes are highly probable reaction intermediates in the carbonylation[1] of diazo compounds,[2] Danheiser Benzannulations,[3] [2+2+2] cycloadditions of diynes and ketenes,[4] and, importantly, the Fisher–Tropsch reaction.[5] As such, some effort has gone into developing methods for synthesizing Ni–ketene complexes and, furthermore, understanding their fundamental reactivity. Unfortunately, effective and general syntheses to these complexes are still lacking. For example, only a handful of Ni–ketene complexes (e.g., complexes **1-7**) have been successfully prepared to date (Figure 4.1) and complex **7**[6] has not been fully characterized. Furthermore, many of these complexes are unstable at ambient conditions thereby hampering detailed reactivity studies.

To further complicate matters, Ni–ketene complexes tend to decompose to form catalytically incompetent Ni–CO complexes (Figure 4.1). Miyashita and co-workers

---

* Reprinted (adapted) with permission from: Staudaher, N. D.; Arif, A. M.; Louie, J. *J. Am. Chem. Soc.* **2016**, *138*, 14083.

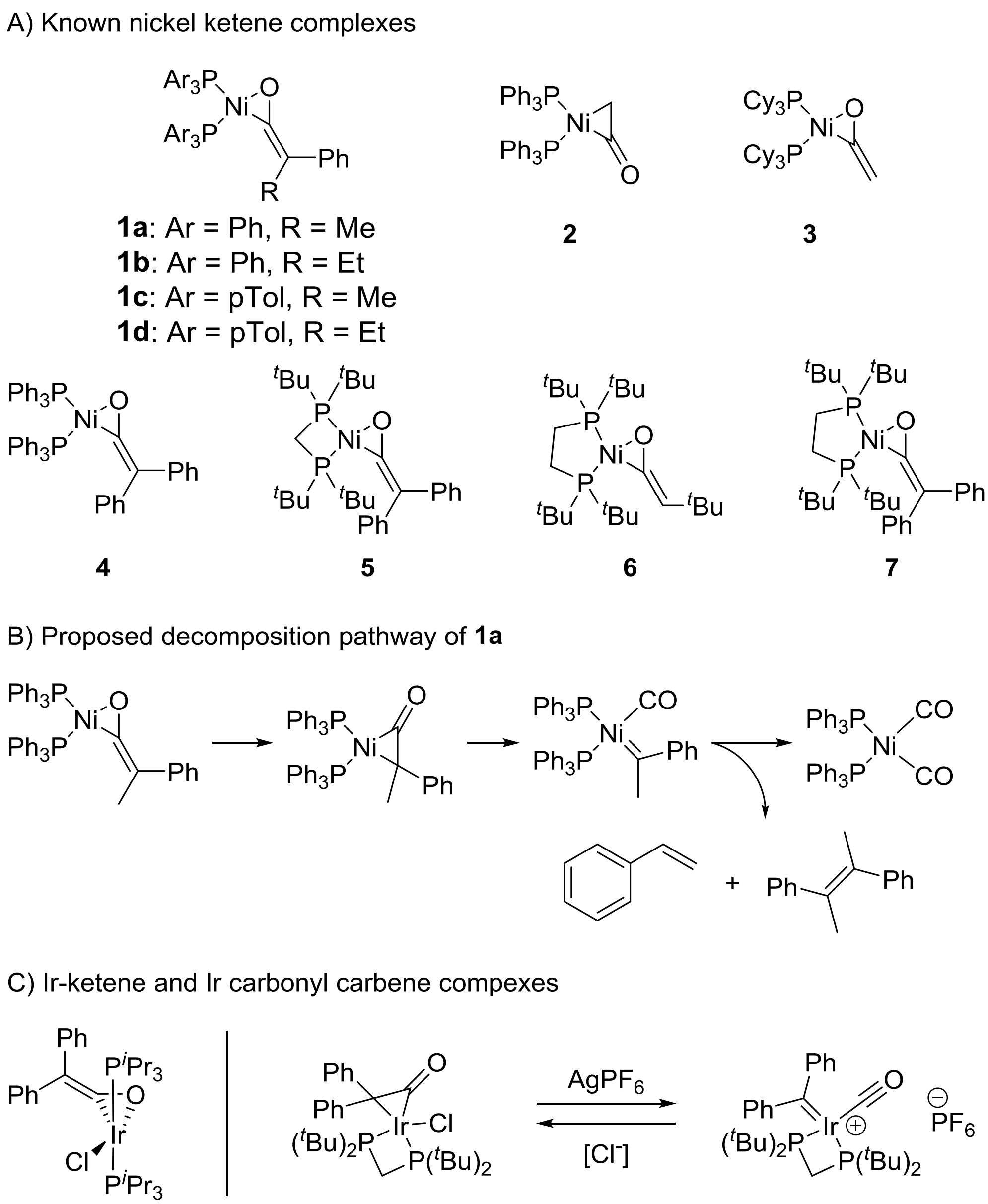

Figure 4.1. Ketene complexes and decomposition pathway of nickel ketene complexes.

showed that the decomposition of complex **1a**, which is stable at -30 ˚C, at room temperature[7] affords $(PPh_3)_2Ni(CO)_2$ as well as styrene and but-2-ene-2,3-diyldibenzene as organic by-products. They propose the decomposition proceeds by an isomerization from η^2-(C,O) to η^2-(C,C) followed by scission of the C=C bond, forming a carbonyl carbene complex. In contrast to the instability of complexes **1-3**, compounds **4-6**[8] are stable at room temperature. Although the thermal decomposition of complexes **5**[9] and **6**[10] were not evaluated, complex **4** decomposes over 24 h at 80 ˚C.

Despite the lack of information on Ni–ketene complexes, Ir– and Rh–ketene complexes have been studied in much more depth and lend insight into the decomposition of Ni–ketene complexes. In fact, coordination through both the C=O[11] and C=C[12] bonds of a ketene have been observed in Ir complexes. Furthermore, The scission of the C=C bond to form an Ir carbonyl carbene complex has been shown to be reversible (Figure 4.1c) and has been studied in depth computationally.[13]

The decomposition of Ni–ketene complexes to Ni–CO complexes is particularly intriguing considering the lack of Ni–CO intermediates in many reaction mechanisms that likely involve Ni–ketene complexes. That is, formation of Ni–CO would prevent product formation in these reactions. Thus, it may be possible that Ni–CO complexes form reversibly in some cases or, more likely, Ni–ketene complexes with higher stability have rates of reactions that are faster than rates of decomposition to Ni–CO. Clearly, a deeper understanding regarding the conversion of Ni–ketene complexes to Ni–CO complexes could aid in the development of new Ni–mediated chemistries of ketenes. Herein we report a detailed evaluation of the structure and mechanism of decomposition of (dppf)Ni(ketene) complexes.

Results and Discussion

Synthesis of (dppf)Ni(ketene) complexes. Our initial efforts focused on the synthesis of a library of Ni–ketene complexes that are stable at room temperature but decompose upon heating. Since all known Ni–ketene complexes have phosphines as supporting ligands, we began by screening the reaction of a variety of monodentate and bidentate phosphine ligands with $Ni(COD)_2$ and butyl phenyl ketene (eq 4.1). Not surprisingly, the use of a monodentate phosphine such as PPh_3 did not afford a long-lived Ni–ketene complex at room temperature as determined by $^{31}P\{^1H\}$ NMR and IR spectroscopy. Indeed, carbonyl peaks, 2002 and 1944 cm^{-1}, were observed and are consistent with the formation of decomposition product $(PPh_3)_2Ni(CO)_2$.[14]

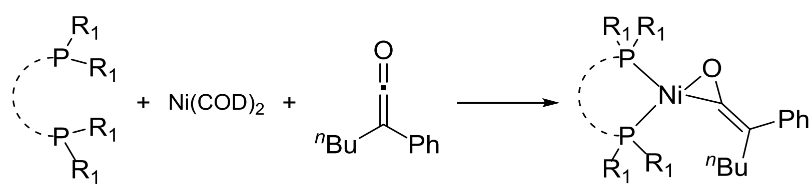

(4.1)

Various bidentate phosphine ligands were also examined. To our dismay, reactions run with dppe, dppp, dppb, or dppbenzene with $Ni(COD)_2$ and diphenylketene also did not afford the desired Ni–ketene complexes. Instead, a mixture of LNi(COD) and L_2Ni species were observed by $^{31}P\{^1H\}$ NMR spectroscopy as we have seen with Xantphos.[15] The formation of these species were confirmed by omitting ketene from the reactions, which led to identical $^{31}P\{^1H\}$ NMR spectra. Furthermore, in the reaction with dppe, only a broad singlet at 44.6 ppm, which is consistent with $(dppe)_2Ni$, was observed.[16] The formation of bis-chelated species is detrimental to Ni–ketene complex formation because for every L_2Ni species, an equivalent of $Ni(COD)_2$ is left over which reacts rapidly with ketene to form nickel carbonyl compounds.[8]

Gratifyingly, the reaction between dppf and $Ni(COD)_2$ formed (dppf)Ni(COD) quantitatively, observed as a sole singlet at 34 ppm in the $^{31}P\{^1H\}$ NMR spectrum; $(dppf)_2Ni$ was not observed.[17] Furthermore, when phenyl butyl ketene was added to a solution of $Ni(COD)_2$ and dppf that was allowed to equilibrate for 60 s, clean formation of Ni–ketene **8b** occurred as indicated by the disappearance of the singlet at 34 ppm and the appearance of two doublets at 42 and 17 ppm, consistent with inequivalent phosphines of a Ni–ketene complex (*vide infra*). Butyl phenyl ketene could be substituted with other alkyl aryl ketenes (eq 4.2) under similar reaction conditions to afford a series of (dppf)Ni(ketene) complexes that were easily recrystallized with pentane (Table 4.1).

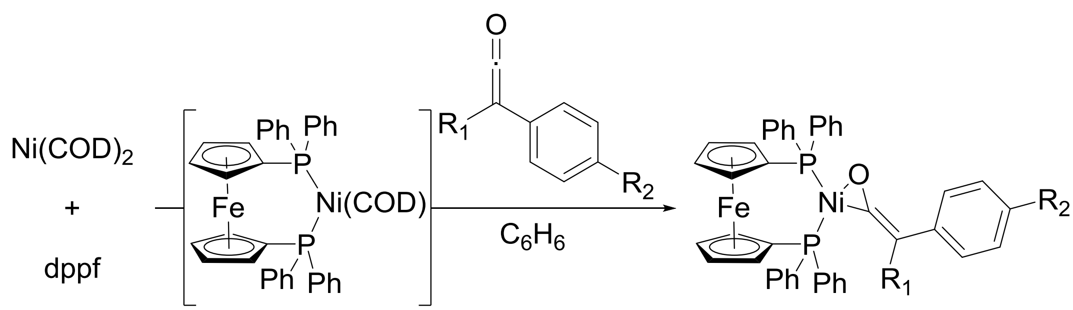

(4.2)

Crystallography. Solid state structures for a variety of complexes are shown in Figure 4.2, and selected bond distances and lengths are in Table 4.2. The structure of **8a** is planar about the Ni center, and the ketene is bound through the C=O bond. The phenyl ring containing C(9) is nearly in plane with the ketene fragment, with a O(1)-C(1)-C(2)-C(9) dihedral angle of -4.6(4)˚, indicating the p orbitals of the ketene and the arene are in conjugation. The other ketene phenyl ring, which contains C(3), is in a π-stacking[18] interaction with the ring containing C(15) on the dppf fragment. The centroid-centroid

Table 4.1. Yields of (dppf)Ni(ketene) complexes.

Complex	R_1	R_2	Yield (%)
8a	Ph	H	85
8b	*n*Bu	H	79
8ca	*i*Bu	F	76
8cb	*i*Bu	H	67
8cc	*i*Bu	Me	75
8cd	*i*Bu	OMe	37
8d	*i*Pr	H	80
8e	*s*Bu	H	78

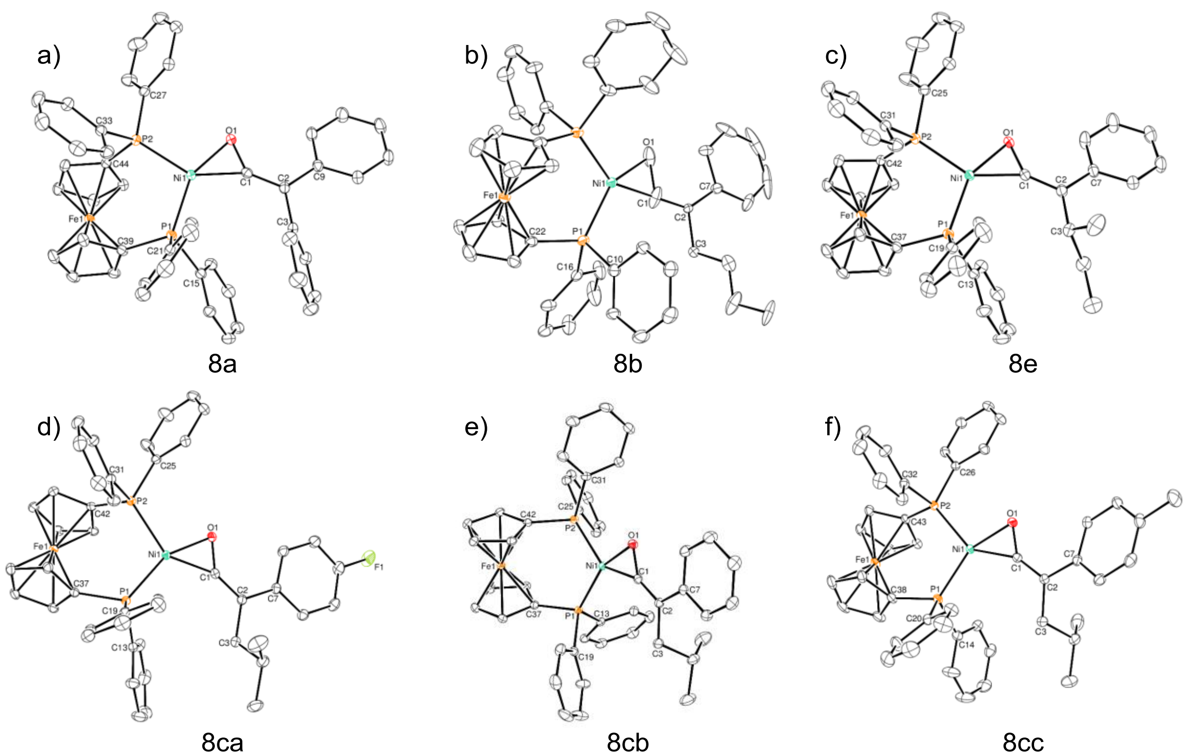

Figure 4.2. ORTEP diagrams of (dppf)Ni(ketene) complexes with ellipsoids set at 30% probability.

Table 4.2. Structural parameters of (dppf)Ni(ketene) complexes from crystal structures.

Complex	P_1-Ni	P_2-Ni	Ni-O_1	Ni-C_1	O_1-C_1	C_1-C_2	O_1-Ni-C_1	P_1-Ni-P_2	O_1-C_1-C_2-C_7
8a	2.1557(6)	2.2252(6)	1.866(1)	1.875(2)	1.297(3)	1.350(3)	40.59(7)	105.60(2)	-4.6(4)
8b	2.1832(15)	2.1833(15)	1.862(5)	1.862(5)	1.383(14)	1.291(11)	43.6(4)	108.13(8)	-19(1)
8e	2.1488(7)	2.2151(7)	1.861(2)	1.878(2)	1.292(2)	1.352(3)	40.42(7)	105.18(2)	-7.1(4)
8ca	2.1551(5)	2.2293(5)	1.851(1)	1.887(2)	1.293(2)	1.352(2)	40.46(6)	104.86(2)	-2.0(3)
8cb	2.1569(6)	2.2306(6)	1.855(1)	1.886(2)	1.292(2)	1.354(3)	40.41(7)	104.78(2)	3.0(3)
8cc	2.1569(6)	2.2277(6)	1.871(1)	1.878(2)	1.291(2)	1.350(3)	40.28(7)	106.34(2)	6.2(3)

distance is 3.644 Å and the planes are skewed by 7.38˚.

The structure of **8b** is, unfortunately, disordered. The unit cell contains four complexes, with random orientation of each ketene fragment relative to the unit cell, i.e., a given unit cell may have all butyl chains down, and another all up, or any combination thereof. As such, **8b** appears to have C_2 symmetry about the line containing the Fe and Ni atoms. Thermal ellipsoids of some carbon atoms have therefore been omitted from Figure 4.2b for clarity, and reliable bond lengths and angles for the metallaoxirane cannot be obtained. Nevertheless, the X-ray structure clearly demonstrates that the ketene is C=O bound; the phenyl ring is oriented away from the dppf fragment and almost in plane with the C=C bond. The structures of **8e**, **8ca**, **8cb**, and **8cc** show similar features in that they are planar, bound through the C=O fragment of the ketene, and have the aromatic ring in plane with the ketene. Interestingly, the structures of **8ca**, **8cb**, and **8cc** reveal that the O(1)-C(1)-C(2)-C(7) dihedral angle increases with more electron rich aromatic rings, indicating slightly better orbital overlap with electron poor ketenes. Also, the O(1)-Ni-C(1) angle decreases slightly from **8ca** to **8cc**, indicating tighter binding of the C=O fragment with electron poor ketenes. The fact that aryl alkyl ketenes have the arene oriented away from the Ni center indicates that the orbital overlap between the arene and the ketene is energetically more favorable than the π-stacking interaction in the structure of **8a**. Finally, the P(1)-Ni (trans to O) bond length is slightly shorter than the P(2)-Ni (trans to C(1)) bond, revealing a modest trans effect. The Ni-O bonds are shorter than the Ni-C bonds, indicating tighter binding of the O atom than the C.

Spectroscopy. The $^{31}P\{^1H\}$ NMR spectrum of **8b** contains two doublets at 42 and 17 ppm with a coupling constant of 23 Hz, consistent with a planar Ni complex with *cis* phosphines and an unsymmetrical π substituent that does not rotate freely. The aromatic region of the ^1H NMR spectrum is complicated, but clearly shows four signals between 4.3–3.6 ppm, the cyclopentadienyl region, consistent with a dppf ligand containing mirror symmetry about the plane containing the Fe and P atoms. In addition, the alkyl region contains signals corresponding to an *n*-butyl chain. The $^{13}C\{^1H\}$ spectrum contains a doublet at 168.7 (J = 48 Hz) corresponding to the ketene O=***C***=C carbon and a doublet of doublets at 79.3 ppm (J = 7, 4 Hz) consistent with the O=C=***C*** carbon. The IR spectrum of **8b** contains only one carbonyl peak at 1624 cm^{-1}, consistent with a C=O coordinated ketene.

Interestingly, the spectral data for **8ca** are much more complicated. The $^{31}P\{^1H\}$ NMR spectrum (Figure 4.3) displays two doublets at 40.8 and 17.3 ppm (J = 22 Hz) as well as two much smaller doublets, each slightly upfield of the first set of doublets at 40.2 and 17.0 ppm (J = 21 Hz) and a singlet at 23.5 ppm (Figure 4.3), indicative of three coordination modes of the ketene. The ^1H NMR spectrum is also consistent with three structural isomers. The Cp region displays this behavior more clearly than the aromatic or alkyl regions. There are three sets of four signals, with integrations 25:4:2; one each of the largest and second largest peaks overlap. The IR spectrum shows two carbonyl peaks at 1597 and 1743 cm^{-1}. The largest signals in the $^{31}P\{^1H\}$ NMR and ^1H NMR spectra and the

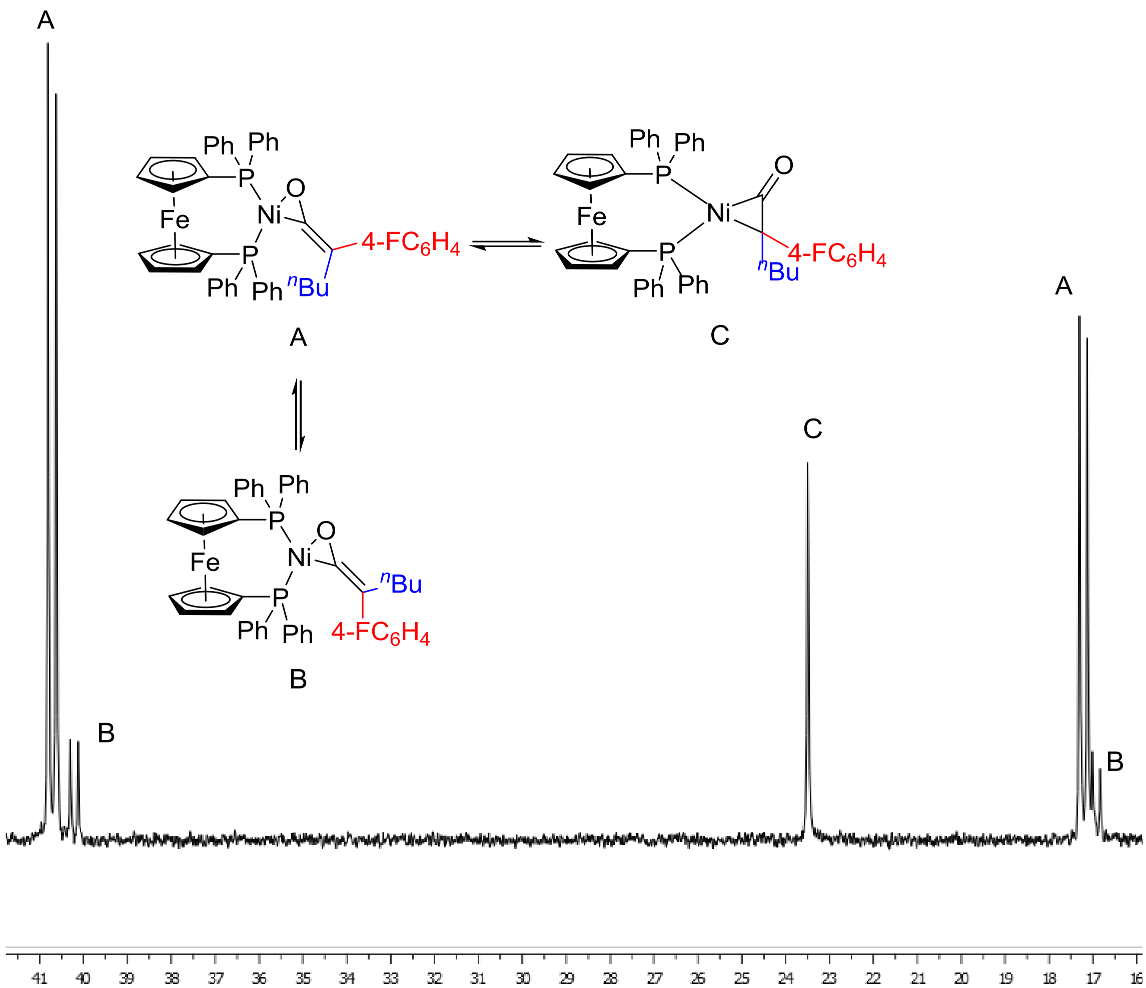

Figure 4.3. ^{31}P spectrum and coordination modes of **8ca**.

carbonyl stretch at 1624 cm^{-1} correspond to a (dppf)Ni–ketene complex where the ketene is C=O coordinated and the aromatic ring is oriented away from the dppf fragment (A, Figure 4.3). This orientation matches what is seen in the solid state by X-ray crystallography. Based on the similarity in chemical shifts and coupling constants, the doublets at 40.2 and 17.0 ppm in the ^{31}P{^{1}H} NMR spectrum and the smallest set of peaks in the ^{1}H NMR spectrum likely correspond to the coordination mode where the ketene is still C=O coordinated, but the aromatic ring is oriented toward the dppf fragment and the isobutyl chain is distal to the Ni center (B, Figure 4.3). Finally, we attribute the singlet that appears at 23.5 ppm in the $^{31}P\{^1H\}$ NMR, the second set of peaks in the Cp region of the ^1H NMR, and the carbonyl stretch at 1743 cm^{-1} to the coordination mode where the ketene is C=C coordinated (C, Figure 4.3), which is often the case in Ir and Rh ketene complexes.[11-12,19] The $^{13}C\{^1H\}$ NMR spectrum of complex **8ca** lacks the signal to noise to see all the peaks for the three coordination modes. Only one carbonyl peak is observed, a ddd at 169.1 ppm (J_{PC} = 41, 7 Hz; J_{FC} = 1 Hz), which we attribute to the coordination mode observed in the solid state (A). The O=C=***C*** carbon gives rise to a doublet of doublets at 76.7 ppm (J_{PC} = 8, 6 Hz). However, the carbon *meta* to fluorine displays a set of three doublets between 117 and 114 ppm, one of each corresponding to each coordination mode. To our knowledge, this is the first example of multiple coordination modes of ketenes observed simultaneously, although it is similar to the coordination of α,β-unsaturated aldehydes and ketones to $CpRe(NO)(PPh3)^+$.[20]

Kinetics of decomposition. The rates of decomposition of **8b**-**e** were measured by ^1H NMR at 100 ˚C in toluene-d_8 (eq 4.3, Table 4.3). The reaction is first order overall and therefore first order in ketene complex with half-lives between 0.48–2.5 h, indicating these complexes are quite stable to thermal decomposition compared to **1a**. A 1:1 mixture of *cis*- and *trans*-alkene products was observed in the decomposition of **8b**. Furthermore, the kinetic isotope effect was investigated by monitoring the decomposition of **8b** and its analogue with a fully deuterated *n*-butyl chain, **8b-*d*₉** (Table 4.3, entries 1 and 2). A k_H/k_D = 1.35 is observed, consistent with secondary kinetic isotope effects, and indicates that in the rate determining step a C-H bond is not broken and that the O=C=***C*** carbon undergoes a change in hybridization. Increasing steric bulk of the alkyl chain from *n*-butyl to *i*-butyl (entry 4) decreases the stability of the complex, but increasing the steric size of the chain

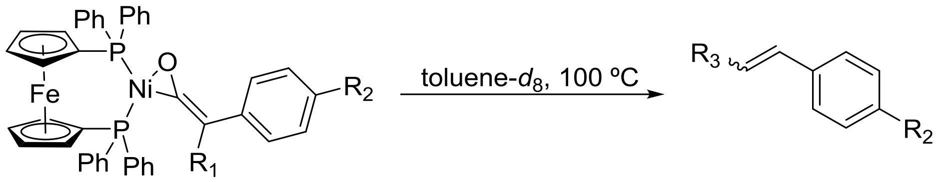

(4.3)

Table 4.3. Kinetics of decomposition of (dppf)Ni(ketene) complexes.

Entry	Complex	R_1	R_2	K_{obs} (x 10^{-4} /s)
1	**8b**	nBu	H	1.0377(5)
2	**8b-*d*$_9$**	nBu-d_9	H	0.771(15)
3	**8ca**	iBu	F	0.997(81)
4	**8cb**	iBu	H	5.02(26)
5	**8cc**	iBu	Me	3.57(32)
6	**8cd**	iBu	OMe	2.69(26)
7	**8d**	iPr	H	2.40(9)

to isopropyl (entry 7) gave a rate constant in-between the *n*-butyl and *i*-butyl. Electronic effects were also investigated with isobutyl alkyl chains. Increasing the donating character from R_2 = H to Me and to OMe (entries 4-6) increases the stability of the complex, and these three data points produce a near perfect Hammett plot with $\rho = 2.31$ vs σ_p (Figure 4.4). These data suggest that negative charge is built up on the O=C=***C*** carbon of the ketene in the rate determining step of the reaction. However, complex **8ca** (entry 3) is an outlier of this relationship, indicating the mechanism of decomposition for this complex is different or has a different rate determining step. Unfortunately, complex **8e** was not kinetically competent. Significant line broadening was observed within the first few time points, indicative of paramagnetic product formation.

Calculation of the reaction coordinate. The mechanism of decomposition of complex **8b** was studied by DFT calculations to gain further insight into the structures and

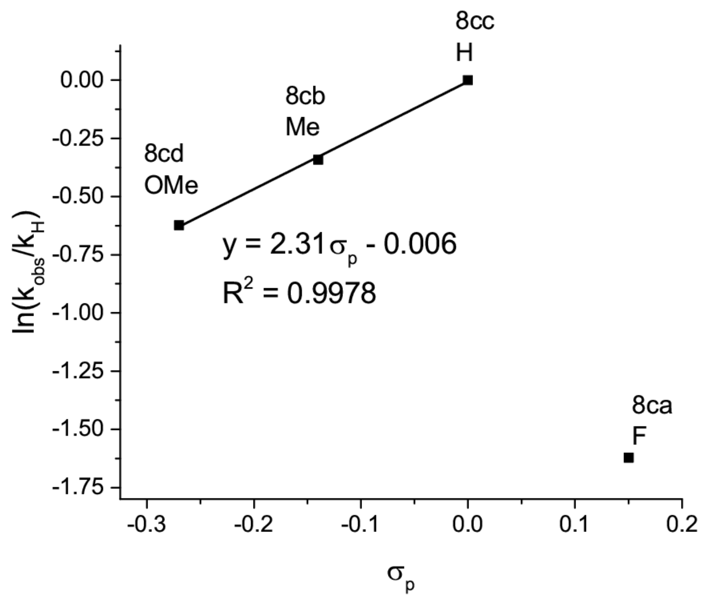

Figure 4.4. Hammett plot of rates of decomposition of (dppf)Ni(aryl isobutyl ketene) complexes.

energies of the intermediates and transition states (Figure 4.5). We found the BP86 functional and a split basis set consisting of tzvp for Ni, P, and the O=C=C fragment and svp for all other atoms reproduced the crystal structure of **8cb**, and this level of theory was used for optimizations and frequency calculations in the study of the decomposition of **8b**. BLYP/6-31G* gave an energy of C=C coordinated complex **9** that was slightly higher than **8b**, consistent with our observation of this species spectroscopically for **8ca**, and the energy of **TS2** (which our experimental data indicate is rate limiting, *vide infra*) that aligned well with the experimental activation energy. Several higher levels of theory were evaluated for single point energy calculations, and they failed to accurately predict these energies (see experimental section for further computational details and benchmarking). Complex **8b** isomerizes from C=O coordination to C=C coordination (**9**) through **TS1**. The C=C bond is then cleaved, leading to carbonyl carbene complex **10** through **TS2**. The energy of this

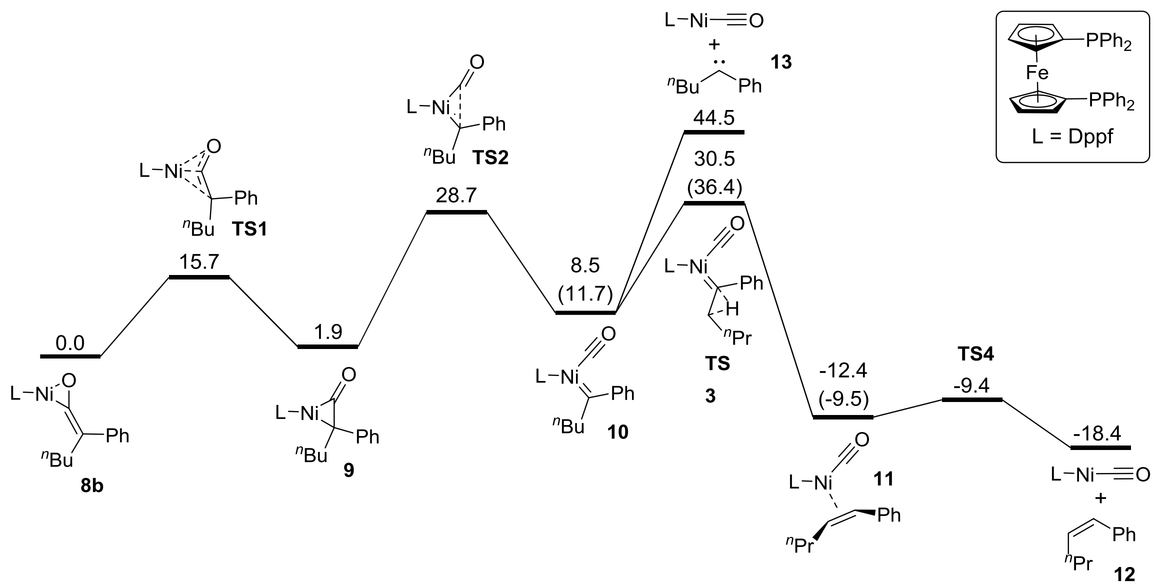

Figure 4.5. Calculated reaction coordinate for the decomposition of **8b**. Units are in kcal/mol relative to **8b**. Numbers in parenthesis describe the formation of the *trans* alkene, where the cis alkene is shown.

transition state, 28.7 kcal/mol agrees with the experimental activation energy of 28.8 kcal/mol, and this step has the largest individual barrier (26.8 kcal/mol) along the calculated pathway. A previous report has found that (dtbpe)Ni(η^2-*(C,C)*-O=C=CH_2) undergoes C-C scission with a $\Delta G^{\ddagger}$ of 41.6 kcal/mol and a ΔG of 38.8 kcal/mol.[21] These numbers are at odds with our theoretical and experimental work, albeit (dtbpe)Ni(O=C=CH_2) is significantly different than our complexes and that work was benchmarked to the dissociation of CO from $Ni(CO)_4$. Subsequent to the decarbonylation event, the carbene rearranges to an alkene via hydrogen transfer in **TS3**. The barrier for this step is 22.0 kcal/mol for the *cis* alkene and 24.7 kcal/mol for the *trans* alkene. Furthermore, the conformation of **10** leading to the *trans* alkene is 3.2 kcal/mol higher in energy than that leading to the *cis* alkene. These barriers for hydrogen migration are less than the barrier for decarbonylation by 2.1–4.8 kcal/mol for the *trans* and *cis* alkenes, respectively. Nevertheless, these transition states represent the second highest individual barrier and the highest point on the reaction coordinate.

We also investigated carbene dissociation of **10** to **13**, which is strongly uphill in energy and therefore not relevant to the decomposition pathway. Complex **11** then undergoes an exergonic alkene dissociation to form three-coordinate (dppf)Ni(CO), which is highly reactive and explains the observation of (dppf)Ni$(CO)_2$ by IR in samples subjected to kinetic analysis.

In addition, we investigated the possible role of partial phosphine dissociation in each step. Dissociation of one P atom from the C=O coordinated complex **8b** was found to be endergonic by 22.2 kcal/mol. Given the lower energy required to reach **TS1**, we believe dissociation of a phosphine from **8b** is irrelevant to the mechanism. In contrast, phosphine dissociation from C=C coordinated complex **9** may be thermodynamically and kinetically competent (Figure 4.6). The barrier for decarbonylation with one P atom coordinated (**9a**) is 20.3 kcal/mol, significantly less than the experimental activation energy of 28.4 kcal/mol. However, the barrier for re-association of the tethered phosphine arm in complex **9a** is only 1.9 kcal/mol. Furthermore, phosphine dissociation from the carbonyl carbene complex **10** has a barrier of only 1.0 kcal/mol (to **TS6**) and is actually downhill in energy by 4.4 kcal/mol (to **10a**) (Figure 4.7). The transition states for hydride transfer with partial phosphine dissociation are 35.0 and 34.6 kcal/mol relative to **8b** for the *cis* and *trans* alkenes, respectively, and the conformation of the carbonyl carbene complex that leads to the *cis* alkene is 1.5 kcal/mol higher in energy than that leading to the *trans* alkene.

Resting state of multiple coordination modes of the ketene. The spectral and crystallographic data of our ketene complexes indicate that the C=O coordination mode

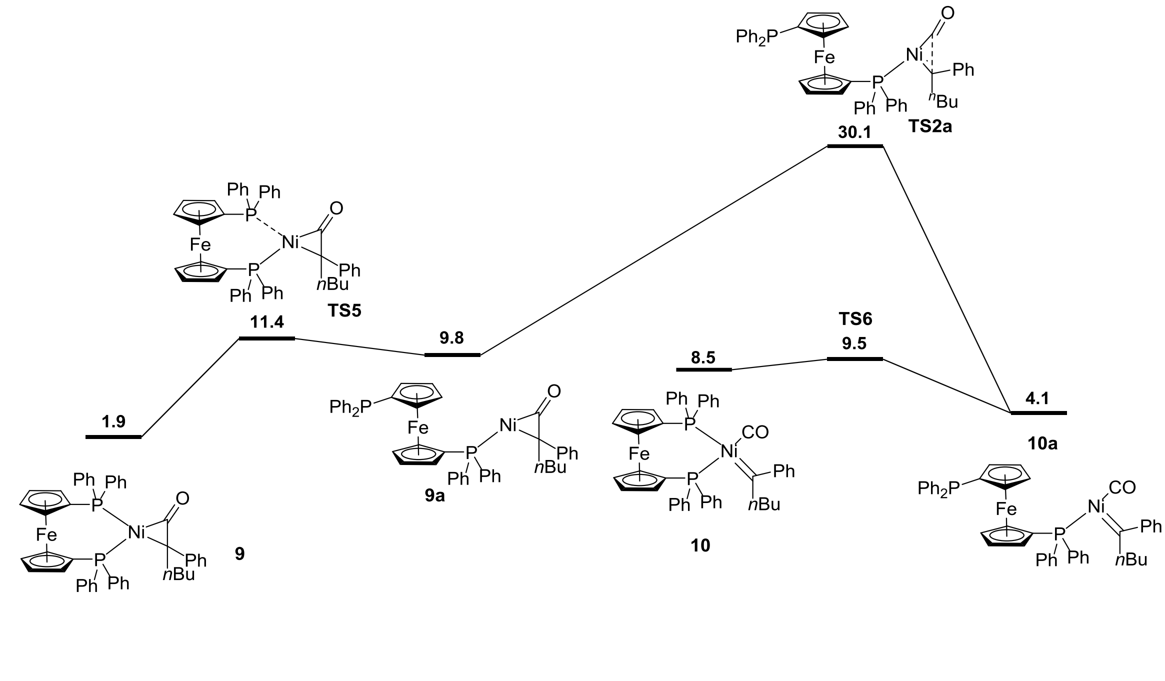

Figure 4.6. Calculated reaction coordinate of decarbonylation with partial phosphine dissociation.

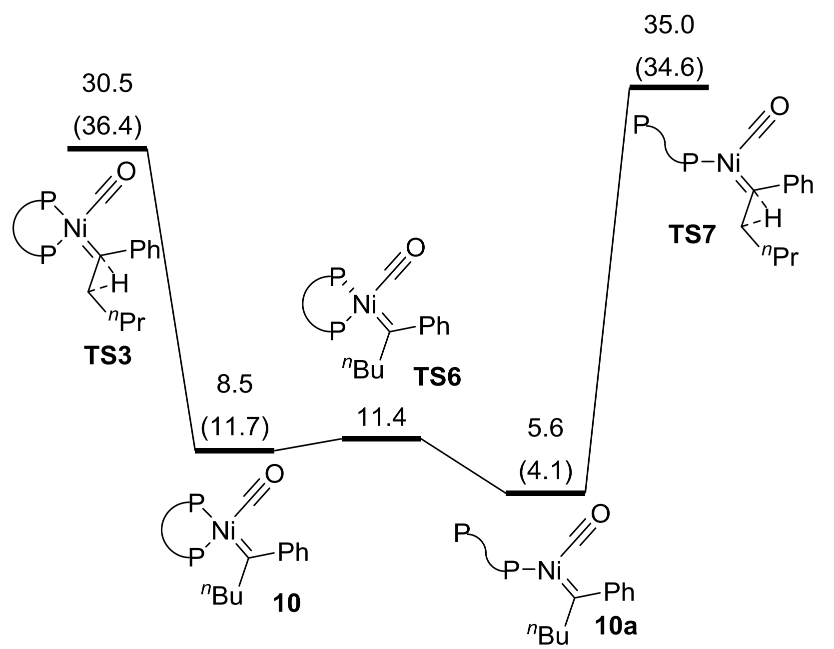

Figure 4.7. Calculated reaction coordinate of hydride migration with partial phosphine dissociation.

with the ketene's aryl group oriented away from the Ni atom is the thermodynamic minimum. In the solid state, the aromatic group of the ketene is oriented away from the Ni atom and the alkyl group is toward the (dppf)Ni fragment. The spectral data of **8ca** indicate the existence of two other coordination modes that have similar energies to the isomer observed in the solid state. The first of these is also CO coordinated, with the aryl and alkyl groups interchanged such that the alkyl group is oriented away from the Ni atom and the arene is in the π-stacking interaction with one of the dppf phenyl rings (B, Figure 4.3). Our calculations indicate this coordination mode is 2.6 kcal/mol higher in energy for complex **8b**. The third isomer has the ketene coordinated via the C=C bond (C, Figure 4.3). Isomer C gives a singlet in the $^{31}P\{^{1}H\}$ NMR, indicating that the ketene is freely rotating. The calculated energy of **9** relative to **8b** (1.9 kcal/mol) also corroborates the assignment of our spectral data to this coordination mode. Furthermore, the calculated barrier for isomerization of **8b** to **9** of 15.7 kcal/mol agrees well with the experimental barrier of 14 kcal/mol for the isomerization of **1a** based on line broadening in the ^{1}H spectrum at low temperature.[7]

Evidence for rate limiting decarbonylation. Our calculations indicate that the decarbonylation step has the highest barrier for an individual step in the pathway, and that the hydride migration is the highest point on the pathway thereby restricting the possible rate determining step to these two options. The kinetic isotope effect observed for **8b** and **8b-*d*$_9$** (1.35) rules out C-H bond scission in the rate determining step, and is consistent with several β and γ secondary KIEs associated with rehybridization of the O=C=***C*** carbon during the rate determining step. Mayer bond order analysis suggests a change of hybridization occurs for the O=C=***C*** carbon during decarbonylation: the difference in C=C bond order in complex **9**, which is 0.948, and the free ketene, which is 1.564, indicates significant back bonding into the C=C bond and that the hybridization of the O=C=***C*** carbon of complex **9** lies in-between sp^3 and sp^2, while in complex **10**, this carbon is a carbene, which is sp^2 hybridized. Furthermore, the value of ρ (2.31) indicates significant buildup of negative charge on the O=C=***C*** carbon during the rate determining step for complexes **8cb-8cd**. Mulliken analysis of intermediates associated with decarbonylation and hydride transfer shows significant buildup of negative charge on the O=C=***C*** carbon atom during decarbonylation and not during hydride migration. This carbon atom has a -0.19 charge in C=C coordinated complex **9**, -0.36 in carbonyl carbene complex **10**, and -0.38 in carbonyl alkene complex **11**. The buildup of charge on this carbon during decarbonylation can be easily rationalized since it gains a lone pair. Thus, the combination of KIE and linear free energy relationship (LFER) analysis, aided by DFT calculations, indicate decarbonylation is rate limiting in most cases. We benchmarked our single point energies accordingly, and the fit is excellent. Applying the rates derived from the DFT calculations to the steady state approximation (eq 4.4) for an equilibrium between C=O and C=C coordinated ketene complexes followed by scission of the C=C bond (eq 4.5) gives a rate constant of 1.28×10^{-4} Hz, which is in excellent agreement with experimental rate of 1.034×10^{-4} Hz. This indicates that our computational model fits the kinetic data very well and that decarbonylation is rate limiting for complex **8b**. Furthermore, Mulliken analysis reveals that **8b** and **9** are essentially Ni(II) species, whereas **10** is nearly Ni(0). Decarbonylation is therefore a reductive process with regard to the Ni center, and we predict that more electron donating phosphines will stabilize Ni–ketene complexes even more effectively than dppf.

$$k = \frac{k_1 k_2[\mathbf{8b}]}{k_{-1} + k_2} \tag{4.4}$$

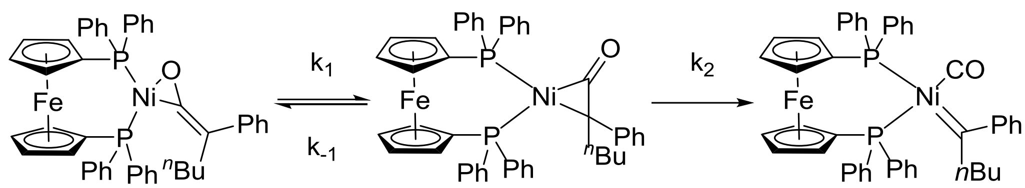

(4.5)

Mechanism of hydrogen atom migration. Following decarbonylation, the carbene ligand rearranges to an alkene. To do so, the β hydrogen must migrate to the α carbon. A close examination of transition state **TS3-cis** (Figure 4.8) shows the migrating hydrogen atom is orthogonal to the nodal plane of the π-bond that is formed. Thus, the hydrogen transfer involves orbital overlap between the carbene sp^2 orbital that contains the lone pair and the C-H σ* as well as overlap between the filled C-H σ and empty carbene p orbitals. Consequently, the transfer involves a hydride rather than a proton or an $H^{\bullet}$. However, from our computational model, it is difficult to say if this step occurs with or without phosphine dissociation. Application of the Curtin-Hammett principle to the energies associated with hydride transfer with both phosphine associated (*vide supra*) gives a cis:trans ratio of 49:1. A ratio of 1:2 is predicted with partial phosphine dissociation, albeit the barriers for hydride migration with one phosphorus coordinated to Ni are unrealistically high. It is difficult to be certain where the error in our computational model is: either the barriers for hydride transfer with partial phosphine dissociation or the $\Delta\Delta G^{\ddagger}$ for the *cis* and *trans* alkene isomers without partial phosphine dissociation have been overestimated.

Hydride transfer is rate limiting in some cases. Complex **8ca**, which possesses

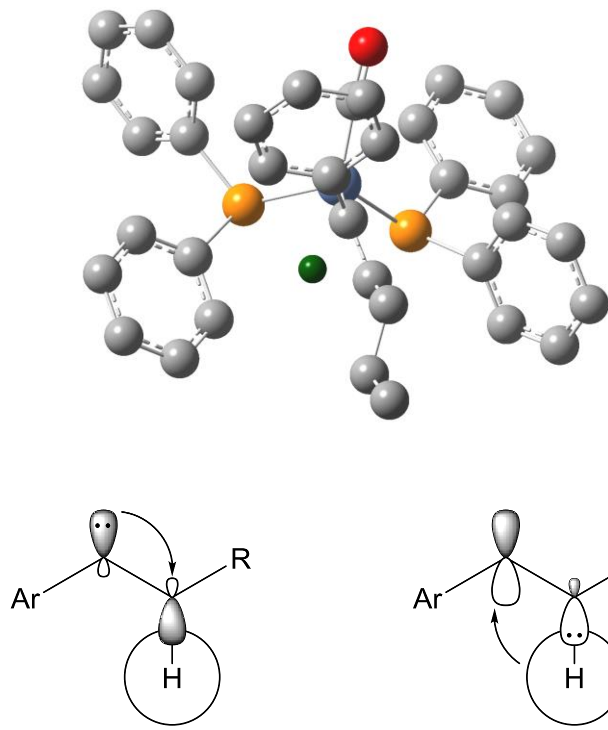

Figure 4.8. Optimized structure of **TS3-Cis** and simplified orbital interactions for hydride migration.

an electron withdrawing *p*-fluorophenyl on the ketene, is a clear outlier of the LFER (Figure 3.4). Extrapolation of the LFER gives a rate of decarbonylation of 7.06 x 10^{-4} Hz, significantly faster than the observed rate. The reason decomposition is much slower for this complex is likely twofold. First, the electron withdrawing group allows for greater stabilization of the buildup of negative charge on the O=C=***C*** carbon during decarbonylation thereby enhancing the rate of this step. Furthermore, the hydride migration step is attenuated by electron withdrawing groups. That is, the nucleophilicity of the carbene sp^2 orbital containing the lone pair and the electrophilicity of the empty carbene p orbital are both attenuated by the electron withdrawing group. We therefore believe **8ca** defies the LFER because of accelerated decarbonylation and decelerated hydride migration to the point where hydride migration, rather than decarbonylation, is rate limiting.

Another outlier of the trends associated with ketene complex decomposition is complex **8d**. Though the electronic character between complexes **8b**, **8cb**, and **8d** are the same, the steric bulk of the alkyl substituent steadily increases (i.e., *n*-butyl < *i*-butyl < *i*-propyl) yet the rate of decomposition both increases then decreases for this series of complexes. That is, complex **8cb** decomposes ~5 fold faster than complex **8b**; yet complex **8d**, which one would expect to have an even higher rate of decomposition than complex **8cb**, decomposes ~2 fold slower than complex **8cb** (i.e., rates of decomposition display the following trend: **8b** < **8cb** > **8d**).

Our calculations suggest that a deviation in the rate limiting step for the decomposition of complex **8d**, as well as **8ca**, occurs, albeit for two different reasons. In these cases, hydrogen migration is rate determining. Inspection of complex **10** (the carbonyl carbene complex of **8b**) reveals that this intermediate has the orbital overlap necessary for hydride migration (Figure 4.9A) in its lowest energy conformation. The Ni–C-C-H dihedral of complex **10** is -122.84˚, similar to that of **TS3-Cis**, which has a dihedral of -81.33˚, a difference of less than an anti–gauche isomerization. On the other hand, the carbonyl carbene complex of **8d** has a Ni–C-C-H dihedral of -9.90˚, indicating that this complex must undergo significant rotation about the C-C bond to adopt the orbital overlap necessary for hydride transfer. Furthermore, rotation of the isopropyl group is significantly more energetically demanding than for an *n*- or *iso*-butyl group. We therefore propose that the hydrogen migration is rate limiting with large alkyl groups (such as those in **8d**) as well in **8ca**).

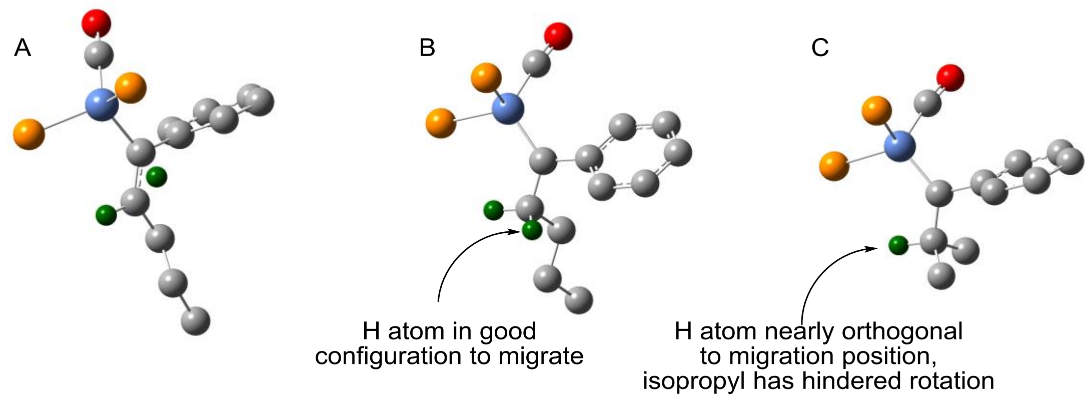

Figure 4.9. A) Truncated structure of **TS3-Cis**. B) Truncated structure of **10**, the carbonyl carbene complex of **8b**. C) The carbonyl carbene complex of **8d**.

Decarbonylation with partial phosphine dissociation is relevant for monodentate phosphines. Despite the lower barrier for the decarbonylation step with one phosphine associated, partial phosphine dissociation is clearly not relevant to the decomposition of ketene complexes with bidentate phosphines. Applying the steady state approximation rate equation (eq 4.4) to the reaction in eq 4.6, where an equilibrium exists between the C=C coordinated complex with either one or two phosphines associated, followed by decarbonylation, gives a k_{obs} of 1.83 x 10^{-5} Hz, which is ~5 fold slower than the experimental rate. Nevertheless, this pathway could be highly relevant for ketene complexes with monodentate phosphines, which are known to be quite unstable. When the phosphine is not tethered to the complex (eq 4.7), phosphine dissociation is entropically favored, thereby increasing the population of species B. Furthermore, the steady state approximation for this pathway (eq 4.8) is distinct from the steady state approximation for a bidentate phosphine, and has the concentration of phosphine in the denominator. The phosphine concentration is very low, and the overall rate of decarbonylation with one phosphine associated should increase greatly compared to bidentate phosphines. This explains the inherent instability of Ni ketene complexes with monodentate phosphine ligands.

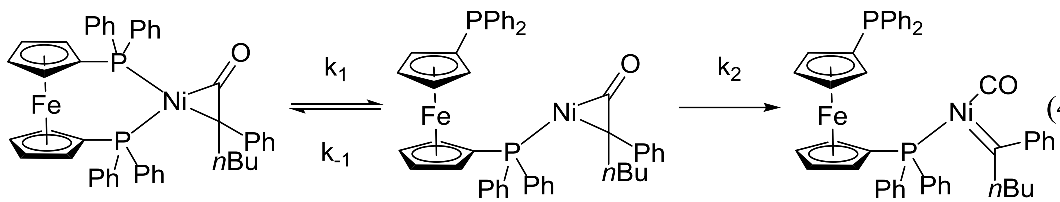

(4.6)

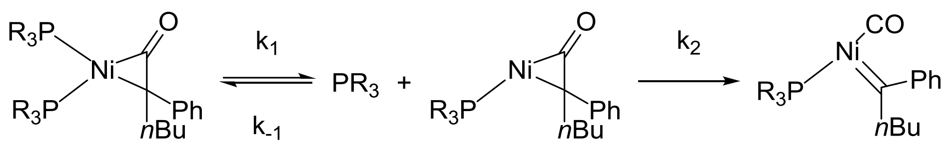

(4.7)

A B

$$k = \frac{k_1 k_2[\mathbf{A}]}{k_{-1}[\mathbf{PR_3}] + k_2} \tag{4.8}$$

DPEphos nickel ketene complexes. In addition to dppf, DPEphos was found suitable for the synthesis and stabilization of nickel–ketene complexes. Several complexes were synthesized in a similar fashion to the dppf complexes (equation 4.9) in good yields (Table 4.4). The characterization data indicate there is some of the η2 CC coordination in solution with complex **13ca**, albeit in a significantly reduced amount compared to **8ca**. This is rationalized by comparing the crystal structures of **13e** (Figure 4.10) and **8e**, which reveals the phenyl ring containing C(25) is significantly closer to the oxygen atom (the centroid to oxygen distance is 4.086 for **8e** and 3.682 for **13e**), blocking η2 CC coordination. Rates of decomposition for some of these complexes were measured at 100º(Table 4.4). The observed rate constants are generally an order of magnitude higher those for the dppf complexes, indicating DPEphos is not as good at stabilizing the ketene as dppf.

Table 4.4. (DPEphos)Ni(ketene) complex yields and decomposition rates.

Complex	R	Ar	Yield (%)	k_{obs} (x10^{-3} /s)
13a	Ph	Ph	87	
13b	*n*Bu	Ph	63	15(5)
13ca	*i*Bu	*p*-FC_6H_4	78	10(2)
13cb	*i*Bu	Ph	70	2.7(2)
13cc	*i*Bu	*p*-MeC_6H_4	78	21(2)
13d	*i*Pr	Ph	61	41(4)
13e	*s*Bu	Ph	76	

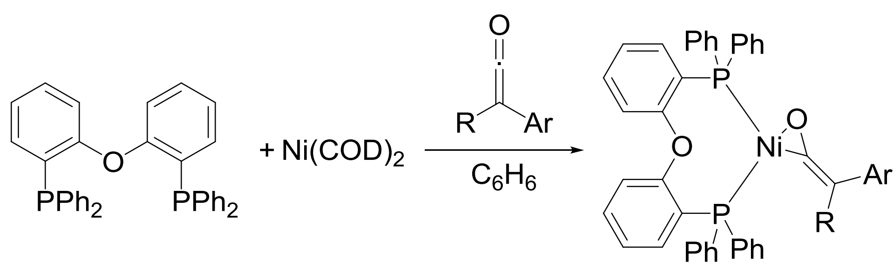

(4.9)

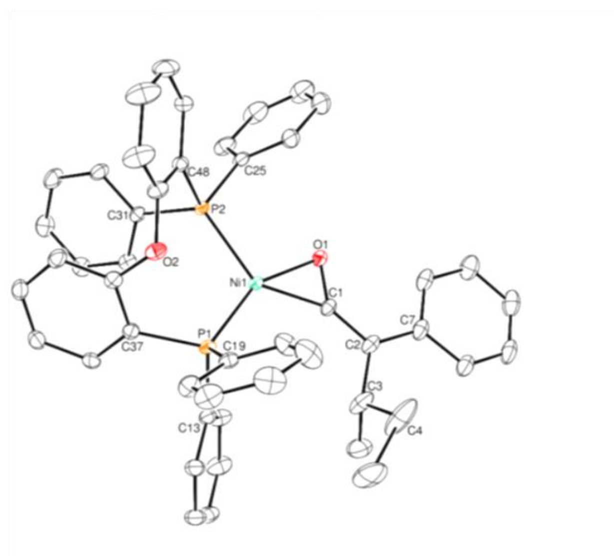

Figure 4.10. ORTEP diagram of **13e**

Interestingly, the trends associated with sterics and electronics are reversed compared to those of the dppf complexes. Increasing steric bulk from *n*Bu to *i*Bu leads to a stark decrease in rate, and increasing again to *i*Pr gives an increase in rate. Similarly, going from the electron poor **8ca** to neutral **8cb** and to electron rich **8cc** gives a decrease and then an increase in rate. These results are difficult to rationalize in light of the mechanistic understanding of the decomposition of the dppf complexes. Perhaps the most likely explanation is that the rates of decomposition of complexes **8** were measured with samples that had passed elemental analysis and were therefore of high purity, whereas samples of **13** subjected to kinetic analysis were not necessarily of such high purity.

Conclusion

Dppf was discovered to be a uniquely suitable ligand for the generation of stable Ni–ketene complexes, and we were able to synthesize and characterize a library of (dppf)Ni[O=C=C(Ar)(R)] complexes. Crystallographic data reveal that the ketene is C=O coordinated with the ketene's aryl group distal to the Ni atom. Spectroscopic data reveal that the coordination mode observed in the solid state predominates in solution, and C=O coordination with the aryl group oriented toward the (dppf)Ni fragment and C=C coordination are both observed. A combined experimental and theoretical approach was used to elucidate the mechanism of decomposition of these complexes which involves a rate determining step of either decarbonylation or hydride transfer. That is, decarbonylation was determined to be the rate determining step for **8b** through kinetic isotope effect and Mayer bond order analyses. Similarly, a LFER for **8cb-8cd** combined with Mulliken analysis suggested decarbonylation and not hydride migration was rate limiting for these complexes. Electron poor and sterically large ketenes decompose with rates that do not fit the trends for the complexes with rate limiting decarbonylation. Our computational model provided a rationale for why the hydride transfer is attenuated and becomes rate limiting in these cases.

Importantly, our calculations revealed that the Ni center is reduced during decarbonylation. We believe that more electron rich phosphines should further stabilize Ni–ketene complexes and are currently investigating this hypothesis. Furthermore, decarbonylation is more facile with one phosphine associated, explaining the instability of known Ni–ketene complexes with monodentate phosphines.

This report bridges the gap between the instability of the known Ni–ketene complexes and their use as intermediates in synthesis. We believe that knowledge of the mechanism of decomposition of Ni–ketene complexes, particularly the fact that bidentate phosphines stabilize these complexes, will lead to improvement of known reactions of Ni–ketene complexes and aid in the development of further reactions that use these complexes as intermediates.

Experimental Section

General considerations. All reactions were carried out under an atmosphere of N_2 in a glovebox. All glassware was oven dried. Benzene and pentane were sparged with nitrogen, dried over neutral alumina, and deoxygenated over Q5 under N_2 using a Grubbs type solvent purification system. Dppf, dppe, dppp, dppb, dppbenzene (strem) triphenylphosphine, 1,3,5-trimethoxybenzene (sigma), and *n*-butyl bromide-d_9 (Cambridge Isotope) were purchased and used as received. $Ni(COD)_2$ was purchased from strem or synthesized according to the literature procedure.[22] Diphenylketene[23] and aryl alkyl ketenes[24] were prepared according to the literature procedures. Deuterated benzene (sigma), deuterated toluene, and deuterated THF (Cambridge isotope), were distilled from CaH_2 and degassed by three freeze pump thaw cycles. Screw-cap NMR tubes were used for all NMRs. The tubes were cleaned by rinsing with acetone, sonicating with 1:1 THF/concentrated HCl for 1 h to remove residual Ni, and rinsed with water. ^{1}H Nuclear Magnetic Resonance spectra were acquired at 300, 400, or 500 MHz. ^{13}C spectra were recorded at 100 or 125 MHz. ^{31}P spectra were recorded at 121 MHz. All ^{13}C and ^{31}P NMR spectra were proton decoupled. ^{1}H and ^{13}C spectra were referenced to residual solvent peaks (C_6D_6 δ 7.15 and δ 128.6; THF-d_8, δ 3.76 and δ 68.0, respectively). ^{31}P NMR shifts were reported with respect to external 85% H_3PO_4 (0 ppm). IR spectra were recorded on a Bruker Tensor 27 FT-IR spectrometer. X-ray crystallography data were collected and analyzed by Dr. Atta Arif at the University of Utah. Elemental analysis was performed by Midwest Microlabs LLC.

Reaction of PPh_3, $Ni(COD)_2$, and phenyl butyl ketene. A solution of PPh_3 (19.6 mg, 0.075 mmol) in 1.5 mL C_6D_6 was added to $Ni(COD)_2$ (20.4 mg, 0.075 mmol) and the solution stirred for 5 min. An aliquot (0.75 mL, 0.0375 mmol) was added to phenyl butyl ketene (19.6 mg, 3 eq) and the two solutions stirred for 2 h, at which point they were analyzed by ^{31}P and ^{1}H NMR. The solution containing no ketene displayed only a sharp singlet at 40.0 ppm in the ^{31}P NMR, consistent with $(PPh_3)_2Ni(COD)$. The ^{1}H NMR spectrum was consistent with a 1:1 mixture of $(PPh_3)_2Ni(COD)$ and free cyclooctadiene. The spectrum of the solution containing ketene had two broad singlets at 41.6 and 33.8, indicating that the $(PPh_3)_2Ni(COD)$ had been consumed. ^{1}H NMR of this sample was not possible due to paramagnetic contaminants. IR spectroscopy revealed six carbonyl peaks, indicative of several carbonyl complexes, including *cis*–$(PPh_3)_2Ni(CO)_2$.

Reaction of $Ni(COD)_2$, dppe, and diphenylketene. A solution of $Ni(COD)_2$ (22.5 mg, 0.0818 mmol) and dppe (32.6 mg, 0.0818 mmol) in C_6H_6 was stirred for 5 min and added to diphenylketene (23.8 mg, 0.123 mmol, 1.5 equiv) and stirred overnight. ^{31}P NMR revealed a singlet at 44.7 ppm, consistent with $(dppe)_2Ni$.

Reaction of $Ni(COD)_2$ with dppe, dppb, dppb, and dppbenzene. $Ni(COD)_2$ (22.5 mg, 0.0818 mmol) and an equimolar amount of bidentate phosphine were dissolved in C_6H_6 (0.75 mmol) and stirred for 4 h before being analyzed by ^{31}P NMR. Dppe resulted in two singlets at 51.3 and 44.6 ppm, the second of which is consistent with $(dppe)_2Ni$[16] while dppp gave two singlets at 21.3 and 12.7 ppm (the second of these is consistent with $(dppp)_2Ni$),[25] dppb gave singlets at 35.5 and 17.6 ppm, and dppbenzene displayed singlets at 55.8 and 47.8 ppm.

(Dppf)Ni(COD). was prepared according to a modified literature procedure. $Ni(COD)_2$ (496.2 mg, 1.8 mmol, 1 equiv) was weighed into a 20 mL scintillation vial. Dppf (1.000 g, 1.8 mmol, 1 equiv) was weighed into a 4 mL vial and transferred to the vial containing $Ni(COD)_2$. Residual dppf was washed into the 20 mL vial with 5x 2mL C_6H_6. Copious orange precipitate forms immediately. The reaction was stirred for 2.5 h, and pentane (10 mL) was added. After an additional hour, the solids were collected by filtration, washed 3x 10 mL pentane, dried under vacuum, and transferred to a tared vial to yield 1.1527 g, 89% of an orange solid. ^{1}H and ^{13}C NMR data agree with the literature.[17]

General procedure for setup of (dppf)Ni(ketene) complexes. In the drybox, $Ni(COD)_2$ (100 mg, 0.363 mmol, 1 eq) and dppf (201.5 mg, 0.363 mmol, 1 eq) were weighed into a 20 mL scintillation vial. Benzene (3 mL) was added and the solution stirred for 2 min, at which point ketene (1.09 mmol, 3 eq) was added in 2 mL benzene.

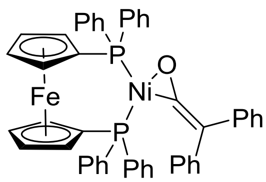

(Dppf)Ni(diphenylketene), 8a. was synthesized according to the general procedure using diphenylketene (141.2 mg, 0.727 mg, 2 eq). The reaction was stirred for 24 h and pentane (15 mL) was added. After an additional 24 h, the solids were collected by filtration, washed 3x 10 mL pentane, and dried under vacuum to yield 249.5 mg (85% yield) of an orange powder. Crystals suitable for X-ray crystallography were obtained by allowing a 1/3 scale reaction to sit unstirred for 48 h, followed by diffusion of pentane into the reaction mixture. ^{1}H NMR (400 MHz, C_6D_6): δ 8.12 (d, J = 8 Hz, 2H), 8.05 (t, J = 10 Hz, 4H), 7.84 (dd, J = 8 Hz, 12 Hz, 4H), 7.31 (t, J = 8 Hz, 2H), 7.12 (s, 1H), 7.00 (m, 14 H), 6.62 (t, J = 8 Hz, 1H), 6.53 (t, J = 8 Hz, 2H), 4.26 (d, 2H), 3.86 (s, 2H), 3.72 (d, 2H), 3.63 (s, 2H). ^{13}C{^{1}H} NMR (100.6 MHz, C_6D_6): δ 168.32 (dd, J = 44, 7 Hz, O=*C*=C) 142.73 (d, J = 3 Hz), 142.34 (d, J = 8 Hz), 125.95 (d, J = 34 Hz), 135.65 (d, J = 14), 135.33 (d, J = 14 Hz), 134.25 (dd, J = 2 Hz, 41 Hz), 133.64 (s), 130.87 (dd, J = 2 Hz, 9 Hz), 129.26 (d, J = 9 Hz), 127.61 (s), 124.92 (s), 123.09 (s), 86.14 (d, J = 56 Hz), 76.06 (d, J = 44 Hz), 75.08 (d, J = 11 Hz), 74.67 (d, J = 9 Hz), 73.36 (d, J = 5 Hz), 71.95 (d, J = 5 Hz). ^{31}P{^{1}H} NMR (121 MHz, C_6D_6): δ 39.59 (d, J = 19.4 Hz), 17.65 (d, J = 20.6 Hz). IR (nujol, NaCl): 2351 (w, CC), 1614 (s), 1581 (s, CO), 1488 (s), 1307 (m), 1292 (m), 1235 (s), 1201 (w), 1169 (m), 1157 (m), 1098 (s), 1071 (m), 1028 (m), 999 (m), 930 (m), 898 (w), 866 (w), 841 (w), 822 (m) cm^{-1}. Several attempts gave elemental analyses that were low in both carbon and hydrogen.

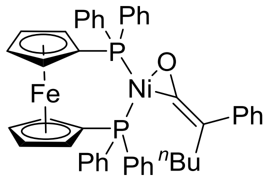

(Dppf)Ni(butylphenylketene), 8b. was prepared according to the general procedure using phenyl butyl ketene (126.7 mg, 0.727 mmol, 2 equiv). The reaction was stirred for 36 h, at which point the reaction was a yellow-orange suspension. The solids were collected by filtration, washed 3x 10 mL pentane, and dried under vacuum to yield 226.1 mg, 79% of a yellow powder. Crystals suitable for X-ray crystallography were obtained by allowing a 1/3 scale reaction to sit unstirred for 48 h, followed by diffusion of pentane into the reaction mixture. Lowering the concentration of the reaction mixture led to no precipitation over several days, followed by precipitation of (dppf)Ni(CO)(μ-dppf)(CO)Ni(dppf) (**14**), which was studied crystallographically (CCDC #1500884). The unit cell of this complex was observed several times in attempts to obtain crystal structures of other complexes **8**. Attempts to study this species spectroscopically failed due to insolubility. ^{1}H NMR (400 MHz, C_6D_6): δ 8.23 (d, *J* = 8 Hz, 2H), 8.11 (m, 4H), 8.00 (t, *J* = 8, 4 H), 7.45 (t, *J* = 8 Hz, 2H), 7.00-7.07 (m, 13H), 4.29 (d, 2H), 3.89 (s, 2H), 3.74 (d, 2H), 3.66 (s, 2H), 2.15 (t, *J* = 8 Hz, 2H), 1.36-1.26 (s, 2H), 0.59 (s, 5H). ^{13}C{^{1}H} NMR (125 MHz, THF-d_8): 168.6 (dd, J = 41, 9 Hz, O=*C*=C), 140.9 (d, J = 8 Hz), 136.7 (d, J = 34 Hz), 136.4 (d, J = 15 Hz), 135.8 (d, J = 13 Hz), 135.7 (dd, J = 41, 3 Hz), 131.6 (dd, J = 69, 1 Hz), 129.9 (d, J = 10 Hz), 129.7 (s), 129.6 (d, J = 10 Hz), 128.6 (s), 126.0 (s), 121.7 (s), 85.6 (dd, J = 49, 6 Hz), 79.1 (dd, J = 8, 6 Hz, O=C=*C*), 76.9 (d, J = 44 Hz), 75.9 (d, J = 11 Hz), 75.4 (d, J = 8 Hz), 74.3 (d, J = 6 Hz), 72.5 (d, J = 6 Hz), 32.9 (d, J = 4 Hz), 31.3 (s), 27.0 (s), 16.4 (s). ^{31}P{^{1}H} NMR (121 MHz, C_6D_6): δ 42.03 (d, *J* = 23 Hz), 17.10 (d, *J* = 23 Hz). IR (nujol, NaCl): 1911 (w), 1657 (w), 1624 (s, CO), 1584 (s), 1491 (s), 1479 (s), 1435 (s), 1337 (w), 1306 (m), 1267 (s), 1213 (m) 1196 (m), 1184 (s) 1166 (s), 1093 (s), 1075 (w), 1031 (s), 1014 (m), 998 (m), 913 (w), 891 (w), 834 (m), 824 (m), 791 (w) cm^{-1}. Anal. Calcd. for $C_{46}H_{42}FeNiOP_2$: C, 70.17; H, 5.23. Found: C, 70.30; H, 5.45.

***n*-Butyl phenyl ketene-*d*$_9$.** was synthesized according to the literature procedure[24] starting from *n*-butyl bromide-*d*$_9$ instead of *n*-butyl bromide. 4.18 g of acyl chloride were used to synthesize the ketene, of which 1.74 (50 %) was isolated with >95% deuteration. ^{1}H NMR (500 MHz, C_6D_6): 7.09 (t, J = 10 Hz, 2H), 6.90 (m, 3H), 2.00 (t, J = 7.5 Hz, 0.08H), 1.25 (m, 0.10H), 1.16 (m, 0.09H), 0.74 (t, J = 7.5 Hz, 0.12H).

(Dppf)Ni(butylphenylketene-*d*$_9$), 8b-*d*$_9$. was prepared in the same fashion as **8b** with *n*-butyl phenyl ketene-*d*$_9$ on the same scale. 206.3 mg (72%) of an orange powder was isolated with >95% deuteration. ^{1}H NMR (500 MHz, C_6D_6): δ 8.23 (d, J = 8 Hz, 2H), 8.11 (m, 4H), 8.00 (m, 4 H), 7.45 (t, J = 8 Hz, 2H), 7.00-7.07 (m, 13H), 4.29 (d, 2H), 3.89 (s, 2H), 3.74 (d, 2H), 3.66 (s, 2H), 2.15 (0.05 H), 1.36-1.26 (0.16 H), 0.59 (0.1 H).

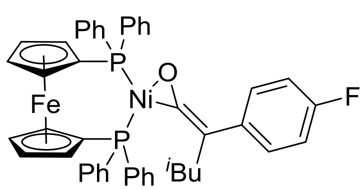

(Dppf)Ni(*p*-fluorophenyl isobutyl ketene), 8ca. was synthesized according to the general procedure with *p*-fluorophenyl isobutyl ketene (129.5 mg, 0.727 mmol, 2 equiv). The reaction was stirred for 2.5 h, pentane (15 mL) was added, and the mixture was stored at -40 ºC overnight. The solids were collected by filtration, washed 4x 10 mL pentane, and dried under vacuum. The product was isolated as a red solid (222.5 mg, 79%). Crystals suitable for X-ray crystallography were grown by layering 1 mL of a saturated benzene solution of the complex with 0.5 mL benzene then 2.5 mL pentane. This crystallization produced a large quantity of red crystals along with two yellow crystals which were identified as (dppf)Ni(*p*-fluorophenyl isobutyl ketene dimer) (**15**) by crystallography (CCDC #1500895). ^{1}H NMR (400 MHz, C_6D_6): δ 8.07 (m, 3.90H), 7.98

(m, 3.79H), 7.93 (m, 2.21H), 7.11 (br, 5.49H), 7.05-6.96 (m, br, 9.36H), 4.26 (d, J = 5 Hz, 1.74H), 4.24 (br, 0.26H), 3.91 (br, 1.75H), 3.86 (br, 0.25H), 3.77 (br, 0.25H), 3.74 (br, 1.74H), 3.65 (br, 1.97H), 2.01 (d, J = 5 Hz, 1.79H), 1.91 (m, J = 5 Hz, 0.86H), 1.15 (d, J = 5 Hz, 0.79H), 0.49 (d, J = 5 Hz, 5.62H). $^{13}C\{^1H\}$ NMR (100.6 MHz, C_6D_6): δ 169.1 (ddd, J_{PC} = 41, 8 Hz, J_{CF} = 1 Hz), 160.5 (d, J_{CF} = 238 Hz), 160.0 (d, J_{CF} = 245 Hz), 137.4 (dd, J = 8, 3 Hz), 136.4 (s), 136.0 (d, J = 34 Hz), 135.7 (d, J = 15 Hz), 135.6 (d, J = 18 Hz), 135.31 (d, J = 32 Hz), 135.26 (d, J = 14 Hz), 134.9 (d, J = 2 Hz), 131.049 (d, J = 2 Hz), 131.046 (dd, J = 50, 2 Hz), 129.9 (d, J = 7 Hz), 129.4 (d, J = 10 Hz), 129.2 (d, J = 10 Hz), 129.1 (s), 128.9 (s), 128.7 (s), 128.5 (s) these three peaks overlap with the residual solvent peak, 127.8 (d, J = 6 Hz), 116.1 (d, J = 21 Hz), 115.8 (d, J = 21 Hz), 115.3 (d, J = 20 Hz), 114.6 (d, J = 20 Hz), 85.9 (dd, J = 42, 5 Hz), 76.8 (d, J = 44 Hz), 76.7 (dd, J = 8, 6 Hz), 75.3 (d, J = 11 Hz), 75.0 (d, J = 10 Hz), 74.8 (d, J = 9 Hz), 74.6 (s) possibly a doublet that overlaps with the previous peak, 73.4 (d, J = 6 Hz), 73.3 (d, J = 6 Hz), 72.0 (d, J = 5 Hz), 71.7 (d, J = 5 Hz), 44.8 (d, J = 6 Hz), 41.1 (d, J = 4 Hz), 33.7 (s), 32.4 (s), 30.7 (s), 29.1 (s), 26.9 (s), 23.6 (s), 23.3 (s), 23.2 (s), 23.1 (s). $^{31}P\{^1H\}$ NMR (121 MHz, C_6D_6): δ 40.8 (d, J = 22 Hz), 40.2 (d, J = 21 Hz), 23.5 (s), 17.3 (d, J = 22 Hz), 17.0 (d, J = 21 Hz). IR (nujol, NaCl): 1743 (s), 1597 (w), 1505 (s), 1436 (s), 1306 (m), 1216 (m), 1611 (s), 1032 (m), 885 (w), 837 (w), 748 (w), 723 (w), 696 (s), 676 (m), 637 (w) cm^{-1}. Anal. Calcd. for $C_{46}H_{41}FFeNiOP_2$: C, 68.61; H, 5.13. Found: C, 68.97; H, 5.40.

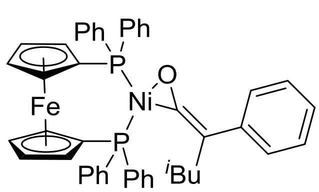

(Dppf)Ni(phenyl isobutyl ketene), 8cb. was synthesized according to the general procedure using phenyl isobutyl ketene (126.7 mg, 0.727 mmol, 2 equiv). The reaction was stirred for 24 h, at which point some orange precipitate had formed. Pentane (15 mL) was added, and precipitation was complete after 4 h. At this point, the solids were collected by filtration, washed 3x 10 mL pentane, and dried under vacuum to yield 191.7 mg, 79% of an orange powder. Crystals suitable for X-ray crystallography were grown by layering 1 mL of a saturated benzene solution of the complex with 0.5 mL benzene then 2.5 mL pentane. ^{1}H NMR (300 MHz, C_6D_6): δ 8.15 (d, *J* = 8 Hz, 2H), 8.10 (m, br, 4H), 8.00 (td, (*J* = 8, 4 Hz, 4H), 7.40 (t, *J* = 8 Hz, 2H), 7.1 (m, 6H), 7.00 (m, 7H), 4.27 (s, 2H), 3.91 (s, 2H), 3.74 (s, 2H), 3.65 (s, 2H), 2.10 (d, *J* = 4 Hz, 2H), 2.03 (pent, *J* = 4 Hz, 1H), 0.50 (d, *J* = 4 Hz, 6H). ^{13}C{^{1}H} NMR (125 MHz, C_6D_6): δ 169.4 (d, *J* = 40, 8 Hz, O=*C*=C), 141.4 (d, *J* = 7 Hz), 136.1 (d, *J* = 34 Hz), 135.7 (d, *J* = 15 Hz), 135.3 (d, *J* = 14 Hz), 135.1 (dd, *J* = 40, 2 Hz), 131.0 (dd, *J* = 51, 1 Hz), 129.4 (d, *J* = 10 Hz), 129.2 (d, *J* = 9 Hz), 129.1 (s), 128.7 (m, overlaps with solvent), 126.9 (s), 122.5 (s), 86.2 (dd, *J* = 48, 6 Hz), 77.6 (dd, *J* = 8, 5 Hz, O=C=*C*), 77.0 (d, *J* = 44 Hz), 75.3 (d, *J* = 11 Hz), 74.8 (d, *J* = 9 Hz), 73.3 (d, *J* = 6 Hz), 71.6 (d, *J* = 6 Hz), 41.2 (d, *J* = 4 Hz), 27.1 (s), 22.7 (s). ^{31}P{^{1}H} NMR (121 MHz, C_6D_6): δ 40.7 (d, *J* = 24.2 Hz), 17.0 (d, *J* = 24.2 Hz). IR (nujol, NaCl): 2813 (s), 1624 (s), 1584 (s), 1479 (s), 1435 (s), 1287 (m), 1229 (m), 1181 (m), 1164 (s), 1095 (s), 1072 (w), 1035 (s), 999 (w), 940 (w), 880 (w), 827 (m), 764 (m), 748 (s), 683 (s), 637 (m), 543 (s), 513 (s), 493 (s), 474 (m), 459 (m) cm^{-1}. Anal. Calcd. for $C_{45}H_{39}FFeNiOP_2$ • ½C_6H_6: C, 71.21; H, 5.49. Found: C, 71.11; H, 5.62.

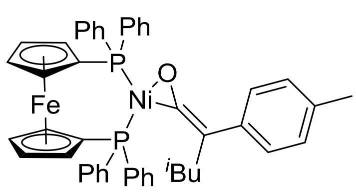

(Dppf)Ni(*p*-methylphenyl iso-butyl ketene), 8cc. was synthesized according to the general procedure using *p*-methylphenyl isobutyl ketene (205.3 mg, 1.09 mmol, 3 equiv). The reaction was stirred for 5 h, and pentane (15 mL) was added. After 16 h, red needles had formed which were collected by filtration, washed with pentane (3x 10 mL), and dried under vacuum to yield the complex (218.5 mg, 75%). Crystals suitable for X-ray crystallography were grown by layering 1 mL of a saturated benzene solution of the complex with 0.5 mL benzene then 2.5 mL pentane. ^{1}H NMR (400 MHz, C_6D_6): δ 8.16-7.97 (br, 10H), 7.20 (d, *J* = 8 Hz, 2H), 7.10 (br, 6H), 7.01 (br, 7H), 4.27 (s with shoulder, 2H), 3.93 (s, 1.82H), 3.87 (s, 0.16H), 3.82 (s, 0.14H), 3.74 (s, 1.89H), 3.66 (s with shoulder, 2H), 2.22 (s, 2.75 H), 2.11-2.00 (br, 3H), 1.95 (s, 0.20H), 1.17 (d, *J* = 4 Hz, 0.59H), 0.52 (d, *J* = 4 Hz, 5.07H). ^{13}C{^{1}H} NMR (100.6 MHz, C_6D_6): δ 169.1 (dd, *J* = 41, 8 Hz, O=*C*=C), 138.6 (d, *J* = 8 Hz), 136.1 (d, *J* = 34 Hz), 135.7 (d, *J* = 15 Hz), 135.3 (d, *J* = 14 Hz), this peak appears to overlap with a smaller peak, 134.9 (d, *J* = 2 Hz), 131.0 (dd, *J* = 40, 2 Hz), 131.1 (s), 129.4 (d, *J* = 12 Hz), 129.3 (d, *J* = 5 Hz), 129.2 (s), 126.9 (s), 86.2 (dd, *J* = 48, 4 Hz, O=C=*C*), 77.2 (dd, *J* = 7, 5 Hz), 76.9 (d, *J* = 44 Hz), 75.3 (d, *J* = 11 Hz), 74.8 (d, *J* = 8 Hz), 73.4 (d, *J* = 6 Hz), 71.7 (d, *J* = 5 Hz), 41.2 (d, *J* = 4 Hz), 27.1 (s), 23.3 (s), 21.8 (s). ^{31}P{^{1}H} NMR (121 MHz, C_6D_6): δ 40.3 (d, *J* = 23.0 Hz), 16.5 (d, *J* = 23.0 Hz). IR (nujol, NaCl): 1959 (w), 1917 (w), 1768 (m), 1754 (m), 1625 (m), 1598 (s), 1508 (s), 1479 (s), 1435 (s), 1330 (w), 1308 (m), 1293 (m), 1284 (m), 1228 (w), 1193 (m), 1165 (s), 1095 (s), 1034 (s), 1000 (w), 883 (w), 820 (s). Anal. Calcd. for $C_{47}H_{44}FeNiOP_2$ $1.5C_6H_6$: C, 73.23; H, 5.82. Found: C, 72.95; H, 6.10.

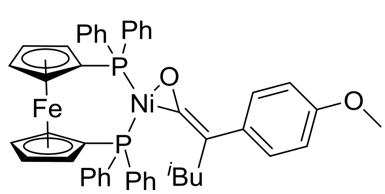

(Dppf)Ni(*p*-methoxyphenyl isobutyl ketene), 8cd. was synthesized according to the general procedure using *p*-methoxyphenyl isobutyl ketene (222.6 mg, 3 equiv). The reaction was stirred for 4 h, pentane (15 mL), was added, and the mixture was stored at -40 °C for 16 h. The solids were collected by filtration, washed 3x 10 mL pentane, dried under vacuum, and collected by filtration to yield the complex as an orange solid (109.9

mg, 37%). ^{1}H NMR (300 MHz, C_6D_6): δ 8.40 (t, *J* = 10 Hz, 0.18H), 8.23 (d, *J* = 10 Hz, 0.20), 8.18 (t, *J* = 10 Hz, 0.25H), 8.11 (m, 3.21H), 8.02 (m, 4.45H), 7.77 (m, 0.72H), 7.67 (m, 0.09H), 7.42 (t, *J* = 7.5 Hz, 0.08H), 7.35 (br, 0.24H), 7.31 (s, 0.19H), 7.25 (m, 0.53H), 7.10 (br, 5.22H), 7.00 (m, 7.66H), 6.94 (m, 0.66H), 6.88 (d, *J* = 5 Hz, 0.34H), 6.82 (d, *J* = 5 Hz, 0.32H), 4.28 (m, 1.67H), 4.23 (s, 0.13H), 4.16 (d, *J* = 10 Hz, 0.21H), 3.91 (s, 1.67H), 3.85 (m, 0.70H), 3.80 (s, 0.17H), 3.74 (m, 1.69H), 3.70 (s, 0.15H), 3.64 (m, 1.62H), 3.38 (s, 2.01H), 3.32 (s, 0.31H), 3.21 (s, 0.23H), 3.11 (m, 0.45H), 2.08 (m, 1.51H), 2.02 (m, 0.76H), 1.86 (m, 0.16H), 1.74 (m, 0.31H), 1.19 (d, *J* = 5 Hz, 0.61H), 1.09 (d, *J* = 5 Hz, 0.37H), 0.93 (d, *J* = 10 Hz, 0.36H), 0.80 (d, *J* = 5 Hz, 0.15H), 0.77 (d, *J* = 5 Hz, 0.30H), 0.63 (d, *J* = 5 Hz, 0.30H), 0.53 (d, *J* = 5 Hz, 4.27H). $^{13}C\{^{1}H\}$ NMR (100.6 MHz, C_6D_6): δ 168.8 (dd, *J* = 40, 4 Hz, O=*C*=C), 158.8 (d, *J* = 43 Hz), 156.24 (s), 137.6 (br), 136.9 (d, *J* = 9 Hz), 136.6 (d, *J* = 7 Hz), 136.2 (d, *J* = 34 Hz), 135.8 (d, *J* = 15 Hz), 135.5 (d, *J* = 8 Hz), 135.3 (d, *J* = 13 Hz), 135.0 (br) 134.8 (br), 134.4 (s), 134.2 (d, *J* = 8 Hz), 133.7 (d, *J* = 12 Hz), 131.0 (d, *J* = 42 Hz), 130.5 (d, *J* = 13 Hz), 130.0 (s), 129.5 (s), 129.3 (d, *J* = 10 Hz), 129.2 (dd, *J* = 9 Hz), 128.7 (s), 128.5 (s). The last two peaks overlap with solvent, 127.9 (s), 127.8 (s), 115.4 (s), 114.5 (s), 114.2 (s), 114.1 (s), 113.9 (s), 86.2 (dd, *J* = 48, 5 Hz), 77.6 (d, *J* = 37 Hz), 76.9 (d, *J* = 44 Hz), 76.6 (t, *J* = 7 Hz, O=C=*C*), 75.3 (d, *J* = 9 Hz), 75.0 (d, *J* = 10 Hz), 74.8 (d, *J* = 8 Hz), 73.4 (d, *J* = 5 Hz), 71.7 (d, *J* = 4 Hz), 55.4 (s), 55.3 (s), 55.25 (s), 55.21 (s), 50.7 (s), 48.5 (s), 41.3 (s), 27.1 (s), 26.4 (s), 25.9 (d, *J* = 4 Hz), 25.5 (s), 24.1 (s), 23.8 (s), 23.7 (s), 23.3 (s). $^{31}P\{^{1}H\}$ NMR (121 MHz, C_6D_6): δ 40.3 (d, *J* = 22 Hz), 33.0 (d, *J* = 30 Hz), 23.0 (s), 21.7 (d, *J* = 30 Hz), 16.5 (d, *J* = 23 Hz). IR (nujol, NaCl): 1915 (w), 1752 (w), 1626 (m), 1506 (s), 1436 (s), 1280 (m), 1244 (s), 1179 (m), 1095 (m), 1036 (m), 830 (m), 746 (s), 697 (s), 637 (m). Anal. Calcd. for

$C_{47}H_{44}FeNiO_2P_2$: C, 69.07; H, 5.43. Found: C, 69.21; H, 5.40.

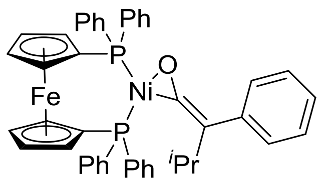

(Dppf)Ni(phenyl isopropyl ketene), 8d. was synthesized according to the general procedure with phenyl isopropyl ketene (174.7 mg, 1.09 mmol, 3 equiv). The reaction was stirred for 48 h, and 15 mL pentane was added. After an additional 24 h, the solids were collected by filtration, washed with 3x 10 mL pentane, and dried under vacuum to afford 224.9 mg, 80% of a yellow powder. ^{1}H NMR (300 MHz, C_6D_6): δ 8.27 (d, J = 8 Hz, 1H), 8.06 (t, J = 8 Hz, 3H), 7.99 (t, J = 8 Hz, 3H), 7.90 (dd, J = 8, 4 Hz, 1H), 7.71 (s, br, 1H), 7.37 (t, J = 8 Hz, 2H), 7.09 (m, br, 5H), 7.00 (m, br, 9H), 6.89 (m, br, 0.77H), 6.81 (t, J = 8 Hz, 0.39H), 6.67 (d, J = 8 Hz, 0.48H), 6.57 (m, 0.46H), 4.28 (s, 1.35H), 4.25 (s, 0.46H), 3.91 (s, 1.42H), 3.87 (0.51H), 3.83 (0.56H), 3.78 (s, 0.60H), 3.75 (s, 0.63H), 3.72 (s, 1.45H), 3.65 (1.63H), 3.34 (quint, J = 8 Hz, 0.14H), 2.57 (quint, J = 8 Hz, 0.62H), 2.35 (quint, J = 8 Hz, 0.24H), 1.67 (d, J = 4 Hz, 0.92H), 1.32 (d, J = 8 Hz, 0.89H), 1.16 (d, J = 8 Hz, 0.82H,), 1.00 (d, J = 4 Hz, 3.86H). ^{13}C{^{1}H} NMR (125 MHz, THF-d_8): δ 168.6 (dd, J = 41, 9 Hz, O=*C*=C), 140.9 (d, J = 8 Hz), 136.7 (d, J = 34 Hz), 136.3 (d, J = 14 Hz), 136.7 (d, J = 13 Hz), 136.6 (dd, J = 41, 3 Hz), 131.9 (d, J = 2 Hz), 131.3 (d, J = 2 Hz), 129.9 (d, J = 10 Hz), 129.6 (d, J = 10 Hz), 128.6 (s), 126.0 (s), 121.8 (s), 86.0 (dd, J = 49, 6 Hz), 79.2 (dd, J = 8, 5 Hz, O=C=*C*), 76.9 (d, J = 45 Hz), 75.9 (d, J = 11 Hz), 75.4 (d, J = 8 Hz), 75.2 (d, J = 6 Hz), 72.5 (d, J = 6 Hz), 35.0 (d, J = 4 Hz), 24.0 (s), 14.8 (s). ^{31}P{^{1}H} NMR (121 MHz, C_6D_6): δ 45.9 (d, J = 24.2 Hz), 45.2 (d, J = 24.2 Hz), 43.4 (d, J = 24.2 Hz), 26.94 (s), 20.6 (d, J = 24.2 Hz). IR (nujol, NaCl): 3105 (m), 3090 (m), 2361 (w), 1915 (w), 1611 (s), 1582 (s), 1491 (s), 1479 (s), 1436 (s), 1381 (m), 1306 (m), 1271 (m), 1196 (m), 1158 (m), 1096 (s), 1070 (w), 1029 (m), 998 (m), 976 (m), 897 (w), 865 (w), 840 (w), 825 (m), 812 (w) cm^{-1}. Anal. Calcd. for $C_{45}H_{40}FeNiOP_2$: C, 69.89; H, 5.21. Found: C, 70.08; H, 5.30.

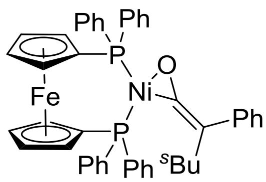

(Dppf)Ni(phenyl *s*-butyl ketene), 8e. was synthesized by adding a solution of phenyl *sec*-butyl ketene (316.5 mg, 1.82 mmol, 5 equiv) in benzene (2 mL) to a suspension of (dppf)Ni(COD) (261.5 mg, 0.363 mmol, 1 equiv) in benzene (3 mL). After 7 h, the reaction had turned from an orange suspension to a red solution, and pentane (15 mL) was added. After an additional 16 h, the solids were collected by filtration, washed 3x 10 mL pentane, and dried under vacuum. The complex is a red crystalline solid (223.3 mg, 78%). Crystals suitable for X-ray diffraction were by layering 1 mL of a saturated solution of the complex in benzene with 0.5 mL benzene followed by 3.5 mL pentane. ^1H NMR (500 MHz, C_6D_6): δ Aromatic region: 8.24 (m, 1.16H), 8.17-8.03 (m, 3.07H), 8.03-7.94 (q, J = 10 Hz, 2.38H), 7.93-7.87 (br, 0.94H), 7.76-7.66 (br, 0.83H), 7.42 (t, J = 7.5 Hz, 0.42H), 7.37 (t, J = 7.5 Hz, 0.90H), 7.22 (d, J = 5 Hz, 0.56H), 7.15-6.91 (m, 12.80H), 6.88 (t, J = 7.5 Hz, 0.47H), 6.81 (t, J = 5 Hz, 0.26H), 6.69 (d, J = 10 Hz, 0.20H), 6.65 (d, J = 10 Hz, 0.27H), 6.60 (m, 0.24H), 6.54 (t, J = 7.5 Hz, 0.39H), Cp region: 4.74 (s, 0.07H), 4.68-4.53 (br, 0.40H), 4.48 (br, 0.11H), 4.40 (s, 0.36H), 4.36 (s, 0.05H), 4.30-4.24 (br, 0.54H), 4.22 (s, 0.17H), 4.12 (s, 0.36H), 4.06 (s, 0.05H), 3.39 (s, 0.46H), 3.90 (s, 0.37H), 3.88-3.85 (m, 0.86H), 3.84-3.79 (m, 0.99H), 3.77 (s, 0.48H), 3.74 (m, 078H), 3.65 (m, 1.83H), 3.02 (q, J = 5 Hz, 0.19H), Alkyl region: 2.30 (m, 0.23H), 2.25-2.11 (m, 0.89H), 1.89-1.76 (m, 0.71H), 1.69-1.59 (m, 1.15H), 1.31 (d, J = 5 Hz, 0.63H), 1.25 (t, J = 7.5 Hz, 0.92H), 1.12 (d, J = 5 Hz, 0.28H), 0.91 (d, J = 0.5 Hz, 1.19H), 0.86 (t, J = 7.5 Hz, 0.85H), 0.76 (m, 0.37H), 0.58 (s, 0.65H), 0.26 (t, J = 5 Hz, 1.18H). $^{13}C\{^1H\}$ NMR (125 MHz, C_6D_6): δ 233.6 (dd, J = 84, 23 Hz), 168.7 (dd, J = 40, 9 Hz), 168.5 (dd, J = 40, 8 Hz), 163.2 (dd, J = 41, 8 Hz), 145.5 (d, J = 2 Hz), 141.0 (d, J = 8 Hz), 140.7 (d, J = 8 Hz), 140.3 (dd, J = 31, 4 Hz), 136.45 (dd, J = 32, 18 Hz), 136.36 (d, J = 1 Hz), 136.14 (s), 136.1 (d, J = 14 Hz), 135.8 (d, J = 5 Hz), 135.7 (d, J = 14 Hz), 135.6 (d, J = 14 Hz), 135.5 (s), 135.4 (d, J = 6 Hz), 135.3 (d, J = 2 Hz), 135.20 (s), 135.19 (d, J = 15 Hz), 134.94 (dd, J = 25, 2 Hz), 134.92 (d, J = 12 Hz), 134.7 (t, J = 2 Hz), 134.3 (t, J = 2 Hz), 132.5 (br), 131.22 (dd, J = 46, 1 Hz), 131.22 (d, J = 2 Hz), 130.9 (d, J = 1 Hz), 130.8 (dd, J = 31, 1 Hz), 130.76 (br), 129.24-129.12 (m, possibly two dd), 129.0 (s, overlaps with solvent), 128.9 (s, overlaps with solvent, possible multiplet with previous peak), 128.2 (s), 128.0 (s), 126.2 (s), 123.4 (s), 123.0 (s), 122.8 (s), 122.6 (s), 122.4 (s), 122.2 (d, J = 6 Hz), 86.3 (d, J = 6 Hz), 86.2 (d, J = 6 Hz), 86.0 (dd, J = 6, 5 Hz), 85.9 (dd, J = 6, 4 Hz), 85.8 (d, J = 5 Hz), 85.5 (d, J = 5 Hz), 84.7 (dd, J = 8, 5 Hz), 79.3 (dd, J = 6, 5 Hz), 77.0 (d, J = 44 Hz), 76.9 (d, J = 44 Hz), 76.62 (t, J = 16 Hz), 76.2 (d, J = 44 Hz), 75.3 (t, J = 14 Hz), 75.2 (dd, J = 11, 4 Hz), 75.0 (d, J = 5 Hz), 74.8 (d, J = 9 Hz), 74.7 (t, J = 9 Hz), 74.5 (d, J = 5 Hz), 74.4 (d, J = 10 Hz), 73.9 (d, J = 8 Hz), 73.5 (d, J = 6 Hz), 73.3 (dd, J = 22, 6 Hz), 72.8 (d, J = 6 Hz), 72.1 (d, J = 5 Hz), 72.0 (dd, J = 26, 6 Hz), 71.7 (d, J = 5 Hz), 71.2 (d, J = 5 Hz), 42.0 (d, J = 6 Hz), 40.1 (d, J = 4 Hz), 33.1 (s), 32.8 (m), 31.9 (t, J = 4 Hz), 30.6 (s), 30.4 (s), 30.0 (s), 27.5 (s), 23.9 (s), 23.3 (s), 21.5 (s), 20.3 (s), 20.2 (s), 16.7 (s), 14.9 (s), 14.2 (s), 13.9 (s), 13.3 (s), 12.3. $^{31}P\{^1H\}$ NMR (121 MHz, C_6D_6): δ 43.6 (d, J = 23 Hz), 42.9 (d, J = 24 Hz), 41.0 (d, J = 24 Hz), 24.7 (s), 18.8 (d, J = 23 Hz), 18.3 (d, J = 24 Hz), 18.1 (d, J = 24 Hz). IR (nujol, NaCl): 2091 (w), 1913 (s), 1727 (w), 1614 (m), 1581 (s), 1435 (s), 1306 (m), 1265 (m), 1160 (m), 1095 (s), 1071 (w), 1028 (s), 998 (m), 894 (w), 821 (m), 748 (s), 695 (s), 678 (s), 637 (w). Anal. Calcd. for $C_{46}H_{42}FeNiOP_2$: C, 70.17; H, 5.38. Found: C, 69.93; H, 5.43.

Kinetic analyses. (Table 4.5) (Dppf)Ni(ketene) complex (0.01 mmol) and 1,3,5-trimethoxybenzene (0.008 mmol) were weighed into a 4-mL scintillation vial in the glovebox and dissolved in toluene-d_8 (0.75 mL). The samples were transferred through a pipet filter with glass wool to screw cap NMR tubes and analyzed by ^{1}H NMR (500 MHz). The tubes were immersed in a 100 ºC oil bath for the indicated amount of time, cooled to room temperature, and analyzed again by ^{1}H NMR. The heating/NMR cycles were repeated until 25-30 time points had been obtained or the starting material was no longer observed. Two or three kinetic data sets were collected for each complex. In several cases, the T_0 did not fit linearly in the ln([A]/[A]$_0$) vs. time plot with the rest of the data. In these cases, the reaction appeared to have a significantly faster rate over the first time point, due to population of the CC coordination mode. The T_0 was omitted and the T_1 treated as the T_0. In some trials, significant line broadening was observed after a few time points. We believe this is due to oxygen permeating into the NMR tube, and these trials were excluded.

Table 4.5. Kinetic data for thermal decomposition of **8**.

Complex	K_{obs} (x10^{-4} /s)	R^2	Timepoints included	Time between points (min)	average K_{obs}	st. dev.
8b	1.038	0.9984	1-25	10	1.038	0.001
	1.037	0.9974	0-30	10		
8b-d9	0.7855	0.9971	1-30	10	0.7709	0.0156
	0.7726	0.9986	0-30	15		
	0.7545	0.9919	0-25	15		
8ca	0.9396	0.9941	1-23	10	0.9971	0.0814
	1.055	0.9979	0-25	15		
8cb	4.745	0.9925	1-23	5	5.020	0.263
	5.270	0.9968	1-17	5		
	5.046	0.9937	1-15	5		
8cc	3.215	0.994	1-27	5	3.570	0.326
	3.637	0.9959	1-27	5		
	3.857	0.9956	1-26	5		
8cd	2.924	0.9959	1-25	5	2.692	0.267
	2.401	0.9934	0-29	5		
	2.750	0.9981	1-29	5		
8d	2.467	0.9958	1-23	5	2.406	0.086
	2.345	0.9923	1-30	5		

General procedure for synthesis of (DPEphos)Ni(ketene) complexes. In the drybox, Ni(COD)$_2$ (100 mg, 0.363 mmol, 1 eq) and DPEphos (195.8 mg, 0.363 mmol, 1eq) were weighed into a 20 mL scintillation vial. Benzene (3 mL) was added and the solution stirred for 2 min, at which point ketene (1.09 mmol, 3 eq) was added in 2 mL benzene. The solution was stirred for 48 h, at which point the vial was filled with pentane and stored at -40 °C for 24 h to complete precipitation. The solids were collected by filtration, washed with pentane, and dried under vacuum.

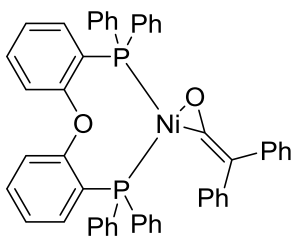

(DPEphos)Ni(diphenylketene). was synthesized according to the general procedure to yield 249.6 mg of a light orange solid (87% yield). ^{1}H NMR (400 MHz, C_6D_6): δ 8.06 (d, J = 8.0 Hz, 3H), 7.34 (t, J = 8.0 Hz, 5H), 7.22 (d, J = 8.0 Hz, 4H), 6.98 (s, br, 20H), 6.70 (t, J = 8.0 Hz, 2H), 6.62 (t, J = 8.0 Hz, 4H). ^{13}C{^{1}H} NMR (100.6 MHz, C_6D_6): δ 169.69 (d, J = 36 Hz, O=*C*=C), 160.16 (d, J = 10 Hz, Ar), 142.90 (s, Ar), 142.42 (m, Ar), 135.26 (s, br, Ar), 133.89 (s, Ar), 132.68 (s, br, Ar), 132.29 (s, br, Ar), 131.81 (s, br, Ar), 130.45 (s, Ar), 129.15 (s, Ar), 129.15 (s, Ar), 128.77 (m, Ar), 128.50 (s, Ar), 127.35 (s, Ar), 126.21 (s, br, Ar), 125.00 (s, Ar), 122.84 (s, Ar), 113.44 (s, Ar), 101.46 (s, Ar), 85.91 (t, J = 6 Hz, O=C=*C*). ^{31}P{^{1}H} NMR (121 MHz, C_6D_6): δ 38-5 – 37.1 (s, br), 15.2 – 13.4 (s, br). IR (nujol, NaCl): 3052 (m), 2098 (m), 1569 (s), 1487 (s), 1435 (s), 1310 (m), 1295 (m), 1262 (s), 1232 (s), 1157 (w), 1124 (w), 1099 (s), 1074 (m), 1029 (m), 999 (w), 929 (m), 883 (m), 802 (m) cm^{-1}. Anal. Calcd. for $C_{48}H_{38}NiOP_2$: C, 75.88; H, 4.84. Found: C, 76.14; H, 4.92.

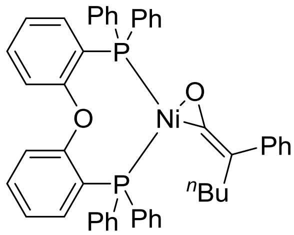

(DPEphos)Ni(butylphenylketene). was synthesized according to the general procedure to yield 179.4 mg of a light orange solid (63% yield). ^{1}H NMR (400 MHz, C_6D_6): δ 8.20 (d, *J* = 8.0 Hz, 2H), 8.05 (s, br, 4H), 7.44 (t, *J* = 8.0 Hz, 2H), 7.25 (s, br, 4H), 7.10 (s, br, 6H), 7.02 (t, *J* = 8.0 Hz, 2H), 6.91 (s, br, 7H), 6.70 (s, br, 1H), 6.59 (s, br, 1H), 6.44 (s, br, 1H), 6.17 (s, br, 2H), 6.08 (s, br, 1H), 2.30 (t, *J* = 8.0 Hz, 2H), 1.41 (s, br, 2H), 0.65 (s, 5H). ^{13}C{^{1}H} NMR (100.6 MHz, C_6D_6): δ 170.12 (d, *J* = 31 Hz, O=*C*=C), 159.96 (m, Ar), 140.75 (d, *J* = 9 Hz, Ar), 137.02 (s, br, Ar), 135.33 (m, Ar), 133.47 (m, Ar), 132.51 (m, Ar), 131.41 (s, br, Ar), 130.66 (m, Ar), 129.25 (s, br, Ar), 126.06 (s, Ar), 125.92 (m, Ar), 123.35 (s, br, Ar), 122.18 (s, Ar), 118.57 (s, br, Ar), 79.08 (td, *J* = 6 Hz, 2 Hz, O=C=*C*), 41.28 (s, $CH_2\mathit{C}H_2CH_2CH_3$), 33.12 (d, *J* = 52 Hz, $\mathit{C}H_2CH_2CH_2CH_3$), 23.94 (s, $CH_2CH_2\mathit{C}H_2CH_3$), 15.00 (s, $CH_2CH_2CH_2\mathit{C}H_3$). ^{31}P{^{1}H} NMR (121 MHz, C_6D_6): δ 40.3 (d, *J* = 34 Hz) 13.0 (d, 34 Hz). IR (nujol, NaCl): 1913 (w), 1624 (s), 1584 (s), 1479 (s), 1435 (s), 1306 (m), 1267 (s), 1213 (m), 1166 (s), 1093 (s), 1031 (s), 998 (w), 913 (w), 891 (w), 824 (m) cm^{-1}.

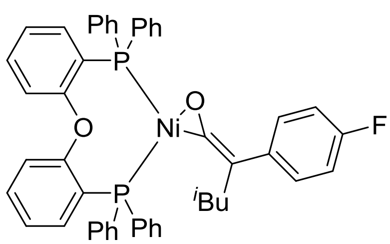

(DPEphos)Ni(*p*-fluorophenyl iso-butyl ketene). was synthesized according to the general procedure to yield 226.8 mg of a light orange solid (78% yield). ^{1}H NMR (300 MHz, $CDCl_3$) The alkyl region is indicative of two coordination modes. The integration of the largest doublet is set to 6. δ 8.02 (s, br, 3.54H), 7.91 (dd, *J* = 8.8, 5.8 Hz, 2.24H), 7.21 (s, br 2.49H), 7.13 – 7.00 (t, *J* = 9 Hz), 3.72H), 6.93 (s, br, 7.72H), 6.73 (m, br, 2.25H), 6.60 (s, br, 1.25H), 6.37 (m, br, 1.62H), 6.12 (m, 3.14H), 3.03 (d, *J* = 7.2 Hz, 0.18H), 2.15 (s, 1.91H), 1.97 (dt, *J* = 14.4, 7.1 Hz, 1.01H), 1.15 (d, *J*

= 6 Hz, 0.60H), 0.87 (t, J = 7.5 Hz 0.50H), 0.56 (d, J = 6.5 Hz, 6.00H). ^{13}C NMR (101 MHz, C_6D_6) δ 170.4 (d, J = 33.9 Hz), 159.9 (dd, J = 124.7, 114.5 Hz), 137.3 (d, J = 47.0 Hz), 135.4 (dd, J = 104.4, 11.2 Hz), 133.5 (s), 133.0 (s), 132.7 (s), 132.5 (s), 132.2 (s), 131.4 (s), 130.7 (d, J = 82.8 Hz), 129.3 (s), 129.2 (s), 127.6 (d, J = 6.8 Hz), 125.4 (s), 123.3 (s), 118.6 (s), 115.2 (d, J = 20.5 Hz), 76.5 (t, J = 6.5 Hz), 41.3 (s), 28.8 (d, J = 29.5 Hz), 27.0 (s), 23.4 (d, J = 31.6 Hz), 22.6 (s), 14.8 (s). ^{31}P{^{1}H} NMR (121 MHz, C_6D_6): δ 38.5 (d, J = 33.9 Hz), 23.2 (s), 12.8 (d, J = 33.3 Hz). IR (nujol, NaCl): 1959 (w), 1913 (w), 1743 (s), 1658 (m), 1597 (m), 1505 (s), 1436 (s), 1306 (m), 1216 (m), 1611 (s), 1119 (m), 1098 (s), 1032 (m), 885 (w), 837 (m), 748 (m), 723 (w), 696 (s), 676 (m), 637 (w) cm^{-1}. Anal. Calcd. for $C_{48}H_{42}NiO_2P_2$: C, 73.02; H, 5.23. Found: C, 73.20; H, 5.37.

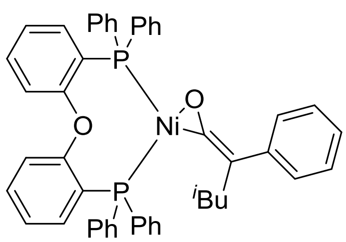

(DPEphos)Ni(phenyl iso-butyl ketene). was synthesized according to the general procedure to yield 194.4 mg of a light orange solid (70% yield). ^{1}H NMR (500 MHz, C_6D_6) contains two coordination modes. Largest doublet in the alkyl region's integration is set to 6.00. δ 8.12 (d, J = 8.2 Hz, 1.95H), 8.04 (s, 3.77H), 7.42 (t, J = 7.6 Hz, 1.97H), 7.31 (d, J = 5.0 Hz, 0.33H), 7.22 (s, 3.60H), 7.15 – 7.06 (m, 4.22H), 7.03 (td, J = 7.3, 0.9 Hz, 1.70H), 6.92 (s, 6.05H), 6.87 – 6.80 (m, 1.39H), 6.80 – 6.72 (m, 1.31H), 6.69 (s, 1.19H), 6.64 (d, J = 7.7 Hz, 0.39H), 6.59 (d, J = 6.4 Hz, 1.10H), 6.47 – 6.39 (m, 1.11H), 6.16 (s, 1.88H), 6.07 (d, J = 6.4 Hz, 1.06H), 3.11 (d, J = 7.4 Hz, 0.10H), 2.33 – 2.16 (m, 1.76H), 2.13 – 2.03 (m, 1.15H), 1.31 – 1.15 (m, 1.32H), 1.12 (d, J = 6.6 Hz, 0.38H), 0.86 (t, J = 7.1 Hz, 1.27H), 0.56 (d, J = 6.5 Hz, 6.00H). ^{13}C NMR (101 MHz, C_6D_6) δ 169.70 (d, J = 31.7 Hz), 158.9 (d, J = 8.6 Hz), 140.4 (d, J = 7.9 Hz), 136.1 (s), 134.44 (dd, J = 104.7, 13.8 Hz), 132.5 (d, J = 6.5 Hz), 132.1 (s), 131.8 (s), 131.50 (s), 131.2 (s), 130.4 (s), 130.1 (s), 129.2 (s), 128.4 (d, J = 9.7 Hz), 128.2 (s), 125.7 (s), 125.4 (s), 124.4 (s), 122.3 (s), 121.4 (s), 117.6 (s), 76.5 (t, J = 6.3 Hz), 40.4 (s), 34.0 (s), 27.7 (s), 26.1 (s), 22.3 (s), 21.7 (s), 13.9 (s). $^{31}P\{^1H\}$ NMR (121 MHz, C_6D_6): δ 38.6 (d, J = 34.5 Hz), 12.7 (d, J = 34.5 Hz). IR (nujol, NaCl): 1633 (m), 1590 (s), 1572 (m), 1489 (s), 1436 (s), 1284 (w), 1261 (s), 1213 (s), 1186 (w), 1157 (w), 1125 (w), 1094 (m), 1070 (m), 1036 (w), 877 (m), 807 (m), 768 (m), 744 (s), 726 (m), 697 (s), 546 (m), 533 (m), 519 (m), 469 (s) cm^{-1}. Anal. Calcd. for $C_{48}H_{42}NiO_2P_2$: C, 74.73; H, 5.49. Found: C, 74.33; H, 5.89.

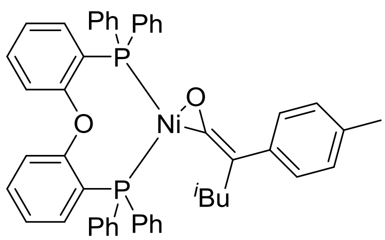

(DPEphos)Ni(*p*-methylphenyl iso-butyl ketene). was synthesized according to the general procedure to yield 222.2 mg of a light orange solid (78% yield). ^{1}H NMR (400 MHz, C_6D_6) contains two coordination modes. The integration of the largest doublet in the alkyl region is set to 6.00. δ 8.04 (d, J = 7.8 Hz, 5.96H), 7.23 (d, J = 7.8 Hz, 6.16H), 6.93 (s, 6.54H), 6.83 (s, 1.16H), 6.77 (s, 1.10H), 6.69 (s, 1.00H), 6.58 (s, 0.90H), 6.43 (s, 0.96H), 6.17 (s, 1.82H), 6.07 (s, 0.82H), 2.24 (s, 3.76H), 2.11 (dt, J = 13.4, 6.6 Hz, 0.96H), 1.99 (s, 0.09H), 1.24 (dd, J = 13.4, 6.8 Hz, 1.33H), 1.14 (d, J = 6.5 Hz, 0.28H), 0.86 (t, J = 7.0 Hz, 1.53H), 0.66 (s, 0.18H), 0.59 (d, J = 6.2 Hz, 6.00H). $^{13}C\{^1H\}$ NMR (100.6 MHz, C_6D_6): δ 169.4 (d, J = 31.6 Hz), 158.9 (d, J = 9.6 Hz), 137.6 (d, J = 8.2 Hz), 136.1 (s), 134.4 (dd, J = 103.9, 12.8 Hz), 131.5 (s), 131.1 (s), 130.3 (s), 130.0 (s), 129.6 (d, J = 86.1 Hz), 128.5 (s), 128.4 (d, J = 9.4 Hz), 128.2 (s), 125.8 (s), 125.4 (s), 124.4 (s), 122.2 (s), 117.6 (s), 76.0 (t, J = 6.3 Hz), 40.5 (s), 34.0 (s), 26.2 (s), 22.3 (s), 21.7 (s), 20.8 (s), 13.9 (s). $^{31}P\{^1H\}$ NMR (121 MHz, C_6D_6): δ 38.09 (d, J = 33.5 Hz), 12.15 (d, J = 34.9 Hz). IR (nujol, NaCl): 2007 (w), 1947 (w), 1634 (s), 1602 (s), 1565 (m), 1507 (s), 1435 (s), 1298 (m), 1281 (m), 1264 (s), 1228 (s), 1184 (w), 1121 (m), 1096 (s), 1067 (s), 1028 (m), 999 (w), 942 (w), 878 (m), 835 (m), 823 (m), 806 (m), 765 (m), 742 (s), 726 (m), 695 (s), 679 (m), 621 (w) cm^{-1}. Anal. Calcd. for $C_{48}H_{42}NiO_2P_2$: C,74.92; H, 5.65. Found: C, 75.08; H, 5.74.

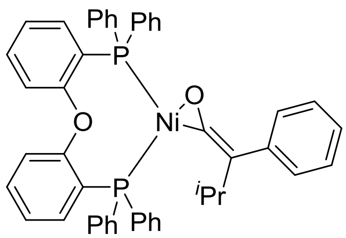

(DPEphos)Ni(phenyl isopropyl ketene). was synthesized according to the general procedure to yield 168.1 mg of a light orange solid (61% yield). ^{1}H NMR (300 MHz, C_6D_6) displays two rotamers of the isopropyl group. The integration of the largest peak in the alkyl region is set to 5.00. δ 8.25 (d, *J* = 7.5 Hz, 1.85H), 8.01 (s, 2.89H), 7.45 – 7.36 (m, 2.85H), 7.25 (s, 3.50H), 7.13 – 6.80 (m, 14.78H), 6.63 (d, *J* = 7.4 Hz, 3.12H), 6.46 (s, 1.62H), 6.17 (s, 2.92H), 3.37 – 3.22 (m, 0.19H), 2.84 – 2.65 (m, 0.93H), 1.63 (d, *J* = 6.8 Hz, 1.14H), 1.09 (s, 5.00H). ^{31}P{^{1}H} NMR (121 MHz, C_6D_6): δ 42.21 (d, *J* = 34.0 Hz), 15.60 (d, *J* = 34.8 Hz). IR (nujol, NaCl): 3069 (m), 3046 (m), 2361 (m), 1966 (w), 1898 (w), 1833 (s), 1586 (m), 1570 (w), 1478 (s), 1431 (s), 1308 (s), 1161 (s), 1119 (w), 1093 (s), 1028 (s), 998 (w), 884 (m), 819 (s), 789 (w) cm^{-1}. Anal. Calcd. for $C_{47}H_{40}NiO_2P_2$: C, 74.53; H, 5.32. Found: C, 74.80; H, 5.29.

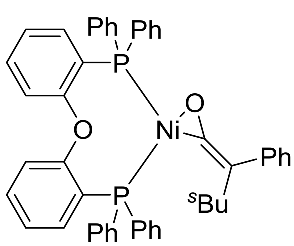

(DPEphos)Ni(phenyl *s*-butyl ketene). was synthesized according to the general procedure to yield 213.1 mg of a light orange solid (76% yield). ^{1}H NMR (300 MHz, C_6D_6): shows multiple rotamers of the sec-butyl chain and/or coordination modes. The integration of the largest triplet in the alkyl region is set to 3.00. δ ^{1}H NMR (400 MHz, C_6D_6) δ 8.19 (d, *J* = 7.9 Hz, 2.38H), 8.00 (m, br, 4.11H), 7.40 (d, *J* = 7.5 Hz, 0.77H), 7.35 (t, *J* = 7.8 Hz, 3.01H), 7.26 (d, *J* = 7.3 Hz, 2.07H), 7.18 (m, br, 4.56H), 7.01 (m, br, 5.36H), 6.98 (t, *J* = 12.0 Hz, 6.58H), 6.94 – 6.70 (m, 10.50H), 6.69 – 6.62 (m, 2.50H), 6.61 – 6.54 (m, 2.62H), 6.41 (s, br, 2.10H), 6.13 (s, br, 2.76H), 6.05 (s, 1.38H), 2.95 (dd, *J* = 14.1, 6.9 Hz, 0.41H), 2.35 (s, 1.03H), 2.30 – 2.14 (m, 0.76H), 1.87 – 1.64 (m, 2.40H), 1.60 (d, *J* = 6.8 Hz, 1.45H), 1.49 (d, *J* = 6.8 Hz, 0.15H), 1.37 (s, 0.30H), 1.22 (dd, *J* = 14.5, 7.4 Hz, 0.62H), 1.14 (t, *J* = 7.3 Hz, 1.64H), 1.09 (d, *J* = 7.7 Hz, 0.24H), 0.98 (s, 2.80H), 0.83 (t, *J* = 7.0 Hz, 1.21H), 0.33 (t, *J* = 7.0 Hz, 3.00H). ^{13}C NMR (101 MHz, C_6D_6) δ 168.8 (d, *J* = 32.0 Hz), 159.2 (d, *J* = 9.6 Hz), 158.9 (d, *J* = 9.6 Hz), 144.6 (s), 140.3 – 140.1 (m), 136.1 (s), 135.5 – 133.1 (m), 132.1 (d, *J* = 40.8 Hz), 131.3 (s), 130.7 (s), 130.4 (s), 130.1 (s), 129.3 (d, *J* = 14.6 Hz), 128.2 (d, *J* = 11.2 Hz), 127.2 (s), 127.0 (s), 125.4 (s), 125.1 (s), 124.5 (s), 122.3 (s), 121.7 (s), 121.2 (s), 117.6 (s), 84.7 (t, *J* = 5.3 Hz), 83.3 (dd, *J* = 6.3, 4.1 Hz), 78.1 (d, *J* = 6.2 Hz), 41.2 (s), 39.15 (s), 34.03 (s), 32.39 (s), 29.58 (s), 29.09 (s), 22.95 (s), 22.31 (s), 20.55 (s), 19.55 (s), 14.02 (s), 13.9 (s), 13.4 (s), 12.4 (s). ^{31}P{^{1}H} NMR (121 MHz, C_6D_6): δ 39.10 (d, *J* = 34.0 Hz, 1H), 12.48 (d, *J* = 33.4 Hz, 1H). IR (nujol, NaCl): 1616 (w), 1585 (m), 1492 (w), 1464 (s), 1434 (s), 1378 (m), 1260 (w), 1214 (m), 1126 (w), 1096 (w), 1070 (w), 875 (w), 805 (w), 746 (m), 696 (m), 677 (m) cm^{-1}.

Kinetics. (DPEphos)Ni(ketene) complex (0.02 mmol) and 1,3,5-trimethoxybenzene (0.016 mmol) were weighed into a 4-mL scintillation vial in the glovebox. Toluene-d_8 (0.75 mL) was added via syringe to produce a final concentration of 0.0267 M. The solids were dissolved by stirring, and if any solids remained after 10 min, the solution was filtered. The samples were transferred to screw cap NMR tubes and analyzed by ^{1}H NMR (500 MHz). The tubes were immersed in a 100 ºC oil bath for the indicated amount of time, cooled to room temperature, and analyzed again by ^{1}H NMR. The heating/NMR cycles were repeated until 25-30 timepoints had been obtained or the starting material was no longer observed. Two or three trials were collected for each complex. In several cases, the $T_{0/1}$ did not fit linearly with the rest of the data, and was omitted (Table 4.6).

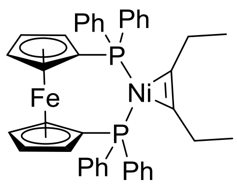

(Dppf)Ni(3-hexyne). In the drybox, $Ni(COD)_2$ (500 mg, 1.81 mmol, 1 eq) and dppf (1.0077 g, 1.81 mmol, 1 eq) were weighed into a 20 mL scintillation vial. Benzene (~10 mL) was added and the solution stirred for 2 min, at which point 3-hexyne (413 μL, 3.64 mmol, 2 eq) was added. The solution was stirred overnight. Pentane (~10 mL) was added and the vial stored at -40 °C for 24 h to complete precipitation. The solids were collected by filtration to yield 1.071 g of a yellow powder (84 %yield). Crystals suitable for X-ray crystallography were grown from diffusion of pentane into a benzene solution of the complex. ^{1}H NMR (300 MHz, C_6D_6): δ 7.97 (s, br, 8H), 7.06 (s, br, 12H), 4.23 (s, 4H), 3.86 (s, 4H), 2.51 (d, J = 9 Hz, 4H), 1.18 (t, J = 9 Hz, 8H). ^{13}C{^{1}H} NMR (100.6 MHz, C_6D_6): δ 139.46 (dt, J = 34, 8 Hz, Ar), 135.14 (t, J = 8 Hz, Ar), 129.77 (s, Ar), 128.68 (s, Ar) 127.60 (dt, J = 29, 15 Hz, *CC*),

Table 4.6. Kinetic data for the decomposition of **13**.

Complex	K_{obs} ($\times 10^{-3}$ /s)	R^2	Timepoints included	Time between points (min)	average K_{obs}	st. dev.
13b	18.302	0.994	1-12	10	15.335	5.022
	14.871	0.994	1-22	5		
	19.7190	0.992	1-23	5		
	8.4480	0.998	1-30	5		
13ca	11.5850	0.996	1-17	10	10.5115	1.5182
	9.4380	0.997	1-20	10		
13cb	3.086	0.994	1-30	20	2.7293	0.2562
	2.492	0.996	2-25	10		
	2.725	0.998	1-25	20		
	2.614	0.996	1-25	20		
13cc	18.649	0.994	1-13	10	20.787	2.017
	21.058	0.991	1-18	5		
	22.655	0.996	1-16	5		
13d	44.580	0.996	1-10	5	41.919	3.763
	39.258	0.994	1-9	5		

85.56 (dt, J = 40, 6 Hz, cp), 75.08 (t, J = 5 Hz, cp), 71.54 (t, J = 3 Hz, cp), 21.97 (t, J = 9 Hz, CH_2), 16.96 (t, J = 2 Hz, CH_3). $^{31}P\{^1H\}$ NMR (121 MHz, C_6D_6): δ 32.23 (s).IR (nujol, NaCl): 2361 (m), 1966 (w), 1898 (w), 1833 (s, CC), 1586 (w, 1570 (w), 1478 (s), 1431 (s), 1308 (m), 1192 (m), 1161 (s), 1119 (w), 1033 (s), 1070 (w), 1028 (s), 998 (w), 884 (m), 819 (m), 789 (w). Anal. Calcd. for $C_{40}H_{38}FeNiP_2$: C, 69.11; H, 5.51. Found: C, 69.09; H, 5.61.

Computational Details. All calculations were performed with the GAUSSIAN09[26] suite of programs. The structure of (Dppf)Ni(Phenyl isobutyl ketene), **8cb**, was optimized with the B3LYP[27] functional and a split basis set consisting of tzvp for the P, Ni, and ketene O=C=C atoms and svp for all other atoms.[28] The structure was also optimized with BP86[29] and the same split basis set and at the B3LYP/tzvp and BP86/tzvp levels of theory. Solvent (benzene) effects were taken into account using the self-consistent reaction field (SCRF) with the PCM model. Analytical frequency calculations at the same level of theory were performed to ensure the calculated structures are local minima and to generate thermal correction factors to ZPE, energy, enthalpy, and gibbs free energy. Several important bond lengths and angles were compared from the crystal structure of this complex and the calculated structures (Table 4.7). The average of the differences between calculated structures and the crystal structure reveal that BP86 reproduces the crystal structure with greater accuracy than B3LYP. In particular, B3LYP overestimates the Ni-P bond lengths. Furthermore, there is no significant difference between the computationally more expensive tzvp basis set and the split tzvp/svp basis set. Further optimizations and frequency calculations were therefore done with the BP86 functional and the split tzvp/svp basis set. Population[30] calculations were performed at the same level of theory and

Table 4.7. Geometrical parameters for **8cb**, experimental and theoretical.

		B3LYP/split		BP86/split		BP86/tzvp		B3LYP/tzvp	
Bonds	Experimental	Length	|difference|	Length	|difference|	Length	|difference|	Length	|difference|
P_1 Ni	2.231	2.316	0.085	2.260	0.029	2.264	0.033	2.322	0.091
P_2 Ni	2.157	2.216	0.059	2.174	0.017	2.178	0.021	2.221	0.064
O Ni	1.855	1.871	0.016	1.893	0.038	1.896	0.041	1.874	0.019
C Ni	1.886	1.898	0.012	1.905	0.019	1.909	0.023	1.901	0.015
C O	1.292	1.280	0.012	1.289	0.004	1.287	0.005	1.278	0.014
C C	1.354	1.355	0.001	1.365	0.011	1.365	0.011	1.354	0.000
		avg	0.031	avg	0.020	avg	0.022	avg	0.034
Angles	Experimental (º)	Angle (º)	|difference|	Angle (º)	|difference|	Angle (º)	|difference|	Angle (º)	|difference|
O Ni P_1	100.98	97.34	3.64	98.62	2.36	98.92	2.06	97.56	3.42
P_1 Ni P_2	104.78	104.71	0.07	104.26	0.52	104.38	0.40	104.84	0.06
P_2 Ni C_1	113.54	118.77	5.23	118.08	4.54	117.91	4.37	118.67	5.13
C Ni O	40.41	39.69	0.72	39.66	0.75	39.55	0.86	39.58	0.83
Ni O C	71.07	71.27	0.20	70.68	0.39	70.80	0.27	71.37	0.30
Ni C O	68.51	69.04	0.53	69.66	1.15	69.65	1.14	69.05	0.54
O C C	135.18	135.12	1.73	135.54	1.62	135.79	1.52	135.40	1.71
		avg	1.32	avg	1.27	avg	1.23	avg	1.31

analyzed with QMForge.[31] Transition states were located by performing 1-dimensional potential energy scans, running a frequency calculation on the highest point from the PES, and using geometries along the negative frequency as input structures for the QST2 method. Frequency calculations were done on the transition structures to ensure they are first order saddle points. Intrinsic reaction coordinate (IRC) calculations were done in most cases to ensure the transition state connects with the desired intermediates, except when the negative frequency clearly describes the desired reaction path such as in the case of phosphine dissociation. IRCs were also not performed if a transition state closely resembled a transition state on which an IRC had been done, i.e., no IRCs were done on **TS3-trans** and **TS2a**, because they resemble **TS3-cis** and **TS2**, respectively.

Several levels of theory were evaluated for single point calculations (Table 4.8). Two factors were taken into account for each level of theory: The CC coordinated complex **9** must be higher in energy than the CO coordinated **8b**, and the barrier for decarbonylation (the energy of **TS2** relative to the energy of **9**) must be close to the experimentally derived

Table 4.8. Energies of TS2 and 9 relative to 8b at several levels of theory.

		Free energy (kcal/mol) Relative to 8b	
Func	Basis	TS2	9
BP86	6-311G+(2d,p)	33.5	0.7
M06	SDD/6-311G+(2d,p)	30.4	0.4
M062x	SDD/6-311G+(2d,p)	34.1	4.0
M06l	tzvp	30.6	-5.5
m06l	6-311g*	26.6	-8.6
PBE	tzvp	32.5	-2.0
PBE	6-311g*	29.2	-4.2
M06l	6-311G+(2d,p)	30.6	-5.6
M06l	SDD/6-311G+(2d,p)	27.9	-1.3
PBE	6-311G+(2d,p)	33.4	-0.9
PBE	SDD/6-311G+(2d,p)	31.9	-0.4
M06l	SDD/6-311G*	30.1	-1.1
BP86	6-311g*	29.2	-2.4
B3LYP	6-311g*	38.3	3.9
M06l	6-31g*	24.6	-7.0
BP86	6-31g*	27.0	-1.5
PBE	6-31g*	27.0	-3.0
M06	6-31g*	29.0	-5.4
BLYP	6-31g*	28.7	1.9
M062x	6-31g*	40.8	5.0

28.8 kcal/mol. Most levels of theory examined predicted that the CC coordination would be preferred and that the barrier for decarbonylation is much higher than the experimental value. For the split basis sets, SDD[32] is used for Ni and the other basis for all other atoms. At a first glance, the M06[33] functional combined with SDD for nickel and 6-311+G(2d,p) for all other atoms, which was used by our collaborators in a mechanistic analysis of the Ni catalyzed [2 + 2 + 2] cycloaddition of diynes and tropone performed the best.[34] However, the energy of carbonyl carbene complex **10** at this level of theory is 50.4 kcal/mol relative to **8b**. We suspect the disparity of applicability of this level of theory for single point energy calculations to the diyne/tropone system vs. the ketene system is because the large SDD basis set was employed for Ni in the optimization and frequency calculations for the tropone/diyne system and not the ketene system. To our surprise (and possibly the chagrin of theoretical chemists), the relatively low level of theory BLYP/6-31g* provided energies of **9** and **TS2** relative to **8b** compatible with our experimental observations. This level of theory was chosen for the rest of the single point energy calculations.

References

1. Zhang, Z.; Zhang, Y.; Wang, J. *ACS Catal.* **2011**, *1*, 1621.

2. Ruchardt, C.; Schrauzer, G. N. *Chem. Ber.* **1960**, *93*, 1840.

3. (a) Auvinet, A. L.; Harrity, J. P. *Angew. Chem., Int. Ed.* **2011**, *50*, 2769. (b) Huffman, M. A.; Liebeskind, L. S. *J. Am. Chem. Soc.* **1991**, *113*, 2771.

4. Kumar, P.; Troast, D. M.; Cella, R.; Louie, J. *J. Am. Chem. Soc.* **2011**, *133*, 7719.

5. Rofer-DePoorter, C. K. *Chem. Rev.* **1981**, *81*, 447.

6. Mindiola, D. J.; Hillhouse, G. L. *J. Am. Chem. Soc.* **2002**, *124*, 9976.
7. Miyashita, A.; Sugai, R.; Yamamoto, J. *J. Organomet. Chem.* **1992**, *248*, 239.

8. Hoberg, H.; Korff, J. *J. Organomet. Chem.* **1978**, *152*, 255.

9. Hofmann, P.; Perez-Moya, L. A.; Stegelmann, O.; Riede, J. *Organometallics* **1992**, *11*, 1167.

10. Curley, J. J.; Kitiachvili, K. D.; Waterman, R.; Hillhouse, G. L. *Organometallics* **2009**, *28*, 2568.

11. Grotjahn, D. B.; Collins, L. S. B.; Wolpert, M.; Bikzhanova, G. A.; Lo, H. C.; Combs, D.; Hubbard, J. L. *J. Am. Chem. Soc.* **2001**, *123*, 8260.

12. Grotjahn, D. B.; Bikzhanova, G. A.; Collins, L. S. B.; Concolino, T.; Lam, K.; Rheingold, A. L. *J. Am. Chem. Soc.* **2000**, *122*, 5222.

13. Urtel, H.; Bikzhanova, G. A.; Grotjahn, D. B.; Hofmann, P. *Organometallics* **2001**, *20*, 3938.

14. Ellgen, P. C. *Inorg. Chem.* **1971**, *10*, 232.

15. Staudaher, N. D.; Stolley, R. M.; Louie, J. *Chem. Commun.* **2014**, *50*, 15577.

16. Le Page, M. D.; Patrick, B. O.; Rettig, S. J.; James, B. R. *Inorg. Chem. Acta.* **2015**, *431*, 276.

17. Yin, G.; Kalvet, I.; Englert, U.; Schoenebeck, F. *J. Am. Chem. Soc.* **2015**, *137*, 4164.

18. Sinnokrot, M. O.; Sherrill, C. D. *J. Phys. Chem. A* **2004**, *108*, 10200.

19. (a) Bleuel, E.; Laubender, M.; Weberndorfer, B.; Werner, H. *Angew. Chem., Int. Ed.* **1999**, *38*, 156. (b) Cordaro, J. G.; van Halbeek, H.; Bergman, R. G. *Angew. Chem., Int. Ed.* **2004**, *43*, 6366. (c) Grotjahn, D. B.; Bikzhanova, G. A.; Hubbard, J. L. *Organometallics* **1999**, *18*, 8614.

20. Wang, Y.; Agbossou, F.; Dalton, D. M.; Liu, Y.; Arif, A. M.; Gladysz, J. E. *Organometallics* **1993**, *12*, 2699.

21. Barcs, B.; Kollár, L.; Kégl, T. *Organometallics* **2012**, *31*, 8082.

22. Montgomery, J. *Science of Synthesis* **2001**, *11*, 61.

23. Taylor, E. C.; McKillop, A.; Hawks, G. H. *Org. Synth.* **1972**, *52*, 36.

24. Staudaher, N. D.; Lovelace, J.; Johnson, M. P.; Louie, J. *Org. Synth.* **2017**, *94*, 1.

25. Chavez, C. A.; Choi, J.; Nesterov, E. E. *Macromolecules* **2014**, *47*, 506.

26. Frisch, M. J.; Trucks, G. W.; Schlegel, H. B.; Scuseria, G. E.; Robb, M. A.; Cheeseman, J. R.; Scalmani, G.; Barone, V.; Mennucci, B.; Petersson, G. A.; Nakatsuji, H.; Caricato, M.; Li, X.; Hratchian, H. P.; Izmaylov, A. F.; Bloino, J.; Zheng, G.; Sonnenberg, J. L.; Hada, M.; Ehara, M.; Toyota, K.; Fukuda, R.; Hasegawa, J.; Ishida, M.; Nakajima, T.; Honda, Y.; Kitao, O.; Nakai, H.; Vreven, T.; Montgomery Jr., J. A.; Peralta, J. E.; Ogliaro, F.; Bearpark, M. J.; Heyd, J.; Brothers, E. N.; Kudin, K. N.; Staroverov, V. N.; Kobayashi, R.; Normand, J.; Raghavachari, K.; Rendell, A. P.; Burant, J. C.; Iyengar, S. S.; Tomasi, J.; Cossi, M.; Rega, N.; Millam, N. J.; Klene, M.; Knox, J. E.; Cross, J. B.; Bakken, V.; Adamo, C.; Jaramillo, J.; Gomperts, R.; Stratmann, R. E.; Yazyev, O.; Austin, A. J.; Cammi, R.; Pomelli, C.; Ochterski, J. W.; Martin, R. L.; Morokuma, K.; Zakrzewski, V. G.; Voth, G. A.; Salvador, P.; Dannenberg, J. J.; Dapprich, S.; Daniels, A. D.; Farkas, Ö.; Foresman, J. B.; Ortiz, J. V.; Cioslowski, J.; Fox, D. J.; Gaussian, Inc.: Wallingford, CT, USA, 2009.

27. (a) Becke, A. D. *J. Chem. Phys.* **1993**, *98*, 5648. (b) Lee, C.; Yang, W.; Parr, R. G. *Phys. Rev. B* **1988**, *37*, 785.

28. (a) Schaefer, A.; Horn, H.; Ahlrichs, R. *J. Chem. Phys.* **1992**, *97*, 2571. (b) Schaefer, A.; Huber, C.; Ahlrichs, R. *J. Chem. Phys.* **1994**, *100*, 1994.

29. (a) Becke, A. D. *Phys. Rev. A* **1988**, *38*, 3098. (b) Perdew, J. P. *Phys. Rev. B* **1986**, *33*, 8822.

30. Glendening, E. D.; Reed, A. E.; Carpenter, J. E.; Weinhold, F. *NBO Version 3.1*.

31. Tenderholt, A. L. *QMForge, Version 2.4, http://qmforge.sourceforge.net*.

32. (a) Szentpaly, L. V.; Fuentealba, P.; Preuss, H.; Stoll, H. *Chem. Phys. Lett.* **1982**, *93*, 1982. (b) Dolg, M.; Wedig, U.; Stoll, H.; Preuss, H. *J. Chem. Phys.* **1987**, *86*, 866. (c) Schwerdtfeger, P.; Dolg, M.; Schwarz, W. H. E.; Bowmaker, G. A.; Boyd, P. D. W. *J. Chem. Phys.* **1989**, *91*, 1762.

33. (a) Zhao, Y.; Truhlar, D. G. *Theor. Chem. Acc.* **2008**, *120*, 215. (b) Zhao, Y.; Truhlar, D. G. *Acc. Chem. Res.* **2008**, *41*, 157.

34. Kumar, P.; Thakur, A.; Hong, X.; Houk, K. N.; Louie, J. *J. Am. Chem. Soc.* **2014**, *136*, 17844.

CHAPTER 5

ON THE MECHANISM OF LIGAND EXCHANGE OF (DPPF)NI(KETENE) WITH FREE KETENE

Introduction

Ni–Ketene complexes have long been thought to be intermediates in several synthetic reactions.[1] Despite this, few have been isolated and little is known about their fundamental reactivity.[2] We have recently investigated the mechanism of thermal decomposition of a series of (dppf)Ni(ketene) complexes.[3] This report bridges the gap between the apparent instability of most previously known Ni–ketene complexes and the success of reactions that involve them as intermediates. As part of our program in developing reactions that involve Ni–ketene complexes as intermediates, we wish to develop a Ni catalyzed Wittig reaction on carbon dioxide. To our knowledge, there are two examples of Wittig reactions on carbon dioxide. One is the stoichiometric reaction of the most prototypical phosphorus ylide, trimethylmethylenephosphane with Aresta's complex, which produced a thermally unstable ketene complex in good yield (eq 5.1).[2e] The other reaction produces symmetrical allenes and requires high reaction temperatures (eq 5.2).[4] Our aim is to expand this reactivity by using nickel to facilitate one Wittig reaction on carbon dioxide, and subsequently trap the ketene in such a way that it will not undergo a second Wittig reaction.

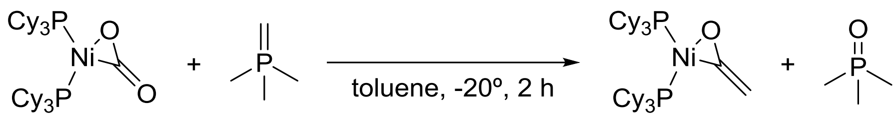

(5.1)

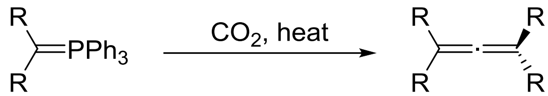

(5.2)

Our initial attempts at developing this reaction failed, because the trapping reagent either reacted with carbon dioxide, or failed to react with the ketene faster than the phosphorus ylide (*vide infra*). This raises the question of whether the trapping reagent should be designed to react with ketene while free or coordinated to Ni. To address this question, we investigated the mechanism of exchange of (dppf)Ni(ketene) with free ketene (Figure 5.1A). In this exchange, there are two mechanistic possibilities. First, the dissociative mechanism (Figure 5.1B) proceeds by dissociation of the ketene followed by association of exogenous ketene. The alternative associative mechanism involves association of the free ketene, producing a 4-coordinate intermediate (Figure 5.1C). Subsequent dissociation of the original ketene completes the ligand exchange. Given that 1 is a 16 electron complex, the associative mechanism is much more likely.[5]

Results and Discussion

With knowledge of how to stabilize ketene complexes in hand, we turned our attention to developing a nickel catalyzed Wittig reaction on carbon dioxide. We selected (dppf)Ni(*trans*-stilbene) as a catalyst owing to dppf's ability to stabilize ketene complexes and stilbene's relative lability.[6] A key feature of a Wittig reaction on carbon dioxide is trapping the intermediate ketene such that the carbonyl cannot undergo a second Wittig

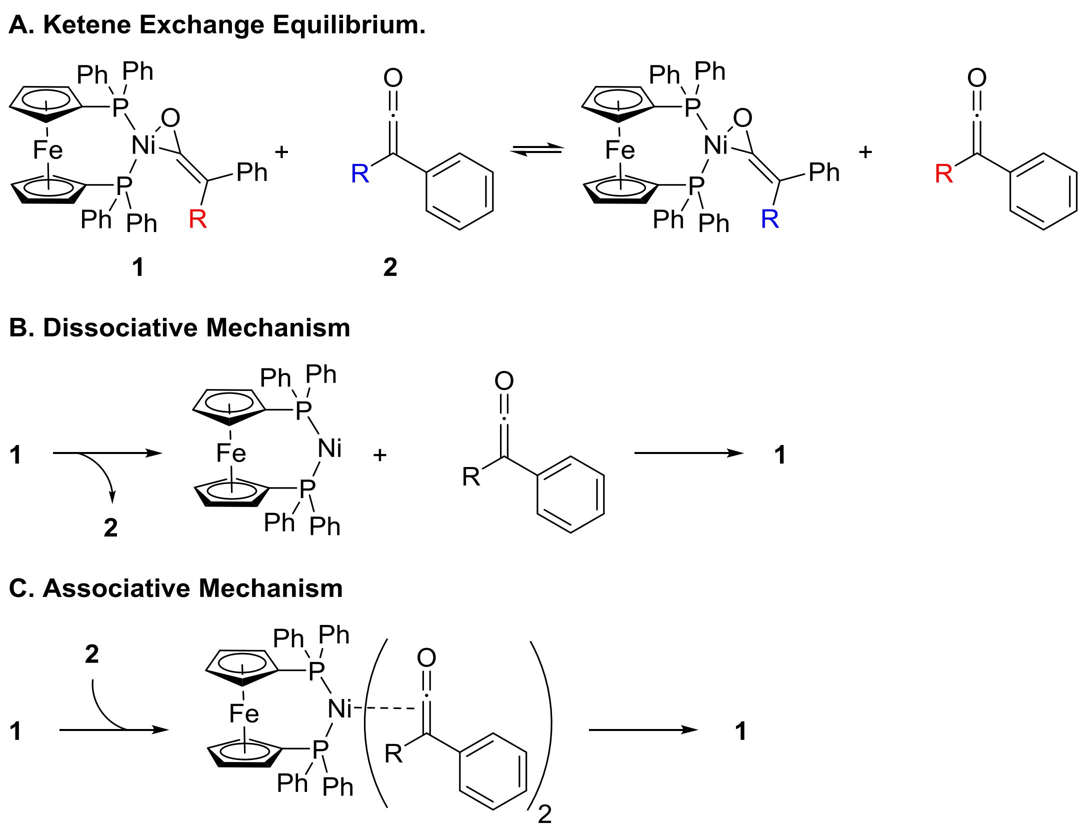

Figure 5.1. Ketene ligand exchange equilibrium and mechanistic possibilities.

reaction, which would produce undesired symmetrical allenes, as was the case in eq 5.2. As such, we selected *para*-methoxybenzylamine, which rapidly reacts with ketenes to form amides,[7] which only react with phosphorus ylides under certain circumstances.[8] Furthermore, the PMB group can be easily removed.[9] Unfortunately, when a solution of phosphorus ylide, *para*-methoxybenzylamine, and catalytic (dppf)Ni(*trans*-stilbene) in C_6D_6 was put under 50 psi of CO_2 in a J.Young tube, a white solid formed at the top of the solution (eq 5.3). This solid was identified as a carbamate salt, which are known to form from amines and carbon dioxide under basic conditions.[10] In an attempt to keep the carbamate salt in solution, DMSO-d_6 was employed as the reaction solvent. No solid formed, and the ylide was consumed within 15 min as assessed by ^{1}H NMR.

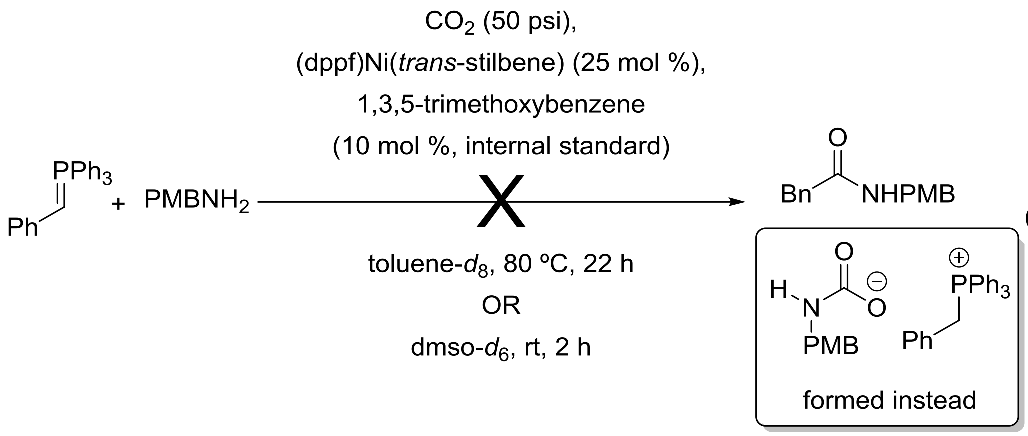

(5.3)

Concomitantly a doublet at 5.16 ppm (J_{PH} = 15.7 Hz) appeared, indicative of ylide protonation by DMSO. Furthermore, the four peaks corresponding to the cp protons on the dppf ligand collapsed into two peaks, indicating catalyst death in DMSO. In a control experiment where the amine and catalyst were omitted, full consumption of ylide and appearance of phosphonium salt was also observed, indicating DMSO is a strong enough acid to protonate the ylide.

Next we attempted a Danheiser type benzannulation (eq 5.4) of carbon dioxide, a vinyl phosphorus ylide, and 3-hexyne (Figure 5.2). Despite $Ni(COD)_2$'s insolubility in ether at low temperature, it is a very proficient catalyst for this reaction starting from cyclobutenones and alkynes (eq 5.4).[1b,11] Given $Ni(COD)_2$'s catalytic ability in this reaction, we thought the Danheiser benzannulation could be an effective method of ketene trapping. When we attempted this reaction, we observed >90% ylide consumption in 3 h

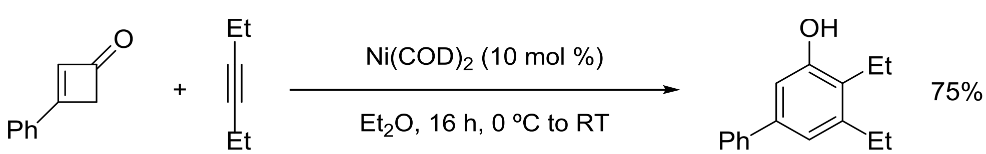

(5.4)

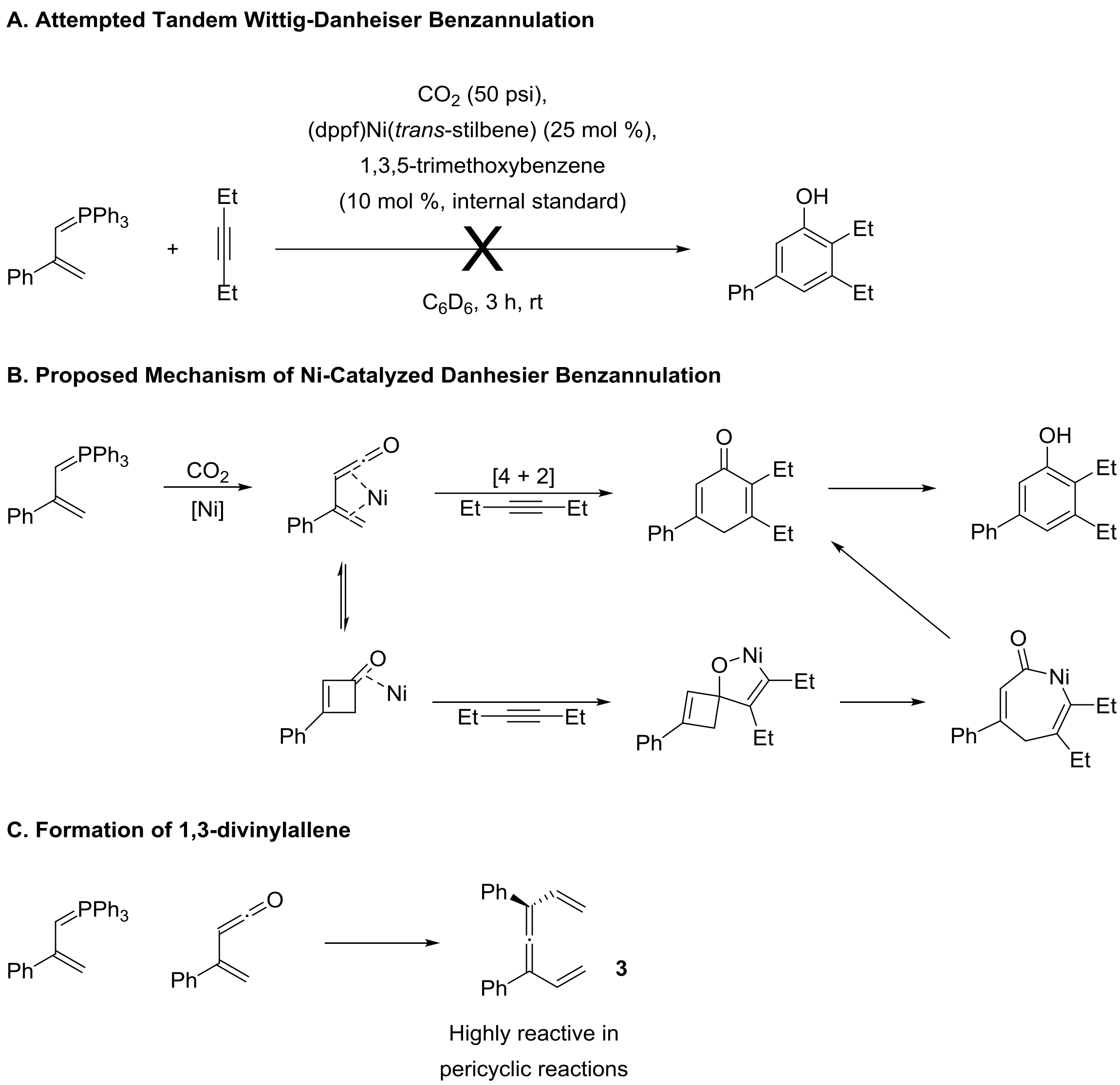

Figure 5.2. A. Wittig Danheiser reaction of ylide, CO_2, and 3-hexyne. B. Proposed mechanism of Wittig Danheiser reaction. C. Formation of 1,3-divinylallene.

by ^{1}H NMR with no consumption of alkyne. Copious triphenylphosphine oxide was observed by ^{31}P NMR and GC/MS, indicating the ylide successfully underwent a Wittig reaction. However, a complex product mixture and no desired product were observed by ^{1}H NMR. Several peaks appear between 5.0 – 5.5 ppm, including a poorly resolved doublet at 5.42 ppm, a triplet at 5.39 (J = 2.2 Hz), and a doublet of doublets at 5.01 ppm (J = 3.4, 2.2 Hz) that integrate 1:1:1 that could be consistent with **3**. Multiple compounds including stilbene, triphenylphosphine oxide, and several unknowns were detected by GC/MS, with no single unknown species accounting for a significant amount of the mass balance. We attribute this to the ketene reacting with a second equivalent of ylide faster than the alkyne, and formation of allene **3**. This allene bears two vinyl substituents and as such is very reactive in [4 + 2] cycloadditions with itself and with alkynes.[12] Furthermore, 1,3-divinylallenes have two possible dienes and four dieneophiles, and could therefore give rise to the observed complex reaction mixture.

Given the failure of our first two attempts to generate a ketene from a Wittig reaction on carbon dioxide and trap that ketene with a reagent other than the Wittig reagent, we turned our attention to the mechanism of ketene trapping. The most fundamental question in this mechanism is if the ketene is trapped when coordinated to the nickel center or if it is displaced and is trapped while free, and we therefore began investigating the mechanism of ketene-ketene exchange: the exchange of **1** and **2**.

Our initial attempts to probe the mechanism of this ligand exchange involved ^{1}H NMR magnetization transfer experiments (Figure 5.3).[13] This experiment works by pulsing the sample at the frequency of a specific peak A before the excitation pulse. This saturates the protons that corresponding to peak A, resulting in a spectrum with no peaks at the saturated frequency. Furthermore, if the proton A chemically exchanges with other protons (B) in the sample faster than the NMR timescale, the peaks corresponding to protons B will also decrease in intensity. First order rate constants for the exchange reaction can be determined from the intensity of peak B with and without saturating A and the T_1 of B according to the equation in Figure 4.3 where T_1 is the spin lattice relaxation time[14] of peak B as determined from a separate inversion recovery experiment, and M_s and M_0 are the

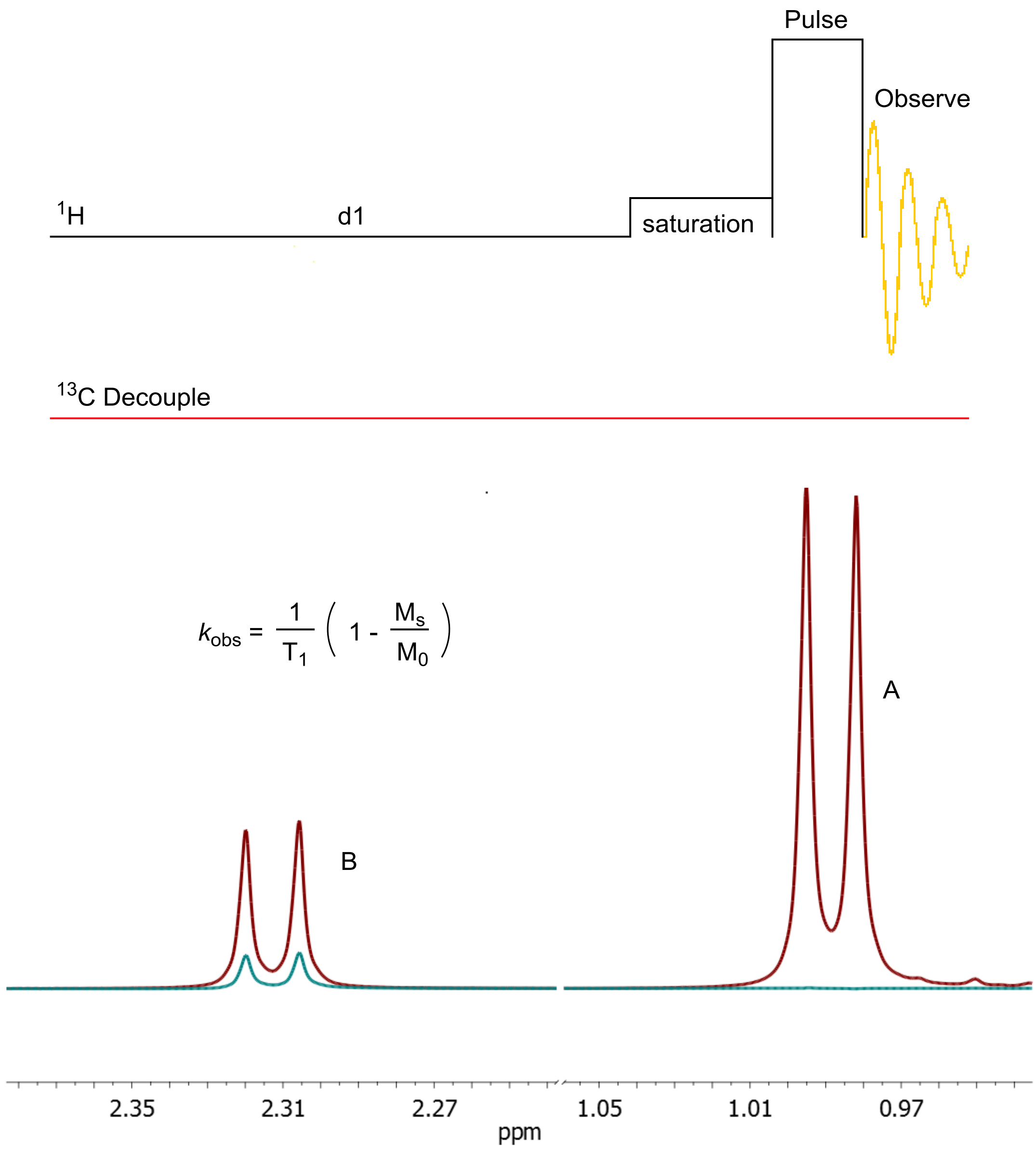

Figure 5.3. Saturation transfer pulse sequence and representative ^{1}H spectrum (red) and saturation transfer spectrum (blue) where the sample is pulsed at the resonant frequency of peak A before excitation, resulting in the disappearance of peak A and a decrease in intensity of peak B due to exchange of protons A and B.

magnetization of nucleus B with and without the saturation pulse. Rate constants between ~10^2 and ~10^{-2} /s can typically be measured by this method.

In our case, we attempted this experiment on samples containing both free ketene and ketene complex. In this experiment, peaks A and B must be at least ~0.5 ppm shifted from each other. Unfortunately, no suitable peaks have this separation in C_6D_6 or toluene-d_8. However, a separation of 1.33 ppm was observed for the terminal methyls on the isobutyl chain of phenyl isobutyl ketene **2a** and (dppf)Ni(phenyl isobutyl ketene) **1a** in THF-d_8. Monitoring a solution of **1a** and excess **2a** by ^{1}H NMR at room temperature led to the disappearance of **1a** and a decrease of **2a** with concomitant appearance of peaks consistent with (dppf)Ni(phenyl isobutyl ketene dimer) **4** over roughly 1 h (eq 4.5). Since the pulse sequences to determine T_1 and the intensity of peak B with and without saturation of A takes roughly 25 min, and significant amounts of **1a** and **2a** are consumed in this timeframe, these conditions are not amenable to determining rate constants for the ligand exchange. However, upon lowering the temperature to -10 ºC, the dimerization reaction is suppressed to the point where the inversion recovery and saturation transfer experiments can be conducted with insignificant ketene dimerization (Figure 5.4). However, the rate constants measured for the exchange were on the cusp of the 10^{-2} /s cutoff. In an attempt to measure accurate rate constants, we raised the relaxation delay to 30 s to obtain quantitative spectra. With this pulse sequence, we obtained rate constants around $3x10^{-2}$ /s.

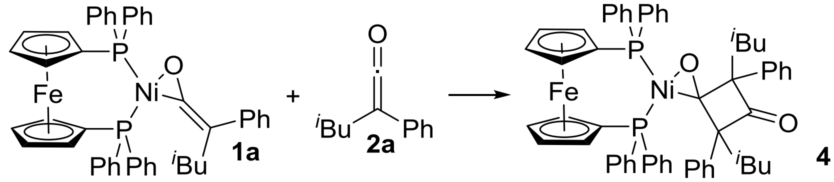

(4.5)

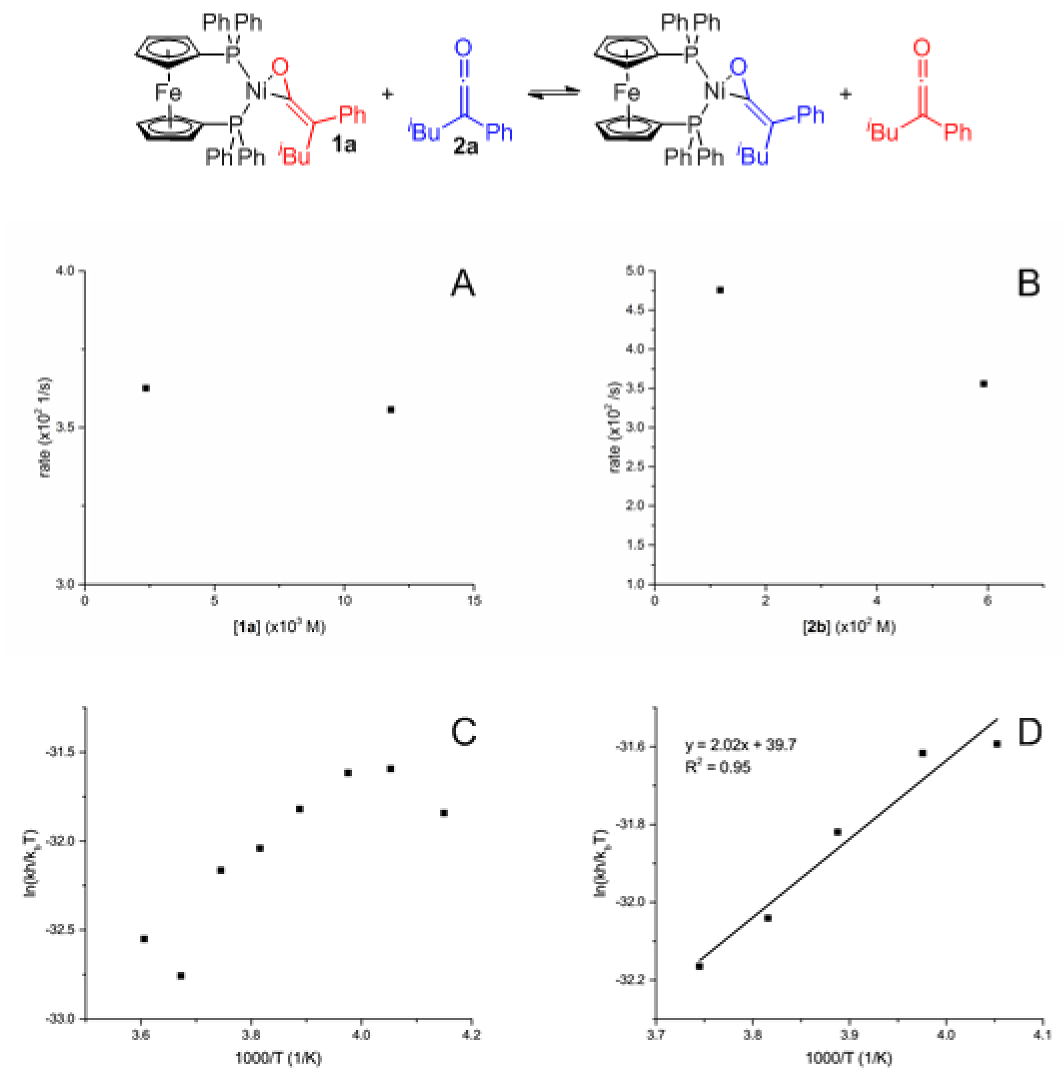

Figure 5.4. Ligand exchange investigated by saturation transfer experiments. A. Effect of complex concentration on rate. B. Effect of ketene concentration on rate. C. Full Erying plot. D. Linear region of Eyring plot showing positive enthalpy of activation and large negative entropy of activation.

However, changing the concentration of ketene and ketene complex led to insignificant changes in observed rate constants. Furthermore, measuring rate constants at several temperatures between +4 and -32 ºC qualitatively gave faster rate constants at lower temperatures. The region between -6 and -26 ºC produced a linear Eyring plot with negative $\Delta H^{\ddagger}$ = -16.8 kcal/mol and extraordinarily large negative $\Delta S^{\ddagger}$ = -78.9 eu. With these nonsensical data in hand, we abandoned saturation transfer as a method of studying the kinetics of the ketene–ketene ligand exchange reaction.

We turned out attention to the exchange of (dppf)Ni(phenyl *n*-butyl ketene) (**1b**) with phenyl *n*-butyl ketene-d_9 (**2b-*d*₉**), where the butyl chain is fully deuterated (Figure 5.5). Monitoring the disappearance **1b** by ^{1}H NMR at -12 ºC upon addition of a solution of excess **2b-d_9** to a solution of **1b** in toluene-d_8 surprisingly did not produce a linear ln([**1b**]/[**1b**]$_0$) vs. time plot, as is expected with pseudo-first order kinetic experiments, and was the case for alkene exchange at a Pd(0) center.[15] Instead, a sigmoidal shape is observed (Figure 5.5A). While dissatisfied with the complexity of the kinetic profile, at least we were vindicated in the failure of our attempts with saturation transfer: the rate of exchange is not constant with respect to time! The best known example of this behavior is in autocatalytic[16] reactions, where the products catalyze the reaction. However, in this case, the reactants and products only differ isotopically. The reaction is likely autoinductive,[17] where an intermediate or side product is catalyzing the reaction. Examination of the region of the sigmoid where the reaction rate is the highest reveals a linear ln([**1b**]/[**1b**]$_0$) vs. time profile. Using rate constants taken from this fast section shows the ligand exchange is first order in free ketene, indicative of an associative mechanism. However, the reaction appears to be inverse-half order in ketene complex **1b**, which is difficult to rationalize, and is likely

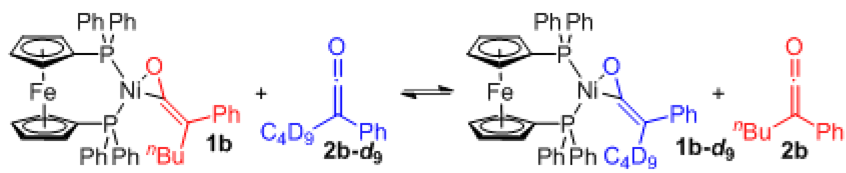

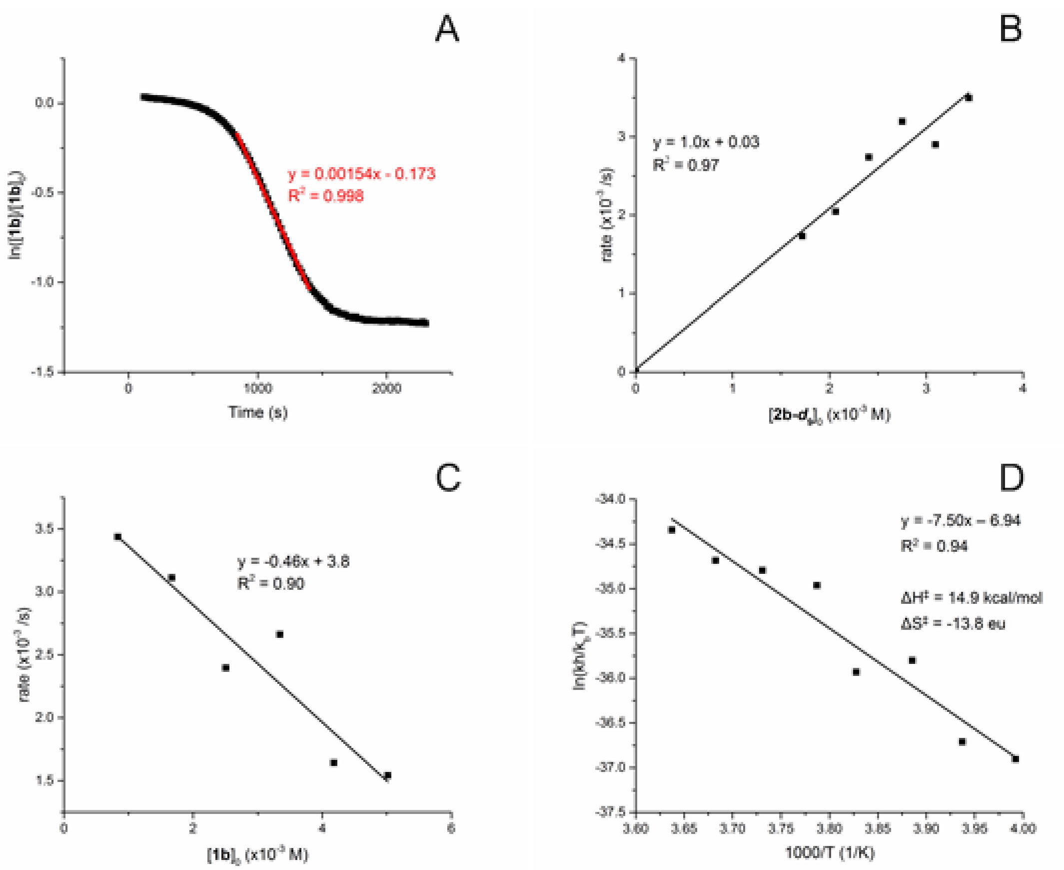

Figure 5.5 . Ligand exchange of **1b** and **2b-*d*₉**. A. ln([**1b**]/[**1b**]$_0$) vs. time with linear portion in red. B. Order in free ketene. C. Order in ketene complex. D. Temperature dependence.

due to error associated with the randomness of the induction period.

Investigating the rate of reaction at different temperatures produced the Eyring plot in Figure 5.5D. The low activation of enthalpy is consistent with the rapid rate of reaction and the negative entropy of activation indicates that entropy decreases during the rate determining step of the reaction. Again, these observations are consistent with an associative ligand exchange.

While the order in **2b-*d*₉** and the activation parameters clearly indicate an associative process, these data only take into account the fastest part of the kinetic profile of each trial, and explanations of why the concentration vs. time plots are sigmoidal and the reaction is inverse half order in ketene complex are lacking. To probe the reaction pathway, we performed cursory DFT calculations (Figure 5.6). Dissociation of ketene to the (dppf)Ni fragment was found to cost 27.1 kcal/mol. Modeling of a (dppf)Ni fragment with two η^2–(C,O) bound ketenes failed to converge with both ketenes bound, ruling out a straightforward ligand exchange. Similarly, modeling of a (dppf)Ni fragment with one η^2 ketene fragment and an η^1 coordinated ketene failed to converge with both ketenes coordinated. However, the structures of the (dppf)Ni fragment with one or two η^1 ketenes both converged. Despite this, isomerization of the ketene from η^2 to η^1 cost 19.9 kcal/mol, and coordination of an additional ketene cost another 5.6 kcal/mol, indicating these species are not likely to be on the exchange pathway. These calculations preclude direct coordination of ketene to **1b** without prior phosphine dissociation. Our previous work on the decomposition of nickel–ketene complexes indicates that partial phosphine dissociation from **1b** is energetically uphill by 22.2 kcal/mol, although **3**, the isomer of complex **1b** that has the ketene coordinated through the C=C bond and two atoms of the aromatic ring, and

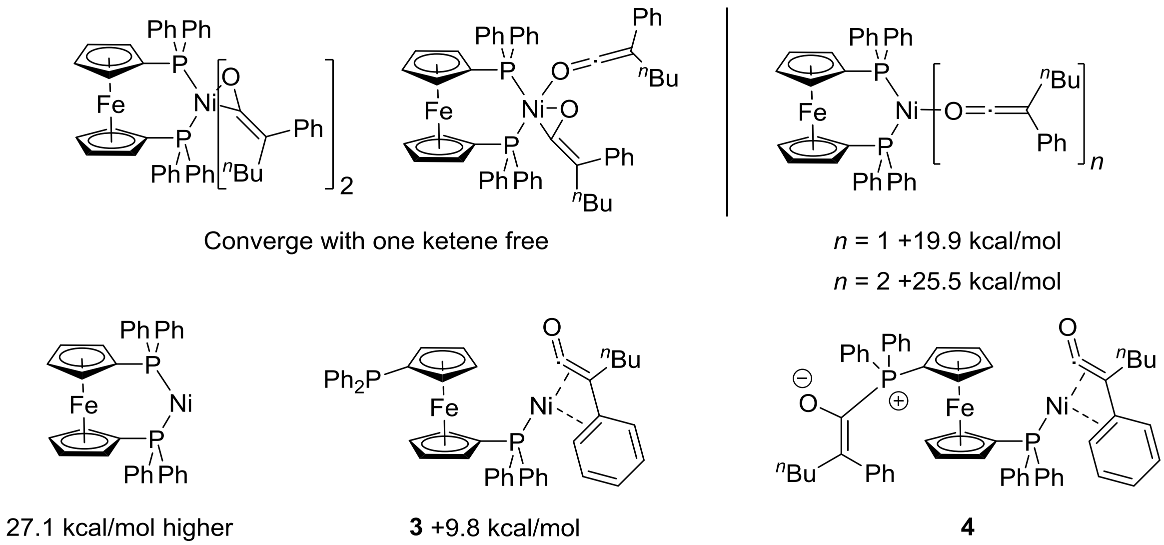

Figure 5.6. DFT calculated energies of possible intermediates on the ketene exchange pathway.

only one phosphine associated is 9.8 kcal/mol higher in energy than **1b** and is kinetically accessible. We therefore propose that association of exogenous ketene occurs to **3** and that the intermediate inducing the ligand exchange facilitates partial phosphine dissociation. Furthermore, addition of the free phosphine to ketene would result in intermediate **4**, the anionic oxygen atom of which could possibly facilitate partial phosphine dissociation.

Blackmond successfully deconvoluted the antoinductive mechanism of the de Sarlo cycloaddition by screening possible by-products of the reaction as additives.[17] It was found that addition of sodium nitrite caused the reaction to skip the induction period, and the reaction gave a straightforward second order kinetic profile. In this vein, we examined several additives that could form during the reaction or modulate our proposed pathway (Figure 5.7). A sample that was left at room temperature overnight was found to contain (dppf)Ni(CO)$_2$ **5** by ^{31}P and ^{1}H NMR and ketene dimer **6** by ^{1}H NMR spectroscopy. However, **5** inhibited the reaction both in terms of induction period and first order rate

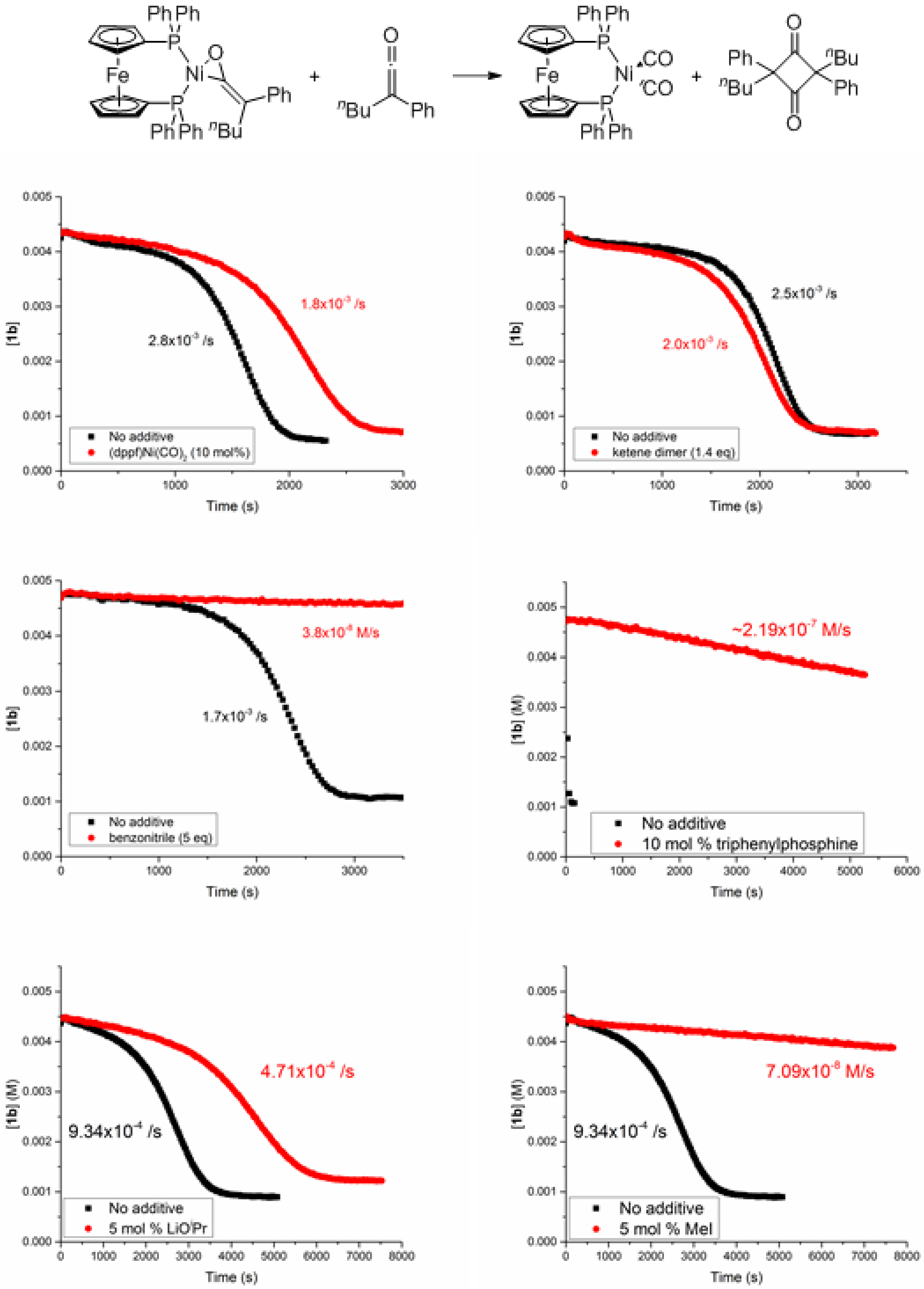

Figure 5.7. Formation of **4** and **5** and concentration vs. time plots with and without additives.

constant and **6** had little effect on the concentration vs. time profile of the exchange. We next evaluated benzonitrile, which is known to facilitate partial phosphine dissociation from $(Xantphos)_2Ni$,[18] but addition of 5 equivalents of benzonitrile resulted in an observed zero order rate constant of ~$4x10^{-8}$ M/s with no reaction induction after 90 min. 10 mol% triphenylphosphine was added to mimic intermediate **3** and resulted in a zero order rate constant of $2.19x10^{-7}$ M/s at room temperature with no induction within 90 min. Under the same conditions without added triphenylphosphine, the reaction goes to completion within 2 min and an accurate rate constant could not be measured. Lithium isopropoxide, which we hypothesized could mimic intermediate **4**, caused the reaction to have a longer induction period and proceed at roughly half the rate as without the additive. Methyl iodide, which could possibly aid in partial phosphine dissociation by trapping the dissociated phosphine arm, was added with a 10 mol % loading, and a zero order rate constant of $7.09x10^{-8}$ M/s was observed with no induction after 2 h.

Thwarted in our attempts to skip the induction period of the ligand exchange with carefully considered additives, we sought to produce the catalyst by addition of a small amount of the ketene stock (~10 μL) at room temperature followed by cooling the sample and adding the rest of the aliquot of ketene. This approach of pre-forming the active catalyst to simplify an inductive kinetic profile has been seen in 1-octene polymerization,[19] and we attempted it even though it would not give us insight into the structure of the catalyst. We observed less coordinated ketene and more free ketene at the outset of the reaction, indicating the reaction comes to equilibrium before the second addition. Furthermore, the induction period was skipped, although this result was observed on the first trial and could not be reproduced. Owing to the irreproducibility of this result, we hypothesized that trace water was entering the sample through the hole created in the septum by the needle. We therefore added trace water to the ketene stock at the beginning of an experiment. To our delight, this removed the induction period from the kinetic profile of the reaction at -12 ºC. Upon investigation of temperature dependence with added water (Figure 5.8), we observed that the induction period returned upon lowering the temperature to -15 ºC or below. Activation parameters of $\Delta H^{\ddagger}$ = 16.2 kcal/mol and $\Delta S^{\ddagger}$ = -6.4 eu were derived from the Eyring plot in Figure 5.8 and are consistent with an associative process with a small enthalpic barrier. For reaction order in each reagent, a temperature of -15 ºC was selected to obtain a longer linear region than at -12 ºC. The reaction is second order in water until about 10 mol%, when the reaction is saturated by water. Despite these seemingly sensical results, the reaction appears to be inverse half order in complex and half order in ketene, with poor R^2 values indicating significant error associated with the induction period.

Given that water accelerates the ligand exchange and that our experimental procedure allows adventitious water to enter the samples (the ketene stock is added to the NMR tube through a syringe, which produces a hole in the septum), we observed the ligand exchange reaction of a sample that had been prepared in the glovebox at -40 ºC in a J.Young tube, and transported in a -78 ºC bath before being allowed to warm to -12 ºC in the spectrometer. Indeed, the ligand exchange showed a similar profile to that of a typical run involving addition of ketene to a septum sealed tube containing ketene complex. This indicates that adventitious water is not the species catalyzing the ligand exchange, and instead water aids in the formation of the active catalyst.

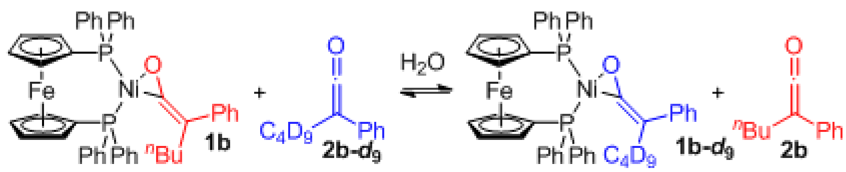

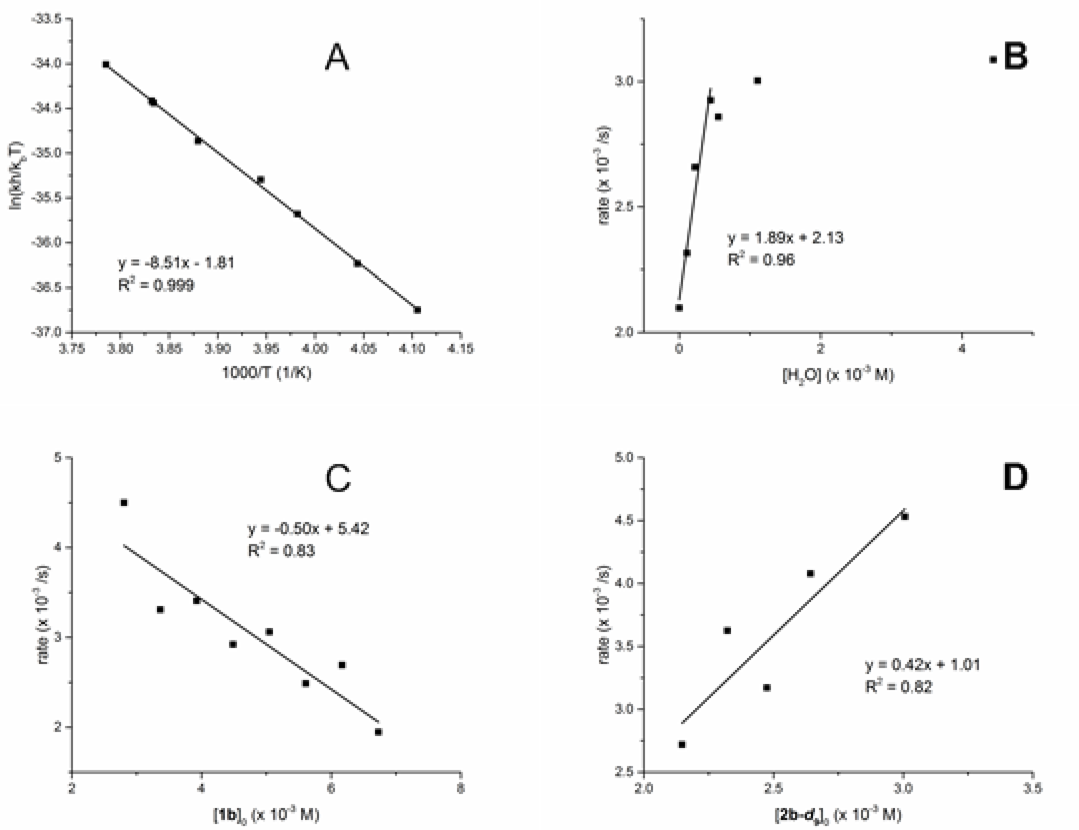

Figure 5.8. Ligand exchange with added water. A. Temperature dependence. B. Water dependence. C. Order in complex. D. Order in free ketene.

Conclusion

To summarize, our attempts at developing a Wittig reaction on carbon dioxide failed because the trapping reagent was either reactive enough to be deactivated by carbon dioxide, or not reactive enough to trap the ketene faster than the ylide. This prompted us to investigate the mechanism of ketene trapping in further detail, beginning with ketene exchange at Ni. Saturation transfer experiments failed to produce meaningful data, so we turned to monitoring the reaction of ketene complex with the ketene's deuterated isotopologue. This showed that the ligand exchange is autoinductive. Examination of the part of the concentration vs. time profile that fits pseudo-first order kinetics at different temperature and reagent concentrations indicates that ketene likely associates during the rate determining step. Based on DFT calculations, we believe that ketene associates to species **3**, where the dppf ligand is partially dissociated and the ketene is coordinated η^4 through the C=C bond of the ketene and two carbon atoms of the aromatic ring. Furthermore, we speculate that an intermediate forms from **1b** and **2b** that catalyzes the conversion of **1b** to **3**, although the identity of this intermediate could not be elucidated by screening additives. Another possibility is the autoinductive intermediate/byproduct facilitates isomerization of the ketene from η^2 to η^1 followed by coordination of exogenous ketene. Addition of water shortened the induction period and increased the rate of ligand exchange. An experiment where water was rigorously excluded from the reaction indicated that adventitious water is not catalyzing the ligand exchange, but is facilitating the formation of the catalyst.

Unfortunately, this study did not provide significant mechanistic insight into the autoinductive nature of the ketene-ketene exchange at the (dppf)Ni center. However, we embarked on this study to determine if we should choose trapping reagents that react with free or coordinated ketene. We have discovered that the exchange is rapid at ambient temperature, and that addition of coordinating additives such as triphenylphosphine inhibits the exchange, providing a switch. The next steps toward developing a Wittig reaction on carbon dioxide should involve studying the rates of reaction of free/coordinated ketene with both phosphorus ylides and potential trapping reagents to find conditions that will allow the ketene to be trapped faster than it undergoes a Wittig reaction.

Experimental Section

General information. All experimental procedures were carried out under intert atmosphere (N_2 or Ar) using standard schlenk techniques or in a glovebox in oven or flame-dried glassware. All protic solvents used in reactions were dried and deoxygenated with a Grubbs type solvent purification system. Deuterated solvents, benzonitrile, 3-hexyne, and methyl iodide were distilled from calcium hydride and subjected to three freeze-pump-thaw cycles prior to use. **1a**, **1b**, **2b-*d*₉**,[3] **2a**, **2b**,[20] **5**[21] and were synthesized as previously reported. **6**[22] was prepared in an analogous fashion to the literature, using **1b** instead of phenyl ethyl ketene. Unless indicated, all other reagents were purchased from commercial sources and used as received. Butyl Lithium was titrated using a known amount of menthol and 1,10-phenanthroline as an indicator in a modification of a literature procedure.[23] ^{1}H NMR spectra of pure compounds were collected either on a Varian Unity 300 or one of two Agilent DirectDrive 500 MHz instruments. ^{13}C spectra were collected on a Varian Inova 400 or one of the two DirectDrive 500 MHz instruments. ^{31}P spectra were collected on either the Unity 300 or one of the DirectDrive instruments (500B). Spectra of Wittig reactions were collected on the DirectDrive 500 equipped with the cold probe (500A). Kinetic data for both the saturation transfer, inversion recovery, and deuterated ketene exchange were collected on the DirectDrive 500B, which has variable temperature capability.

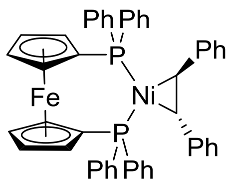

(Dppf)Ni(trans-stilbene). To (dppf)Ni(COD)[24] (251.3 mg, 0.349 mmol) in a 20 mL vial with a stir bar was added a solution of trans-stilbene (360.5 mg, 1.75 mmol, 5 eq) in benzene (4 mL). The reaction was stirred overnight and carefully layered with pentane (5 mL). The vial was allowed to sit for 3 days, at which point the solids were collected by filtration, washed with several portions of pentane, and dried under high vacuum to yield the product as red crystals (245.1 mg, 88.4%). ^{1}H NMR (300 MHz, C_6D_6) δ 7.79 (s, br, 4H), 7.19 (s, br, 4H), 7.07 (m, 18H), 6.91 (d, J = 6.6 Hz, 4H), 4.38 (s, 2H), 4.12 (s, 2H), 3.90 (s, 2H), 3.82 (s, 4H). ^{13}C NMR (101 MHz, C_6D_6) δ 145.7 (s), 140.0 (t, J = 17.1 Hz), 136.5 (t, J = 18.2 Hz), 135.7 (t, J = 7.5 Hz), 133.4 (t, J = 6.6 Hz), 129.6 (d, J = 30.4 Hz), 125.8 (s), 123.3 (s), 81.9 (dd, J = 21.7, 20.2 Hz), 75.2 (m), 72.0 (d, J = 38.7 Hz), 63.0 (t, J = 6.9 Hz). ^{31}P NMR (121 MHz, C_6D_6) δ 26.2. IR (nujol) 1589, 1488, 1463, 1433, 1379, 1305, 1250, 1224, 1161, 1093, 1069, 1035, 1024, 997, 891, 840, 813, 757, 741, 700, 691, 637. Anal. Calcd. for $C_{48}H_{40}FeNiP_2$: C, 72.67; H, 5.08. Found: C, 72.70; H, 5.33.

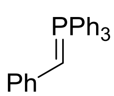

Benzylidenetriphenyl-λ^5-phosphane. In the glovebox, benzyltriphenylphosphonium bromide (246.3 mg, 0.562 mmol) was weighed into a 5 mL vial and suspended in pentane (2 mL) with stirring. Freshly titrated butyl lithium in hexanes (2.67 M, 0.2 mL, 0.534 mmol, 0.95 equiv) was added dropwise over 2 min. An immediate color change to orange was observed. The vial was capped and the reaction was allowed to stir for an additional 6 h, at which point it was filtered through celite, washing with THF (2 mL) into a tared 5 mL vial. The vial was placed in the freezer (-40 ºC) overnight. The supernatant was decanted and the remaining solids dried under high vacuum to yield 62.6 mg (33%) of the ylide as an orange powder. ^{1}H NMR (500 MHz, C_6D_6) δ 7.70 – 7.62 (m, 6H), 7.11 (t, J = 7.6 Hz, 2H), 7.06 (d, J = 7.1 Hz, 2H), 7.01 (td, J = 7.1, 1.2 Hz, 3H), 6.93 (td, J = 7.5, 2.4 Hz, 6H), 6.69 (t, J = 7.0 Hz, 1H), 2.85 (d, J = 19.0 Hz, 1H). ^{13}C NMR (126 MHz, $CDCl_3$) δ 147.9 (d, J = 7.5 Hz) 133.8 (d, J = 10 Hz), 132.07, 131.46, 130.75, 129.4 (d, J = 12.5 Hz), 122.4 (d, J = 13.8 Hz), 116.32, 28.8 (d, J = 128.8 Hz). ^{31}P NMR (121 MHz, C_6D_6) δ 8.40. IR (NaCl, C_6D_6) 3235, 2389, 2282 (s), 1618, 1591, 1483, 1453, 1391, 1330 (s), 1290, 1162, 1097, 957, 812 (s), 745, 719, 694.

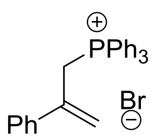

Triphenyl(2-phenylallyl)phosphonium bromide. (3-bromoprop-1-en-2-yl)benzene[25] (512.1 mg, 2.55 mmol) was weighed into an oven-dried 20 mL vial that had been cooled to room temperature under a stream of nitrogen. Dichloromethane (5 mL) was added and the solids dissolved with stirring. Triphenylphosphine (703.6 mg, 2.55 mmol, 1 eq) was added in one portion and the vial was capped. The reaction was stirred for 24 h, and the vial was filled with pentane, causing an immediate formation of a white solid. The crystallization was allowed to go to completion for 24 h, at which point the solids were collected by filtration on a 15 mL medium porosity fritted funnel. The solids were transferred to a tared 20 mL and dried under high vacuum to yield the phosphonium salt as a white powder (1.03 g, 86%). ^{1}H NMR (500 MHz, $CDCl_3$) δ 7.80 (dd, J = 12.5, 8.2 Hz, 6H), 7.67 (t, J = 7.5 Hz, 3H), 7.55 (m, 6H), 7.24 (m, 2H), 7.09 (m, 3H), 5.52 (d, J = 5.2 Hz, 1H), 5.48 (d, J = 4.5 Hz, 1H), 5.34 (d, J = 15.4 Hz, 1H). ^{13}C NMR (126 MHz, $CDCl_3$) δ 139.6 (d, J = 2.5 Hz), 136.1 (d, J = 10 Hz), 134.8 (d, J = 2.5 Hz), 134.3 (d, J = 10

Hz), 130.1 (d, J = 12.5 Hz), 128.6 (s), 128.2 (s), 126.9 (s), 123.7 (d, J = 11.2 Hz), 118.2 (d, J = 85 Hz), 31.1 (d, J = 46 Hz). ^{31}P NMR (121 MHz, $CDCl_3$) δ 21.9.

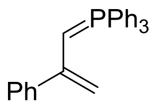

Triphenyl(2-phenylallylidene)-λ^5-phosphane. In the glovebox, triphenyl(2-phenylallyl)phosphonium bromide (134.0 mg, 0.281 mmol) was weighed into a 5 mL vial and suspended in pentane (2 mL). Freshly titrated butyl lithium (2.67 M, 0.1 mL, 0.267 mmol, 0.95 eq) was added dropwise over 1 min, causing an immediate color change to orange. The reaction was stirred an additional 10 min, filtered through celite, washing with pentane (2 mL) into a tared 5 mL vial. The solution was placed in the freezer (-40 C) overnight. The mother liquor was decanted and the solids dried under high vacuum to yield the ylide as an orange solid (43.4 mg, 43%). ^{1}H NMR (500 MHz, C_6D_6) δ 8.04 (d, *J* = 8.0 Hz, 2H), 7.78 (dd, *J* = 11.4, 7.6 Hz, 6H), 7.27 (t, *J* = 7.6 Hz, 2H), 7.03 (m, 10H), 4.57 (s, 1H), 4.28 (s, 1H), 2.60 (d, *J* = 21.0 Hz, 1H). ^{13}C NMR (126 MHz, C_6D_6) δ 151.7 (d, *J* = 9.2 Hz), 148.9 (d, *J* = 17.9 Hz), 134.0 (d, *J* = 9.7 Hz), 131.9 (d, *J* = 2.8 Hz), 131.0 (s), 130.3 (s), 129.4 (d, *J* = 11.6 Hz), 128.1 (s), 127.5 (s), 91.5 (d, *J* = 5.9 Hz), 28.9 (d, *J* = 122.0 Hz). ^{31}P NMR (121 MHz, C_6D_6) δ 9.84.

Wittig reactions. Triphenyl(2-phenylallylidene)-λ^5-phosphane (4.7 mg, 0.013 mmol) was weighed into a 5 mL vial and dissolved in toluene-d_8 (0.5 mL) and transferred to a vial containing *para*-methoxybenzyl amine (1.6 mg, 0.012 mmol, 0.9 eq). The vial was swirled to dissolve the amine and the solution transferred to vial containing (dppf)Ni(*trans*-stilbene) (2.5 mg, 0.0033 mmol, 25 mol%). The complex was dissolved with stirring, and the solution was transferred to a J.Young tube. A ^{1}H NMR was acquired and the tube was pressurized with 100 psi of instrument grade CO_2 using a high pressure schlenk line. Upon addition of carbon dioxide, a white solid appeared at the top of the tube. Another ^{1}H NMR was acquired, revealing consumption of the starting materials without apparent formation of any new products. The reaction mixture was heated to 80 ºC and analyzed by ^{1}H NMR after 1 h, 3 h, and 17.5 h. No new product formation was observed.

Triphenyl(2-phenylallylidene)-λ^5-phosphane (19.7 mg, 0.0536 mmol) and trimethoxybenzene (0.6 mg, 0.00536 mmol, 10 mol%) were dissolved in dmso-*d*6 (2 mL). A 0.5 mL aliquot of this solution was transferred to J.Young tube A. A 1 mL aliquot of the solution was transferred to a vial containing paramethoxybenzylamine (4.5 mg, 0.0241 mmol, 0.9 eq). 0.5 mL of this solution was transferred to J.Young tube B. The remaining 0.5 mL was transferred to a vial containing (dppf)Ni(*trans*-stilbene) (2.8 mg, 0.00335 mmol, 25 mol%) and stirred until no more complex dissolved. The suspension was transferred to J.Young tube C. The samples were analyzed by ^{1}H NMR before being pressurized with 50 psi of instrument grade CO_2 using a high pressure schlenk line. Tubes A and B were analyzed again, and an array of ^{1}H spectra was collected of tube C. Tube A turned clear after 2 h and no ylide was detected. B turned clear and some precipitate formed. C turned from orange to yellow. In all cases, the ylide was completely consumed and a doublet at 5.17 ppm appeared, consistent with phosphonium salt, indicating that dmso is a strong enough acid to protonate the ylide.

Triphenyl(2-phenylallylidene)-λ^5-phosphane (9.6 mg, 0.026 mol) and trimethoxybenzene (0.3 mg, 0.0026 mmol, 10 mol%) were weighed into a 5 mL vial and dissolved in C_6D_6 (1.5 mL). A 0.75 mL aliquot was transferred to a screw-cap NMR tube. The remainder was added to (dppf)Ni(*trans*-stilbene) (2.4 mg, 0.0033 mmol, 25 mol%) and 3-hexyne (7.5 µL, 0.066 mmol, 5 eq) was added to this solution, and it was transferred to a J.Young tube. Both solutions were analyzed by ^{1}H NMR. The J.Young tube was pressurized with instrument grade CO_2. 93% consumption of the ylide and no consumption of the alkyne were observed within 3 h with no phenol formation. ^{31}P NMR revealed copious formation of triphenylphosphine oxide along with leftover ylide. Ylide was observed by IR. By GC/MS, stilbene, triphenylphosphine oxide were observed along with several significantly smaller peaks whose mass spectra could not be identified. In a separate experiment, the ylide's ability to react with CO_2 in the absence of 3-hexyne and (dppf)Ni(*trans*-stilbene). triphenyl(2-phenylallylidene)-λ^5-phosphane (5.1 mg, 0.013 mmol) and trimethoxybenzene (0.2 mg, 0.0013 mmol, 10 mol%) were dissolved in C_6D_6 (0.5 mL) and transferred to a J.Young tube. The tube was analyzed by ^{1}H NMR, pressurized with CO_2 (50 psi). In 4.5 h, 73% ylide consumption was observed. The longer timeframe, higher CO_2 pressure, and lower consumption indicate that (dppf)Ni(*trans*-stilbene) is in fact catalyzing the Wittig reaction.

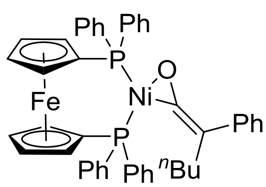

(Dppf)Ni(butylphenylketene), 1b. was prepared using a modification to the literature procedure.[3] Ni(COD)$_2$ (100 mg, 0.363 mmol, 1 eq) and dppf (201.5 mg, 0.363 mmol, 1 eq) were weighed into a 20 mL scintillation vial. Benzene (3 mL) was added and the solution stirred for 2 min, at which point the stirring was ceased and butyl phenyl ketene **2b** (126.7 mg, 0.727 mmol, 2 equiv) was added in 2 mL benzene. The solution was shaken briefly to homogenize the reaction mixture and left to sit undisturbed for 24 h, at which point a few small red crystals had formed at the bottom of the vial. Precipitation was completed by careful layering with pentane and allowing the vial to sit for an additional 24 h. The mother liquor was filtered through a fritted funnel, and the red crystalline solids were collected on the same frit by washing the vial with pentane. The yield is 310.9 mg, 75%. The spectroscopic data are identical to that previously reported, but the careful precipitation of the product described here results in samples that consistently pass elemental analysis.

Ketene complex and ketene addition reaction. **1b** (4.6 mg, 0.00584 mmol) was dissolved in C_6D_6 (0.75 mL) and added to **2b-*d*₉** (1.9 mg, 0.0058 mmol, 1.8 eq). The solution was transferred to a screw-cap NMR tube and monitored by taking a ^{1}H NMR every 5 min for 3.75 h. Over this time period, the four cp peaks shrank significantly as four new cp peaks appeared, indicating dimerization of the ketene at room temperature. Additionally, two cp peaks indicative of **5** also appeared.

Temperature dependence by saturation transfer. In the glovebox, **1a** (7.0 mg, 8.9 mmol) was dissolved in THF-d_8 (0.75 mL) and cooled to -40 ºC in the freezer, then added to **2a** (7.9 mg, 5 eq). The resulting solution was transferred to a screw-cap NMR tube, removed from the glovebox, and maintained at -40 ºC in a dry ice-acetonitrile bath while it was transported to the spectrometer. The sample was inserted into the spectrometer, which was set at 0 ºC (calibrated at 4.18 ºC with a methanol standard[26]). An inversion recovery experiment was performed to determine the T_1 of the peaks corresponding to the terminal methyl. Then a saturation transfer experiment is performed. The pulse sequence involves a 29 s d_1 followed by saturation at the selected frequency for 1 s with satpwr=5 for a total relaxation delay of 30 s. A 90º pulse is applied followed by 2.555 s of acquisition time. Four steady state or “dummy” scans (ss=4) are performed to ensure homogenous magnetization across scans, followed by four real scans. Three frequencies are used: one significantly away from any peaks in the spectrum (to determine the peak intensities without saturation), and at the frequency of the peaks corresponding to the terminal methyls on the ketene complex and free ketene. These scans are performed twice. One of the residual THF peaks is used as an internal standard. After the data were collected at 0 ºC, the spectrometer temperature was lowered 5 degrees, another temperature calibration run (the sample was placed in the -40 ºC bath when not in the spectrometer) and the inversion recovery and saturation transfer experiments repeated. Data were collected every 5 degrees from 0 to -35 ºC (Table 5.1). Notably, the rate constants are roughly an order of magnitude off depending on if the coordinated or free ketene methyl was saturated. The data where the coordinated ketene methyl were used to construct the eyring plot.

Order in reagents by saturation transfer. In the glovebox, stock solution A was prepared using **1a** (69.7 mg, 0.0885 mmol) in THF-d_8 (5 mL) in a volumetric flask and cooled to -40 ºC. Another stock solution (B) of **2a** (58.7 mg, 0.337 mmol) in THF-d_8 was prepared in a 2 mL volumetric flask and cooled to -40 ºC. Sample 1 was prepared using stock solution A (500 μL, 0.00885 mmol) and stock solution B (250 μL, 0.0421 mmol, 4.7 eq). Sample 2 was prepared using stock solution A (500 μL, 0.00885 mmol) and stock solution B (50 μL, 0.00842 mmol, 0.95 eq), and THF- d_8 (200 μL). Sample 3 was prepared using stock solution A (100 μL, 0.00177 mmol) and stock solution B (250 μL, 0.0421 mmol, 23 eq), and THF-d_8 (400 μL). The samples were removed from the glovebox and frozen in liquid nitrogen until they were inserted into the spectrometer, which was pre-

Table 5.1. Data for Magnetization Transfer Experiments at Multiple Temperatures.

Temp	Temp (calibrated, °C)	T_1 (free, s)	T_1 (coordinated, s)	K_{obs} (pulse coordinated)	K_{obs} (pulse free)
0	4.18	1.92	0.40	4.8(2)x10^{-3} /s	4.22(2)x10^{-2} /s
-5	-0.86	1.78	0.42	4.3(2)x10^{-3} /s	3.3(1)x10^{-2} /s
-10	-6.11	1.65	0.37	4.0(1)x10^{-3} /s	5.9(2)x10^{-2} /s
-15	-11.07	1.50	0.35	5.1(1)x10^{-3} /s	6.64(5)x10^{-2} /s
-20	-15.93	1.35	0.34	5.75(6)x10^{-3} /s	8.1(2)x10^{-2} /s
-25	-21.61	1.22	0.32	6.4(5)x10^{-3} /s	9.73(8)x10^{-2} /s
-30	-26.39	1.12	0.31	6.86(7)x10^{-3} /s	9.7(2)x10^{-2} /s
-35	-32.15	1.00	0.30	7.3(3)x10^{-3} /s	7.4(2)x10^{-2} /s

cooled to -20 ºC (calibrated at -16.22 ºC). The inversion recovery and saturation transfer experiments as described above were performed on each sample. Despite drastic concentration changes in reagents, little to no change in rate constant was observed.

Order in free ketene by deutero-ketene exchange. A stock solution (A) wasprepared in a volumetric flask using **1b** (33.6 mg, 0.0426 mmol) and toluene-d_8 (5 mL). Stock solution B was prepared in a volumetric flask using **2b-d_9** (50.4 mg, 0.275 mmol). One sample was prepared in a screw-cap NMR tube using 400 μL of stock solution A and toluene-d_8 (350 μL) and analyzed by ^{1}H NMR as a T_0. Six samples were prepared in septum-sealed screw-cap NMR tubes using 400 μL of stock solution A and the requisite amount of toluene-d_8 for a final volume of 750 μL after the stock solution B is added. Stock solution B was transferred to a 5 mL vial and sealed with a septum cap, which was pierced with a thin gauge 6" needle with a gastight 250 μL syringe. The samples and stock solution B were removed from the glovebox and brought to the NMR spectrometer, which was pre-cooled to -12 ºC (calibrated at -12.12 ºC). In turn, each sample was cooled in an isopropanol bath regulated between -25 to -35 ºC by addition of small pieces of dry ice. The requisite amount of stock solution B was added via syringe. A volume of gas equal to the amount of stock solution B was removed from the tube and added to the vial containing stock solution B using the syringe. The sample was briefly shaken, inserted into the spectrometer, and analyzed by a ^{1}H NMR array until the reaction had gone to completion. The furthest downfield cp peak was used as an internal standard. Sample 1, 250 μL ketene stock, 7.6 eq, 3.49 x 10^{-3} /s. Sample 2, 225 μL ketene stock, 6.8 eq, 2.90 x 10^{-3} /s. Sample 3, 200 μL ketene stock, 6.0 eq, 3.20 x 10^{-3} /s. Sample 4, 175 μL ketene stock, 5.3 eq, 2.74 x 10^{-3} /s. Sample 5, 150 μL ketene stock, 4.5 eq, 2.04 x 10^{-3} /s. Sample 6, 125 μL ketene stock, 3.8

eq, 1.73 x 10^{-3} /s.

Order in ketene complex by deutero-ketene exchange. A stock solution (A) was prepared in a volumetric flask using **1b** (32.9 mg, 0.0418 mmol) and toluene-d_8 (5 mL). Stock solution B was prepared in a volumetric flask using **2b-*d*$_9$** (40.3 mg, 0.220 mmol). One sample was prepared in a screw-cap NMR tube using 400 μL of stock solution A and toluene-d_8 (350 μL) and analyzed by ^{1}H NMR as a T_0. Six samples were prepared in septum-sealed screw-cap NMR tubes using the amount of stock solution A specified below and the requisite amount of toluene-d_8 for a final volume of 750 μL after the stock solution B is added. Stock solution B was transferred to a 5 mL vial and sealed with a septum cap, which was pierced with a thin gauge 6" needle with a gastight 250 μL syringe. The samples and stock solution B were removed from the glovebox and brought to the NMR spectrometer, which was pre-cooled to -12 ºC (calibrated at -12.54 ºC). In turn, each sample was cooled in an isopropanol bath regulated between -25 to -35 ºC by addition of small pieces of dry ice. 150 μL of stock solution B was added via syringe. A volume 150 μL of gas was removed from the tube and added to the vial containing stock solution B using the syringe. The sample was briefly shaken, inserted into the spectrometer, and analyzed by a ^{1}H NMR array until the reaction had gone to completion. The furthest downfield cp peak was used as an internal standard. Sample 1, 600 μL stock solution A, 4.4 eq ketene, 1.54 x 10^{-3} /s. Sample 2, 500 μL stock solution A, 5.3 eq ketene, 1.64 x 10^{-3} /s. Sample 3, 400 μL stock solution A, 6.6 eq ketene, 2.66 x 10^{-3} /s. Sample 4, 300 μL stock solution A, 8.8 eq ketene, 2.40 x 10^{-3} /s. Sample 5, 200 μL stock solution A, 13.2 eq ketene, 3.11 x 10^{-3} /s. Sample 6, 100 μL stock solution A, 26.3 eq ketene, 3.44 x 10^{-3} /s.

Temperature dependence by deutero-ketene exchange. A stock solution (A) was prepared in a volumetric flask using **1b** (33.8 mg, 0.0429 mmol) and toluene-d_8 (5 mL). Stock solution B was prepared in a volumetric flask using **2b-*d*$_9$** (42.0 mg, 0.229 mmol). One sample was prepared in a screw-cap NMR tube using 400 μL of stock solution A and toluene-d_8 (350 μL) and analyzed by ^{1}H NMR as a T_0. Eight samples were prepared in septum-sealed screw-cap NMR tubes using 400 μL of stock solution A and 200 μL of toluene-d_8 Stock solution B was transferred to a 5 mL vial and sealed with a septum cap, which was pierced with a thin gauge 6” needle with a gastight 250 μL syringe. The samples and stock solution B were removed from the glovebox and brought to the NMR spectrometer, which was pre-cooled, stabilized, and calibrated at the temperatures indicated below. In turn, each sample was cooled in an isopropanol bath regulated at least 10 ºC colder than the spectrometer temperature by addition of small pieces of dry ice. 150 μL of stock solution B (5.0 eq) was added via syringe. A volume of 150 μL of gas was removed from the tube and added to the vial containing stock solution B using the syringe. The sample was briefly shaken, inserted into the spectrometer, and analyzed by a ^{1}H NMR array until the reaction had gone to completion. The furthest downfield cp peak was used as an internal standard. Spectrometer temperature 0 ºC, calibrated 1.78 ºC, 6.98 x 10^{-3} /s. Spectrometer temperature -3 ºC, calibrated -1.59 ºC, 4.89 x 10^{-3} /s. Spectrometer temperature -6 ºC, calibrated -5.11 ºC, 4.32 x 10^{-3} /s. Spectrometer temperature -9 ºC, calibrated -9.09 ºC, 3.60 x 10^{-3} /s. Spectrometer temperature -12 ºC, calibrated -11.89 ºC, 1.35 x 10^{-3} /s. Spectrometer temperature -15 ºC, calibrated -15.78 ºC, 1.52 x 10^{-3} /s. Spectrometer temperature -18 ºC, calibrated -19.16 ºC, 6.03 x 10^{-4} /s. Spectrometer temperature -21 ºC, calibrated -22.66 ºC, 4.91 x 10^{-4} /s.

(Dppf)Ni(CO)$_2$ additive. Stock solution A was prepared with **1b** (32.1 mg, 0.0408 mmol) and toluene-d_8 in a 5 mL volumetric flask. Stock B was prepared with **2b-d_9** (51.4 mg, 0.281 mmol) and toluene-d_8 in a 2 mL volumetric flask. A sample was prepared with 400 μL of stock solution A and 350 μL of toluene-d_8 and analyzed by ^{1}H NMR as a T_0. Two samples were prepared with 400 μL of stock solution A and 200 μL of toluene-d_8. One of these solutions was added to **5** (0.2 mg, 0.000299 mmol, 9 mol%). Both solutions were transferred to screw-cap NMR tubes and removed from the glovebox with stock solution B in a septum-sealed vial pierced with a 6" needle and 250 μL syringe. In turn, each sample was cooled to ~-25 ºC and 150 μL of stock solution B was added. 150 μL of gas was removed from the tube and added to the vial containing stock solution B. The sample was briefly shaken, inserted into the spectrometer, which was pre-cooled at -12 ºC (calibrated to -12.54 ºC), and analyzed by a ^{1}H NMR array.

Ketene dimer additive. Stock solution A was prepared with **1b** (31.5 mg, 0.0400 mmol) and toluene-d_8 in a 5 mL volumetric flask. Stock B was prepared with **2b-d_9** (23.0 mg, 0.126 mmol) and toluene-d_8 in a 1 mL volumetric flask. A sample was prepared with 400 μL of stock solution A and 350 μL of toluene-d_8 and analyzed by ^{1}H NMR as a T_0. Two samples were prepared with 400 μL of stock solution A and 200 μL of toluene-d_8. One of these solutions was added to **6** (1.6 mg, 0.00459 mmol, 1.4 eq). Both solutions were transferred to screw-cap NMR tubes and removed from the glovebox with stock solution B in a septum-sealed vial pierced with a 6" needle and 250 μL syringe. In turn, each sample was cooled to ~-25 ºC and 150 μL of stock solution B was added. 150 μL of gas was removed from the tube and added to the vial containing stock solution B. The sample was briefly shaken, inserted into the spectrometer, which was pre-cooled at -12 ºC (calibrated at -12.54 ºC), and analyzed by a ^{1}H NMR array.

Benzonitrile and triphenylphosphine additives. Stock solution A was prepared with **1b** (35.1 mg, 0.0446 mmol) and toluene-d_8 in a 5 mL volumetric flask. Stock B was prepared with **2b-d_9** (44.4 mg, 0.242 mmol) and toluene-d_8 in a 2 mL volumetric flask. Stock solution C was prepared using benzonitrile (19.9 mg, 0.139 mmol) and toluene-d_8 in a 1 mL volumetric flask. Stock solution D was prepared using triphenylphosphine (1.1 mg, 0.00419 mmol) and toluene-d_8 in a 1 mL volumetric flask. A sample was prepared with 400 μL of stock solution A and 350 μL of toluene-d_8 and analyzed by ^{1}H NMR as a T_0. Samples 1 and 2 were prepared with 400 μL of stock solution A and 200 μL of toluene-d_8. Samples 3 and 4 were prepared with 400 μL of stock solution A and 100 μL of toluene-d_8. 100 μL of stock solution C (5 eq) was added to sample 3, and 100 μL of stock solution D was added to tube 4. All samples were transferred to screw-cap NMR tubes and removed from the glovebox with stock solution B in a septum-sealed vial pierced with a 6” needle and 250 μL syringe. At room temperature, 150 μL of stock solution B was added to samples 1 and 4 in turn, and each sample was analyzed by a ^{1}H NMR array. The spectrometer was cooled to -12 ºC (calibrated at -12.28 ºC) and samples 2 and 3 in turn were cooled to ~-25 ºC and 150 μL of stock solution B was added. 150 μL of gas was removed from the tube and added to the vial containing stock solution B. The sample was briefly shaken, inserted into the spectrometer, and analyzed by a ^{1}H NMR array.

Lithium isopropoxide and methyl iodide. Stock solution A was prepared with **1b** (33.9 mg, 0.0430 mmol) and toluene-d_8 in a 5 mL volumetric flask. Stock B was prepared with **2b-d_9** (33.1 mg, 0.181 mmol) and toluene-d_8 in a 2 mL volumetric flask. Stock solution C was prepared using Lithium isopropoxide (0.2 mg, 0.00303 mmol) and toluene-d_8 in a 1 mL volumetric flask. Stock solution D was prepared using methyl iodide

(0.4 mg, 0.00282 mmol) and toluene-d_8 in a 1 mL volumetric flask. A sample was prepared with 400 μL of stock solution A and 350 μL of toluene-d_8 and analyzed by ^{1}H NMR as a T_0. Sample 1 was prepared with 400 μL of stock solution A and 200 μL of toluene-d_8. Samples 2 and 3 were prepared with 400 μL of stock solution A, 100 μL of toluene-d_8, and 100 μL of stock solution C and D, respectively. All samples were transferred to screw-cap NMR tubes and removed from the glovebox with stock solution B in a septum-sealed vial pierced with a 6" needle and 250 μL syringe. In turn, each sample was cooled to ~-25 ºC and 150 μL of stock solution B was added. 150 μL of gas was removed from the tube and added to the vial containing stock solution B. The sample was briefly shaken, inserted into the spectrometer, which was pre-cooled at -12 ºC (calibrated at -12.51 ºC), and analyzed by a ^{1}H NMR array.

Kinetics with added water. Deionized water (~10 mL) was added to a 25 mL round bottom flask with a 14/20 ground glass joint and a sidearm with a ground glass stopcock. The joint was fitted with a rubber septum and the water was sparged with argon for 2 h through a needle with the sidearm open. The sidearm was closed and the needle was removed. The septum was fastened with electrical tape and the water brought into the glovebox. A stock solution was prepared using 1.5 μL of water in 5 mL toluene-d_8 in a volumetric flask. This stock solution was used where specified in kinetic runs.

Temperature dependence. A stock solution (A) was prepared in a volumetric flask using **1b** (32.8 mg, 0.0416 mmol) and toluene-d_8 (5 mL). Stock solution B was prepared in a 2mL volumetric flask using **2b-*d*₉** (47.7 mg, 0.260 mmol) and water (3 μL, 0.167 mmol). One sample was prepared in a screw-cap NMR tube using 400 μL of stock solution A and toluene-d_8 (350 μL) and analyzed by ^{1}H NMR as a T_0. Nine samples were prepared in septum-sealed screw-cap NMR tubes using 400 μL of stock solution A and 200 μL of toluene-d_8 Stock solution B was transferred to a 5 mL vial and sealed with a septum cap, which was pierced with a thin gauge 6” needle with a gastight 250 μL syringe. The samples and stock solution B were removed from the glovebox and brought to the NMR spectrometer, which was pre-cooled, stabilized, and calibrated at the temperatures indicated below. In turn, each sample was cooled in an isopropanol bath regulated at least 10 ºC colder than the spectrometer temperature by addition of small pieces of dry ice. 150 μL of stock solution B (5.0 eq) was added via syringe. A volume 150 μL of gas was removed from the tube and added to the vial containing stock solution B using the syringe. The sample was briefly shaken, inserted into the spectrometer, and analyzed by a ^{1}H NMR array until the reaction had gone to completion. The furthest downfield cp peak was used as an internal standard. Spectrometer temperature -6 ºC, calibrated -5.34 ºC, 1.13 x 10^{-2} /s. Spectrometer temperature -9 ºC, calibrated -8.96 ºC, 9.35 x 10^{-3} /s. Spectrometer temperature -12 ºC, calibrated -12.34 ºC, 6.00 x 10^{-3} /s. Spectrometer temperature -12 ºC, calibrated -12.20 ºC, 6.15 x 10^{-3} /s. Spectrometer temperature -15 ºC, calibrated -15.41 ºC, 3.88 x 10^{-3} /s. Spectrometer temperature -18 ºC, calibrated -19.62 ºC, 2.45 x 10^{-3} /s. Spectrometer temperature -21 ºC, calibrated -22.02 ºC, 1.67 x 10^{-3} /s. Spectrometer temperature -24 ºC, calibrated -25.85 ºC, 9.45 x 10^{-4} /s. Spectrometer temperature -27 ºC, calibrated -29.57 ºC, 5.57 x 10^{-4} /s.

Order in water. A stock solution (A) was prepared in a volumetric flask using **1b** (33.7 mg, 0.0428 mmol), trimethoxybenzene (0.1 mg, 0.00059 mmol, 1 mol%), and toluene-d_8 (5 mL). Stock solution B was prepared in a volumetric flask using **2b-*d*₉** (44.6 mg, 0.244 mmol). One sample was prepared in a screw-cap NMR tube using 400 μL of stock solution A and toluene-d_8 (350 μL) and analyzed by ^{1}H NMR as a T_0. Eight samples were prepared in septum-sealed screw-cap NMR tubes using 400 μL of stock solution A, the amount of water stock solution specified below, and the requisite amount of toluene-d_8 for a final sample volume of 750 μL. Stock solution B was transferred to a 5 mL vial and sealed with a septum cap, which was pierced with a thin gauge 6" needle with a gastight 250 μL syringe. The samples and stock solution B were removed from the glovebox and brought to the NMR spectrometer, which was pre-cooled and stabilized at -15 ºC (calibrated at -15.78 ºC). In turn, each sample was cooled in an isopropanol bath regulated at -25-30 ºC by addition of small pieces of dry ice. 150 μL of stock solution B was added via syringe. A volume 150 μL of gas was removed from the tube and added to the vial containing stock solution B using the syringe. The sample was inserted into the spectrometer and analyzed by a ^{1}H NMR array until the reaction had gone to completion. The upfield trimethoxybenzene peak was used as an internal standard. Sample 1, 200 μL water stock, 97 mol%, 3.09 x 10^{-3} /s. Sample 2, 100 μL water stock, 49 mol%, 2.45 x 10^{-3} /s. Sample 3, 50 μL water stock, 24 mol%, 3.00 x 10^{-3} /s. Sample 4, 25 μL water stock, 12 mol%, 2.86 x 10^{-3} /s. Sample 5, 20 μL water stock, 9.7 mol%, 2.92 x 10^{-3} /s. Sample 6, 10 μL water stock, 4.9 mol%, 2.66 x 10^{-3} /s. Sample 7, 5 μL water stock, 2.4 mol%, 2.31 x 10^{-3} /s. Sample 8, 0 μL water stock, 0 mol%, 2.10 x 10^{-3} /s.

Order in ketene complex. A stock solution (A) was prepared in a volumetric flask using **1b** (33.1 mg, 0.0420 mmol), trimethoxybenzene (0.1 mg, 0.00059 mmol, 1 mol%), and toluene-d_8 (5 mL). Stock solution B was prepared in a volumetric flask using **2b-*d*₉** (45.8 mg, 0.250 mmol) and water (1 μL, 0.056 mmol). One sample was prepared in a screw-cap NMR tube using 400 μL of stock solution A and toluene-d_8 (350 μL) and analyzed by ^{1}H NMR as a T_0. Eight samples were prepared in septum-sealed screw-cap NMR tubes using the amount of stock solution A specified below, and the requisite amount of toluene-d_8 for a final sample volume of 750 μL. Stock solution B was transferred to a 5 mL vial and sealed with a septum cap, which was pierced with a thin gauge 6” needle with a gastight 250 μL syringe. The samples and stock solution B were removed from the glovebox and brought to the NMR spectrometer, which was pre-cooled and stabilized at -15 ºC (calibrated at -19.47 ºC). In turn, each sample was cooled in an isopropanol bath regulated at -25 ºC by addition of small pieces of dry ice. 150 μL of stock solution B was added via syringe. A volume 150 μL of gas was removed from the tube and added to the vial containing stock solution B using the syringe. The sample was briefly shaken, inserted into the spectrometer, and analyzed by a ^{1}H NMR array until the reaction had gone to completion. The upfield trimethoxybenzene peak was used as an internal standard. Sample 1, 500 μL stock solution A, 3.7 eq ketene, 1.94×10^{-3} /s. Sample 2, 550 μL stock solution A, 4.0 eq ketene, 2.69×10^{-3} /s. Sample 3, 500 μL stock solution A, 4.46 eq ketene, 2.49×10^{-3} /s. Sample 4, 450 μL stock solution A, 5.0 eq ketene, 3.06×10^{-3} /s. Sample 5, 400 μL stock solution A, 5.6 eq ketene, 2.92×10^{-3} /s. Sample 6, 350 μL stock solution A, 6.4 eq ketene, 3.41×10^{-3} /s. Sample 7, 300 μL stock solution A, 7.4 eq ketene, 3.31×10^{-3} /s. Sample 8, 250 μL stock solution A, 8.9 eq ketene, 4.50×10^{-3} /s.

Order in free ketene. A stock solution (A) was prepared in a 5 mL volumetric flask using **1b** (32.8 mg, 0.0416 mmol), trimethoxybenzene (0.1 mg, 0.00059 mmol, 1 mol%), water stock solution (250 μL, 0.0042 mmol, 10 mol%) and diluted to the line with toluene-d_8. Stock solution B was prepared in a 2 mL volumetric flask using **2b-*d*$_9$** (49.8 mg, 0.271 mmol) and diluted to the line with toluene-d_8. One sample was prepared in a screw-cap NMR tube using 400 µL of stock solution A and toluene-d_8 (350 µL) and analyzed by ^{1}H NMR as a T_0. Five samples were prepared in septum-sealed screw-cap NMR tubes using 400 µL of stock solution A and the requisite amount of toluene-d_8 for a final sample volume of 750 µL. Stock solution B was transferred to a 5 mL vial and sealed with a septum cap, which was pierced with a thin gauge 6" needle with a gastight 250 µL syringe. The samples and stock solution B were removed from the glovebox and brought to the NMR spectrometer, which was pre-cooled and stabilized at -15 ºC (calibrated at -15.76 ºC). In turn, each sample was cooled in an isopropanol bath regulated at -25 ºC by addition of small pieces of dry ice. The amount of stock solution B specified below was added via syringe. An equal volume of gas was removed from the tube and added to the vial containing stock solution B using the syringe. The sample was inserted into the spectrometer and analyzed by a ^{1}H NMR array until the reaction had gone to completion. The upfield trimethoxybenzene peak was used as an internal standard. Sample 1, 250 µL stock solution B, 10.2 eq ketene, 3.00 x 10^{-3} /s. Sample 2, 225 µL stock solution B, 9.2 eq ketene, 2.64 x 10^{-3} /s. Sample 3, 200 µL stock solution B, 8.2 eq ketene, 2.32 x 10^{-3} /s. Sample 4, 175 µL stock solution B, 7.1 eq ketene, 2.48 x 10^{-3} /s. Sample 5, 150 µL stock solution B, 6.1 eq ketene, 2.14 x 10^{-3} /s.

Ketene exchange in a J.Young tube. **1b** (2.6 mg, 0.0033 mmol) and trimethoxybenzene (<0.1 mg) were weighed into a 5 mL vial, and dissolved in toluene-d_8 (0.75 mL). **2b-*d*₉** (4.4 mg, 0.024 mmol, 7.3 eq) was weighed into a separate 5 mL vial. Both vials, a 1 mL syringe, and a J.Young tube were cooled to -40 ºC in the glovebox freezer. The solution was transferred to the ketene, and the vial was shaken to dissolve the ketene. The resulting reaction mixture was transferred to the J.Young tube, which was sealed, removed from the glovebox, and immediately placed in a -45 ºC bath. The tube was inserted into the spectrometer and analyzed by an array of ^{1}H NMRs.

Density functional theory. All calculations were performed with the GAUSSIAN09[27] suite of programs. The same levels of theory were used as in the ketene decomposition study.[3] All geometries were optimized using the BP86 functional and a split basis set consisting of tzvp for Ni, P and the O=C=C atoms and svp for all other atoms. Solvent (benzene) effects were taken into account using the self-consistent reaction field (SCRF) with the PCM model. Frequency calculations were carried out at this level of theory to ensure the structures were local minima and to generate thermal corrections to gibbs free energy. Single point calculations were performed at the BLYP/6-31G(d) level of theory. Where possible, a total of two ketenes were included in the calculations to provide more accurate energies. The exception to this is the (dppf)Ni fragment with no coordinated ketenes. This calculation was attempted with the (dppf)Ni fragment and two ketenes, each ~10 Å apart. The calculation converged, but the frequency calculation showed negative values. The optimization was re-run with Opt=VTight, but would not converge and negative frequencies were still present. For this species, (dppf)Ni was optimized alone and the energies of two free ketenes added for comparison to the other species. Energies and coordinates of calculated structure can be found in the Appendix.

References

1. (a) Auvinet, A.-L.; Harrity, J. P. A. *Angew. Chem. Int. Ed.* **2011**, *50*, 2769. (b) Huffman, M. A.; Liebeskind, L. S. *J. Am. Chem. Soc.* **1991**, *113*, 2771. (c) Kumar, P.; Troast, D. M.; Cella, R.; Louie, J. *J. Am. Chem. Soc.* **2011**, *133*, 7719. (d) Rofer-DePoorter, C. K. *Chem. Rev.* **1981**, *81*, 447. (e) Ruchardt, C.; Schrauzer, G. N. *Chem. Ber*. **1960**, *93*, 1621. (f) Zhang, Z.; Zhang, Y.; Wang, J. *ACS Catal.* **2011**, *1*, 1621.

2. (a) Sugai, R.; Miyashita, A.; Nohira, H. *Chem. Lett.* **1988**, 1403. (b) Miyashita, A.; Shitara, H.; Nohira, H. *J. Chem. Soc., Chem. Commun.* **1985**, 850. (c) Miyashita, A.; Sugai, R.; Yamamoto, J. *J. Organomet. Chem.* **1992**, *428*, 239. (d) Mindiola, D. J.; Hillhouse, G. L. *J. Am. Chem. Soc.* **2002**, *124*, 9976. (e) Wright, C. A.; Thorn, M.; McGill, J. W.; Sutterer, A.; Hinze, S. M.; Prince, R. B.; Gong, J. K. *J. Am. Chem. Soc.* **1996**, *118*, 10305. (f) Curley, J. J.; Kitiachvili, K. D.; Waterman, R.; Hillhouse, G. L. *Organometallics* **2009**, *28*, 2568. (g) Hofmann, P.; Perez-Moya, L. A.; Steigelmann, O.; Riede, J. *Organometallics* **1992**, *11*, 1167.

3. Staudaher, N. D.; Arif, A. M.; Louie, J. *J. Am. Chem. Soc.* **2016**, *138*, 14083.

4. Bestmann, H. J.; Denzel, T.; Salbaum, H. *Tetrahedron Lett.* **1974**, *14*, 1275.

5. Hartwig, J. F. *Organotransition Metal Chemistry*; University Science Books, 2010.

6. (a) Tolman, C. A. *J. Am. Chem. Soc.* **1974**, *96*, 2780. (b) Tolman, C. A.; Seidel, W. C. *J. Am. Chem. Soc.* **1974**, *96*, 2774.

7. de Lucas, N. C.; Netto-Ferreira, J. C.; Andraos, J.; Scaiano, J. C. *J. Org. Chem.* **2001**, *66*, 5016.

8. J. Murphy, P.; E. Lee, S. *J. Chem. Soc., Perkin Trans. 1* **1999**, 3049.

9. Iqbal, N.; Cho, E. J. *Adv. Synth. Catal.* **2015**, *357*, 2187.

10. Penny, D. E.; Ritter, T. J. *J. Chem. Soc., Faraday Trans. 1* **1983**, *79*, 2103.

11. Stalling, T.; Harker, W. R. R.; Auvinet, A.-L.; Cornel, E. J.; Harrity, J. P. A. *Chemistry – A European Journal* **2015**, *21*, 2701.

12. (a) Mödlhammer, U.; Hopf, H. *Angew. Chem., Int. Ed. Engl.* **1975**, *14*, 501. (b) Chen, H.-T.; Chen, H.-L.; Ho, J.-J. *Journal of Physical Organic Chemistry* **2010**, *23*, 134. (c) Phongsatha, A.; Klaboe, P.; Hopf, H.; Cyvin, B. N.; Cyvin, S. J. *Spectrochim. Acta, Part A* **1978**, *34*, 537.

13. (a) Jarek, R. L.; Flesher, R. J.; Shin, S. K. *J. Chem. Educ.* **1997**, *74*, 978. (b) Wolff, S. D.; Balaban, R. S. *Journal of Magnetic Resonance (1969)* **1990**, *86*, 164.

14. Spencer, R. G. S.; Fishbein, K. W. *J. Magn. Reson.* **2000**, *142*, 120.

15. Popp, B. V.; Thorman, J. L.; Morales, C. M.; Landis, C. R.; Stahl, S. S. *J. Am. Chem. Soc.* **2004**, *126*, 14832.

16. Blackmond, D. G. *Angew. Chem. Int. Ed.* **2009**, *48*, 386.

17. Mower, M. P.; Blackmond, D. G. *J. Am. Chem. Soc.* **2015**, *137*, 2386.

18. Staudaher, N. D.; Stolley, R. M.; Louie, J. *Chem. Commun.* **2014**, *50*, 15577.

19. Cueny, E. S.; Johnson, H. C.; Anding, B. J.; Landis, C. R. *J. Am. Chem. Soc.* **2017**, *139*, 11903.

20. Staudaher, N. D.; Lovelace, J.; Johnson, M. P.; Louie, J. *Org. Synth.* **2017**, *94*, 1.

21. Hamann, B. C.; Hartwig, J. F. *J. Am. Chem. Soc.* **1998**, *120*, 3694.

22. Dehmlow, E. V. *Liebigs Ann. Chem.* **1979**, *4*, 572.

23. Ireland, R. E.; Meissner, R. S. *J. Org. Chem.* **1991**, *56*, 4566.

24. Yin, G.; Kalvet, I.; Englert, U.; Schoenebeck, F. *J. Am. Chem. Soc.* **2015**, *137*, 4164.

25. Tripathi, C. B.; Mukherjee, S. *Angew. Chem. Int. Ed.* **2013**, *52*, 8450.

26. Van Geet, A. L. *Anal. Chem.* **1970**, *42*, 679.

27. Frisch, M. J.; Trucks, G. W.; Schlegel, H. B.; Scuseria, G. E.; Robb, M. A.; Cheeseman, J. R.; Scalmani, G.; Barone, V.; Mennucci, B.; Petersson, G. A.; Nakatsuji, H.; Caricato, M.; Li, X.; Hratchian, H. P.; Izmaylov, A. F.; Bloino, J.; Zheng, G.; Sonnenberg, J. L.; Hada, M.; Ehara, M.; Toyota, K.; Fukuda, R.; Hasegawa, J.; Ishida, M.; Nakajima, T.; Honda, Y.; Kitao, O.; Nakai, H.; Vreven, T.; Montgomery, J. A.; Peralta, J. E.; Ogliaro, F.; Bearpark, M.; Heyd, J. J.; Brothers, E.; Kudin, K. N.; Staroverov, V. N.; Kobayashi, R.; Normand, J.; Raghavachari, K.; Rendell, A.; Burant, J. C.; Iyengar, S. S.; Tomasi, J.; Cossi, M.; Rega, N.; Millam, J. M.; Klene, M.; Knox, J. E.; Cross, J. B.; Bakken, V.; Adamo, C.; Jaramillo, J.; Gomperts, R.; Stratmann, R. E.; Yazyev, O.; Austin, A. J.; Cammi, R.; Pomelli, C.; Ochterski, J. W.; Martin, R. L.; Morokuma, K.; Zakrzewski, V. G.; Voth, G. A.; Salvador, P.; Dannenberg, J. J.; Dapprich, S.; Daniels, A. D.; Farkas; Foresman, J. B.; Ortiz, J. V.; Cioslowski, J.; Fox, D. J. Wallingford CT, 2009.

APPENDIX

Table A.1. (Dppf)Ni(η2-CO-phenyl *n*-butyl ketene) + phenyl *n*-butyl ketene.

Zero-point energy (BLYP/6-31G(d)=	-5847.81600025
Zero-point correction=	0.946222 (Hartree/Particle)
Thermal correction to Energy=	1.010537
Thermal correction to Enthalpy=	1.011481
Thermal correction to Gibbs Free Energy=	0.825808
Sum of electronic and zero-point Energies=	-5847.218723
Sum of electronic and thermal Energies=	-5847.154409
Sum of electronic and thermal Enthalpies=	-5847.153464
Sum of electronic and thermal Free Energies=	-5847.339137

Coordinates:

C	-6.00990100	-2.16965900	0.28680400
C	-7.26209800	-2.37459400	-0.39166900
C	-6.98538400	-2.61458300	-1.78305700
C	-5.56069900	-2.56883700	-1.97221500
C	-4.94268500	-2.29403100	-0.69042600
H	-5.88207300	-1.94982200	1.35429400
H	-8.25669300	-2.32948300	0.07150200
H	-7.73218800	-2.78365500	-2.57017900
H	-5.02742700	-2.70065200	-2.92174400
Fe	-6.22598200	-0.78730700	-1.19689500
C	-5.21787300	0.78281500	-2.02654700
C	-6.49091500	0.62760200	-2.67667400
C	-5.45283800	0.99942400	-0.60955200
H	-4.23178000	0.73102000	-2.50650900
C	-7.51965600	0.74726800	-1.67818300
H	-6.64715300	0.42789200	-3.74496900
C	-6.88899300	0.97573000	-0.40550000
H	-8.60010600	0.65060100	-1.84993100
H	-7.40637600	1.07963000	0.55582000
P	-3.15412800	-2.00369700	-0.36652300
P	-4.08478700	1.22841000	0.60098000
Ni	-2.32710600	0.03956500	0.13069500
O	-0.48069200	-0.36122300	0.01369800
C	-0.63685700	0.91490600	0.10221600
C	0.19079800	2.00068000	0.10648100
C	1.66048200	1.82682900	0.09794300
C	2.52387900	2.94941700	0.26656200
C	2.29345400	0.55867800	-0.05762700
C	3.92100500	2.81229500	0.28313000
H	2.09348100	3.95304000	0.39840200
C	3.68944600	0.42712200	-0.04377600
H	1.67127400	-0.33694500	-0.19693200
C	4.52119500	1.55046500	0.12704000
H	4.54828800	3.70891300	0.42072000
H	4.13570400	-0.57340600	-0.17109100

Table A.1 continued

C	-4.07369300	3.08167200	0.79952800
C	-3.52020400	3.64707400	1.97193900
C	-4.59586700	3.93752000	-0.19367100
C	-3.50353800	5.03947200	2.15101600
H	-3.10134800	2.99426500	2.75445700
C	-4.57283400	5.33307300	-0.01306200
H	-5.03295300	3.51563000	-1.11171000
C	-4.03194200	5.88732900	1.15976100
H	-3.07339000	5.46522600	3.07152200
H	-4.98818300	5.98926500	-0.79456500
H	-4.01963500	6.97955400	1.30175600
C	-4.80832200	0.73241900	2.24521700
C	-5.89695100	1.42479800	2.82453500
C	-4.22819400	-0.34317000	2.95213400
C	-6.41512100	1.02219600	4.06708600
H	-6.33182500	2.29809400	2.31350200
C	-4.74298200	-0.74054100	4.19971500
H	-3.35871400	-0.86612000	2.52081700
C	-5.84206900	-0.06347500	4.75559600
H	-7.26604700	1.56748900	4.50589500
H	-4.27577700	-1.57902300	4.73987200
H	-6.24597700	-0.37240300	5.73287200
C	-2.39001400	-2.59478600	-1.95657800
C	-2.36670900	-3.96194200	-2.31241100
C	-1.82657900	-1.64397500	-2.83472300
C	-1.80017700	-4.36625700	-3.53288800
H	-2.78504400	-4.71774500	-1.62903000
C	-1.26336700	-2.05066600	-4.05763800
H	-1.81520400	-0.57988300	-2.54785600
C	-1.25005200	-3.41151700	-4.40874200
H	-1.78299300	-5.43525100	-3.79923700
H	-0.82270300	-1.29941400	-4.73201200
H	-0.80217400	-3.73165300	-5.36303900
C	-2.71339900	-3.35391300	0.83304600
C	-3.55858000	-4.45205700	1.10885500
C	-1.46532100	-3.25830800	1.49340100
C	-3.15861200	-5.44135000	2.02572500
H	-4.53643000	-4.53586900	0.60966200
C	-1.06898100	-4.25321900	2.40294400
H	-0.80434900	-2.40039200	1.28880400
C	-1.91410000	-5.34549900	2.67278600
H	-3.82609400	-6.29306400	2.23383100
H	-0.09358300	-4.17028500	2.90834700
H	-1.60332300	-6.12129600	3.39061000
C	-0.40404400	3.39321300	0.06332300

Table A.1 continued

C	-0.27093600	4.08619200	-1.31206200
H	0.05858700	4.04111000	0.84439300
H	-1.47679400	3.33008200	0.32940200
C	-0.73392000	5.55085300	-1.32054900
H	0.78597900	4.03347600	-1.65803300
H	-1.78428600	5.60525800	-0.95496200
H	-0.13150400	6.12713100	-0.58069600
H	5.61764500	1.44344400	0.13681200
H	-0.85697800	3.50325700	-2.05896600
C	-0.62988300	6.22051600	-2.69690300
H	-0.96509800	7.27889700	-2.66840600
H	0.41566300	6.21193200	-3.07400400
H	-1.25361900	5.69362800	-3.45122200
O	14.54385800	-2.97648400	0.59279800
C	13.89506400	-2.00816100	0.43042700
C	13.15899500	-0.91833300	0.24807600
C	13.81502200	0.36916700	-0.07492400
C	13.03516100	1.53669600	-0.27223000
C	15.22606800	0.48546800	-0.19805200
C	13.64456700	2.76610400	-0.57934800
H	11.93975800	1.49159000	-0.18655200
C	15.82672300	1.71289400	-0.50417800
H	15.86418100	-0.40212400	-0.05117700
C	15.04027900	2.86589200	-0.69780300
H	13.01273000	3.65679500	-0.72735400
H	16.92354300	1.77070400	-0.59283900
H	15.51373100	3.83051300	-0.93845000
C	11.64174300	-1.03952800	0.38089600
H	11.30655900	-0.31854600	1.16142700
H	11.18448300	-0.69496900	-0.57491800
C	11.11137100	-2.44018300	0.72192300
H	11.44074100	-3.16556900	-0.05692800
H	11.56178900	-2.78849700	1.67957000
C	9.57930000	-2.48892100	0.83917800
H	9.12932900	-2.13596900	-0.11638600
H	9.24968700	-1.76031300	1.61417300
C	9.03784800	-3.88274500	1.17937700
H	9.43975100	-4.24824700	2.14857900
H	7.93099400	-3.88092900	1.25613400
H	9.31818900	-4.62695400	0.40346700

Table A.2. (Dppf)Ni(η1-phenyl *n*-butyl ketene)$_2$.

Zero-point energy (BLYP/6-31G(d)=			-5847.774389
Zero-point correction=			0.944029 (Hartree/Particle)
Thermal correction to Energy=			1.009246
Thermal correction to Enthalpy=			1.010190
Thermal correction to Gibbs Free Energy=			0.824859
Sum of electronic and zero-point Energies=			-5847.187380
Sum of electronic and thermal Energies=			-5847.122164
Sum of electronic and thermal Enthalpies=			-5847.121220
Sum of electronic and thermal Free Energies=			-5847.306550
Coordinates:			
C	3.80620400	-0.79593600	-1.86811100
C	5.23858500	-0.85762200	-1.99281100
C	5.74026300	-1.70894500	-0.94628700
C	4.61908500	-2.18250100	-0.17719400
C	3.40810200	-1.62267200	-0.74343300
H	3.12710900	-0.21059500	-2.50077700
H	5.84253900	-0.32541800	-2.73984100
H	6.79658600	-1.93953600	-0.75213200
H	4.66916700	-2.83571000	0.70293500
Fe	4.68007900	-0.13260500	-0.14815600
C	4.08002300	0.59857800	1.65948900
C	5.51666100	0.52617000	1.61384000
C	3.63051300	1.46623700	0.58622300
H	3.42998600	0.07485700	2.37163500
C	5.96831600	1.33397000	0.51156200
H	6.15241600	-0.06456700	2.28683100
C	4.81301900	1.91463300	-0.12153700
H	7.01117600	1.46710300	0.19313800
H	4.81912400	2.56712100	-1.00358300
P	1.66335700	-1.78617400	-0.16050500
P	1.85277300	1.80018300	0.20887700
Ni	0.57144800	0.06519300	0.04174400
O	-0.84966500	0.01730400	1.58918500
C	-1.95821700	-0.13806000	1.99092600
C	-3.20392600	-0.30081700	2.42209900
C	-3.72375500	-1.65997500	2.70062400
C	-5.11044500	-1.88169100	2.89979900
C	-2.85953100	-2.78684000	2.76463700
C	-5.60780900	-3.17371800	3.14298100
H	-5.81551200	-1.03816700	2.85689200
C	-3.36107100	-4.07354000	3.00158700
H	-1.77265700	-2.64717000	2.63886200
C	-4.74154000	-4.27890000	3.19386100
H	-6.69060400	-3.31405800	3.29361200

Table A.2 continued

H	-2.66329400	-4.92523700	3.04586400
C	1.42864000	3.08527100	1.49908000
C	0.10634800	3.59083800	1.50101700
C	2.32897400	3.54201900	2.48693000
C	-0.29931700	4.53960300	2.45301400
H	-0.61177500	3.23257800	0.74427100
C	1.91654800	4.48142400	3.45129700
H	3.36247200	3.16281900	2.50433400
C	0.60493600	4.98569300	3.43640100
H	-1.32972400	4.92999900	2.43201900
H	2.63123900	4.82485100	4.21695800
H	0.28515200	5.72305800	4.18996200
C	2.00503200	2.88472100	-1.30996900
C	2.50189900	4.20707100	-1.26112400
C	1.59285300	2.35686700	-2.55307300
C	2.59469100	4.97728700	-2.43378300
H	2.81304300	4.64139000	-0.29747800
C	1.68995500	3.12542700	-3.72749900
H	1.18066600	1.33440100	-2.58474100
C	2.19198300	4.43773500	-3.66984300
H	2.98153600	6.00803900	-2.38166900
H	1.36338200	2.69938400	-4.68985400
H	2.26281800	5.04420600	-4.58704300
C	1.88367100	-2.83679600	1.37295100
C	2.26501900	-4.19694800	1.32045900
C	1.64395100	-2.24404400	2.63193200
C	2.41604000	-4.94103300	2.50386000
H	2.43909500	-4.68101600	0.34607300
C	1.79884800	-2.98718500	3.81668500
H	1.32054400	-1.19043900	2.66990700
C	2.18640400	-4.33754800	3.75458300
H	2.71224800	-6.00123800	2.44906000
H	1.60753800	-2.51043200	4.79156600
H	2.30260400	-4.92332800	4.68055400
C	0.98427900	-3.06264000	-1.34546200
C	1.70150900	-3.57442000	-2.44940400
C	-0.34808400	-3.49693200	-1.14235600
C	1.10185400	-4.49861800	-3.32629500
H	2.73931800	-3.25197100	-2.62596100
C	-0.93958700	-4.43078900	-2.00812900
H	-0.92676500	-3.10046300	-0.29117800
C	-0.21670400	-4.93278700	-3.10801400
H	1.67588600	-4.88635800	-4.18367300

Table A.2 continued

H	-1.97283300	-4.76752500	-1.82487200
H	-0.68232900	-5.65992900	-3.79227300
C	-4.05201200	0.95857700	2.61550700
C	-4.30055500	1.32687300	4.09129000
H	-5.02141900	0.81328000	2.08650300
H	-3.56455000	1.81227700	2.09946500
C	-5.21820900	2.54821700	4.26269500
H	-4.73836600	0.45427200	4.62539800
H	-4.78010800	3.41539800	3.71760700
H	-6.19419000	2.34572900	3.76498200
H	-5.13467900	-5.28941400	3.38649800
H	-3.32070300	1.52104100	4.58222700
C	-5.45814600	2.92971000	5.72896700
H	-6.12455700	3.81281800	5.81805800
H	-5.93035600	2.09615600	6.29186200
H	-4.50499000	3.17654500	6.24388700
O	-0.96418900	0.22928900	-1.26785500
C	-2.03013500	0.31143300	-1.79259100
C	-3.22588000	0.37968000	-2.36932400
C	-3.85610900	1.69622300	-2.62369400
C	-5.22817400	1.79248900	-2.97174200
C	-3.11869800	2.90677700	-2.51372000
C	-5.83323400	3.04237400	-3.18959300
H	-5.83770000	0.88138400	-3.06625900
C	-3.72749400	4.15051300	-2.72661000
H	-2.04379000	2.86691300	-2.26987000
C	-5.09237800	4.23011500	-3.06718200
H	-6.90147400	3.08383300	-3.45810500
H	-3.12604300	5.06944000	-2.63490400
H	-5.56922700	5.20754300	-3.24066000
C	-3.90683700	-0.93835600	-2.74738200
H	-3.38468700	-1.77737900	-2.24144900
H	-4.93877900	-0.93697500	-2.32717500
C	-3.95212900	-1.20749600	-4.26435300
H	-4.42484800	-0.34406400	-4.78356500
H	-2.90942100	-1.25887200	-4.65008700
C	-4.70273100	-2.49909200	-4.62680300
H	-5.74257500	-2.44227500	-4.23058800
H	-4.22821100	-3.35782400	-4.09934300
C	-4.74178000	-2.77949700	-6.13444000
H	-3.71766800	-2.88121500	-6.55322600
H	-5.29072100	-3.71690800	-6.36246400
H	-5.24312700	-1.95566500	-6.68641100

Table A.3. (Dppf)Ni(η^1-CO-phenyl *n*-butyl ketene) + phenyl *n*-butyl ketene.

Zero-point energy (BLYP/6-31G(d)=	-5847.7730321
Zero-point correction=	0.943800 (Hartree/Particle)
Thermal correction to Energy=	1.009516
Thermal correction to Enthalpy=	1.010460
Thermal correction to Gibbs Free Energy=	0.814520
Sum of electronic and zero-point Energies=	-5847.186045
Sum of electronic and thermal Energies=	-5847.120330
Sum of electronic and thermal Enthalpies=	-5847.119385
Sum of electronic and thermal Free Energies=	-5847.315326

Coordinates:

C	-4.87972400	-3.20373900	0.61744300
C	-5.79056100	-4.11277600	-0.02692300
C	-5.23846300	-4.46251900	-1.30934200
C	-3.98005300	-3.77838000	-1.45678200
C	-3.74398500	-2.99547700	-0.26119500
H	-5.02286900	-2.73778200	1.60069400
H	-6.75116000	-4.45624200	0.37972900
H	-5.70484500	-5.11947100	-2.05596900
H	-3.31742200	-3.82340200	-2.33022600
Fe	-5.49718900	-2.42511900	-1.16674400
C	-5.20943500	-0.74228900	-2.28685700
C	-6.11250100	-1.63350700	-2.96568600
C	-5.78393300	-0.40295800	-0.99747800
H	-4.24147000	-0.38881900	-2.66566500
C	-7.24290600	-1.86228100	-2.10448500
H	-5.95251600	-2.08077000	-3.95581300
C	-7.04546100	-1.10819800	-0.89405500
H	-8.09692300	-2.51837100	-2.32097200
H	-7.71926400	-1.08906900	-0.02823100
P	-2.34510800	-1.84510700	0.11239500
P	-4.92250500	0.66337100	0.23601200
Ni	-2.82479700	0.22634400	0.44224000
O	-1.54882600	1.58986600	0.69123800
C	-0.75943700	2.48710800	0.59833400
C	0.08941900	3.50740500	0.52758700
C	1.55272900	3.26382100	0.50756700
C	2.47580600	4.32829800	0.67259600
C	2.08227700	1.95557100	0.33813300
C	3.86149700	4.09135400	0.67642000
H	2.11156600	5.35745400	0.80912800
C	3.46352400	1.72296400	0.34614300
H	1.39194000	1.10866400	0.18732400

Table A.3 continued

C	4.36753500	2.79057900	0.51542500
H	4.55265700	4.93975800	0.80858600
H	3.83994000	0.69598600	0.21085800
C	-5.43006900	2.37503800	-0.31301100
C	-5.05350700	3.46533100	0.50855700
C	-6.10231900	2.64140000	-1.52628500
C	-5.35697400	4.78394200	0.13465600
H	-4.51892400	3.27491200	1.45464700
C	-6.39196200	3.96559300	-1.90731800
H	-6.40617900	1.80847500	-2.17916300
C	-6.02490900	5.03978300	-1.07913400
H	-5.06836800	5.61932300	0.79307600
H	-6.91614700	4.15571400	-2.85808700
H	-6.25679600	6.07482800	-1.37676800
C	-5.97759900	0.46565200	1.76252000
C	-7.29968600	0.95833600	1.84666900
C	-5.41505500	-0.17910300	2.88601600
C	-8.04798300	0.78947000	3.02490200
H	-7.74440200	1.48686600	0.98815800
C	-6.16382600	-0.34794300	4.06475900
H	-4.37352700	-0.53881000	2.82727000
C	-7.48313500	0.13369900	4.13486600
H	-9.07802200	1.17766700	3.07893400
H	-5.71095000	-0.85085700	4.93432500
H	-8.07023500	0.00646700	5.05851700
C	-1.21869300	-2.15875500	-1.34716100
C	-0.53771700	-3.37925300	-1.55452500
C	-1.03088900	-1.10619900	-2.26998600
C	0.30411200	-3.54371700	-2.66855800
H	-0.65780400	-4.20595800	-0.83626000
C	-0.19400200	-1.27249400	-3.38803900
H	-1.54383600	-0.14517500	-2.09165700
C	0.47530200	-2.49276400	-3.58911200
H	0.83372700	-4.49875200	-2.81711800
H	-0.05755900	-0.44204300	-4.09928200
H	1.13749400	-2.62366500	-4.45996600
C	-1.46640300	-2.76992600	1.47841000
C	-1.71201300	-4.12406900	1.79956900
C	-0.51320800	-2.05214700	2.23738600
C	-1.01103300	-4.74656000	2.84904700
H	-2.46054100	-4.69665900	1.22959200
C	0.19413200	-2.67738900	3.27755300
H	-0.33543300	-0.98783900	2.00932100
C	-0.05477200	-4.02749700	3.58772100

Table A.3 continued

H	-1.21485800	-5.80253200	3.09017800
H	0.93629300	-2.10429700	3.85637400
H	0.49206900	-4.51664300	4.40967500
C	-0.49068400	4.92353600	0.45476600
C	-0.37175000	5.58155600	-0.93411700
H	0.01546500	5.55490700	1.22090700
H	-1.55915100	4.89390400	0.75480900
C	-0.90149800	7.02406800	-0.96818300
H	0.69059200	5.56727000	-1.26542500
H	-1.96329400	7.03129800	-0.63140700
H	-0.34602200	7.63611300	-0.22087100
H	5.45373800	2.60860600	0.51688100
H	-0.92723600	4.96097100	-1.67245700
C	-0.79634900	7.68098900	-2.35037000
H	-1.18552800	8.72047300	-2.34055500
H	0.25764800	7.72183000	-2.69987900
H	-1.37435100	7.11469900	-3.11177000
O	14.03823200	-3.03949300	-1.10727000
C	13.45579300	-2.11325500	-0.67418300
C	12.79432000	-1.07063500	-0.18600400
C	13.53086000	0.15311200	0.20421200
C	12.83124500	1.27004400	0.72689100
C	14.94217900	0.25658600	0.07328000
C	13.51769400	2.43869300	1.10135300
H	11.73856400	1.23272600	0.84504000
C	15.61981100	1.42335200	0.44809100
H	15.51901700	-0.59277900	-0.32967500
C	14.91267700	2.52648300	0.96621100
H	12.94737400	3.29107900	1.50465000
H	16.71470900	1.47269300	0.33434900
H	15.44664600	3.44341100	1.26057700
C	11.27687600	-1.17792600	-0.04467300
H	11.01717200	-0.99105500	1.02262600
H	10.81807700	-0.34460300	-0.62482400
C	10.65696300	-2.51009800	-0.49233600
H	10.90903100	-2.70073500	-1.56066200
H	11.10954700	-3.34743700	0.08665500
C	9.12962000	-2.54796500	-0.32129100
H	8.67773900	-1.70812100	-0.89639900
H	8.87758700	-2.35220700	0.74570000
C	8.49902400	-3.87368100	-0.76460200
H	8.90281700	-4.72928100	-0.18211800
H	7.39801300	-3.86611000	-0.62740400
H	8.70094600	-4.07964600	-1.83753500

Table A.4. (Dppf)Ni.

Zero-point energy (BLYP/6-31G(d)=	-4766.4212397
Zero-point correction=	0.500962 (Hartree/Particle)
Thermal correction to Energy=	0.535447
Thermal correction to Enthalpy=	0.536392
Thermal correction to Gibbs Free Energy=	0.430920
Sum of electronic and zero-point Energies=	-4766.258849
Sum of electronic and thermal Energies=	-4766.224363
Sum of electronic and thermal Enthalpies=	-4766.223419
Sum of electronic and thermal Free Energies=	-4766.328890

Coordinates:

C	0.96087000	1.65947500	1.59317700
C	0.93107500	1.68295800	3.03150700
C	1.59072400	0.49558600	3.50920900
C	2.03858300	-0.25900100	2.36660100
C	1.66110400	0.46211400	1.16961100
H	0.52334100	2.41081500	0.92344200
H	0.46130100	2.45663400	3.65355300
H	1.71216100	0.20338300	4.56123800
H	2.56451400	-1.22182500	2.39181900
Fe	-0.00007800	-0.00210500	2.30680500
C	-0.96122300	-1.66262100	1.59082100
C	-0.93131600	-1.68817700	3.02911300
C	-1.66135100	-0.46457500	1.16903000
H	-0.52384500	-2.41305900	0.91997400
C	-1.59081100	-0.50143200	3.50858000
H	-0.46157900	-2.46281200	3.64999300
C	-2.03866600	0.25486000	2.36709200
H	-1.71213100	-0.21073800	4.56104100
H	-2.56444100	1.21773000	2.39374100
P	1.91168600	0.00375200	-0.60387700
P	-1.91181700	-0.00360500	-0.60381200
Ni	-0.00006400	0.00012600	-1.49001500
C	-3.30148000	-1.15124500	-1.10151300
C	-3.56665400	-1.28316800	-2.48438100
C	-4.06743100	-1.90765400	-0.18634500
C	-4.58690100	-2.13303400	-2.94184100
H	-2.95480600	-0.71649900	-3.20723700
C	-5.08142700	-2.76875000	-0.64600900
H	-3.86727000	-1.82764800	0.89386300
C	-5.34655700	-2.88101700	-2.02226500
H	-4.78394600	-2.22096000	-4.02256700
H	-5.66907500	-3.35570500	0.07860900
H	-6.14022100	-3.55639800	-2.37988700

Table A.4 continued

C	-2.80432300	1.63258000	-0.47222900
C	-4.13745400	1.76352200	-0.02381200
C	-2.09614500	2.79050700	-0.86349200
C	-4.74245800	3.03136600	0.04406500
H	-4.71115600	0.86878300	0.26688900
C	-2.69971300	4.05830000	-0.79293000
H	-1.06298800	2.67187900	-1.23500500
C	-4.02502000	4.18059700	-0.33726200
H	-5.78391100	3.12230200	0.39316900
H	-2.13584100	4.95306800	-1.10259000
H	-4.50316700	5.17201500	-0.28621400
C	2.80553400	-1.63188400	-0.47451800
C	4.13888000	-1.76229500	-0.02657300
C	2.09817800	-2.78989300	-0.86698800
C	4.74492500	-3.02972600	0.03958700
H	4.71190400	-0.86743700	0.26509400
C	2.70278600	-4.05729000	-0.79813500
H	1.06480500	-2.67166300	-1.23802700
C	4.02831400	-4.17906800	-0.34298300
H	5.78653500	-3.12026200	0.38832400
H	2.13955100	-4.95213700	-1.10872500
H	4.50727700	-5.17016100	-0.29327900
C	3.30034200	1.15322300	-1.10019300
C	4.06600900	1.90874200	-0.18405900
C	3.56497400	1.28759300	-2.48293400
C	5.07920100	2.77136400	-0.64264900
H	3.86629800	1.82682800	0.89608900
C	4.58441100	2.13899200	-2.93933800
H	2.95334700	0.72163300	-3.20653000
C	5.34379500	2.88607900	-2.01879900
H	5.66662400	3.35758000	0.08274900
H	4.78104300	2.22882000	-4.01998300
H	6.13681200	3.56265900	-2.37558800

Table A.5. Free phenyl *n*-butyl ketene.

Zero-point energy (BLYP/6-31G(d)=	-540.65782882
Zero-point correction=	0.220961 (Hartree/Particle)
Thermal correction to Energy=	0.234283
Thermal correction to Enthalpy=	0.235227
Thermal correction to Gibbs Free Energy=	0.179481
Sum of electronic and zero-point Energies=	-540.456959
Sum of electronic and thermal Energies=	-540.443637
Sum of electronic and thermal Enthalpies=	-540.442692
Sum of electronic and thermal Free Energies=	-540.498439

Coordinates:

O	0.66057400	2.86477100	-0.00024400
C	0.37333100	1.72366000	0.00025400
C	0.05415500	0.43481200	0.00055200
C	-1.36937100	0.02743000	0.00025400
C	-1.71743800	-1.34698200	0.00018900
C	-2.42494300	0.97895700	0.00002700
C	-3.06505900	-1.74838100	-0.00008900
H	-0.93192200	-2.11655900	0.00035600
C	-3.76505200	0.57256300	-0.00024800
H	-2.19130800	2.05691900	0.00006900
C	-4.09761300	-0.79667900	-0.00030900
H	-3.30548300	-2.82388100	-0.00013200
H	-4.56096500	1.33459800	-0.00041800
H	-5.15175900	-1.11498900	-0.00052700
C	1.18663700	-0.59068700	0.00027300
H	1.05552900	-1.24761700	0.89066100
H	1.05527300	-1.24742500	-0.89021900
C	2.61020400	-0.01354800	0.00012600
H	2.74923800	0.64138500	-0.89032500
H	2.74950700	0.64117400	0.89069000
C	3.69761600	-1.10044500	-0.00016500
H	3.55538500	-1.75780300	-0.88785300
H	3.55565400	-1.75801100	0.88741300
C	5.12353700	-0.53594300	-0.00031400
H	5.30942100	0.09571400	0.89456700
H	5.88165100	-1.34613900	-0.00052400
H	5.30915000	0.09592500	-0.89510300